Molekulare Mechanismen der Neurodegeneration in der Grosshirnrinde von Kathepsin B und L-Doppelknockoutmäusen

Dissertation zur Erlangung des
naturwissenschaftlichen Doktorgrades
der Bayerischen Julius-Maximilians-Universität Würzburg

vorgelegt von

Sonja Stahl

aus
Marktheidenfeld

Würzburg 2006

Eingereicht am:

Mitglieder der Promotionskommission:

Vorsitzender:Prof. Dr. M. Müller
Gutachter: PD Dr. U. Felbor
Gutachter: Prof. Dr. G. Krohne

Tag des Promotionskolloquiums:

Doktorurkunde ausgehändigt am:

Summary

Cathepsins B and L are lysosomal cysteine proteases which have been implicated in a variety of pathological processes such as cancer, tumor angiogenesis, and neurodegeneration. However, only a few protein substrates have thus far been described and the mechanisms by which cathepsins B and L regulate cell proliferation, invasion, and apoptosis are poorly understood. Combined deficiency of both cathepsins results in early-onset neurodegeneration in mice reminiscent of neuronal ceroid lipofuscinoses in humans. Therefore, we intended to quantify protein changes in brain lysosomes of double deficient mice. A combination of subcellular fractionation and LC-MS/MS using isobaric tagging for relative and absolute quantitation (iTRAQ^{TM}) allowed us to simultaneously assess wildtype and cathepsin $B^{-/-}L^{-/-}$ cerebral lysosomes. Altogether, 19 different proteins were significantly increased in cathepsin $B^{-/-}L^{-/-}$ lysosomes. Most elevated proteins had previously been localized to neuronal biosynthetic, recycling/endocytic or lysosomal compartments. The increase of calcyon, the Delta/Notch-like epidermal growth factor-related receptor, neurochondrin, phospholipase D3, Rab14, cathepsin D, and apolipoprotein E suggests a potential role for cathepsins B and L in axon outgrowth and synapse formation during postnatal development of the central nervous system.

Zusammenfassung

Kathepsin B und L sind lysosomale Cysteinproteasen, die mit einer Reihe von pathologischen Prozessen, wie z. B. Cancerogenese, Tumorangiogenese und Neurodegeneration in Verbindung gebracht werden. Dennoch sind bis jetzt nur wenige Proteinsubstrate beschrieben. Ausserdem sind die Mechanismen der Regulation von Zellproliferation, -invasion und -apoptose durch Kathepsin B und L weitgehend unverstanden. Ein kombinierter Mangel beider Kathepsine führt zu einer frühzeitigen Neurodegeneration in Mäusen, die an neuronale Lipofuszinosen beim Menschen erinnert. In der vorliegenden Studie wurden Unterschiede in der Proteinzusammensetzung von wildtypischen und doppelt-defizienten Gehirnlysosomen quantifiziert. Eine Kombination von subzellulärer Fraktionierung und LC-MS/MS unter Verwendung einer isobarischen Markierung (iTraq^{TM}) erlaubte uns die gleichzeitige Untersuchung von zerebralen Lysosomen aus Wildtyp und Kathepsin

$B^{-/-}L^{-/-}$ Mäusen. Ingesamt waren 19 Proteine signifikant erhöht in Kathepsin $B^{-/-}L^{-/-}$ Lysosomen. Die meisten erhöhten Proteine wurden der neuronalen Biosynthese, regenerierenden bzw. endozytotischen oder lysosomalen Kompartimenten zugeordnet. Der Anstieg von Calcyon, dem Delta/Notch- verwandten epidermalen Wachstumsfaktor-Rezeptor (DNER), Neurochondrin, Phospholipase D3, Rab14, Cathepsin D und Apolipoprotein E lässt eine potentielle Rolle von Kathepsin B und L im Axonwachstum und der Synapsenbildung während der postnatalen Entwicklung des Zentralnervensystems vermuten.

1. Einleitung

1.1 Proteasen im lysosomalen Kompartiment

Proteasen katalysieren die intra- und extrazelluläre Hydrolyse von Amidbindungen. Proteolyse findet überall im Organismus statt. Sie ist wichtig für die normale Funktion eines Organismus und muss strikt kontrolliert werden. Viele Krankheiten werden durch Fehlregulation von Proteasen verursacht. Im Zytosol werden Proteine durch das Proteasom, einen Proteasekomplex abgebaut. Von grosser Bedeutung für die Proteinreifung und den terminalen Proteinabbau ist jedoch das endosomal-lysosomale System. Die lysosomalen Cysteinproteasen, auch Kathepsine genannt, sind ubiquitäre Proteasen der Papainfamilie. Im humanen Genom sind 11 Kathepsine vorhanden (B, C, F, L, K, V, S, X/Z, H, W und O). Sie unterscheiden sich im Expressionsmuster und der Substratspezifität. Konstitutive Proteasen mit geringer Spezifität sind hierbei Kathepsin B, H und L. Sie sind involviert in den intrazellulären Proteinabbau, die Immunantwort, die Proteinprozessierung und andere wichtige zelluläre Prozesse (Barrett et al., 1998). Im extrazellulären Raum wird ihnen eine grosse Bedeutung bei der Hormonregulation zugeschrieben (Brix *et al.,* 2001). In pathologisch veränderten Geweben können Proteasen sezerniert werden und beispielsweise beim Lungenemphysem (Mason et al., 1986; Takeyabu et al., 1998) oder bei der Tumordisseminierung (Joyce and Hanahan, 2004) zur unkontrollierten Degradation der extrazellulären Matrix führen. Ferner wurde für Kathepsin B und L in einem neuronalen *in vitro* System nachgewiesen, dass diese beiden Cysteinproteasen Prionproteine abbauen (Luhr et al., 2004). Gen-Knockoutmäuse haben bestätigt, dass Kathepsine individuelle und spezifische Funktionen haben, die für zahlreiche physiologische Prozesse eines Organismus wichtig sind und nicht nur den lysosomalen Proteinabbau betreffen (Gowen et al., 1999; Honey et al., 2002; Nakagawa et al., 1998; Roth et al., 2000; Saftig et al., 1998; Stypmann et al., 2002).

1.2 Mutationen in humanen Kathepsingenen

Auch Erbkrankheiten konnten auf Fehlregulation von Kathepsinen zurückgeführt werden. So wird die autosomal-rezessiv vererbte Pyknodysostose (OMIM #265800) durch Nonsense-, Missense- und Stopmutationen im Kathepsin K-Gen verursacht (Gelb et al., 1996), das in Osteoklasten stark exprimiert wird (Gowen et al., 1999). Die Pyknodysostose zeichnet sich durch verkürzte und sklerotisierte Röhrenknochen aus. Der menschliche Phänotyp konnte auch bei Kathepsin K-Knockoutmäusen

reproduziert werden und lässt sich auf eine defizitäre Matrix-Degradation in den Resorptionslakunen zurückführen (Gowen et al., 1999; Saftig et al., 1998). Da Östrogen die Kathepsin K-Expression negativ reguliert, lag der Umkehrschluss nahe, dass überschüssiges Kathepsin K eine Rolle bei der postmenopausalen Osteoporose spielen könnte (Lazner et al., 1999). Inzwischen werden selektive Kathepsin K-Inhibitoren für eine potentielle therapeutische Anwendung bei Osteoporose entwickelt (Kim and Tasker, 2006). Eine weitere autosomal-rezessive Erkrankung, die auf eine Kathepsin-Mutation zurückzuführen ist, ist das Papillon-Lefevre Syndrom (PLS, OMIM #245000, Hart et al., 2000a; Hart et al., 2000b; Toomes et al., 1999). PLS ist gekennzeichnet durch eine Palmoplantarkeratose mit früh beginnender Parodontitis. Bei PLS-Patienten wurde ein nahezu kompletter Verlust der Kathepsin C-Aktivität festgestellt, verursacht durch Nonsense- und Missensemutationen sowie durch Deletionen und Insertionen. Hart et al. (2000) stellten ausserdem fest, dass das PLS und das Haim-Munk Syndrom (HMS, OMIM #245010) allelische Variationen der Kathepsin C-Mutationen sind. HMS ist ein auf eine jüdische Bevölkerungsgruppe begrenztes Syndrom, das dem PLS sehr ähnlich ist.

Dass eine Kathepsin D-Defizienz zu einer menschlichen neurodegenerativen Erkrankung führt, wurde durch zwei Tiermodelle bereits gezeigt: Eine Missensemutation, die ein für die katalytische Aktivität essentielles Aspartat betrifft, ist in Schafen homozygot mutiert die eine angeborene lysosomale Speicherkrankheit haben. Diese führt zu einer progressiven psychomotorischen Retardierung, Blindheit und frühem Tod (Tyynelä et al., 2000). Auch Kathepsin D-Knockoutmäuse werden durch Krampfanfälle phänotypisch auffällig und versterben um den 26. postnatalen Tag blind (Koike et al., 2000). In Nervenzellen dieser Mäuse akkumulieren Lysosomen-ähnliche Strukturen, die denen der neuronalen Ceroid-Lipofuszinose (NCL, OMIM #610127) ähneln. Im Rahmen einer genetischen Analyse von 25 Kindern mit NCL-ähnlichen Erkrankungen wurde vor kurzem der erste Mensch mit einer Kathepsin D-Defizenz identifiziert (Steinfeld et al., 2006). Das Mädchen fiel mit Ataxie und Sehstörungen im Grundschulalter auf. Bereits mit 17 Jahren war sie an den Rollstuhl gebunden und mental stark retardiert. Zwei heterozygote Missense-Mutationen wurden im Kathepsin D-Gen identifiziert. Zeitgleich entdeckte eine finnische Forschergruppe eine homozygote Nukleotidduplikation (c.764.dupA) bei einem Jungen pakistanischer Herkunft, dessen Eltern Vetter und Base 1. Grades

sind (Ramirez-Montealegre et al., 2006; Siintola et al., 2006). Die Duplikation führt zu einem vorzeitigen Stopkodon und theoretisch somit zu einem trunkierten Kathepsin D Protein (p.Tyr255X). Allerdings scheint es bedingt durch die Duplikation zu einer Degradation der Kathepsin-mRNA oder des Proteins zu kommen. Hirngewebeproben von Geschwistern des Patienten zeigten, dass kein Kathepsin D vorhanden war. Die Existenz einer humanen kongenitalen Form der NCL, die durch Kathepsin D-Defizienz verursacht wird, wurde auch in einem weiteren englischen Patienten bestätigt (Siintola et al., 2006).
Obwohl Kathepsin B und L-Doppelknockoutmäuse einen viel ausgeprägteren Phänotyp aufweisen als Kathepsin D-Knockoutmäuse, erscheint es unwahrscheinlich, dass ein humanes Pendant für die Doppelknockoutmäuse gefunden wird. Bei einem autosomal-rezessiven Erbgang würde dies vier Mutationen vorraussetzen, zwei im Kathepsin B- und zwei im Kathepsin L-Gen.

1.3 Struktur der Kathepsine

Die Grundstruktur der Kathepsine wurde initial anhand von Kathepsin B geklärt (Musil et al., 1991). Enzyme der Papainfamilie bestehen aus zwei Domänen, der R- und der L-Domäne. Die L-Domäne wird von einer α-Helix dominiert und bildet mit der R-Domäne, die hauptsächlich aus einer β-Faltblattstruktur besteht, einen V-förmigen Spalt, in dem das Substrat bindet (McGrath, 1999). Das katalytisch aktive Cystein im aktiven Zentrum befindet sich in der N-terminalen Region der α-Helix an Position 25. Neben dem Cystein findet sich im Homologievergleich der Papain-verwandten Kathepsine auch noch ein konserviertes Histidin an Position 159. Es ist auf der gegenüberliegenden Seite in der β-Faltblattstruktur lokalisiert. Zusätzlich zu diesen beiden Aminosäureresten existiert noch ein weiteres hoch konserviertes Asparagin an Position 175, welchem die Zugehörigkeit zu einer „katalytische Triade“ zugeschrieben wird, vergleichbar mit der Serin-Histidin-Asparagin Triade von Serin Proteasen (Chapman et al., 1997).

1.4 Aktivierung und proteolytische Wirkweise von Kathepsinen

Kathepsine werden als Vorläufermoleküle, sogenannte Zymogene, im endosomal-lysosomalen System synthetisiert, wo sie unter sauren pH-Bedingungen zum enzymatisch aktiven Molekül heranreifen. Das Präproenzym wird am membran-gebundenen Ribosomen des rauen endoplasmatischen Reticulums hergestellt. Der

Transport in das endoplasmatischen Reticulum erfolgt über eine cotranslationale Abspaltung eines terminalen Signalpeptids. In den „späten Endosomen“ und Lysosomen kommt es nach einer Absenkung des pH-Wertes zu einer Konformationsänderung und dadurch zu einer proteolytischen N-terminalen Propeptidabspaltung. Im Lysosom besitzen Kathepsine die höchste enzymatische Aktivität. Ausserhalb dieses Systems sind die meisten Cysteinproteasen relativ instabil (B, L, H, K, V, F). Kathepsin S gehört zu den Ausnahmen, die auch auch ausserhalb des Lysosoms stabil sind (Bromme and McGrath, 1996).

Cysteinproteasen lassen sich in zwei Klassen einteilen: Exopeptidasen, zu denen Kathepsin C und X gehören, und Endopeptidasen, die den größten Teil dieser Enzymgruppe stellen (Kathepsine F, K, L, S und V). Nur Kathepsin B und H besitzen sowohl Exo- als auch Endopeptidaseaktivität. Endopeptidasen können sich selbst aktivieren, wohingegen Exopeptidasen wie Kathepsin X und C einer Aktivierung durch Endopeptidasen bedürfen (Dahl et al., 2001; Nagler et al., 1999).

Die meist monomer vorliegenden Cysteinproteasen haben eine ungefähre molekulare Masse von 22 - 28 kDa. Eine Ausnahme bildet Kathepsin C, welches als Oligomer vorkommt und eine Masse von ca. 200 kDa hat (Dolenc et al., 1995). Neben den Cysteinproteasen gibt es unter den Kathepsinen auch noch Aspartasen (Kathepsin D und E) und Serinproteasen (Kathepsin A und G).

1.5 Substrate für Kathepsin B und L

Natürliche Substrate von Kathepsin B und L sind die Bestandteile der extrazellulären Matrix, beispielsweise Laminin, Kollagen, Elastin und Fibronektin (Bromme et al., 1996; Ishidoh and Kominami, 1995; Lombardi et al., 2005). Intrazellulär spielt Kathepsin L eine wichtige Rolle bei der Degradation der MHC-Klasse II-assoziierten invarianten Kette in kortikalen Thymuszellen (Chapman et al., 1997; Nakagawa et al., 1998). Prohormon-prozessierende Aktivität wird Kathepsin L im Zusammenhang mit der Enkephalin-Produktion zugeschrieben (Yasothornsrikul et al., 2003). Weiterhin sind Kathepsin B, L und K an der Prozessierung von Thyroglobulin und damit an der Freisetzung von Tyroxin beteiligt (Friedrichs et al. 2003). Es wird vermutet, dass Kathepsin L an einem bisher unbekannten Weg der Biosynthese von Peptidneurotransmittern und -hormonen beteiligt ist (Hook et al., 2004; Hook, 2006). Kathepsin B ist weiterhin verantwortlich für die proteolytische Spaltung von Insulin-like growth factor-1 (IGF-1) im Endosom (Authier et al., 2005). Ebenfalls im Endosom

findet die Prozessierung von Epidermal growth factor (EGF) und Glucagon durch Kathepsin B statt (Authier et al., 1999; Authier et al., 1995).

Neuste Forschungen mit Vero-Affenzellen zeigten, dass sowohl Kathepsin B als auch Kathepsin L an der endosomalen Proteolyse des Ebola Glycoproteins G1 beteiligt sind (Chandran et al., 2005). Erst die endosomale Prozessierung ermöglicht dem Virus, die Wirtszelle zu infizieren. Einen ähnlichen Mechanismus verwenden die für SARS verantwortlichen Coronaviren beim Eintritt in Wirtszellen (Simmons et al., 2005). Kontrovers wird die Rolle von Kathepsin B und L bei Prionprotein-Erkrankungen diskutiert. Die Akkumulation von PrP^{Sc} in Kathepsininhibitor-behandelten GTI-1 Scrapie-infizierten Zellen (Luhr et al., 2004) steht allerdings im Gegensatz zur Reduktion von PrP^{Sc} in Neuro2a Scrapie-infizierten Zellen nach Kathepsininhibitor Zugabe (Zhang et al., 2003).

Bekannt ist auch eine nukleäre Wirkung von Kathepsinen. Durch die proteolytische Prozessierung des Transkriptionsfaktors CDP/Cux greift Kathepsin L in die Regulation des Zellzyklus ein (Goulet et al., 2004). Hierbei ist eine verkürzte Form von Kathepsin L im neutralen Milieu des Kerns aktiv. Ein weiterer Zellzyklusregulator wurde bei Versuchen mit Seneszenz-initiierenden Zellen als Kathepsin L-Substrat identifiziert (Zheng et al., 2004). p21/WAF ist ein Cyclin-abhängiger Kinaseinhibitor, der durch das Tumorsuppressorgen p53 kontrolliert wird. Die Zugabe von Kathepsin L Inhibitoren führte zu einer erhöhten Expression des Zellzyklusinhibitors p21/WAF.

Unter pathologischen Bedingungen ist auch hochmolekulares Kininogen, ein Plasmaglykoprotein mit antiproteolytischer Wirkung, ein Substrat für Kathepsin B (Barros et al., 2004). Der Kathepsin-Inhibitor wird bei einem pH-Wert von 6,35 in drei Fragmente zerschnitten und ist daraufhin inaktiv. Kathepsin L generiert aus hochmolekularem Kininogen *in vitro* immunoreaktive Kinine (Desmazes et al., 2003; Desmazes et al., 2001). Die biologische Relevanz der Kininogenprozessierung durch Kathepsine ist noch unklar. Es deutet jedoch vieles darauf hin, dass Kathepsine als Kininogen-spaltende Enzyme wirken und damit bei Entzündungsreaktionen eine grosse Rolle spielen. Kinine wirken im Zusammenhang mit inflammatorischen Erkrankungen als Vasodilatatoren und bewirken eine Relaxation der glatten Muskulatur. Eine intravenöse Injektion von Kathepsin L in Ratten führte zu einer erhöhten Kininfreisetzung und als Folge zu Blutdruckabfall. *In vitro* Experimente zeigten, dass der Archetyp der Kinine, Bradykinin, entsteht (Puzer et al., 2005).

Eine erhöhte elastolytische Aktivität von Kathepsinen hat die Prozessierung des Secretory Leukoprotease inhibitor SLPI zur Folge (Taggart et al., 2001). Dieser kommt in den schleimproduzierenden Schichten von Epithelzellen vor und wird außerdem von Makrophagen und neutrophilen Zellen produziert. Er wird von Kathepsin B, L und S geschnitten und inaktiviert. Im Organismus konnte eine erhöhte Aktivität von Kathepsin L und Inaktivierung von SLPI im Bronchialsekret bei Erkrankungen der oberen Atemwege wie z.B. beim Lungenemphysem festgestellt werden. α_1-Proteinase Inhibitor (α_1PI), ein im Blutplasma vorkommender Elastase-, Trypsin- und Chymotrypsininhibitor, kann von Kathepsin L katalytisch inaktiviert werden (Johnson et al., 1986). Ein im humanen Sputum vorkommender Inhibitor von Kathepsin B ist α_2-Makroglobulin. Eine Bindung von Kathepsin B an α_2-Makroglobulin verhindert den Proteoglykanabbau (Buttle et al., 1991; Starkey and Barrett, 1973). Damit gewinnen Kathepsin B und L indirekt weiter an Bedeutung in Verbindung mit der Degradation von extrazellulären Matrixproteinen.

Therapeutisch relevant könnte die Tatsache sein, dass Kathepsin B, L und K Amyloidproteine und Amyloidablagerungen abbauen. Amyloidablagerungen findet man bei chronischen oder wiederkehrenden inflammatorischen Erkrankungen wie z.B. der rheumatoiden Arthritis (Bohne et al., 2004; Rocken et al., 2005). Eine Kolokalisation von Kathepsin B und dem beta-Amyloid wurde *in vitro* in sekretorischen Vesikeln von neuronalen chromaffinen Zellen beobachtet. Kathepsin B wirkt eventuell als beta-Sekretase und produziert so aus dem Amyloid-Precursor-Protein unlösliches, extrazellulär vorkommendes beta-Amyloid, das sich bei Alzheimerpatienten vermehrt im Gehirn anreichert. In diesem Zusammenhang werden Kathepsin B-Inhibitoren als therapeutische Ansatzpunkte gesehen, um beta-Amyloidanreicherung im Gehirn von Alzheimerpatienten zu vermindern (Hook et al., 2005).

1.6 Inhibitoren

Cysteinpeptidasen werden *in vivo* durch endogene nicht selektive Inhibitoren, sogenannte Cystatine, gehemmt (Turk et al., 1993). Cystatine inhibieren Endo- und Exopeptidasen, indem sie an das aktive Zentrum von Kathepsinen binden. Cystatine teilt man in drei Gruppen ein. Neben den eigentlichen Cystatinen kennt man noch Stefine und Kininogene. Stefine sind intrazelluläre Inhibitoren, Cystatine und Kininogene werden im extrazellulären Raum gefunden. Somit werden die aktivierten

Kathepsine außerhalb des lysosomal-endosomalen Systems nicht nur durch den pH Wert kontrolliert, sondern auch aktiv und effektiv durch Cystatine. Der Mechanismus der Inhibierung durch Cystatine ist noch nicht ganz geklärt.

Mutationen im Cystatin B-Gen verursachen das familiäre Unverricht-Lundborg Syndrom, eine autosomal-rezessiv vererbte progressive Myoklonusepilepsie (Lehesjoki, 2003). Die häufigste Mutationsart ist eine homozygote Expansion eines instabilen Minisatellitenrepeats in der Promotorregion des Cystatin B-Gens, die zur Cystatin B-mRNA-Reduktion führt. Trunkierende Mutationen innerhalb der translatierten Genregion führen entweder zu instabilen Genprodukten oder ebenso wie bei den zwei bekannten Missense-Mutationen zu diffus im Zytoplasma verteilten Produkten, die nicht mit lysosmalen Markern kolokalisieren. Bei den Missense-Mutationen wurde zudem gezeigt, dass die Bindung an Zielproteasen eingeschränkt ist. Eine erhöhte Aktivität von Kathepsin B, L und S scheint für die Pathogenese des Unverricht-Lundborg Syndroms von Bedeutung zu sein (Alakurtti et al., 2005; Lehesjoki, 2003).

Als weiterer natürlicher Cysteinproteaseinhbitor wurde 1975 E-64 entdeckt (Aoyagi and Umezawa, 1975). Der aus dem Schimmelpilz *Aspergillus japonicus* stammende Epoxidinhibitor E-64 interagiert über eine Epoxysuccinyl-Gruppe kovalent mit dem Cystein des aktiven Zentrums. Dieser Vorgang ist irreversibel. E-64 hemmt Kathepsin B, H und L.

Thyroglobulin Typ-1 (Tg-1) Domäne enthaltende Proteine sind ebenfalls effiziente Inhibitoren von Kathepsinen, so z.B. Testican-1 (Bocock et al., 2003; Meh et al., 2005). Testican ist ein Proteoglycan, welches von Gehirnzellen sezerniert wird. Testicans genaue *in vivo* Funktion ist nicht bekannt. Andere Tg-1-Domänenproteine mit Kathepsin L-inhibierender Funktion sind das p41 invariant chain fragment (Bevec et al., 1996), Equistatin (Lenarcic et al., 1997), Saxiphilin (Lenarcic et al., 2000) und der aus Hundslachs (*Oncorhynchus keta)* stammende Eicysteinpeptidaseinhibitor (Yamashita and Konagaya, 1996).

Eine weitere umfassende Gruppe der Kathepsin-Inhibitoren sind die Serpine (**Ser**in-**P**rotease-**In**hibitoren). Serpine präsentieren in einer „reaktiven Zentralschleife“ eine Art Pseudosubstrat für Proteasen. Während der Reaktion der Serin-Protease mit dem Serpin kommt es zu einer Konformationsänderung des Serpins und damit zu einem irreversiblen Komplex aus Protease und Inhibitor. Squamous cell carcinoma antigen-1 und -2 sind Inhibitoren von Kathepsin K, L und S aus der Serpin-

Superfamilie (Irving et al., 2002). Sie haben ähnlich wie auch CrmA eine Köderfunktion, im Bezug auf Cystein-Proteasen. CrmA ist ein virales Serpin mit hoher Sequenzhomologie zum Plasminogen-Aktivator-Inhibitor Typ II (PAI II). Hurpin (SerpinB13) wird zusammen mit Kathepsin L häufig bei inflammatorischen und neoplastischen Erkrankungen gefunden. Beispielsweise wurden hohe Expressionslevels von Kathepsin L bei Psoriasis und Plattenepithelkarzinom-patienten gefunden. Gleichzeitig wurden in der Haut der Erkrankten erhöhte Mengen an Hurpin detektiert (Bylaite et al., 2006). Der genaue Mechanismus der Cystein-Protease-Inhibierung ist noch nicht bekannt.

1.7 Kathepsin B-defiziente Mäuse

Kathepsin B ist das erste beschriebene Mitglied der grossen Familie der Cysteinproteasen. 1983 wurde die erste komplette Aminosäuresequenz für Kathepsin B aus Rattenleber publiziert (Takio et al., 1983). Zehn Jahre später wurde die Kristallstruktur gelöst (Musil et al., 1991). Obwohl Kathepsin B in viele pathologische Vorgänge involviert zu sein scheint, zeigten Kathepsin B-Knockoutmäuse keinen augenscheinlichen Phänotyp (Deussing et al., 1998). Auch histologische Analysen von verschiedenen Gewebetypen deckten keine Veränderungen auf. Fertilität und Mortalität sind ebenfalls nicht signifikant unterschiedlich im Vergleich zu Wildtypmäusen. Allerdings wurde in diesem Mausmodell die seit längerem diskutierte Rolle von Kathepsin B bei der Auslösung einer akuten Pankreatitis bestätigt. Eine akute Pankreatitis, induziert in Kathepsin B Knockoutmäusen und Wildtypmäusen, zeigte, dass die Trypsinaktivierung im Pankreas von erkrankten Knockoutmäusen um 80% geringer war als in der Vergleichsgruppe (Figarella et al., 1988; Halangk et al., 2000). Dafür könnte eine Trypsinogenaktivierung durch Kathepsin B verantwortlich sein, die nach der Aktivierung von Trypsin Aktivierungen von vielen weiteren Proteasen nach sich zieht. Unter experimentellen Zellkulturbedingungen wurde ferner in Leberzellen eine erhöhte Resistenz gegen TNFα-induzierte Apoptose festgestellt (Guicciardi et al., 2000). Fibroblastenzelllinien von Kathepsin B- und L-defizienten Mäusen waren darüber hinaus essentiell für den Nachweiss, dass Ebolaviren diese beiden Proteasen benötigen, um in Zellen eindringen zu können (Chandran et al., 2005).

1.8 Kathepsin L-defiziente Mäuse

Roth et al. (2000) berichteten, dass Kathepsin L Knockoutmäuse im Vergleich zu Kontrollmäusen in der Entwöhnungsphase eine höhere Mortalitätsrate besitzen (15% gegenüber 5% bei Wildtypmäusen). Dies konnten wir in unseren von AstraZeneca überlassenen Kathepsin $L^{-/-}$ Mäusen nicht bestätigen (Felbor et al., 2002). Homozygote $L^{-/-}$ Mäuse sind ab der zweiten Lebenswoche anhand einer verzögerten Entwicklung des Fells zu erkennen. Später weisen sie einen periodischen Haarausfall und eine epitheliale Hyperplasie auf (Potts et al., 2004; Roth et al., 2000; Tobin et al., 2002). Vieles deutet darauf hin, dass Kathepsin L in die epidermale Homöostase und die Regulation des Haarzyklus involviert ist (Reinheckel et al., 2001). So wurden in den Keratinozyten und Melanozyten der Haarfollikel von Kathepsin $L^{-/-}$ Mäusen höhere Proliferations- und Apoptoseraten festgestellt. Als Folge treten Hyperkeratosen auf. Verantwortlich für die Hyperproliferation ist nach neuesten Erkenntnissen ein verstärktes Zirkulieren von EGF und seinen Rezeptoren von den Endosomen zur Keratinozyten-Plasmamembran (Reinheckel et al., 2005). Eine Fellanomalie bei Mäusen, die sogenannte *furless*-Mutante, wurde bereits Mitte der 50er Jahre beschrieben (Green, 1954). Roth und Mitarbeiter zeigten, dass der *furless*-Mutante eine Mutation im Kathepsin L-Gen zu Grunde liegt. Es handelt sich um einen Nukleotidaustausch, der einen Aminosäureaustausch von G zu A (G149A) bedingt. Dieser liegt nahe am aktiven Zentrum und führt zu einem Komplettverlust an enzymatischer Aktivität (Roth et al., 2000). Ferner wurde bei Kathepsin L-defizienten Tieren eine immunologische Abnormalität beschrieben. Eine Reduktion der $CD4^+$ T-Lymphozyten um 70% (Nakagawa et al., 1998) weist auf eine verschlechterte positive Selektion in den kortikalen Thymusepithelzellen hin. Zusätzlich ist die Anzahl an V(α)14(+)NK 1.1(+) T-Zellen massiv verringert (Honey et al., 2002). Dies deutet darauf hin, dass Kathepsin L nicht nur eine Rolle bei der klassischen MHCII Antigen-Präsentation spielt, sondern auch wichtig für die nicht-klassische CD1D Präsentation ist. Auch die Mausmutante *nackt*, die durch eine diffuse Alopezie und eine deutliche Reduktion der $CD4^+$T-Zellen charakterisiert ist, wird durch eine Mutation im Kathepsin L-Gen verursacht. Dabei handelt es sich um eine 118 Basenpaare umfassende Deletion, die die Exons 6 und 7 betrifft (Benavides et al., 2001).

Im Zusammenhang mit Osteoporose ist zu erwähnen, das Östrogenentzug bei Kathepsin L Knockoutmäusen zu einem geringeren trabekulären Knochenverlust führte als bei Kontrollmäusen und heterozygoten Geschwistern (Potts et al., 2004).

Neben dem Hautphänotyp fand sich bei einjährigen Kathepsin $L^{-/-}$ Mäusen eine dilatative Kardiomyopathie, verbunden mit einer geringen Erhöhung des Herzgesamtgewichts (Stypmann et al., 2002). Schließlich wurde eine reduzierte Menge von Enkephalin im Gehirn von Kathepsin L-Knockoutmäusen gefunden (Yasothornsrikul et al., 2003).

Aktuelle Forschungsarbeiten bringen Kathepsin L in direkten Bezug zu vaskulären Erkrankungen wie Aneurysmata der Aorta Abdominalis und Atherosklerose (Liu et al., 2006). Die Cysteinprotease ist in betroffenen Geweben überexprimiert. Ihre Expression in vaskulären Zellen dieser Gewebe wird durch Cytokine reguliert. Weiterhin stellte sich heraus, dass Kathepsin L nach einer Ischämie wichtig für die durch endotheliale Progenitorzellen induzierte Neovaskularisation ist (Urbich et al., 2005).

1.9 Kathepsin B und L-defiziente Mäuse

Um die Rolle von Kathepsin L in der Angiogenese zu untersuchen, wurden Kathepsin B und L-Einzelknockoutmäuse gekreuzt, da Kathepsin B und L überlappende Substratspezifitäten haben. Ausgangspunkt für die Annahme, dass Kathepsin L eine duale pro- und antiapoptotische Rolle spielen könnte, war die Entdeckung, dass Kathepsin L den Angiogeneseinhibitor Endostatin aus Kollagen XVIII generiert (Felbor et al., 2000). Doppelknockoutmäuse zeigten jedoch einen dramatischen neurodegenerativen Phänotyp (Felbor et al., 2002). In den ersten Tagen nach der Geburt unterscheiden sich die Kathepsin B- und L-defiziente Mäuse phänotypisch nicht von ihren Geschwistern. Ab dem siebten Tag ist jedoch die für Kathepsin L-Einzelknockoutmäuse beschriebene Fellanamolie sichtbar (Roth et al., 2000). Hinzu kommt eine deutliche Gewichtsreduktion im Vergleich zu heterozygoten Geschwistern. Die meisten doppeltdefizienten Mäuse sterben zwischen Tag 12 und 17. Um die Überlebenschancen zu steigern, müssen die Wurfgrößen auf drei bis vier Junge reduziert werden, sobald der Phänotyp am 7. Tag erkennbar wird. Dennoch überleben nur wenige Doppelknockoutmäuse die Entwöhnungsphase von der Mutter. Diese bedürfen einer intensiven Pflege nach der Entwöhnungsphase, d.h. sie benötigen zweimal täglich angefeuchtetes Futter. Der Bewegungsablauf dieser Tiere ist von einem leichten Tremor und einer Spastizität der Hinterbeine gekennzeichnet. Obwohl man für beide Kathepsine eine ubiquitäre Expression nachweisen konnte, zeigten sich bei der histologischen Analyse der Kathepsin B- und L-defizienten

Mäuse neben der Hyperproliferation der Keratinozyten nur pathologische Veränderungen im Gehirn (Felbor et al., 2002). Es kommt in selektiven Nervenzellen der Gross- und Kleinhirnrinde der Kathepsin B und L-Doppelknockoutmäuse zu einer massiven Akkumulation lysosomaler Strukturen, der Apoptose und reaktive Astrozytose folgt. Als Folge dieser Neurodegeneration kommt es zu einer ausgeprägten Gross- und Kleinhirnatrophie. Etwa die Hälfte der Neuronen im zerebralen Kortex reichern grosse Mengen ultrastrukturell elektronendichter Strukturen an, bei denen es sich um Lysosomen handelt. Die Struktur der Einschlusskörperchen unterscheidet sich allerdings von denen, die für bekannte lysosomale Speicherkrankheiten typisch sind. Auch Standardmarker für neuronale Lipofuszinosen wie Antikörper gegen die mitochondriale F_1F_0-ATP-Synthase zeigten keine spezifische Anreicherung in den Doppelknockoutmäusen. In den Doppelknockoutmäusen war ferner die Aktivität der Tripeptidylpeptidase I, sowie der Palmitoylproteinthioesterase nicht reduziert (Felbor et al., 2002). Im hippocampalen Ammonshorn von Kathepsin B und L-defizienten Mäusen ließen sich am 7. postnatalen Tag elektronenmikroskopisch geringe lysosomale Akkumulationen in vereinzelten Nervenzellen nachweisen (Stahl *et al.,* unpublizierte Daten). In der Literatur war bereits beschrieben, dass eine Suppression von Kathepsin B und L *in vitro* zu einer Meganeuritenbildung und zu einer Degradation von τ durch Kathepsin D in kultivierten hippocampalen Schnitten führt (Bednarski and Lynch, 1996; Bednarski et al., 1997).

Eine mit histologischen Methoden nachweisbare lysosomale Akkumulation, Nervenzellapoptose sowie reaktive Gliose fand sich jedoch in keinem der untersuchten Entwicklungsstadien im Hippocampus von Doppelknockoutmäusen. Stattdessen erschien das Ammonshorn ab dem dritten postnatalen Tag verbreitert und zweigeteilt. Besonders prominent stellen sich axonale Schwellungen von Geburt an im zentralen Nervensystem von Doppelknockoutmäusen dar (Felbor et al., 2002). Die Phänotypen doppeltdefizienter Mäuse lassen sich zusammenfassend wie folgt auflisten:

Alter	Phänotyp
P 0.5	Vereinzelt axonale Schwellungen in weisser Substanz
P 3.5	Dichte Häufung axonaler Schwellungen in weisser Substanz
P 3.5	Hippocampaler Laminationsdefekt
P10.5	Klüver-Barrera-positive Einschlüsse in corticalen Neuronen
P17.5	Apoptose der Purkinje-Zellen
P21.5	Apoptose von selektiven Neuronen der Grosshirnrinde

1.10 Das lysosomale Kompartiment

Lysosomen sind in tierischen Zellen ubiquitär vorkommende Vesikel. Sie enthalten verschiedene Arten von hydrolytischen Enzymen mit optimaler Aktivität im sauren pH-Bereich. Hydrolasen spalten Proteine, Kohlenhydrate, Nukleinsäuren, Fette und andere Zellbausteine. Sie werden im endoplasmatischen Retikulum synthetisiert und glykosyliert. Der Transport in die Lysosomen erfolgt über den Golgiapparat, von wo sie durch Vesikelabschnürung in primären Lysosomen an ihren Zielort gelangen. Ein molekularer Marker, der die Hydrolasen in die Lysosomen lenkt, ist Mannose-6-phosphat (McIntyre and Erickson, 1991). Im *cis*-Kompartiment des Golgiapparates wird durch eine Phosphotransferase eine Phospho-N-acetylglucosamineinheit an die 6-OH Gruppe eines Mannoserestes angehängt. Durch eine Phosphodiesterase wird der Zucker wieder entfernt und ein Mannose-6-phosphatrest bleibt als Markierung erhalten. In der Membran des Golgiapparates befindet sich ein integrales Membranprotein, der Mannose-6-phosphat-Rezeptor, der markierte Proteine bindet. Vesikel mit diesem Membran-Rezeptor-Komplex schnüren sich vom Golgiapparat ab und verschmelzen mit prälysosomalen Vesikeln (Gu et al., 2001). Saure pH-Bedingungen führen zu einer Dissoziation von lysosomalen Hydrolasen und Mannose-6-Rezeptor. Die Enzyme gelangen in die Lysosomen, der Rezeptor kehrt in den Golgiapparat zurück. Patienten mit Mukolipidose II oder I-Zell-Krankheit (OMIM #252500) besitzen nur unmodifizierte Mannose. Ursache ist das Fehlen der GlcNAc-Phosphotransferase (Kudo et al., 2006; Waheed et al., 1982). Wichtige saure Hydrolasen können daher nicht an ihren Bestimmungsort gelangen. In den Fibroblasten der Patienten kommt es zu lysosomaler Speicherung von Glykolipiden und Glykosaminoglykanen. Die sogenannten „inclusions“ in kultivierten Fibroblasten (=“I-cells“) führen zur Namensgebung dieser schweren, autosomal-rezessiv vererbten lysosomalen Speicherkrankheit. Da die posttranslationalen Modifikation zahlreicher Enzyme defekt ist, kommt es zu einem breiten Spektrum klinischer Befunde von Wachstumsretardierung über Skelettdeformationen bis zur psychomotorischen Retardierung. Betroffene Kinder werden durschschnittlich 5 bis 7 Jahre alt.

Substrate, die von lysosomalen Enzymen abgebaut werden, stammen aus endozytotischen oder autophagozytotischen Vesikeln. Dazu verschmelzen die Membranen der Vesikel mit denen von primären Lysosomen. Autophagie und Endozytose finden statt, um die Homöostase der Zelle zu erhalten. Autophagie dient

hauptsächlich dem Abbau von cytoplasmatischem Material, während durch Endozytose extrazelluläres Material degradiert wird. Die beiden lysosomalen Abbauwege stehen in der Zelle aber auch in Zusammenhang, da Autophagosomen während ihrer Entstehung durch endozytotische Vesikel gespeist werden (Kroemer and Jäättelä, 2005). Lysosomale Speicherkrankheiten sind meist autosomal-rezessiv vererbte Stoffwechselerkrankungen. Ausnahmen bilden die Mukopolysaccharidose vom TypII (Morbus Hunter, OMIM #309900) und die Sphingolipidose Morbus Fabry (OMIM #301500), die einem X-chromosomalen Erbgang folgen. Durch Fehlfunktionen im endosomal-lysosomalen System kommt es in verschiedenen Geweben und Organen wie z.B. Leber, Milz, Nervensystem und Haut zur Anreicherung von nicht abgebauten Stoffwechselmolekülen. Die Degradation hochmolekularer Substrate, wie Glykoproteine, Glykosaminglykane, Proteine und Lipide durch saure Hydrolasen ist bei lysosomalen Speicherkrankheiten gestört. Klinisch unterscheidet man zwischen Glykoproteinosen, Mukopolysaccharidosen, Gangliosidosen und Lipidosen. So werden bei Mukopolysaccharidosen komplexe Kohlenhydrate, die Mukopolysaccharide, die als Teile der Proteoglykane wesentliche Strukturkomponenten der extrazellulären Matrix darstellen, nicht mehr abgebaut. Bekannte Mukopolysaccharidosen sind Morbus Hunter und Morbus Hurler (OMIM #607014). Beide Krankheiten sind gekennzeichnet durch mentale Retardierung, Skelettdeformationen und die Speicherung von Dermatansulfat und Heparansulfat in den Körperzellen. Charakteristisch für Lipidspeicherkrankheiten sind Abbaustörungen von Membranlipiden, meist im Zentralnervensystem. Beispiele hierfür sind das Niemann-Pick Syndrom (OMIM #257200) oder Morbus Gaucher (OMIM #230800). Ferner treten Lipidspeichersubstanzen auch bei neuronalen Ceroid-Lipofuszinosen auf (Kohlschütter, 2005). Neuronale Ceroid-Lipofuszinosen (NCL) sind eine heterogene Gruppe progredient verlaufender lysosomaler Speicherkrankheiten, die meist im Kindesalter beginnen, vorwiegend Gehirn und Augen betreffen und zu Visusverlust und Demenz führen. Sie werden durch Gendefekte in lysosomalen Hydrolasen oder Membranproteinen verursacht, die zur vermehrten Bildung von Autophagosomen führen. Mutierte Moleküle sind beispielsweise bei der infantilen Form (CLN1) die Palmitoyl-Proteinthioesterase-1 (PPT1), oder bei der spätinfantilen form (CLN2) die Tripeptidyl-Aminopeptidase. Die Akkumulation der hochmolekularen Substanzen führt nach massiven Störungen des Zellstoffwechsels schließlich zum Tod der Zelle. *Post mortem* findet man bei Patienten histologisch und

elektronenmikroskopisch charakteristische Einschluss-Körperchen in betroffenen Geweben. Weder die für CLN1 typischen granulären Lipopigmenteinschlüsse, noch die für CLN2 charakteristischen kurvilinearen Profile wurden in Kathepsin B und L Doppelknockoutmäusen gefunden (Felbor et al., 2002).
Inzwischen wurden Therapieformen für lysosomale Speicherkrankheiten entwickelt, die nicht nur Symptome behandeln, sondern auch eine weitere Akkumulation verhindern können. So werden für Morbus Gaucher Enzymersatztherapien angeboten (Mistry, 2005). Ausserdem besteht die Möglichkeit, die Synthese der Speichersubstanzen durch Inhibitoren zu hemmen (Aerts et al., 2006; Mattocks et al., 2006). Die Bedeutung der Kathepsine im Bezug auf lysosomale Speicherkrankheiten ist weitgehend ungeklärt.

1.11 Kathepsine und Apoptose

Der programmierte Zelltod ist ein unentbehrlicher Bestandteil der normalen Entwicklung und Funktion eines Lebewesens. Eine zentrale Rolle spielen dabei die Mitochondrien. Hier beginnt sowohl die Caspase-abhängige Apoptose als auch die ATP-abhängige Nekrose. Die Apoptose hat eine wichtige Bedeutung für die Homöostase von Geweben. Ein genetisch programmierter Prozess ist dafür verantwortlich, dass in Geweben und Organen eine konstante Anzahl von Zellen vorhanden ist. Es entsteht ein Gleichgewicht aus Proliferation und Apoptose. Gealterte, geschädigte oder erkrankte Zellen werden eliminiert. Aber auch bei Differenzierungs- und Entwicklungsprozessen werden unnötige Zellen gezielt ausgeschaltet. Die Selbstzerstörung ist auch Selbstschutz, so werden beispielsweise Immunzellen, die sich autoreaktiv verhalten, durch Apoptose entfernt. Dabei kommt es zu typischen morphologischen Veränderungen: nach Chromatin-Kondensation, DNA Fragmentierung und der Bildung von membrangebundenen apoptotischen Vesikeln folgt eine Veränderung im Zytoskelett der Zellen und eine Zellschrumpfung. Kommt es zu Fehlregulationen bzw. wird das Gleichgewicht gestört, treten übermässige Zellverluste auf, was unter anderem bei Krebs und neurodegenerativen Erkrankungen sehr ausgeprägt ist.
Die Identifizierung der für die Apoptose regulatorischen Proteine gelang durch Beobachtungen an der Nematode *C. elegans* (Steller, 1995). Für zentrale Moleküle in *C. elegans* konnten homologe Gene und Proteine in Säugerzellen gefunden werden. Am apoptotischen Programm sind die pro- und antiapoptotischen Mitglieder

der *Bcl-2* Familie sowie Caspasen beteiligt. Eine Aktivierung der Caspasekaskade gilt als typisches Merkmal von Apoptose. Caspasen sind aber nicht alleine verantwortlich für das Ablaufen des programmierten Zelltodes. Extrazelluläre Signale, übertragen durch sogenannte „Todesrezeptoren“ (death receptors), verursachen z. B. den Fas- und TNFα vermittelten programmierten Zelltod. In letzter Zeit werden immer häufiger Kathepsine als Apoptosefaktoren diskutiert (Fehrenbacher and Jäättelä, 2005; Foghsgaard et al., 2001). Eine Prozessierung des Apoptosemediators *Bid*, durch Kathepsin B in Lysosomenextrakten (Stoka et al., 2001) konnte mit dem TNFα vermittelten Zelltod in Zusammenhang gebracht werden. Kathepsin B wird von den Lysosomen ins Zytosol abgegeben, schneidet *Bid* und verursacht eine Permeabilisierung der Mitochondrien und damit eine Freisetzung von Cytochrom c (Guicciardi et al., 2005). Aber auch *Bid*-unabhängige Apoptose wird durch Kathepsine vermittelt (Houseweart et al., 2003).

1.12 Kathepsine und Krebs

Tumorentstehung und Tumorprogression sind sehr stark abhängig vom Gleichgewicht zwischen Zellproliferation und Zelltod. Kommt es zu Störungen in der Regulierung des programmierten Zelltods kann Krebs entstehen. Während der Tumorentwicklung verändern sich in den Zellen Genexpressionsmuster und Proteinfunktionen: Tumorsuppressorgene werden inaktiviert und Onkogene aktiviert. Für Kathepsine ist bekannt, dass sie in manchen Tumoren an der Zelloberfläche vorkommen oder sogar sezerniert werden (Joyce and Hanahan, 2004). Ausserdem wurde eine verstärkte Expression mancher Kathepsine bei Krebs in Mensch und Maus beobachtet (Joyce et al., 2004; Tardy et al., 2005).

1.13 Kathepsine in der Nervenzellentwicklung

Proteasen im neuronalen System, sogenannte Neuroproteasen, sind zum einen für die Biosynthese von Neurotransmittern wichtig. So ist Kathepsin L in den Biosynthesewegen von Enkephalin involviert (Hook, 2006). Andererseits nehmen Neuropeptidasen eine Schlüsselrolle bei der Produktion von toxischen Proteinfragmenten ein (Hook, 2006). Da für sehr viele neuropathologische Zustände noch keine Behandlungsmöglichkeiten bestehen, sind die Neuroproteasen ein neues Feld für die Medikamentenentwicklung.

In Kathepsin B und L-Doppelknockoutmäusen finden sich bereits kurz nach der Geburt ausgeprägte axonale Schwellungen. Innerhalb der ersten und zweiten murinen Lebenswoche findet die sekundäre Neurogenese, die Vernetzung von Nervenzellen und die Myelinisierung der Axone statt (Aggelopoulos et al., 1989). Um die Rolle von Kathepsinen in der Nervenzellentwicklung zu analysieren, wurden neuronale Stammzellkulturen von Wildtypmäusen und Doppelknockoutmäusen untersucht.

1.14.1 Neuronale Stammzellen

Neuronale Stammzellen sind multipotente Zellen, die sich nahezu unbegrenzt vermehren können und dazu fähig sind, sämtliche Zelltypen des ZNS zu bilden. Es entstehen viele Arten von Vorläuferzellen (Progenitorzellen), die sich wiederum in alle Arten von Neuronen, Oligodendrozyten und Astrozyten differenzieren. Progenitorzellen besitzen jedoch ein eingeschränktes Differenzierungspotential und produzieren terminal differenzierte Zellen (Weiss and Orkin, 1996).

Die Isolierung embryonaler neuronaler Stammzellen kann aus dem Vorderhirn, dem Kleinhirn und dem Rückenmark erfolgen (Temple, 2001). Während der Embryonalentwicklung sinkt der Anteil neuronaler Stammzellen von 50% im Neuralrohr bei acht Tage alten Embryonen (E8) auf 5 bis 20% im Telenzephalon bei zehn Tage alten Mäusembryonen (E10) (Temple, 2001). Im Rückenmark sind am Tag E12 10% der Zellen Stammzellen, am 1. postnatalen Tag (P1) sind nur noch 1% Stammzellen vorhanden (Kalyani et al., 1997; Kalyani et al., 1998). In der ventrikulären Keimzone (VZ) entstehen während der Entwicklung Neuronal- und Glia-Vorläuferzellen. Stammzellen des frühen zerebralen kortikalen Neuroepithels teilen sich symmetrisch, d.h. sie expandieren nur, ohne sich zu differenzieren. Etwa um den Tag E13 teilen sich diese Stammzellen ausgehend von der VZ asymmetrisch, viele differenzierte Zellen werden jetzt gebildet. Es entstehen junge Neuronen. Entlang radialer Gliazellen wandern die Neuronen nach außen und bilden die unterschiedlichen Schichten des Kortex. Diese Phase der Gehirnentwicklung bezeichnet man als neurogene Phase. In der gliogenen Phase ab E18 entstehen in der VZ Gliavorläuferzellen, die in der subventrikulären Zone (SVZ) proliferieren. Oligodendrozyten findet man erst ab P0 (Qian et al., 2000). Ab der Geburt verschwinden die Radialgliazellen und Astrozyten entstehen, die VZ bildet sich zurück. In der SVZ, die weiterhin existiert, besteht im adulten Tier die höchste

Neurogeneserate. Die SVZ ist eine dünne Schicht, die an den lateralen Ventrikel des Telencephalons grenzt. Diese Region stellt den Rest des embryonalen Neuroepitheliums dar und besitzt lebenslange mitotische Aktivität. Es gibt dort zwei vorherrschende Zelltypen: proliferierende und migrierende Neuroblasten sowie Astrozyten. Die Astrozyten formen ein Röhrensytem, die sogenannten Gliatuben, in dem die Neuroblasten eng gruppiert bis zur distalen Spitze des Bulbus olfaktorius wandern. Neuronale Vorläuferzellen migrieren von der SVZ aus entlang eines festgelegten Weges, dem rostromigratorischen Strom (RMS) rostral in den Bulbus olfaktorius. Täglich wandern ca. 30000 neu gebildete Vorläuferzellen an ihren Zielort, an dem sie sich ausdifferenzieren. Dort fungieren sie als spezialisierte Neuronen z.B. als Interneurone. Adulte neuronale Stammzellen können aus der subventrikulären Zone (SVZ) und dem Hippocampus entnommen werden (Gage, 2003; McKay, 1997; Rao and Mayer-Proschel, 1997).

1.14.2 Stammzelltherapie

Die Transplantation von Stammzellen ins Gehirn von Patienten mit neurodegenerativen Erkrankungen wie Parkinson oder Alzheimer wird als mögliche Therapiemethode der Zukunft angesehen. Begründet ist diese Hoffnung darin, dass man die Möglichkeit hat, transplantationsfähige Stammzellen in Kultur zu züchten (Lindvall et al., 2004). Außerdem wurde schon in den frühen sechziger Jahren entdeckt, dass neue Neuronen auch im adulten Gehirn als Reaktion auf Verletzungen entstehen (Altman and Das, 1965; Altman and Das, 1966). Daraus ergibt sich in Zukunft eventuell die Chance, verletzte Bereiche des ZNS gezielt zu regenerieren (Okano, 2002). Die Entwicklung von Stammzell-basierenden Therapien steht allerdings noch am Anfang. Bislang ist nicht klar ob embryonale Stammzellen oder adulte Stammzellen aus dem Gehirn oder eventuell aus anderen Geweben verwendet werden können. Die Kontrolle der Stammzellproliferation und die Differenzierung in spezifische Zelltypen sowie die Integration der Zellen in neuronale Netzwerke ist noch weitgehend unverstanden. Da die Lebensspanne von Kathepsin B und L-Doppelknockoutmäusen limitiert ist, ist ihre Verwendung für stammzelltherapeutische Studien fraglich.

1.14.3 Neurosphärenkultur von Kathepsin $B^{-/-}$ $L^{-/-}$ Mäusen

Die Kultivierung von embryonalen Stammzellen erfolgt in Suspensionskulturflaschen in serumfreiem Medium unter Zusatz von speziellen Wachstumsfaktoren wie EGF und FGF-2. Die entstehenden Neurosphären sind ein heterogenes, kugelförmiges Aggregat aus Stamm- (10-50%) und Progenitorzellen sowie ausdifferenzierten und apoptotischen Zellen. Dissoziiert man Neurosphären, haben die darin enthaltenen Stammzellen nach neuer Aussaat die Möglichkeit, neue Neurosphären zu bilden (Galli et al., 2003). Um Stamm- und Progenitorzellen zu Neuronen, Astrozyten und Oligodendrozyten ausdifferenzieren zu lassen, ist allerdings ein adhäsives Substrat nötig (Reynolds and Weiss, 1996).

Ein immunologischer Marker, der eine neuronale Stammzelle eindeutig als solche identifiziert, existiert nicht, dies ist allein durch das Potential einer Zelle ableitbar, Neurosphären zu bilden. Ein grosses Problem besteht darin, dass aus neuronalen Stammzellen eine heterogene Population von neuronalen Zellen entsteht. Neuronale Progenitorzellen erkennt man durch Marker wie Nestin, ein Intermediärfilament, das in undifferenzierten Zellen exprimiert wird (Lendahl et al., 1990). Inzwischen gelang es, eine homogene Population von *pax-6* positiven radialen Gliazellen herzustellen (Bibel et al., 2004). Diese entwickeln sich sehr schnell zu Neuronen mit biochemischen und funktionalen Eigenschaften einer Linie zerebraler Kortexneuronen.

Der Phänotyp der Kathepsin $B^{-/-}L^{-/-}$ Mäuse liess sich in vitro im Neurosphärenmodell nicht eindrucksvoll reproduzieren. Die Ausdifferenzierung der Nervenzellen erschien zwar zeitlich leicht verzögert, aber eine deutliche Akkumulation LAMP1-positiver Vesikel liess sich beispielsweise nicht beobachten. Ausserdem war die Neurosphärenbildung in Kathepsin $B^{-/-}L^{-/-}$-Kulturen reduziert (Poster, Anlage 1). Folglich stellte sich das Neurosphärenmodell für die beabsichtigte biochemische Charakterisierung als ungeeignet heraus. Zur Aufklärung der in vivo-Funktion von Kathepsin B und L in Nervenzellen der Grosshirnrinde und zur Identifizierung nervenzellspezifischer *in vivo* Substrate von Kathepsin B und L sollten biochemische Methoden wie subzelluläre Fraktionierung, Gelelektrophorese und Massenspektrometrie angewandt werden.

2. Subzelluläre Proteomanalyse von Kathepsin $B^{-/-}$ $L^{-/-}$ Lysosomen

Die subzelluläre Proteomanalyse ist ein vielversprechender moderner Ansatz, um einzelne Zellkompartimente zu analysieren. Für lysosomale Membranproteine (Bagshaw et al., 2005) und die lysosomenähnlichen Neuromelaningranulae (Tribl et al., 2005; Tribl et al., 2006) wurde dieses Verfahren beispielsweise erfolgreich angewandt. Für die biochemische Charakterisierung von Kathepsin $B^{-/-}L^{-/-}$ Lysosomen wurde das lysosomale Kompartiment aus Grosshirnlysaten zunächst mittels subzellulärer Fraktionierung angereichert. Daraufhin wurde die iTRAQ™ (isobaric Tag for Relative and Absolute Quantification) Methode mit der massenspektrometrischen Analyse (LC-MS/MS) kombiniert, da sich die 2D-Gelelektrophorese für die Auftrennung der lysosomalen Fraktion nicht eignete.

2.1. Subzelluläre Fraktionierung

Die Prozessierung von Prokathepsin D zu Kathepsin D war in Gehirnlysaten von Kathepsin B und L-Doppelknockoutmäusen nicht beeinträchtigt. Eine Anreicherung des Intermediats und der reifen Kathepsin D-Form suggerierte im Gegenteil, dass nicht nur das lysosomale, sondern auch das endosomale Kompartiment akkumuliert (Felbor et al., 2002). Folglich wurden zunächst endosomal-lysosomale Fraktionen aus homogenisierten Grosshirnextrakten von 17 Tage alten Wildtyp- und Doppelknockoutmäusen angereichert. Dieses Stadium wurde gewählt, da Doppelknockoutmäuse in der Regel ein Lebensalter von 17 Tagen erreichen, wenn die Wurfgröße am 7. Lebenstag reduziert wird. Ferner ist zu diesem Zeitpunkt die lysosomale Akkumulation in Grosshirnnervenzellen prominent und keine ausgeprägte Apoptose im Grosshirn doppeltdefizienter Mäuse vorhanden. Das Kleinhirn wurde abgetrennt, da in diesem primär die einreihige Purkinjezellschicht betroffen zu sein scheint, die eine geringe lysosomale Akkumulation aufweist und am Tag 17 bereits apoptotisch ist.

Einer intracardialen Perfusion mit 10 ml 10 mM Tris-HCl, 140 mM NaCl, pH 7.4, 4°C folgend wurde das native Grosshirngewebe in einem zehnfachen Volumen Homogenisierungspuffer (0.25 M Saccharose, 10 mM Tris-HCl, pH 7.2, 1 mM EDTA) aufgenommen und mittels eines Potter S Homogenisators (Braun Biotech, Deutschland) aufgeschlossen. Nach einem kurzen Zentrifugationsschritt wurde der postnukleäre Überstand auf einen selbstformenden isoosmotischen Percoll-Gradienten aufpipettiert und in einer Beckman L8-70M Ultrazentrifuge mit

Vertikalrotor (Beckman VT 65.1; 25000 rpm) aufgetrennt. Eine deutliche Bande (Pfeil, Stahl et al., 2006, Abb.1B, Anlage 2) erschien im Bereich der „schweren“ Doppelknockoutlysosomen (DKO), die im Wildtypgradienten (WT) nicht sichtbar ist. Trotz unterschiedlicher Gehirnmasse –Doppelknockoutgehirne wiegen durchschnittlich nur 211 mg im Gegensatz zu 305 mg im Wildtyp (Stahl et al., 2006, Abb. 1A, Anlage 2)– zeigte eine Silberfärbung nach Auftrennung in 10-20% SDS-PAGE Gradientengelen eine extreme Materialzunahme in den „schweren“ Doppelknockoutfraktionen im niedermolekularen Bereich.

Zur genauen Bestimmung der Position von schweren Lysosomen und allen anderen Zellkompartimenten wurden enzymatische Aktivitätstests mit allen gesammelten Fraktionen der Wildtyp- und Doppelknockoutgradienten durchgeführt. Dem ersten optischen Eindruck entsprechend, zeigte sich ein deutlicher Unterschied im Aktivitätsprofil des lysosomalen Leitenzyms Hexosaminidase zwischen Doppelknockout- und Wildtypgrosshirnen (Stahl et al., 2006, Abb. 1C, Anlage 2). Leitenzymtests für alle übrigen Zellorganellen erbrachten, dass durch diesen ersten Percollgradienten die relevante lysosomale Fraktion (Fraktionen 3-5) fast vollständig separiert werden konnte (Stahl et al., 2006, Abb. 1E, Anlage 2). Westernblotanalysen mit Antikörpern gegen LAMP-1 und Kathepsin D bestätigten einen deutlichen Anstieg des lysosomalen Kompartiments in den Doppelknockoutgehirnen (Stahl et al., 2006, Abb.1D, Anlage 2).

Zur Kontrolle wurden die gepoolten Doppelknockoutfraktionen 3-5 durch elektronenmikroskopische Analysen überprüft. Es konnte eine lysosomale Anreicherung mit sehr gutem Strukturerhalt bestätigt werden (Stahl et al., 2006, Abb. 1F, Anlage 2). Das so erhaltene Material wurde in Kollaboration mit Dr. A. Sickmann und Dr. Y. Reinders durch iTRAQ^{TM} und massenspektrometrische Untersuchungen analysiert.

2.2. Massenspektrometrie

Zur vergleichenden Analyse von unterschiedlich stark exprimierten Proteinen wurde eine massenspektrometrische Methode entwickelt, bei welcher Proteine verschiedener Proben unterschiedlich markiert werden können. Durch Anhängen verschiedener Massen (Tag) werden bei ICAT® (**I**sotope-**c**oded **A**ffinity **T**ag) cysteinhaltige Proteine markiert (Gygi et al., 1999). Eine neue verbesserte Methode, die erstmals von Ross et al. (2004) beschrieben wurde, ist iTRAQ^{TM} (**i**sobaric **T**ag

for **R**elative and **A**bsolute **Q**uantification; Applied Biosystems). Im Gegensatz zu ICAT werden nicht nur Cysteine markiert, sondern ein aminoreaktives, stabiles Isotopenreagenz markiert den N-Terminus aller Peptide. Ein weiterer Vorteil ergibt sich daraus, dass vier verschiedene Massen zur Verfügung stehen, mit denen unterschiedliche Proben, z. B. unterschiedliche Stadien, markiert werden können. Differentiell exprimierte Proteine können zeitgleich untersucht werden, da die „Tags" aminspezisch und isobarisch sind (DeSouza et al., 2005; Hardt et al., 2005; Ross et al., 2004; Shadforth et al., 2005). Durch Ausgleichs-, Reporter- und Reaktionseinheiten wird sichergestellt, dass alle Peptide gekennzeichnet sind und in der Massenspektrometrie ein identisches Verhalten zeigen. Nach der Markierung können die Proben gemischt werden. Eine relative bzw. absolute Quantifizierung mittels MS/MS folgt einer Fraktionierung durch Umkehrphasen-Nano-LC. Gemessen wird die Intensität der Reporterionen, d.h. markierte Peptide von gleichen Proteinen. Verschiedene Proben zeigen im Massenspektrometer gleiche Spektren, können aber durch die Reportereinheit quantifiziert werden. Die Analyse der Daten kann direkt online durch QStar erfolgen.

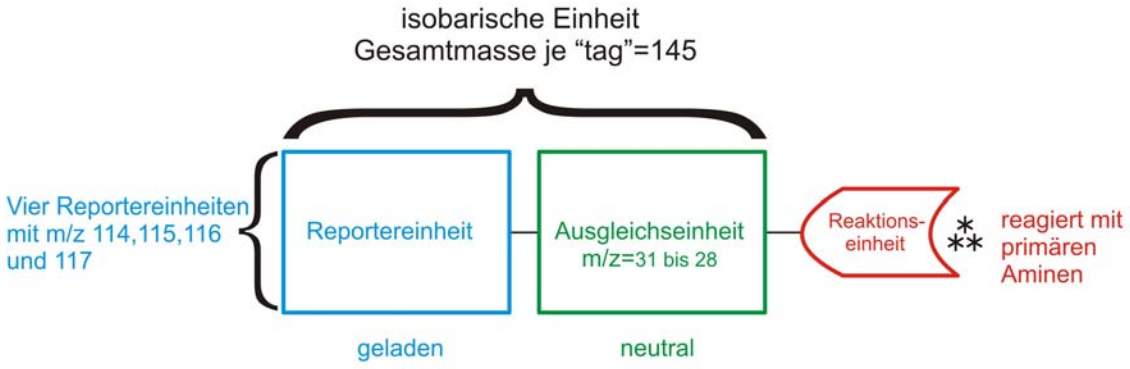

Abb. 1 (modifiziert nach Applied Biosystems):
Der Tag ist aufgebaut aus einer Reporter-, einer Ausgleichs- und einer Reaktionseinheit. Die Reaktionseinheit bindet in der Probe an die N-terminale Gruppe eines Peptids. Die Reportereinheit ist bei unterschiedlichen Proben verschieden schwer. Sie dient damit der Quantifizierung. Daraus ergibt sich die Möglichkeit vier Proben gleichzeitig analysieren zu können. Dies wird durch die Ausgleichseinheit ermöglicht. Die unterschiedlichen Tags haben gleiche Gesamtmassen.

2.2.1. Identifizierung von nervenzellspezifischen Kathepsin-Substraten

Nachdem sich die 2D-Gelelektrophorese für die Analyse der Kathepsin $B^{-/-}L^{-/-}$-Fraktionen als nicht geeignet herausstellte, ergab der Vergleich von Wildtyp- und

Doppelknockout-Lysosomenfraktionen mittels iTRAQ™, dass es in doppeltdefizienten Grosshirnnervenzellen zu einer Akkumulation zahlreicher Zellbestandteile kommt. Neben lysosomalen Proteinen wurden in Doppelknockout-Lysosomen auch Cytoplasma-, Golgi-, Mitochondrien-, Ribosomen- und Membranproteine verstärkt gefunden. Weiterhin konnten auch nukleäre Proteine und Proteine mit unbekannter Funktion detektiert werden. Prominente Peptide, die in Kathepsin $B^{-/-}L^{-/-}$-Fraktionen mindestens vierfach erhöht sind, sind in Tabelle 1 (Stahl et al., 2006, Anlage 2) gelistet.

Beispielsweise wurden die lysosomen-typischen Proteasen Hexosaminidase A und Kathepsin D angereichert gefunden. Die Anreicherung von Hexosaminidase A war bereits im Rahmen der subzellulären Fraktionierung durch enzymatische Aktivitätstests gezeigt worden (Stahl et al., 2006, Abb.1C, Anlage 2). Auch Kathepsin D war durch Westernblotanalysen vermehrt in Doppelknockoutgehirnlysaten (Felbor et al. 2002) detektiert worden. Westernblotanalysen von Gehirnfraktionen bestätigten auch für Kathepsin D die Resultate der iTRAQ™-Analyse (Stahl et al., 2006, Abb.1D, Anlage 2).

Die in Tabelle 1 der Anlage 2 nicht gelistete Detektion von Hämoglobin in den lysosomalen $B^{-/-}L^{-/-}$ Fraktionen hat vermutlich präparative Gründe. Bei Vorversuchen zur subzellulären Fraktionierung stellte sich heraus, dass die Erythrozyten nach der Zentrifugation im Percollgradienten mit den schweren Lysosomen kolokalisieren. Eine intrakardiale Perfusion schien dieses Problem zu lösen. iTRAQ™ ist aber eine hoch sensitive Methode, durch die vermutlich auch minimale Mengen Restblut erkannt werden. Es wurde zwar beschrieben, dass bei Morbus Alzheimer Hämoglobin an einer Oligomerbildung von Aβ und an Amyloidablagerung beteiligt ist (Oyama et al., 2000; Wu et al., 2004), dennoch scheint hier ein Fehler im Versuchsablauf wahrscheinlicher.

Hervorzuheben sind eine Reihe von Proteinen mit prominenter Expression im Gehirn (Stahl et al., 2006, Tabelle 1 und Diskussion in Anlage 2). Dazu gehören Calcyon und der Delta/Notch-like epidermal growth factor-related Rezeptor sowie Neurochondrin, Phospholipase D3, Rab14 und Apolipoprotein E. Vor allem für bislang wenig charakterisierte Moleküle wie Calcyon und Neurochondrin, denen eine Rolle in der Gehirnentwicklung zugeschrieben wird, werden weitere zellbiologische Kolokalisations- und Funktionsanalysen von Bedeutung sein.

2.2.2. Diskussion

Zahlreiche lysosomale Proteine, die durch iTRAQ^{TM} in Doppelknockoutmäusen vermehrt identifiziert wurden (Stahl et al., 2006, Tabelle 1, Anlage 2), sind bei einer Reihe von lysosomalen Speicherkrankheiten mutiert bzw. involviert. Neben Kathepsin D (Ceroid Lipofuszinose CLN10, OMIM #610127), sind dies die Palmitoyl-Proteinthioesterase-1 (Ceroid Lipofuszinose CLN1, OMIM #256730) und die Tripeptidyl-Aminopeptidase (Ceroid Lipofuszinose CLN2, OMIM #204500). Ferner wurden drei Proteine nachgewiesen, die bei G_{M2}-Gangliosidosen mutiert sind: Prosaposin, ein integrales Membranprotein und die Vorstufe von Saposin, dem G_{M1}-Aktivator Protein, ist bei der Cerebrosidlipidose Morbus Gaucher (OMIM #230800) herunterreguliert oder fehlt komplett. Ein Hexosaminidase A-Mangel führt zu psychomotorischer Retardierung und muskulärer Hypertonie und tritt häufig bei jüdischen Patienten auf (Morbus Tay-Sachs, OMIM #272800). Vermehrt nachgewiesen wurde auch Hexosaminidase B, die bei Patienten mit Morbus Sandhoff (OMIM #268800) mutiert vorliegt. Die bei Morbus Farber (OMIM #228000) defiziente saure Ceramidase ASAH1, spaltet bei gesunden Menschen Ceramid in Sphingosin und Fettsäuren. Das Fehlen führt zu intrazellulärer Ceramidspeicherung.
Enzymatische Aktivitäten von vielen Proteasen sind bei humanen NCL-Formen sowie im Gehirngewebe von Kathepsin $D^{-/-}$ Schafen (Tyynelä et al., 2000) und in Kathepsin $B^{-/-}L^{-/-}$-Mäusen erhöht. Es ist aber gerade ein mutationsbedingter Verlust dieser Enzyme, der durch Akkumulation von Speichersubstanzen zu spezifischen hereditären Krankheitsbildern führt. Folglich kann es sich um eine kompensatorische Erhöhung oder eine fehlerhafte Degradation oder Prozessierung der Enzyme in Kathepsin $B^{-/-}L^{-/-}$-Mäusen handeln. Für PPT und TPP1 war bereits in der Initialbeschreibung der Kathepsin $B^{-/-}L^{-/-}$-Mäuse eine erhöhte und nicht eine verminderte enzymatische Aktivität beschrieben worden. Daraus wurde geschlossen, dass der Kathepsin $B^{-/-}L^{-/-}$-Phänotyp sich von diesen beiden klassischen NCL-Formen eindeutig unterscheidet (Felbor et al., 2002). Diese Ergebnisse wurden in der vorliegenden Arbeit bestätigt und spezifiziert. Vergleichbar zur Kathepsin D-Defizienz (Ceroid Lipofuszinose CLN10, OMIM #610127) wäre ein humanes Pendant der Kathepsin $B^{-/-}L^{-/-}$-Mäuse theoretisch denkbar. Da dies aber vier rezessive Mutationen in zwei Genen voraussetzen würde, die zudem lethal wären, ist es sehr unwahrscheinlich, dass ein humanes $B^{-/-}L^{-/-}$-Krankheitsbild identifiziert werden wird.

Dennoch können die Kathepsin $B^{-/-}L^{-/-}$-Mäuse als Modellsystem für NCL betrachtet werden (Koike et al., 2005).

Dem Kathepsin $B^{-/-}L^{-/-}$-Phänotyp vergleichbare Ergebnisse wurden auch durch die Inaktivierung des Ionenkanalproteins ClC-7 in Mäusen (*Clcn7*$^{-/-}$) erzielt. Diese resultierte nicht nur in einem osteopetrotischen Phänotyp in der Maus, sondern führte auch zur Identifizierung humaner Mutationen bei der infantilen malignen Osteopetrose führte (Kornak et al., 2001). *Clcn7*$^{-/-}$ Mäuse zeigten darüber hinaus eine Retina- und Neurodegeneration, die vorwiegend die hippocampale CA3-Region, aber auch den zerebralen Kortex und die zerebelläre Purkinjezellschicht betrifft (Kasper et al., 2005). Ein Rettungsversuch durch Überexpression von ClC-7 in Osteoklasten von *Clcn7*$^{-/-}$ Mäusen führte möglicherweise aufgrund der schweren Neurodegeneration zu einer um nur etwa drei Wochen erhöhten Lebenserwartung. Obwohl die Funktion des lysosomalen Ionenkanalproteins in Nervenzellen unklar bleibt, handelt es sich bei *Clcn7*$^{-/-}$ Mäusen um eine NCL-ähnliche lysosomale Speicherkrankheit mit Akkumulation von autofluoreszentem Lipopigment, granulären und lamellären Ultrastrukturen, einer intralysosomalen Anreicherung der c-Untereinheit der mitochondrialen ATP-Synthase und von Saposin D, einer Akkumulation von Kathepsin D und erhöhten enzymatischen Aktivitäten der Hexosaminidasen und von TPP1. Da allerdings die neuronalen Ceroidlipofuszinosen nicht mit einer Osteopetrose assoziiert sind, erscheint es unwahrscheinlich, dass *CLCN7* ein Kandidatengen für NCLs ist.

In $B^{-/-}L^{-/-}$-Lysosomen akkumulieren einige ATP-abhängige Membrankanalproteine, die im Nervensystem exprimiert sind (McGrail et al., 1991) und bei neurologischen Erkrankungen mutiert sind: Mutationen in der α-3 Untereinheit der Na^+/K^+-ATPase führen beispielsweise zu einer autosomal-dominant vererbten Dystonieform mit Parkinsonismus (OMIM #128235) (de Carvalho Aguiar et al., 2004). Mutationen in der α-2 Untereinheit der Natriumkaliumpumpe wurden mit einer familiären Form der Migräne assoziiert (FHM2, OMIM #602481) (Estevez and Gardner, 2004). Diese aus vielen Untereinheiten bestehenden Proteinkomplexe transportieren unter ATP-Verbrauch Protonen über biologische Membranen und erzeugen dadurch beispielsweise in Lysosomen ein saures Milieu, so dass die in den Lysosomen enthaltenen Enzyme ausreichend aktiv sind. Membranproteine wurden allerdings nicht in Tabelle 1 der Anlage 2 gelistet, da sie im Vergleich zu Wildtyplysosomen nicht mindestens vierfach erhöht waren.

Bei zahlreichen neuronalen Speicherkrankheiten liegt der zugrundeliegende Defekt in ubiquitär exprimierten Molekülen. Der nervenzellspezifische Phänotyp konnte bei der Tay Sachs-Speicherkrankheit durch ein nervenzellspezifisches Substrat der Hexosaminidase, das GM_2-Gangliosid, erklärt werden. In der vorliegenden Studie wurde gezeigt, dass dies für die Kathepsin B- und L-Defizienz mit grosser Wahrscheinlichkeit nicht zutrifft, obwohl die lysosomalen Akkumulationen nur selektiv in bestimmten Nervenzellpopulationen zu finden sind und nicht in anderen Organen (Felbor und Goebel, unpublizierte Daten). Die Nervenzellspezifität des $B^{-/-}L^{-/-}$-Phänotyps könnte dadurch begründet werden, dass den betroffenen Zellen eine kompensierende Protease fehlt. Allerdings ist der Nachweis dieser Hypothese experimentell ausserordentlich schwierig. Denkbar ist auch, dass eine defekte Autophagozytose in Abwesenheit von Kathepsin B und L vulnerable Nervenzellen besonders betreffen könnte, die sich nicht mehr teilen, eine hohe Lebensspanne bei hohem Umsatz von Membranlipiden und Proteinen haben und mit ihren langen axonalen Fortsätzen eine einzigartige Anatomie aufweisen.

Zusammenfassend gehört die Kathepsin B- und L-Defizienz ebenso wie die Defizienz des Chloridkanalproteins ClC-7 und die Gruppe der menschlichen neuronalen Ceroidlipofuszinosen zu den Speicherkrankheiten mit unspezifischer Anreicherung lysosomaler Proteine und Proteasen bzw. deren enzymatischer Aktivitäten. Diese unspezifische Anreicherung wurde als Ausdruck eines Kompensations-mechanismusses bei suboptimaler lysosomaler Funktion interpretiert (Ezaki and Kominami, 2004). Nachfolgende Studien werden u.a. klären müssen, ob es sich bei der Anreicherung nervenzellspezifischer Substrate wie Calcyon, dem Delta/Notch-like epidermal growth factor-related Rezeptor und Neurochondrin in Kathepsin $B^{-/-}L^{-/-}$-Doppelknockoutmäusen um primäre und/oder sekundäre/reaktive Phänomene handelt. Für Apolipoprotein E wurde beschrieben, dass es stressinduziert in Nervenzellen hochreguliert wird und protektive Funktionen übernimmt (Übersicht in Mahley et al., 2006). Die entwicklungbiologische und/oder protektive Bedeutung von erst kürzlich beschriebenen Molekülen wie Calcyon (Lezcano et al., 2000; Xiao et al., 2006) und Neurochondrin (Istvanffy et al., 2004; Shinozaki et al., 1999) bedarf hingegen einer soliden experimentellen Aufarbeitung. Folglich bleibt derzeit offen, ob eines der gespeicherten Proteine eine pathogenetische Rolle bei der Entstehung des Kathepsin $B^{-/-}L^{-/-}$-Phänotyps spielt.

3. Teilprojekt II: Lokalisierung von Endostatinrezeptoren und Charakterisierung der Endostatinbindung

Endostatin ist ein endogener Inhibitor der Angiogenese und des Tumorwachstums (O'Reilly et al., 1997). Das Molekül ist 20 kDa schwer und wird durch sekretiertes Kathepsin L von Kollagen XVIII abgespalten (Felbor et al., 2000). Die Wirkweise des Angiogeneseinhibitors Endostatin ist nach wie vor ungenügend charakterisiert. Eine Reihe von niedrigaffinen Endostatinrezeptoren wurde inzwischen beschrieben. Dazu gehören Heparansulfatproteoglykane (Glypikane), Integrin $\alpha_5\beta_1$ und das Basalmembranprotein Laminin. Im Vordergrund der meisten Studien stand die Heparinaffinität von Endostatin und die Charakterisierung der Heparinbindungsstelle (Übersicht in Sasaki et al., 2002).

Um einen hochaffinen Endostatinrezeptor lokalisieren und identifizieren zu können, wurde Endostatins prominente Heparinbindungsstelle mittels Alanin *in vitro* Mutagenese eliminiert. Diese Endostatinmutante zeigte zwar keine antiangiogene Aktivität in einem murinen embryonalen Knochenangiogenesemodell, band aber an murine Gewebe *in situ*, an aussprossende Endothelzellen in Organkulturen und an Endothelzelllinien. In Übereinstimmung mit dem menschlichen Phänotyp, wurde eine ausgeprägte Bindung an die Tunica vasculosa lentis von Mäuseembryonen beobachtet (Gaetzner et al., 2005, Anlage 4; Rychkova et al., 2005, Anlage 3). Im Gegensatz zur Heparinmutante führte eine weitere Mutante, in der zwei an der Moleküloberfläche ungewöhnlich exponierte, hydrophobe Phenylalaninreste durch Alanin ersetzt worden waren, zu einem kompletten Bindungsverlust an Gewebe und Endothelzellen bei unveränderter Heparinaffinität. Endostatins Heparinaffinität ist folglich für die Bindung *in situ* nicht ausschlaggebend. Durch systematische *in vitro* Mutagenese und Bindungsstudien konnte gezeigt werden, dass Endostatin an einen von Heparansulfaten unabhängigen, noch zu identifizierenden hochaffinen Endostatinrezeptor binden muss (Stahl et al., 2005).

Die Identifizierung dieses hochaffinen Endostatinrezeptors auf Endothelzellen sollte durch Expressionsklonierung unter Verwendung der AP-Tag^{TM}-Technologie erfolgen. Die Konstruktion und Expression von AP-Fusionsproteinen sowie die Identifizierung einer Rezeptor-positiven Zelllinie als Quelle für die Generierung einer cDNA-Expressionsbibliothek verliefen problemlos. Als problematisch stellte sich jedoch die Identifizierung einer eindeutig Rezeptor-negativen und zugleich leicht transfizierbaren Zelllinie heraus, die mit gepoolter DNA der zu erstellende Expressionsbibliothek aus

CPAE-Zellen transfiziert werden sollte. Allein die schwer zu transfizierende neuronale Modellzelllinie PC12 erwies sich als eindeutig Rezeptor-negativ (Neumann und Felbor, unpubliziert). Im Rahmen einer vergleichenden Analyse der homologen Endostatindomänen von Kollagen XV und XVIII in Angiogenese und Neurogenese stellte sich heraus, dass weder Endostatin noch die homologe Endostatindomäne von Kollagen XV mit neuronalen Geweben reagierten (Rychkova et al., 2005, Anlage 3). AP-VEGF hingegen zeigte eine stark positive Färbung der neuronalen Modellzelllinie PC12 und muriner Nervengewebe (Berger et al., 2006, Anlage 5). Da der dritte Meilenstein der Expressionsklonierung, die Identifizierung einer Rezeptor-negativen Zelllinie, nicht zu dem erhofften Ergebnis führte, liegt der Schluss nahe, den Endostatinrezeptor nicht über den genetischen Ansatz, sondern mit biochemischen Methoden zu identifizieren.

Homozygote und compound heterozygote trunkierende Mutationen im Kollagen XVIII Gen (*COL18A1*) verursachen das autosomal rezessiv vererbte Knobloch Syndrom (MIM# 267750), das durch eine angeborene Myopie, vitreoretinale Degeneration und okzipitale Enzephalozele charakterisiert wird. Eine verzögerte Regression der Vasa hyaloidea, die während der Embryonalzeit die Linse und den Glaskörper versorgen, scheint pathogenetisch relevant zu sein (Fukai et al., 2002). Bemerkenswert ist, dass sechs von neun bekannten Mutationen in den Exonen 35, 36, 40 und 41 liegen und durch vorzeitige Stopkodons entweder die gesamte oder einen Teil der Endostatindomäne deletieren, die durch die terminalen drei Exone (41 bis 43) von *COL18A1* kodiert wird.

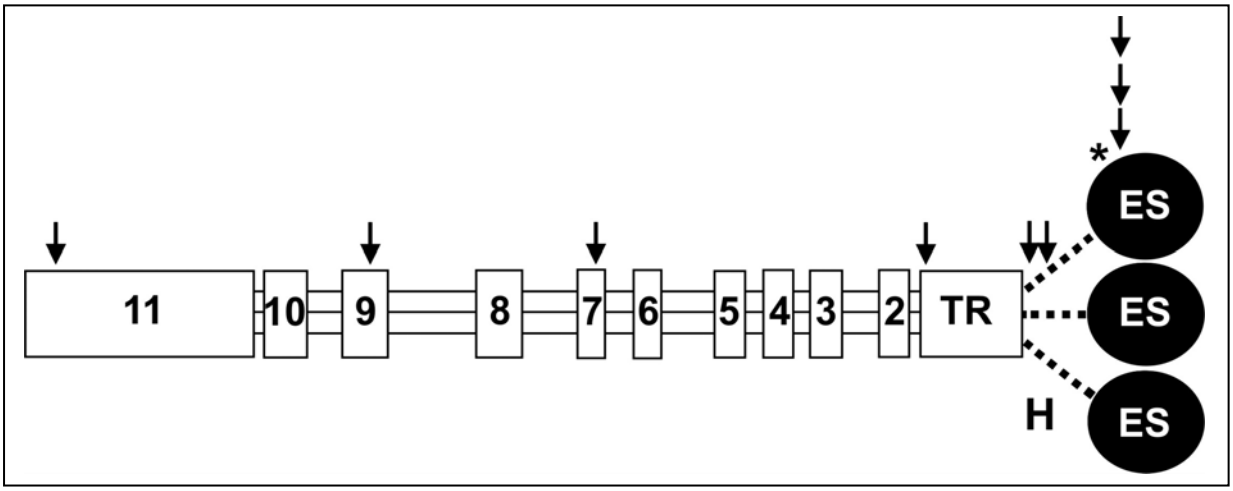

Abb.2: Schematische Darstellung von humanen Mutationen im homotrimeren Kollagen XVIII. ES= Endostatin, TR=Trimerisierungsdomäne, H= Hinge-Region, * = Missense-Mutation

Die einzige bisher bekannte humane Missense Mutation in der Endostatindomäne führt nicht zu einer Veränderung im Bindungsverhalten an Gewebe, Endothelzellen, Heparin und Laminin. Diese Endostatinmutante wird jedoch schwächer exprimiert (Stahl et al., 2005, Anlage 6). Diese Beobachtung lässt sich durch eine reduzierte Faltungskinetik erklären, die durch die Lage von A48 im räumlich begrenzten, hydrophoben Innern des Moleküls verursacht sein könnte. Endostatin spielt folglich nicht nur als freigesetztes Molekül im Rahmen pathologischer Neovaskularisationen, sondern auch als C-terminale Kollagen XVIII-Domäne während der normalen Entwicklung eine herausragende Rolle.

4. Teilprojekt III: Etablierung der molekulargenetischen Kavernomdiagnostik

Zerebrale kavernöse Malformationen (CCM, OMIM #116860, 603284, 603285), kurz Kavernome, sind häufige Blutgefässfehlbildungen im zentralen Nervensystem, welche vor allem in der 2.-4. Lebensdekade symptomatisch werden. Die dieser Krankheitsgruppe zugrunde liegenden pathogenetischen Mechanismen sind noch größtenteils unbekannt. Die Blutgefässfehlbildungen treten sowohl sporadisch als auch familiär auf. Hereditäre Formen werden autosomal dominant vererbt. Die Penetranz ist inkomplett und die Expressivität variabel. Die Symptomatik umfasst Kopfschmerzen, Krampfanfälle und Schlaganfälle mit nachfolgenden neurologischen Ausfällen. Bisher wurden drei ursächliche Gene identifiziert: *CCM1/KRIT1*, *CCM2/ MGC4607/Malcavernin/OSM* und *CCM3/PDCD10* (Übersicht in Felbor et al., 2006).

Da die molekulargenetische Kavernomdiagnostik in Deutschland bis zum Jahr 2005 nicht angeboten wurde, wurde diese für Patienten mit positiver Familienanamnese und/oder multiplen Kavernomen etabliert. Sie wird als Stufendiagnostik durchgeführt. In den ersten vier Stufen werden sukzessive die kodierenden Abschnitte inklusive der Exon-Intron Übergänge von allen drei *CCM*-Genen mittels Sequenzanalyse untersucht. Bei negativem Ergebnis nach Direktsequenzierung aus genomischer DNA erfolgt in der 5. Stufe eine quantitative PCR mit Hilfe der MLPA-Methode zur Beurteilung von grösseren Deletionen und Duplikationen. Die Multiplex Ligation Dependent Probe Amplification (MLPA) für die drei *CCM*-Gene wurde von MRC Holland auf Anfrage erst im Jahr 2005 entwickelt. Inzwischen wurden nicht nur zahlreiche neue *CCM*-Mutationen identifiziert, die beispielsweise das Leseraster verschieben (Sürücü et al., 2006, Anlage 7 und unpublizierte Daten), sondern auch grosse genomische Deletionen wie z.B. die in der Literatur zuvor noch nicht beschriebene Deletion des gesamten *CCM1*-Gens (Gaetzner et al., 2006, eingereicht, Anlage 8). Aus wissenschaftlicher Sicht dient die genetische Mutationsanalyse mittelfristig einerseits einer molekularen Reklassifizierung hereditärer vaskulärer Malformationen (Bilguvar et al., 2006, Anlage 10; Stahl and Felbor, 2006, Anlage 9). Andererseits werden die Identifizierung spezifischer humaner Mutationen und humane Zelllinien mit diesen Mutationen zum Verständnis der Genfunktionen beitragen. Gegenwärtiger Forschungsschwerpunkt ist die Funktionsanalyse von *CCM3*. Im *CCM3*-Gen wurden erst 2005 humane Mutationen bei CCM-Patienten identifiziert. Es ist derzeit nicht bekannt, welche Funktionen das CCM3-Protein hat.

Literaturverzeichnis

Aerts, J. M., Hollak, C. E., Boot, R. G., Groener, J. E., and Maas, M. (2006). Substrate reduction therapy of glycosphingolipid storage disorders. J Inherit Metab Dis *29*, 449-456.

Aggelopoulos, N., Parnavelas, J. G., and Edmunds, S. (1989). Synaptogenesis in the dorsal lateral geniculate nucleus of the rat. Anat Embryol (Berl) *180*, 243-257.

Alakurtti, K., Weber, E., Rinne, R., Theil, G., de Haan, G. J., Lindhout, D., Salmikangas, P., Saukko, P., Lahtinen, U., and Lehesjoki, A. E. (2005). Loss of lysosomal association of cystatin B proteins representing progressive myoclonus epilepsy, EPM1, mutations. Eur J Hum Genet *13*, 208-215.

Altman, J., and Das, G. D. (1965). Autoradiographic and histological evidence of postnatal hippocampal neurogenesis in rats. J Comp Neurol *124*, 319-335.

Altman, J., and Das, G. D. (1966). Autoradiographic and histological studies of postnatal neurogenesis. I. A longitudinal investigation of the kinetics, migration and transformation of cells incorporating tritiated thymidine in neonate rats, with special reference to postnatal neurogenesis in some brain regions. J Comp Neurol *126*, 337-389.

Aoyagi, T., and Umezawa, H. (1975). In Proteases in Biological Control, D. B. Rifkin, and E. Shaw, eds. (Cold Spring Habour Laboratory Press), pp. 429-454.

Authier, F., Kouach, M., and Briand, G. (2005). Endosomal proteolysis of insulin-like growth factor-I at its C-terminal D-domain by cathepsin B. FEBS Lett *579*, 4309-4316.

Authier, F., Metioui, M., Bell, A. W., and Mort, J. S. (1999). Negative regulation of epidermal growth factor signaling by selective proteolytic mechanisms in the endosome mediated by cathepsin B. J Biol Chem *274*, 33723-33731.

Authier, F., Mort, J. S., Bell, A. W., Posner, B. I., and Bergeron, J. J. (1995). Proteolysis of glucagon within hepatic endosomes by membrane-associated cathepsins B and D. J Biol Chem *270*, 15798-15807.

Bagshaw, R. D., Mahuran, D. J., and Callahan, J. W. (2005). A proteomic analysis of lysosomal integral membrane proteins reveals the diverse composition of the organelle. Mol Cell Proteomics *4*, 133-143.

Barrett, A. J., Rawlings, N. D., and Woessner, J. F. (1998). Handbook of Proteolytic Enzymes, Academic Press.).

Barros, N. M., Tersariol, I. L., Oliva, M. L., Araujo, M. S., Sampaio, C. A., Juliano, L., and da Motta, G. (2004). High molecular weight kininogen as substrate for cathepsin B. Biol Chem *385*, 551-555.

Bednarski, E., and Lynch, G. (1996). Cytosolic proteolysis of tau by cathepsin D in hippocampus following suppression of cathepsins B and L. J Neurochem *67*, 1846-1855.

Bednarski, E., Ribak, C. E., and Lynch, G. (1997). Suppression of cathepsins B and L causes a proliferation of lysosomes and the formation of meganeurites in hippocampus. J Neurosci *17*, 4006-4021.

Benavides, F., Venables, A., Poetschke Klug, H., Glasscock, E., Rudensky, A., Gomez, M., Martin Palenzuela, N., Guenet, J. L., Richie, E. R., and Conti, C. J. (2001). The CD4 T cell-deficient mouse mutation nackt (nkt) involves a deletion in the cathepsin L (Ctsl) gene. Immunogenetics *53*, 233-242.

Berger, I., Stahl, S., Rychkova, N., and Felbor, U. (2006). VEGF receptors on PC12 cells mediate transient activation of ERK1/2 and Akt: Comparison of nerve growth factor and vascular endothelial growth factor. J Negat Results Biomed *5*, 8.

Bevec, T., Stoka, V., Pungercic, G., Dolenc, I., and Turk, V. (1996). Major histocompatibility complex class II-associated p41 invariant chain fragment is a strong inhibitor of lysosomal cathepsin L. J Exp Med *183*, 1331-1338.

Bibel, M., Richter, J., Schrenk, K., Tucker, K. L., Staiger, V., Korte, M., Goetz, M., and Barde, Y. A. (2004). Differentiation of mouse embryonic stem cells into a defined neuronal lineage. Nat Neurosci *7*, 1003-1009.

Bilguvar, K., Ozturk, A. K., Gunel, M., and Guclu, B. (2006). Response to Letter by Stahl and Felbor. Stroke.

Bocock, J. P., Edgell, C. J., Marr, H. S., and Erickson, A. H. (2003). Human proteoglycan testican-1 inhibits the lysosomal cysteine protease cathepsin L. Eur J Biochem *270*, 4008-4015.

Bohne, S., Sletten, K., Menard, R., Buhling, F., Vockler, S., Wrenger, E., Roessner, A., and Rocken, C. (2004). Cleavage of AL amyloid proteins and AL amyloid deposits by cathepsins B, K, and L. J Pathol *203*, 528-537.

Brix, K., Linke, M., Tepel, C., and Herzog, V. (2001). Cysteine proteinases mediate extracellular prohormone processing in the thyroid. Biol Chem *382*, 717-725.

Bromme, D., and McGrath, M. E. (1996). High level expression and crystallization of recombinant human cathepsin S. Protein Sci *5*, 789-791.

Bromme, D., Okamoto, K., Wang, B. B., and Biroc, S. (1996). Human cathepsin O2, a matrix protein-degrading cysteine protease expressed in osteoclasts. Functional expression of human cathepsin O2 in Spodoptera frugiperda and characterization of the enzyme. J Biol Chem *271*, 2126-2132.

Buttle, D. J., Abrahamson, M., Burnett, D., Mort, J. S., Barrett, A. J., Dando, P. M., and Hill, S. L. (1991). Human sputum cathepsin B degrades proteoglycan, is inhibited by alpha 2-macroglobulin and is modulated by neutrophil elastase cleavage of cathepsin B precursor and cystatin C. Biochem J *276 (Pt 2)*, 325-331.

Bylaite, M., Moussali, H., Marciukaitiene, I., Ruzicka, T., and Walz, M. (2006). Expression of cathepsin L and its inhibitor hurpin in inflammatory and neoplastic skin diseases. Exp Dermatol *15*, 110-118.

Chandran, K., Sullivan, N. J., Felbor, U., Whelan, S. P., and Cunningham, J. M. (2005). Endosomal proteolysis of the Ebola virus glycoprotein is necessary for infection. Science *308*, 1643-1645.

Chapman, H. A., Riese, R. J., and Shi, G. P. (1997). Emerging roles for cysteine proteases in human biology. Annu Rev Physiol *59*, 63-88.

Dahl, S. W., Halkier, T., Lauritzen, C., Dolenc, I., Pedersen, J., Turk, V., and Turk, B. (2001). Human recombinant pro-dipeptidyl peptidase I (cathepsin C) can be activated by cathepsins L and S but not by autocatalytic processing. Biochemistry *40*, 1671-1678.

de Carvalho Aguiar, P., Sweadner, K. J., Penniston, J. T., Zaremba, J., Liu, L., Caton, M., Linazasoro, G., Borg, M., Tijssen, M. A., Bressman, S. B*., et al.* (2004). Mutations in the Na+/K+ -ATPase alpha3 gene ATP1A3 are associated with rapid-onset dystonia parkinsonism. Neuron *43*, 169-175.

Desmazes, C., Galineau, L., Gauthier, F., Bromme, D., and Lalmanach, G. (2003). Kininogen-derived peptides for investigating the putative vasoactive properties of human cathepsins K and L. Eur J Biochem *270*, 171-178.

Desmazes, C., Gauthier, F., and Lalmanach, G. (2001). Cathepsin L, but not cathepsin B, is a potential kininogenase. Biol Chem *382*, 811-815.

DeSouza, L., Diehl, G., Rodrigues, M. J., Guo, J., Romaschin, A. D., Colgan, T. J., and Siu, K. W. (2005). Search for cancer markers from endometrial tissues using differentially labeled tags iTRAQ and cICAT with multidimensional liquid chromatography and tandem mass spectrometry. J Proteome Res *4*, 377-386.

Deussing, J., Roth, W., Saftig, P., Peters, C., Ploegh, H. L., and Villadangos, J. A. (1998). Cathepsins B and D are dispensable for major histocompatibility complex class II-mediated antigen presentation. Proc Natl Acad Sci U S A *95*, 4516-4521.

Dolenc, I., Turk, B., Pungercic, G., Ritonja, A., and Turk, V. (1995). Oligomeric structure and substrate induced inhibition of human cathepsin C. J Biol Chem *270*, 21626-21631.
Estevez, M., and Gardner, K. L. (2004). Update on the genetics of migraine. Hum Genet *114*, 225-235.
Ezaki, J., and Kominami, E. (2004). The intracellular location and function of proteins of neuronal ceroid lipofuscinoses. Brain Pathol *14*, 77-85.
Fehrenbacher, N., and Jäättelä, M. (2005). Lysosomes as targets for cancer therapy. Cancer Res *65*, 2993-2995.
Felbor, U., Dreier, L., Bryant, R. A., Ploegh, H. L., Olsen, B. R., and Mothes, W. (2000). Secreted cathepsin L generates endostatin from collagen XVIII. EMBO J *19*, 1187-1194.
Felbor, U., Kessler, B., Mothes, W., Goebel, H. H., Ploegh, H. L., Bronson, R. T., and Olsen, B. R. (2002). Neuronal loss and brain atrophy in mice lacking cathepsins B and L. Proc Natl Acad Sci U S A *99*, 7883-7888.
Felbor, U., Sure, U., Grimm, T., and Bertalanffy, H. (2006). Genetics of cerebral cavernous angioma. Zentralbl Neurochir *67*, 110-116.
Figarella, C., Miszczuk-Jamska, B., and Barrett, A. J. (1988). Possible lysosomal activation of pancreatic zymogens. Activation of both human trypsinogens by cathepsin B and spontaneous acid. Activation of human trypsinogen 1. Biol Chem Hoppe Seyler *369 Suppl*, 293-298.
Foghsgaard, L., Wissing, D., Mauch, D., Lademann, U., Bastholm, L., Boes, M., Elling, F., Leist, M., and Jäättelä, M. (2001). Cathepsin B acts as a dominant execution protease in tumor cell apoptosis induced by tumor necrosis factor. J Cell Biol *153*, 999-1010.
Friedrichs, B., C. Tepel, T. Reinheckel, J. Deussing, K. von Figura, V. Herzog, C. Peters, P. Saftig, and K. Brix. 2003. Thyroid functions of mouse cathepsins B, K, and L. J Clin Invest 111:1733-45.
Fukai, N., Eklund, L., Marneros, A. G., Oh, S. P., Keene, D. R., Tamarkin, L., Niemela, M., Ilves, M., Li, E., Pihlajaniemi, T., and Olsen, B. R. (2002). Lack of collagen XVIII/endostatin results in eye abnormalities. EMBO J *21*, 1535-1544.
Gaetzner, S., Deckers, M. M., Stahl, S., Lowik, C., Olsen, B. R., and Felbor, U. (2005). Endostatin's heparan sulfate-binding site is essential for inhibition of angiogenesis and enhances in situ binding to capillary-like structures in bone explants. Matrix Biol *23*, 557-561.
Gaetzner, S., Stahl, S., Sürücü, O., Schaafhausen, A., Halliger-Keller, B., Bertalnaffy, H., Sure, U., and Felbor, U. (2006). CCM1 gene deletion identified by MLPA in cerebral cavernous malformation. Neurosurg Rev *submitted*.
Gage, F. H. (2003). Brain, repair yourself. Sci Am *289*, 46-53.
Galli, R., Gritti, A., Bonfanti, L., and Vescovi, A. L. (2003). Neural stem cells: an overview. Circ Res *92*, 598-608.
Gelb, B. D., Shi, G. P., Chapman, H. A., and Desnick, R. J. (1996). Pycnodysostosis, a lysosomal disease caused by cathepsin K deficiency. Science *273*, 1236-1238.
Goulet, B., Baruch, A., Moon, N. S., Poirier, M., Sansregret, L. L., Erickson, A., Bogyo, M., and Nepveu, A. (2004). A cathepsin L isoform that is devoid of a signal peptide localizes to the nucleus in S phase and processes the CDP/Cux transcription factor. Mol Cell *14*, 207-219.
Gowen, M., Lazner, F., Dodds, R., Kapadia, R., Feild, J., Tavaria, M., Bertoncello, I., Drake, F., Zavarselk, S., Tellis, I.*, et al.* (1999). Cathepsin K knockout mice develop osteopetrosis due to a deficit in matrix degradation but not demineralization. J Bone Miner Res *14*, 1654-1663.
Green, F. L. (1954). The genetics of a new hair deficiency, furless. J Hered *45*,, 115–118.
Gu, F., Crump, C. M., and Thomas, G. (2001). Trans-Golgi network sorting. Cell Mol Life Sci *58*, 1067-1084.
Guicciardi, M. E., Bronk, S. F., Werneburg, N. W., Yin, X. M., and Gores, G. J. (2005). Bid is upstream of lysosome-mediated caspase 2 activation in tumor necrosis factor alpha-induced hepatocyte apoptosis. Gastroenterology *129*, 269-284.
Guicciardi, M. E., Deussing, J., Miyoshi, H., Bronk, S. F., Svingen, P. A., Peters, C., Kaufmann, S. H., and Gores, G. J. (2000). Cathepsin B contributes to TNF-alpha-mediated hepatocyte apoptosis by promoting mitochondrial release of cytochrome c. J Clin Invest *106*, 1127-1137.
Gygi, S. P., Rist, B., Gerber, S. A., Turecek, F., Gelb, M. H., and Aebersold, R. (1999). Quantitative analysis of complex protein mixtures using isotope-coded affinity tags. Nat Biotechnol *17*, 994-999.
Halangk, W., Lerch, M. M., Brandt-Nedelev, B., Roth, W., Ruthenbuerger, M., Reinheckel, T., Domschke, W., Lippert, H., Peters, C., and Deussing, J. (2000). Role of cathepsin B in intracellular trypsinogen activation and the onset of acute pancreatitis. J Clin Invest *106*, 773-781.
Hardt, M., Witkowska, H. E., Webb, S., Thomas, L. R., Dixon, S. E., Hall, S. C., and Fisher, S. J. (2005). Assessing the effects of diurnal variation on the composition of human parotid saliva: quantitative analysis of native peptides using iTRAQ reagents. Anal Chem *77*, 4947-4954.
Hart, P. S., Zhang, Y., Firatli, E., Uygur, C., Lotfazar, M., Michalec, M. D., Marks, J. J., Lu, X., Coates, B. J., Seow, W. K., *et al.* (2000a). Identification of cathepsin C mutations in ethnically diverse papillon-Lefevre syndrome patients. J Med Genet *37*, 927-932.
Hart, T. C., Hart, P. S., Michalec, M. D., Zhang, Y., Firatli, E., Van Dyke, T. E., Stabholz, A., Zlotogorski, A., Shapira, L., and Soskolne, W. A. (2000b). Haim-Munk syndrome and Papillon-Lefevre syndrome are allelic mutations in cathepsin C. J Med Genet *37*, 88-94.
Honey, K., Benlagha, K., Beers, C., Forbush, K., Teyton, L., Kleijmeer, M. J., Rudensky, A. Y., and Bendelac, A. (2002). Thymocyte expression of cathepsin L is essential for NKT cell development. Nat Immunol *3*, 1069-1074.
Hook, V., Toneff, T., Bogyo, M., Greenbaum, D., Medzihradszky, K. F., Neveu, J., Lane, W., Hook, G., and Reisine, T. (2005). Inhibition of cathepsin B reduces beta-amyloid production in regulated secretory vesicles of neuronal chromaffin cells: evidence for cathepsin B as a candidate beta-secretase of Alzheimer's disease. Biol Chem *386*, 931-940.
Hook, V., Yasothornsrikul, S., Greenbaum, D., Medzihradszky, K. F., Troutner, K., Toneff, T., Bundey, R., Logrinova, A., Reinheckel, T., Peters, C., and Bogyo, M. (2004). Cathepsin L and Arg/Lys aminopeptidase: a distinct prohormone processing pathway for the biosynthesis of peptide neurotransmitters and hormones. Biol Chem *385*, 473-480.
Hook, V. Y. (2006). Protease Pathways in Peptide Neurotransmission and Neurodegenerative Diseases. Cell Mol Neurobiol.
Houseweart, M. K., Vilaythong, A., Yin, X. M., Turk, B., Noebels, J. L., and Myers, R. M. (2003). Apoptosis caused by cathepsins does not require Bid signaling in an in vivo model of progressive myoclonus epilepsy (EPM1). Cell Death Differ *10*, 1329-1335.
Irving, J. A., Pike, R. N., Dai, W., Bromme, D., Worrall, D. M., Silverman, G. A., Coetzer, T. H., Dennison, C., Bottomley, S. P., and Whisstock, J. C. (2002). Evidence that serpin architecture intrinsically supports papain-like cysteine protease inhibition: engineering alpha(1)-antitrypsin to inhibit cathepsin proteases. Biochemistry *41*, 4998-5004.
Ishidoh, K., and Kominami, E. (1995). Procathepsin L degrades extracellular matrix proteins in the presence of glycosaminoglycans in vitro. Biochem Biophys Res Commun *217*, 624-631.
Istvanffy, R., Vogt Weisenhorn, D. M., Floss, T., and Wurst, W. (2004). Expression of neurochondrin in the developing and adult mouse brain. Dev Genes Evol *214*, 206-209.

Johnson, D. A., Barrett, A. J., and Mason, R. W. (1986). Cathepsin L inactivates alpha 1-proteinase inhibitor by cleavage in the reactive site region. J Biol Chem *261*, 14748-14751.
Joyce, J. A., Baruch, A., Chehade, K., Meyer-Morse, N., Giraudo, E., Tsai, F. Y., Greenbaum, D. C., Hager, J. H., Bogyo, M., and Hanahan, D. (2004). Cathepsin cysteine proteases are effectors of invasive growth and angiogenesis during multistage tumorigenesis. Cancer Cell *5*, 443-453.
Joyce, J. A., and Hanahan, D. (2004). Multiple roles for cysteine cathepsins in cancer. Cell Cycle *3*, 1516-1619.
Kalyani, A., Hobson, K., and Rao, M. S. (1997). Neuroepithelial stem cells from the embryonic spinal cord: isolation, characterization, and clonal analysis. Dev Biol *186*, 202-223.
Kalyani, A. J., Piper, D., Mujtaba, T., Lucero, M. T., and Rao, M. S. (1998). Spinal cord neuronal precursors generate multiple neuronal phenotypes in culture. J Neurosci *18*, 7856-7868.
Kasper, D., Planells-Cases, R., Fuhrmann, J. C., Scheel, O., Zeitz, O., Ruether, K., Schmitt, A., Poet, M., Steinfeld, R., Schweizer, M.*, et al.* (2005). Loss of the chloride channel ClC-7 leads to lysosomal storage disease and neurodegeneration. EMBO J *24*, 1079-1091.
Kim, T. S., and Tasker, A. S. (2006). Non-covalent cathepsin k inhibitors for the treatment of osteoporosis. Curr Top Med Chem *6*, 355-360.
Kohlschütter, A., Goebel, H. H., Schulz, A., Lukacs, Z. (2005). Die neuronalen Ceroid-Lipofuszinosen: Demenzerkrankungen bei Kindern und Jugendlichen. Deut Ärzteblatt *102*, 285-288.
Koike, M., Nakanishi, H., Saftig, P., Ezaki, J., Isahara, K., Ohsawa, Y., Schulz-Schaeffer, W., Watanabe, T., Waguri, S., Kametaka, S.*, et al.* (2000). Cathepsin D deficiency induces lysosomal storage with ceroid lipofuscin in mouse CNS neurons. J Neurosci *20*, 6898-6906.
Koike, M., Shibata, M., Waguri, S., Yoshimura, K., Tanida, I., Kominami, E., Gotow, T., Peters, C., von Figura, K., Mizushima, N.*, et al.* (2005). Participation of autophagy in storage of lysosomes in neurons from mouse models of neuronal ceroid-lipofuscinoses (Batten disease). Am J Pathol *167*, 1713-1728.
Kornak, U., Kasper, D., Bosl, M. R., Kaiser, E., Schweizer, M., Schulz, A., Friedrich, W., Delling, G., and Jentsch, T. J. (2001). Loss of the ClC-7 chloride channel leads to osteopetrosis in mice and man. Cell *104*, 205-215.
Kroemer, G., and Jäättelä, M. (2005). Lysosomes and autophagy in cell death control. Nat Rev Cancer *5*, 886-897.
Kudo, M., Brem, M. S., and Canfield, W. M. (2006). Mucolipidosis II (I-cell disease) and mucolipidosis IIIA (classical pseudo-hurler polydystrophy) are caused by mutations in the GlcNAc-phosphotransferase alpha / beta -subunits precursor gene. Am J Hum Genet *78*, 451-463.
Lazner, F., Gowen, M., Pavasovic, D., and Kola, I. (1999). Osteopetrosis and osteoporosis: two sides of the same coin. Hum Mol Genet *8*, 1839-1846.
Lehesjoki, A. E. (2003). Molecular background of progressive myoclonus epilepsy. EMBO J *22*, 3473-3478.
Lenarcic, B., Krishnan, G., Borukhovich, R., Ruck, B., Turk, V., and Moczydlowski, E. (2000). Saxiphilin, a saxitoxin-binding protein with two thyroglobulin type 1 domains, is an inhibitor of papain-like cysteine proteinases. J Biol Chem *275*, 15572-15577.
Lenarcic, B., Ritonja, A., Strukelj, B., Turk, B., and Turk, V. (1997). Equistatin, a new inhibitor of cysteine proteinases from Actinia equina, is structurally related to thyroglobulin type-1 domain. J Biol Chem *272*, 13899-13903.
Lendahl, U., Zimmerman, L. B., and McKay, R. D. (1990). CNS stem cells express a new class of intermediate filament protein. Cell *60*, 585-595.
Lezcano, N., Mrzljak, L., Eubanks, S., Levenson, R., Goldman-Rakic, P., and Bergson, C. (2000). Dual signaling regulated by calcyon, a D1 dopamine receptor interacting protein. Science *287*, 1660-1664.
Lindvall, O., Kokaia, Z., and Martinez-Serrano, A. (2004). Stem cell therapy for human neurodegenerative disorders-how to make it work. Nat Med *10 Suppl*, S42-50.
Liu, J., Sukhova, G. K., Yang, J. T., Sun, J., Ma, L., Ren, A., Xu, W. H., Fu, H., Dolganov, G. M., Hu, C.*, et al.* (2006). Cathepsin L expression and regulation in human abdominal aortic aneurysm, atherosclerosis, and vascular cells. Atherosclerosis *184*, 302-311.
Lombardi, G., Burzyn, D., Mundinano, J., Berguer, P., Bekinschtein, P., Costa, H., Castillo, L. F., Goldman, A., Meiss, R., Piazzon, I., and Nepomnaschy, I. (2005). Cathepsin-L influences the expression of extracellular matrix in lymphoid organs and plays a role in the regulation of thymic output and of peripheral T cell number. J Immunol *174*, 7022-7032.
Luhr, K. M., Nordstrom, E. K., Low, P., and Kristensson, K. (2004). Cathepsin B and L are involved in degradation of prions in GT1-1 neuronal cells. Neuroreport *15*, 1663-1667.
Mahley, R. W., Weisgraber, K. H., and Huang, Y. (2006). Apolipoprotein E4: a causative factor and therapeutic target in neuropathology, including Alzheimer's disease. Proc Natl Acad Sci U S A *103*, 5644-5651.
Mason, R. W., Johnson, D. A., Barrett, A. J., and Chapman, H. A. (1986). Elastinolytic activity of human cathepsin L. Biochem J *233*, 925-927.
Mattocks, M., Bagovich, M., De Rosa, M., Bond, S., Binnington, B., Rasaiah, V. I., Medin, J., and Lingwood, C. (2006). Treatment of neutral glycosphingolipid lysosomal storage diseases via inhibition of the ABC drug transporter, MDR1. Cyclosporin A can lower serum and liver globotriaosyl ceramide levels in the Fabry mouse model. Febs J *273*, 2064-2075.
McGrail, K. M., Phillips, J. M., and Sweadner, K. J. (1991). Immunofluorescent localization of three Na,K-ATPase isozymes in the rat central nervous system: both neurons and glia can express more than one Na,K-ATPase. J Neurosci *11*, 381-391.
McGrath, M. E. (1999). The lysosomal cysteine proteases. Annu Rev Biophys Biomol Struct *28*, 181-204.
McIntyre, G. F., and Erickson, A. H. (1991). Procathepsins L and D are membrane-bound in acidic microsomal vesicles. J Biol Chem *266*, 15438-15445.
McKay, R. (1997). Stem cells in the central nervous system. Science *276*, 66-71.
Meh, P., Pavsic, M., Turk, V., Baici, A., and Lenarcic, B. (2005). Dual concentration-dependent activity of thyroglobulin type-1 domain of testican: specific inhibitor and substrate of cathepsin L. Biol Chem *386*, 75-83.
Mistry, P. (2005). Therapeutic goals in Gaucher disease. Rev Med Interne *27*, 30-38.
Musil, D., Zucic, D., Turk, D., Engh, R. A., Mayr, I., Huber, R., Popovic, T., Turk, V., Towatari, T., Katunuma, N., and et al. (1991). The refined 2.15 A X-ray crystal structure of human liver cathepsin B: the structural basis for its specificity. EMBO J *10*, 2321-2330.
Nagler, D. K., Zhang, R., Tam, W., Sulea, T., Purisima, E. O., and Menard, R. (1999). Human cathepsin X: A cysteine protease with unique carboxypeptidase activity. Biochemistry *38*, 12648-12654.
Nakagawa, T., Roth, W., Wong, P., Nelson, A., Farr, A., Deussing, J., Villadangos, J. A., Ploegh, H., Peters, C., and Rudensky, A. Y. (1998). Cathepsin L: critical role in Ii degradation and CD4 T cell selection in the thymus. Science *280*, 450-453.
Okano, H. (2002). Stem cell biology of the central nervous system. J Neurosci Res *69*, 698-707.
O'Reilly, M. S., Boehm, T., Shing, Y., Fukai, N., Vasios, G., Lane, W. S., Flynn, E., Birkhead, J. R., Olsen, B. R., and Folkman, J. (1997). Endostatin: an endogenous inhibitor of angiogenesis and tumor growth. Cell *88*, 277-285.

Oyama, R., Yamamoto, H., and Titani, K. (2000). Glutamine synthetase, hemoglobin alpha-chain, and macrophage migration inhibitory factor binding to amyloid beta-protein: their identification in rat brain by a novel affinity chromatography and in Alzheimer's disease brain by immunoprecipitation. Biochim Biophys Acta *1479*, 91-102.
Potts, W., Bowyer, J., Jones, H., Tucker, D., Freemont, A. J., Millest, A., Martin, C., Vernon, W., Neerunjun, D., Slynn, G.*, et al.* (2004). Cathepsin L-deficient mice exhibit abnormal skin and bone development and show increased resistance to osteoporosis following ovariectomy. Int J Exp Pathol *85*, 85-96.
Puzer, L., Vercesi, J., Alves, M. F., Barros, N. M., Araujo, M. S., Aparecida Juliano, M., Reis, M. L., Juliano, L., and Carmona, A. K. (2005). A possible alternative mechanism of kinin generation in vivo by cathepsin L. Biol Chem *386*, 699-704.
Qian, X., Shen, Q., Goderie, S. K., He, W., Capela, A., Davis, A. A., and Temple, S. (2000). Timing of CNS cell generation: a programmed sequence of neuron and glial cell production from isolated murine cortical stem cells. Neuron *28*, 69-80.
Ramirez-Montealegre, D., Rothberg, P. G., and Pearce, D. A. (2006). Another disorder finds its gene. Brain *129*, 1353-1356.
Rao, M. S., and Mayer-Proschel, M. (1997). Glial-restricted precursors are derived from multipotent neuroepithelial stem cells. Dev Biol *188*, 48-63.
Reinheckel, T., Deussing, J., Roth, W., and Peters, C. (2001). Towards specific functions of lysosomal cysteine peptidases: phenotypes of mice deficient for cathepsin B or cathepsin L. Biol Chem *382*, 735-741.
Reinheckel, T., Hagemann, S., Dollwet-Mack, S., Martinez, E., Lohmuller, T., Zlatkovic, G., Tobin, D. J., Maas-Szabowski, N., and Peters, C. (2005). The lysosomal cysteine protease cathepsin L regulates keratinocyte proliferation by control of growth factor recycling. J Cell Sci *118*, 3387-3395.
Reynolds, B. A., and Weiss, S. (1996). Clonal and population analyses demonstrate that an EGF-responsive mammalian embryonic CNS precursor is a stem cell. Dev Biol *175*, 1-13.
Rocken, C., Menard, R., Buhling, F., Vockler, S., Raynes, J., Stix, B., Kruger, S., Roessner, A., and Kahne, T. (2005). Proteolysis of serum amyloid A and AA amyloid proteins by cysteine proteases: cathepsin B generates AA amyloid proteins and cathepsin L may prevent their formation. Ann Rheum Dis *64*, 808-815.
Ross, P. L., Huang, Y. N., Marchese, J. N., Williamson, B., Parker, K., Hattan, S., Khainovski, N., Pillai, S., Dey, S., Daniels, S.*, et al.* (2004). Multiplexed protein quantitation in Saccharomyces cerevisiae using amine-reactive isobaric tagging reagents. Mol Cell Proteomics *3*, 1154-1169.
Roth, W., Deussing, J., Botchkarev, V. A., Pauly-Evers, M., Saftig, P., Hafner, A., Schmidt, P., Schmahl, W., Scherer, J., Anton-Lamprecht, I.*, et al.* (2000). Cathepsin L deficiency as molecular defect of furless: hyperproliferation of keratinocytes and pertubation of hair follicle cycling. Faseb J *14*, 2075-2086.
Rychkova, N., Stahl, S., Gaetzner, S., and Felbor, U. (2005). Non-heparan sulfate-binding interactions of endostatin/collagen XVIII in murine development. Dev Dyn *232*, 399-407.
Saftig, P., Hunziker, E., Wehmeyer, O., Jones, S., Boyde, A., Rommerskirch, W., Moritz, J. D., Schu, P., and von Figura, K. (1998). Impaired osteoclastic bone resorption leads to osteopetrosis in cathepsin-K-deficient mice. Proc Natl Acad Sci U S A *95*, 13453-13458.
Sasaki, T., Hohenester, E., and Timpl, R. (2002). Structure and function of collagen-derived endostatin inhibitors of angiogenesis. IUBMB Life *53*, 77-84.
Shadforth, I. P., Dunkley, T. P., Lilley, K. S., and Bessant, C. (2005). i-Tracker: for quantitative proteomics using iTRAQ. BMC Genomics *6*, 145.
Shinozaki, K., Kume, H., Kuzume, H., Obata, K., and Maruyama, K. (1999). Norbin, a neurite-outgrowth-related protein, is a cytosolic protein localized in the somatodendritic region of neurons and distributed prominently in dendritic outgrowth in Purkinje cells. Brain Res Mol Brain Res *71*, 364-368.
Siintola, E., Partanen, S., Stromme, P., Haapanen, A., Haltia, M., Maehlen, J., Lehesjoki, A. E., and Tyynelä, J. (2006). Cathepsin D deficiency underlies congenital human neuronal ceroid-lipofuscinosis. Brain *129*, 1438-1445.
Simmons, G., Gosalia, D. N., Rennekamp, A. J., Reeves, J. D., Diamond, S. L., and Bates, P. (2005). Inhibitors of cathepsin L prevent severe acute respiratory syndrome coronavirus entry. Proc Natl Acad Sci U S A *102*, 11876-11881.
Stahl, S., and Felbor, U. (2006). Controversial molecular classification of human cerebrovascular malformations. Stroke *37*, 2214; author reply 2215-2216.
Stahl, S., Gaetzner, S., Mueller, T. D., and Felbor, U. (2005). Endostatin phenylalanines 31 and 34 define a receptor binding site. Genes Cells *10*, 929-939.
Stahl, S., Reinders, Y., Asan, E., Conzelmann, E., Sickmann, A., and Felbor, U. (2006). A proteomic analysis of Cathepsin B and L-deficient brain lysosomes. Mol Cell Proteomics *submitted*.
Starkey, P. M., and Barrett, A. J. (1973). Inhibition by alpha-macroglobulin and other serum proteins. Biochem J *131*, 823-831.
Steinfeld, R., Reinhardt, K., Schreiber, K., Hillebrand, M., Kraetzner, R., Bruck, W., Saftig, P., and Gartner, J. (2006). Cathepsin d deficiency is associated with a human neurodegenerative disorder. Am J Hum Genet *78*, 988-998.
Steller, H. (1995). Mechanisms and genes of cellular suicide. Science *267*, 1445-1449.
Stoka, V., Turk, B., Schendel, S. L., Kim, T. H., Cirman, T., Snipas, S. J., Ellerby, L. M., Bredesen, D., Freeze, H., Abrahamson, M.*, et al.* (2001). Lysosomal protease pathways to apoptosis. Cleavage of bid, not pro-caspases, is the most likely route. J Biol Chem *276*, 3149-3157.
Stypmann, J., Glaser, K., Roth, W., Tobin, D. J., Petermann, I., Matthias, R., Monnig, G., Haverkamp, W., Breithardt, G., Schmahl, W.*, et al.* (2002). Dilated cardiomyopathy in mice deficient for the lysosomal cysteine peptidase cathepsin L. Proc Natl Acad Sci U S A *99*, 6234-6239.
Sürücü, O., Sure, U., Gaetzner, S., Stahl, S., Benes, L., Bertalanffy, H., and Felbor, U. (2006). Clinical impact of CCM mutation detection in familial cavernous angioma. Childs Nerv Syst.
Taggart, C. C., Lowe, G. J., Greene, C. M., Mulgrew, A. T., O'Neill, S. J., Levine, R. L., and McElvaney, N. G. (2001). Cathepsin B, L, and S cleave and inactivate secretory leucoprotease inhibitor. J Biol Chem *276*, 33345-33352.
Takeyabu, K., Betsuyaku, T., Nishimura, M., Yoshioka, A., Tanino, M., Miyamoto, K., and Kawakami, Y. (1998). Cysteine proteinases and cystatin C in bronchoalveolar lavage fluid from subjects with subclinical emphysema. Eur Respir J *12*, 1033-1039.
Takio, K., Kominami, E., Wakamatsu, N., Katunuma, N., and Titani, K. (1983). Amino acid sequence of rat liver thiol proteinase inhibitor. Biochem Biophys Res Commun *115*, 902-908.
Tardy, C., Codogno, P., Autefage, H., Levade, T., and Andrieu-Abadie, N. (2005). Lysosomes and lysosomal proteins in cancer cell death (new players of an old struggle). Biochim Biophys Acta.
Temple, S. (2001). The development of neural stem cells. Nature *414*, 112-117.
Tobin, D. J., Foitzik, K., Reinheckel, T., Mecklenburg, L., Botchkarev, V. A., Peters, C., and Paus, R. (2002). The lysosomal protease cathepsin L is an important regulator of keratinocyte and melanocyte differentiation during hair follicle morphogenesis and cycling. Am J Pathol *160*, 1807-1821.

Toomes, C., James, J., Wood, A. J., Wu, C. L., McCormick, D., Lench, N., Hewitt, C., Moynihan, L., Roberts, E., Woods, C. G., *et al.* (1999). Loss-of-function mutations in the cathepsin C gene result in periodontal disease and palmoplantar keratosis. Nat Genet *23*, 421-424.
Tribl, F., Gerlach, M., Marcus, K., Asan, E., Tatschner, T., Arzberger, T., Meyer, H. E., Bringmann, G., and Riederer, P. (2005). "Subcellular proteomics" of neuromelanin granules isolated from the human brain. Mol Cell Proteomics *4*, 945-957.
Tribl, F., Marcus, K., Meyer, H. E., Bringmann, G., Gerlach, M., and Riederer, P. (2006). Subcellular proteomics reveals neuromelanin granules to be a lysosome-related organelle. J Neural Transm *113*, 741-749.
Turk, B., Dolenc, I., Turk, V., and Bieth, J. G. (1993). Kinetics of the pH-induced inactivation of human cathepsin L. Biochemistry *32*, 375-380.
Tyynelä, J., Sohar, I., Sleat, D. E., Gin, R. M., Donnelly, R. J., Baumann, M., Haltia, M., and Lobel, P. (2000). A mutation in the ovine cathepsin D gene causes a congenital lysosomal storage disease with profound neurodegeneration. EMBO J *19*, 2786-2792.
Urbich, C., Heeschen, C., Aicher, A., Sasaki, K., Bruhl, T., Farhadi, M. R., Vajkoczy, P., Hofmann, W. K., Peters, C., Pennacchio, L. A., *et al.* (2005). Cathepsin L is required for endothelial progenitor cell-induced neovascularization. Nat Med *11*, 206-213.
Waheed, A., Hasilik, A., Cantz, M., and von Figura, K. (1982). Phosphorylation of lysosomal enzymes in fibroblasts. Marked deficiency of N-acetylglucosamine-1-phosphotransferase in fibroblasts of patients with mucolipidosis III. Hoppe Seylers Z Physiol Chem *363*, 169-178.
Weiss, M. J., and Orkin, S. H. (1996). In vitro differentiation of murine embryonic stem cells. New approaches to old problems. J Clin Invest *97*, 591-595.
Wu, C. W., Liao, P. C., Yu, L., Wang, S. T., Chen, S. T., Wu, C. M., and Kuo, Y. M. (2004). Hemoglobin promotes Abeta oligomer formation and localizes in neurons and amyloid deposits. Neurobiol Dis *17*, 367-377.
Xiao, J., Dai, R., Negyessy, L., and Bergson, C. (2006). Calcyon, a novel partner of clathrin light chain, stimulates clathrin-mediated endocytosis. J Biol Chem *281*, 15182-15193.
Yamashita, M., and Konagaya, S. (1996). A novel cysteine protease inhibitor of the egg of chum salmon, containing a cysteine-rich thyroglobulin-like motif. J Biol Chem *271*, 1282-1284.
Yasothornsrikul, S., Greenbaum, D., Medzihradszky, K. F., Toneff, T., Bundey, R., Miller, R., Schilling, B., Petermann, I., Dehnert, J., Logvinova, A., *et al.* (2003). Cathepsin L in secretory vesicles functions as a prohormone-processing enzyme for production of the enkephalin peptide neurotransmitter. Proc Natl Acad Sci U S A *100*, 9590-9595.
Zhang, Y., Spiess, E., Groschup, M. H., and Burkle, A. (2003). Up-regulation of cathepsin B and cathepsin L activities in scrapie-infected mouse Neuro2a cells. J Gen Virol *84*, 2279-2283.
Zheng, X., Chou, P. M., Mirkin, B. L., and Rebbaa, A. (2004). Senescence-initiated reversal of drug resistance: specific role of cathepsin L. Cancer Res *64*, 1773-1780.

Anlage 1

Neurodegeneration in cathepsin B- and L-deficient mice

S. Stahl[1], Y. Reinders[2], E. Asan[3], E. Conzelmann[4], A. Sickmann[2], U. Felbor[1]

[1]Department of Human Genetics, [2]Protein Mass Spectrometry & Functional Proteomics Group, [3]Department of Anatomy and Cell Biology, [4]Department of Physiological Chemistry II, University of Würzburg, Germany

Abstract

Mice deficient for the two lysosomal proteases cathepsin B and cathepsin L develop a severe neurodegeneration during infancy. Select neurons in the cerebral and cerebellar cortex accumulate massive amounts of ultrastructurally unique lysosomal bodies prior to apoptosis and death of the animals during the third and fourth postnatal week. Apoptosis of cathepsin $B^{-/-}L^{-/-}$ neurons was confirmed by TUNEL-stainings, immunohistochemistry with an antibody against activated caspase-3, and electron microscopy. Thus, we have shown that cathepsins B and L functionally compensate for each other *in vivo*. To further analyze the molecular basis of neuronal loss in cathepsin B- and L-deficient mice, we primarily intend to identify neuron-specific *in vivo* substrates for cathepsins B and L. In parallel, we aim at reproducing the phenotype in an *in vitro* cell culture model system. Therefore, we isolated and expanded neural stem and progenitor cells from 12-day-old fetal forebrains of wild-type and cathepsin $B^{-/-}L^{-/-}$ mice. Their proliferative potential was quantified based on their capacity to generate primary and secondary neurospheres in culture. Furthermore, neurospheres were tested for their ability to differentiate into intact neurons and astrocytes. Neurosphere generation was reduced in double mutant cultures, and neural stem cell differentiation was slightly delayed in the absence of cathepsins B and L.

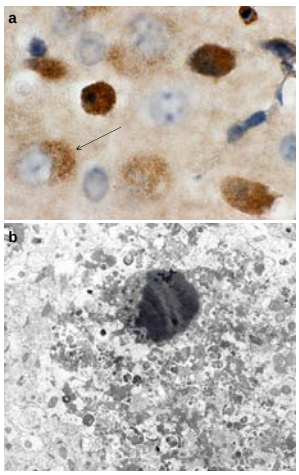

Fig. 1 **(a)** Apoptosis of 24-day-old cathepsin $B^{-/-}L^{-/-}$ forebrain neurons. Immunohistochemistry with an anti-activated caspase-3 antibody showed DAB-positive (brown) shrunken neurons and apoptotic bodies. Punctuate immunostaining (arrow) within perikarya reflects the accumulation of lysosomes prior to cell death. **(b)** Electron microscopy demonstrated globular chromatin compaction. Taken together, apoptosis of double-mutant neurons was confirmed by TUNEL positivity (Felbor et al., *PNAS*, 2002), anti-activated caspase-3 immunostaining and electron microscopy.

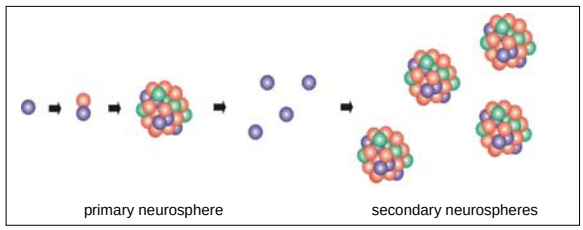

Fig. 2 Schematic representation of neurosphere formation.

An asymmetric division is shown: a stem cell (blue) divides into a stem and a progenitor cell (red). Alternatively, a stem cell can proliferate into two stem cells (symmetric division). Finally, a primary neurosphere arises which contains stem, progenitor and precursor (green) cells. After dissociation of primary neurospheres into single cells, suspensions are cultured in medium which selects for neural stem cells. Only these give rise to a secondary neurosphere. Less than 20% of neurosphere cells are stem cells.

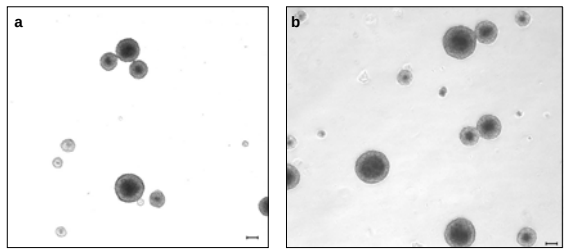

Fig. 3 Neurospheres after 14 days in culture. **(a)** Wildtype neurospheres, **(b)** double-mutant neurospheres (bar = 50 µm).

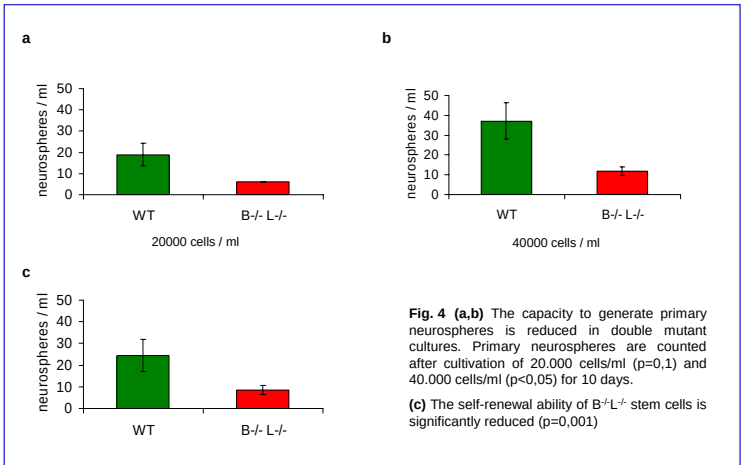

Fig. 4 **(a,b)** The capacity to generate primary neurospheres is reduced in double mutant cultures. Primary neurospheres are counted after cultivation of 20.000 cells/ml (p=0,1) and 40.000 cells/ml (p<0,05) for 10 days.

(c) The self-renewal ability of $B^{-/-}L^{-/-}$ stem cells is significantly reduced (p=0,001)

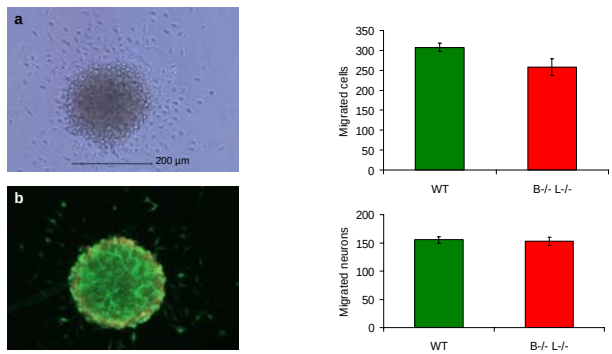

Fig. 5 Double knockout neurospheres differentiated slightly slower than wildtype neurospheres. **(a)** Phase-contrast picture of a double-mutant neurosphere, plated on a poly-L-ornithine coated coverslip and cultured in 1% horse serum for 4 days (bar = 200 µm). Fewer cells have migrated out of double mutant neurosheres (p<0,05). **(b)** Neurons are stained with anti-neuronal class III ß tubulin (green) and astrocytes with anti-GFAP (red). While significantly less $B^{-/-}L^{-/-}$ neurons migrate out of neurospheres after 2-3 days (data not shown), no difference is observed after 4 days (p=0,78).

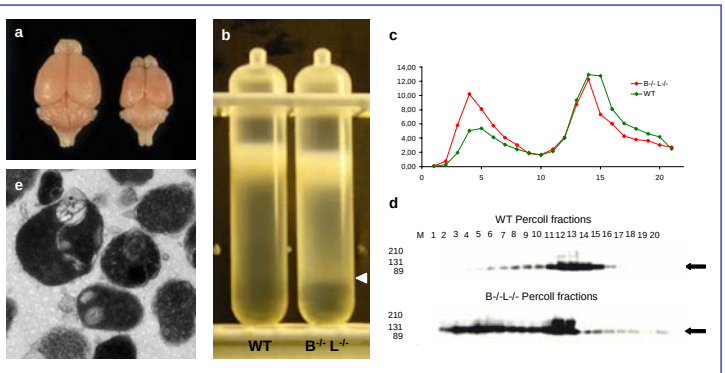

Fig. 6 The lysosomal compartment is increased in cathepsin $B^{-/-}L^{-/-}$ cerebral neurons. **(a)** Freshly prepared cerebral tissue was homogenized. **(b)** The post nuclear supernatant was loaded onto percoll gradients and centrifuged at 25000 rpm. Double mutant lysosomes formed a visible band in the lower region of the tube (arrowhead). **(c)** The late lysosomal fractions 3 to 5 showed a much higher hexosaminidase activity when compared to the wildtype. **(d)** Wild-type and double knockout fractions were also loaded onto 10-20% SDS-PAGE gels and probed with antibodies against e.g. LAMP1 which confirmed a striking accumulation of heavier lysosomes in double mutant brains. **(e)** Intact electron-dense lysosomes in the pooled fractions 3 to 5.

Summary

Cathepsin $B^{-/-}L^{-/-}$ stem and progenitor cells could be cultivated and differentiated into neurons and astrocytes. However, their proliferation potential differed significantly at the primary and secondary neurosphere stage.

In addition, double-mutant neurospheres required longer time periods for differentiation although there was no striking difference between wildtype and double-mutant neurospheres in general appearance and cell composition in later stages.

Accumulating heavy lysosomes from murine cerebral cortices were successfully purified using subcellular fractionation techniques. After biochemical characterization of the fractions with enzymatic activity tests and western blot analyses, the ultrastructure of the purified lysosomes was visualized. Since 2D gel electrophoresis turned out to be unsuitable for the material purified from cathepsin B- and L- double knockout brains, a proteomics approach using iTRAQ™ reagents is currently evaluated.

Reference

Felbor U, Kessler B, Mothes W, Ploegh HL, Bronson RT, Olsen BR, Neuronal loss and brain atrophy in mice lacking cathepsins B and L. *PNAS* 99, 7883-7888 (2002).

Acknowledgements

We thank C. Peters for cathepsin $B^{-/-}$ mice, Astra Zeneca for cathepsin $L^{-/-}$ mice, E. Hösl and S. Gätzner for expert assistance. This work was supported by the Graduiertenkolleg 1048 „Molecular basis of organ development in vertebrates“.

'CELL DEATH & DISEASE'
Mont Sainte-Odile, 2005

Anlage 2

Proteomic analysis of cathepsin B and L-deficient mouse brain lysosomes

Sonja Stahl[1], Yvonne Reinders[2], Esther Asan[3], Ernst Conzelmann[4], Albert Sickmann[2], Ute Felbor[1]

[1]Departments of Human Genetics, [2]Protein Mass Spectrometry & Functional Proteomics, [3]Anatomy and Cell Biology, and [4]Physiological Chemistry II, University of Würzburg, Germany

To whom correspondence should be addressed to:

Dr. U. Felbor

Department of Human Genetics

University of Würzburg

Biozentrum, Am Hubland

D-97074 Würzburg

Tel.: (+)49-931-888 4097

Fax: (+)49-931-888 4058

felbor@biozentrum.uni-wuerzburg.de

Abstract

Cathepsins B and L are lysosomal cysteine proteases which have been implicated in a variety of pathological processes such as cancer, tumor angiogenesis, and neurodegeneration. However, only a few protein substrates have thus far been described and the mechanisms by which cathepsins B and L regulate cell proliferation, invasion, and apoptosis are poorly understood. Combined deficiency of both cathepsins results in early-onset neurodegeneration in mice reminiscent of neuronal ceroid lipofuscinoses in humans. Therefore, we intended to quantify protein changes in brain lysosomes of double deficient mice. A combination of subcellular fractionation and LC-MS/MS using isobaric tagging for relative and absolute quantitation (iTRAQ™) allowed us to simultaneously assess wildtype and cathepsin $B^{-/-}L^{-/-}$ cerebral lysosomes. Altogether, 19 different proteins were significantly increased in cathepsin $B^{-/-}L^{-/-}$ lysosomes. Most elevated proteins had previously been localized to neuronal biosynthetic, recycling/endocytic or lysosomal compartments. The increase of calcyon, the Delta/Notch-like epidermal growth factor-related receptor, neurochondrin, phospholipase D3, Rab14, cathepsin D, and apolipoprotein E suggests a potential role for cathepsins B and L in axon outgrowth and synapse formation during postnatal development of the central nervous system.

Introduction

Cathepsins B and L belong to a family of 11 cysteine proteases (cathepsins B, C, H, F, K, L, O, S, V, W, and X/Z) with major roles in terminal protein degradation within the lysosome. Specific protein processing functions in other cellular compartments have more recently been recognized for the widely expressed cathepsins B and L. These include regulation of cell cycle progression through proteolytic processing of the CDP/Cux transcription factor in the nucleus (18), major histocompatibility complex class II antigen presentation (35) and control of growth factor recycling in endosomes (38), and hormone production within the regulated secretory pathway (16, 50). Notably, cathepsin L has been shown to convert proenkephalin to the active enkephalin opioid peptide neurotransmitter within secretory vesicles of neuroendocrine chromaffin cells (50). Cathepsin B has been proposed to act as a β-secretase producing neurotoxic Aβ (20). However, it was just shown that cathepsin B also degrades preformed extracellular oligomeric and fibrillar amyloid in aged APP transgenic mice (34). Furthermore, cathepsin B was identified as the major enzyme responsible for endosomal proteolysis of internalized epidermal growth factor receptor complexes (3) and insulin-like growth factor-I (2). Multistep endosomal proteolysis involving cathepsins B and L is also required for Ebola virus (5) and SARS-coronavirus infection (41).

During certain pathological conditions such as tumor invasion and tumor angiogenesis, both cathepsins have been reported to be upregulated, translocated to the cell surface, and secreted. Secreted procathepsin L generates the angiogenesis inhibitor endostatin from collagen XVIII after conversion to mature cathepsin L in the acidic extracellular milieu of murine hemangioendothelioma cells (13). In a mouse model of pancreatic islet cell carcinogenesis, impaired tumor invasion in cathepsin $B^{-/-}$ mice and cathepsin $L^{-/-}$ mice was in part attributed to maintenance of E-cadherin protein levels. It was subsequently demonstrated that both cathepsins release the extracellular domain of E-cadherin *in vitro* which abrogates its

adhesive function (17). Both single knockout mice also showed a reduction of tumor cell proliferation and increased cell death. The latter could be correlated with observed defects in tumor angiogenesis only in cathepsin $B^{-/-}$ mice. Thus, apoptosis occurred independently of angiogenesis defects in cathepsin $L^{-/-}$ mice (17).

The role of cathepsins in apoptosis appears to be complex. Cathepsin B has been reported to be an essential downstream mediator during tumor cell apoptosis induced by tumor necrosis factor (TNF-α) (15). This lysosomal pathway of apoptosis requires the release of lysosomal enzymes into the cytoplasm (reviewed in (29)) and can be inhibited by suppression of cytosolic cathepsin B activity (32). Furthermore, increased proteolysis by cathepsin B contributes to neuronal apoptosis in cystatin B-deficient mice, a murine model of Unverricht-Lundborg progressive myoclonus epilepsy (21). However, the biological relevance of the reported *in vitro* cleavage of the proapoptotic BCl-2 family member Bid by cathepsins (43) has been questioned *in vivo* (22), and further cytosolic target proteins of cathepsin B are not known. In contrast to the observed increased resistance of cathepsin $B^{-/-}$ cells to TNF-α-triggered apoptosis (15), cathepsin L-deficient lung carcinoma cells showed increased sensitivity to apoptosis (48) wich is in agreement with increased tumor cell death in the mouse model of multistage pancreatic tumorigenesis after deletion of cathepsin L (17). Increased apoptosis in the absence of cathepsin L could be rescued by inhibition of the aspartic protease cathepsin D whose single-chain isoform was subsequently shown to be specifically degraded by cathepsin L. Therefore, it was proposed that cathepsin L contributes to control death receptor-induced apoptosis via proteolysis of cathepsin D (48).

Cathepsin $B^{-/-}L^{-/-}$ mice display extensive neuron death in the central nervous system and develop a pronounced brain atrophy during the fourth postnatal week (14). Most double mutant animals die during the weaning period even if they are carefully nursed. Procathepsin D and correctly processed mature cathepsin D were found to be increased in cathepsin $B^{-/-}L^{-/-}$

brain lysates (14) which potentially adds to the terminal apoptotic process. However, prior to neuronal cell death, cathepsin $B^{-/-}L^{-/-}$ neurons develop a lysosomal storage disorder reminiscent of human neuronal ceroid lipofuscinoses (14, 28). This suggests that cathepsins B and L have other essential roles during postnatal maturation and in maintaining the integrity of the central nervous system. In addition, cathepsin D deficiency or dysfunction itself causes a congenital form of neuronal ceroid lipofuscinoses in mice (27), sheep (46) and humans (40, 42).

Cathepsins B and L can compensate for each other *in vivo* since only cathepsin $B^{-/-}L^{-/-}$ double mutant mice and not the respective single knockout mice develop autophagosomal and lysosomal accumulations within neurons. Importantly, the phenotype is restricted to select neurons in the cerebral and cerebellar cortex. In order to identify common neuronal substrates of cathepsins B and L, we performed a subcellular proteomics approach combining subcellular fractionation and amine-specific isobaric tag-based protein quantification by LC-MS/MS. Here, we present 19 proteins which are significantly increased in cathepsin $B^{-/-}L^{-/-}$ brain lysosomes.

Experimental Procedures

Mice

Cathepsin $B^{-/-}L^{-/-}$ mice were described previously (Felbor et al. 2002). Both double mutant and wild-type controls were from a mixed genetic background (C57BL/6 x 129/sv). All animal experiments were performed in compliance with institutional guidelines.

Subcellular Fractionation

P17.5 double mutant and control cerebral tissues were dissected after intracardiac perfusion with cold 140 mM NaCl, 10 mM Tris-HCl, pH 7.4, in order to minimize red blood cell content. All following steps were performed at 4°C. Perfused mouse brains were immediately homogenized in an isoosmotic homogenization buffer (0.25 M sucrose containing 1 mM EDTA, 100 μM leupeptin, 100 μM elastinatinal, 50 μM pepstatinA) by five passes with 1000 U/min using a Potter S homogenizer (Braun). After a centrifugation step of 1,000 rpm for 2 min, 2 ml postnuclear supernatants were loaded onto 10 ml 41% Percoll (Amersham Pharmacia Biotech) in 0.25 M sucrose which had been layered on top of a 1-ml cushion of 90% Percoll. After 30 min centrifugation at 25,000 rpm and 4°C (Beckman L8-70M), 500 μl subcellular fractions were collected from the bottom of the tube.

Biochemical Characterization of Subcellular Fractions

10 μl of each fraction were mixed with 90 μl 0.25% Triton X-100 to disrupt lysosomes and the specific hexosaminidase substrate 4-methylumbelliferyl-β-D-N-acetylglucosaminide (Sigma) was added. After 30 min of incubation at 37°C, the amount of the fluorescent product 4-methylumbelliferol was detected with a fluorimeter at 366 nm. Further enzymatic activities analyzed were 2',3'-phosphodiesterase for myelin, katalase for peroxisomes, succinate-dehydrogenase for mitochondria, and cholin acetyl transferase for synaptosomes

using the substrates adenosine 2'3'-cyclic monophosphate (Sigma), hydrogen peroxide, natrium succinate (Sigma), and [1-^{14}C]accetyl CoA, respectively.

10 µl of all wild-type and double knockout fractions were also loaded onto 10-20% SDS-PAGE gels, electroblotted onto nitrocellulose and probed with a polyclonal rat anti mouse LAMP-1 antibody (PharMingen, 553792). Further antibodies were a goat anti-human cathepsin D antibody (Santa Cruz Biotechnology, sc-6486), and a goat anti-human apolipoprotein E antibody (Calbiochem, 178479). Secondary antibodies conjugated to peroxidase were purchased from Dianova.

Electron Microscopy

To eliminate Percoll particles, pooled fractions 3-5 containing double knockout lysosomes were centrifuged at 100,000 g (4°C). The white interphase was diluted with 0.25 M sucrose (60 µl) and fixed for 90 min with 2% glutaraldehyde in 0.1M phosphate-buffered saline, pH 7.4, at 4°C. A light yellow pellet became visible that was washed with PBS and spun at 4,0000 rpm for 15 min at 4°C three times. The pellet was then incubated in 4% OsO_4 and epon-embedded. Ultrathin sections were examined with a transmission electron microscope (LEO 912 AB, LEO Elektronenmikroskopie, Oberkochen, Germany).

Isobaric Tagging for Relative and Absolute Quantitation (iTRAQ™ labeling)

Lysosomes derived from fractions 3 to 5 were resuspended in 20 µL digestion buffer (0.5 M triethylammonium bicarbonate, pH 8.5, and 0.1% SDS). The final protein concentration was determined with the bicinchoniic acid assay (Pierce). iTRAQ™ reagents were dissolved in 70 µL ethanol. The samples were reduced for 60 minutes at 37 °C using reducing reagent, blocked for 10 minutes at room temperature using MMTS, and digested with trypsin over

night. Afterwards, each sample was incubated with a different iTRAQ™ reagent for one hour.

Cation Exchange Chromatography

After pooling the samples, the mixture was separated directly by cation exchange chromatography as previously described (Wagner *et. al.*, 2003). Prior to nano-LC-MS/MS, each fraction was concentrated in a vacuum centrifuge to diminish the acetonitrile concentration.

Nano-Rechromatography and MS/MS

The sample was preconcentrated on a C_{18} precolumn (C_{18} PepMap™ RP, 300 µm ID x 1mm, Dionex, Idstein, Germany) for 5 min at a flow rate of 25 µL/min using an HPLC system consisting of a Famos™ autosampler, a Switchos™ microcolumn switching module and an Ultimate™ micropump (all Dionex). Afterwards, peptides were eluted and separated on a C_{18} main column (C_{18} PepMap™ RP, 75 µm ID x 150 mm, Dionex) by a binary gradient composed of solvent A (0.1% formic acid) and solvent B (0.1% formic acid in 84% acetonitrile). Solvent B was increased linearly from 5% to 50% within 30 minutes, then to 95% for 10 minutes, and afterwards the column was reequilibrated to 5% solvent B. The flow rate was set to 250 nL/min. Peptides were directly eluted into an ESI-mass spectrometer. For mass spectrometric analysis a Quad-TOF QStar®XL (Applied Biosystems, Darmstadt, Germany) was used.

Data Analysis

Data analysis of the derived spectra was accomplished using the ProQUANT 1.0 software (Applied Biosystems, Darmstadt, Germany) for both identification and quantification.

Database searching was restricted to tryptic peptides of the NCBI mouse protein database (June 2005). For iTRAQ™ experiments, side reactions with tyrosine were also taken into account. Doubly and triply charged ions were considered, respective mass tolerances were set to 0.2 Da. Proteins were identified on the basis of having at least one peptide whose individual ion score was above the 98% confidence threshold. The iTRAQ ratios reported are the average ratios calculated from the ratios of the individual peptides determined for each protein. All spectra were verified manually in order to avoid false positive hits derived from the search algorithms.

Results

Isolation of lysosomes

On postnatal days 16 to 17 (P16.5-P17.5), cathepsin $B^{-/-}/L^{-/-}$ cerebral neurons contain large amounts of lysosomal accumulations while apoptotic cell death becomes prominent between P21.5-P24.5 (14). Since most double knockouts survive until P16.5-P17.5, this stage was chosen for further analyses. The cerebellum was excluded because apoptosis already peaks around day 17.5 in the Purkinje cell monolayer (14).

For resolution of lysosomal fractions, freshly perfused murine cerebral tissues (Fig. 1A) were homogenized. The postnuclear supernatants were subjected to density gradient subcellular fractionation. A 41% Percoll gradient allowed separation of a high-density (fractions 3-6) and a low-density peak (fractions 13-16) of β-hexosaminidase activity (Fig. 1 B,C). Despite a significantly reduced mean wet weight of 203 mg for double mutants when compared to 313 mg for controls, a distinct white band became visible at the bottom of the double mutant gradient (Fig. 1 B). Direct comparison of the distribution profile of β-hexosaminidase activity between wild-type and $B^{-/-}/L^{-/-}$ fractions revealed an obvious shift towards heavier lysosomes in $B^{-/-}/L^{-/-}$ brains (Fig. 1 C). A similar difference in the profile of the endosomal-lysosomal compartment was observed upon SDS-PAGE and western blot analyses of all wild-type and double knockout fractions using an antibody against LAMP1 (Fig. 1D). Again, a prominent enrichment of late-stage lysosomes was found in double mutant mice.

To assess the purity of the late-stage lysosomal fractions, all fractions were analyzed using enzymatic markers specific for mitochondria, synaptosomes, peroxisomes and myelin which proved to be absent in cathepsin $B^{-/-}/L^{-/-}$ lysosomal fractions 3-5 (Fig. 1 E). Furthermore, electron microscopy demonstrated the high purity of intact, membrane-bound lysosomes containing electron-dense material in the pooled fractions 3-5 from double mutants (Fig. 1F). Therefore, these fractions were chosen for further analyses.

Identification of proteins increased in cathepsin $B^{-/-}/L^{-/-}$ lysosomes

In order to compare the protein composition of cathepsin $B^{-/-}/L^{-/-}$ and wildtype lysosomes, a quantitative proteomic strategy using iTRAQ™ reagents and nano-LC-MS/MS was employed. For protein quantification only peptides that had been identified by more than one, manually verified spectrum were considered. Furthermore, only proteins that were increased by at least a factor of three were taken into account. Thereby, a total of 19 unique murine proteins, summarized in Table 1, were found to be increased in cathepsin $B^{-/-}/L^{-/-}$ lysosomes. These include five lysosomal enzymes: acid ceramidase-like protein, cathepsin D, hexosaminidase A and B, and palmitoyl-protein thioesterase 1. In addition, the acid glycoprotein prosaposine, a precursor of four activator proteins of various lysosomal enzymes was found to be increased. Two further proteins, ubiquitin B, and sequestosome 1, are part of ubiquitination-dependent degradation. Calcyon (49), apolipoprotein E (8, 9), Rab14 (4), phospholipase D (25), carboxypeptidase E (6), and the Delta/Notch-like epidermal growth factor-related receptor (DNER) (10) have been found in secretory and recycling pathways. Thus, most of the proteins presented in Table 1 have been associated with biosynthetic, endocytic, and lysosomal compartments. Moreover, the majority of the proteins identified are known to be expressed in neurons and to have important functions in neuronal development and/or maintenance of neuronal integrity (see discussion).

To confirm iTRAQ quantitation, western blot analyses of two selected proteins were performed. In agreement with the iTRAQ results, cathepsin D, and apolipoprotein E were increased in cathepsin $B^{-/-}/L^{-/-}$ lysosomal fractions 3-5 (Fig. 2). Together with the previously reported increase of palmitoyl-protein thioesterase 1 activity in cathepsin $B^{-/-}/L^{-/-}$ brain lysates (14) the iTRAQ results of three proteins have been corroborated using two experimental methods.

Discussion

The proteomics-approach involving relative quantification of protein abundance has led to the identification of 19 different proteins with significantly increased abundance levels in cathepsin $B^{-/-}/L^{-/-}$ cerebral lysosomes. Comparable strategies have recently been employed successfully for similar analyses, e.g. directed towards lysosomal membranes or neuromelanine granules (4, 23, 45). Although such a proteomics-approach cannot guarantee completeness of the obtained dataset, it has added valuable information for deeper insight into lysosomal function.

The largest group of those proteins that were increased at least three-fold in cathepsin $B^{-/-}/L^{-/-}$ cerebral lysosomes were lysosomal enzymes as well as molecules associated with the ubiquitin-conjugating system. Elevated levels of lysosomal enzymes have been found in other diseases with impaired lysosomal function such as the neuronal ceroid lipofuscinoses. This has been interpreted as a compensatory mechanism (12) which is supported by the observation that palmitoyl-protein thioesterase 1 and tripeptidyl-peptidase 1 activities were normal in 12-day-old and elevated only in older cathepsin $B^{-/-}/L^{-/-}$ brain lysates in response to disease progression (14). Similarly, ubiquitin-positive inclusion bodies are common findings in neurodegenerative diseases including lysosomal storage disorders (51). Therefore, increased levels of lysosomal and ubiquitin-associated proteins presumably are an unspecific epiphenomenon rather than a major disease-causing mechanism in cathepsin $B^{-/-}/L^{-/-}$ mice. This view is supported by the fact that both the intermediate and the mature forms of cathepsin D are proportionally elevated in cathepsin $B^{-/-}/L^{-/-}$ brain lysosomes (Fig. 2).

Carboxypeptidase E (6), phospholipase D3 (37), and Rab14 (26) are three proteins that deserve to be highlighted due to their predominant expression in brain and role in biosynthesis and recycling. Secretory vesicle cathepsin L and Arg/Lys aminopeptidase have recently been found to form a proteolytic pathway generating peptide neurotransmitters that

is distinct from the pathway mediated by subtilisin-like prohormone convertases and carboxypeptidase E/H (19). It is possible that neuropeptide production or sorting in the regulated secretory pathway or neuropeptide secretion might be disturbed in the absence of cathepsins B and L. However, since the biosynthesis of most neuropeptides requires a carboxypeptidase, the upregulation of carboxypeptidase E might also be a secondary, compensatory phenomenon rather than the accumulation of a disease-causing substrate. Similarly, neurons in the central nervous system can synthesize apolipoprotein E in response to stress or injury (reviewed in (33)). Apolipoprotein E is a prototypic secretory and endocytosed protein which has also been colocalized with CD63- and cathepsin D-positive lysosomes in cultured human brain neurons (8). Apolipoprotein E plays important roles in maintenance and repair of neurons including stimulation of neurite outgrowth and synaptic plasticity. Therefore, the expression of apolipoprotein E by cathepsin $B^{-/-}/L^{-/-}$ neurons, astrocytes or activated microglia may be induced to promote neuron protection. Further studies will have to reveal whether pathological proteolysis of apolipoprotein E in cathepsin $B^{-/-}/L^{-/-}$ neurons contributes to the disease phenotype.

Calcyon and the Delta/Notch-like epidermal growth factor-related receptor (DNER) are prominently increased in cathepsin $B^{-/-}/L^{-/-}$ cerebral lysosomes compared to wildtype lysosomes (Table 1). Calcyon is a 24-kDa transmembrane protein predominantly expressed in brain and localized to vesicular compartments in neuronal cell bodies, dendrites, spines, and synaptic structures. Initially, calcyon was found to interact with the D1 dopamine receptor in pyramidal cells of the prefrontal cortex (31). Later, the clathrin light chain was identified as a further interaction partner of calcyon which was found to be a stimulator of clathrin-mediated endocytosis in cortical neurons (49). Thus far, nothing is known about calcyon expression and function in early postnatal development of the murine brain. Intriguingly, cathepsin $B^{-/-}/L^{-/-}$ mice develop their neuronal phenotype during early postnatal development, a phase

characterized by intensive synaptogenesis as well as extensive growth and degeneration (1). Furthermore, a hallmark of the cathepsin $B^{-/-}/L^{-/-}$ phenotype are densely packed axonal inclusions which precede lysosomal accumulations in perikarya (14). Therefore, it will be interesting to analyze whether cathepsins B and L influence calcyon-mediated synaptic plasticity, vesicle recycling or retrograde transport in postnatal neuronal development. Since clathrin-coated vesicles are responsible for internalization of receptor-bound ligands, it is conceivable that degradation or recycling of DNER is impaired. The neuron-specific transmembrane protein DNER is expressed in somatodentritic endosomal compartments of the developing central nervous system (10), promotes neuron-glia interaction by activating Notch signalling (11), and is essential for cerebellar development (44). A further protein which is six-fold increased in cathepsin $B^{-/-}/L^{-/-}$ lysosomes is neurochondrin. Neurochondrin has been reported to be prominently expressed in zones of neurite outgrowth and to bind to the cytoplasmic domain of the synaptic transmembrane-type semaphorin4C (24, 36, 39). Neurochondrin also binds to phosphatic acid (30) which is produced by phospholipase D1 and has been implicated in vesicular trafficking and phagocytosis (7). The phospholipase D3 isoform is elevated in cathepsin $B^{-/-}/L^{-/-}$ cerebral lysosomes. While phospholipase D1 plays an important role in neurotransmitter release (47), phospholipase D3 is thus far not intensively characterized but known to be expressed in the murine telencephalon during postnatal development (37). Consequently, it appears conceivable that a group of proteins with roles in early postnatal development of the central nervous system may be directly or indirectly regulated by degradation or processing through cathepsins B and L.

Acknowledgements

We thank C. Peters for providing cathepsin $B^{-/-}$ mice, AstraZeneca for cathepsin $L^{-/-}$ mice, and S. Gätzner for expert technical assistance. This work was supported by the Graduiertenkolleg 1048 and an Emmy Noether-grant from the Deutsche Forschungsgemeinschaft (Fe 432/6-5).

Figure legends

FIG 1. **Purification of cathepsin $B^{-/-}/L^{-/-}$ lysosomes from cerebral tissues.** A, 24-day old wildtype (wt) and cathepsin $B^{-/-}/L^{-/-}$ mouse brains demonstrating reduced brain size in the double mutant mainly attributable to neuronal apoptosis (Felbor et al., 2002). In the present study, only the cerebrum (c) was analysed (cb = cerebellum, ob = olfactory bulb). B, Percoll gradients revealing a white band (arrow) after centrifugation of cathepsin $B^{-/-}/L^{-/-}$ postnuclear supernatants. C, hexosaminidase assays of wildtype (green) and $B^{-/-}/L^{-/-}$ (red) fractions (average of five independent experiments). D, fractions loaded onto 10-20% SDS-PAGE gels and probed with an antibody against LAMP1. E, the lysosomal fractions 3-5 are clearly separated from mitochondria, synaptosomes, peroxisomes, and myelin in cathepsin $B^{-/-}/L^{-/-}$ lysosomes (average of five independent experiments). F, electron microscopy of purified intact cathepsin $B^{-/-}/L^{-/-}$ lysosomes.

FIG2. **Western blot analysis of lysosomal fractions corroborating the iTRAQ results.** A, a proportional increase of the 47-kDa intermediate form of cathepsin D and mature cathepsin D composed of a 31-kDa and a 14-kDa fragment was observed in cathepsin $B^{-/-}/L^{-/-}$ fractions when compared to the corresponding wild type fractions.

TABLE I *Summary of proteins that show more than three-fold increased iTRAQ™ ratios in cathepsin $B^{-/-}/L^{-/-}$ lysosomes (iTRAQ™114: cathepsin $B^{-/-}/L^{-/-}$ lysosomes; iTRAQ™117: wild type).*

Acc.No.	Protein	unique Peptides	AvG.: 114:117	SD
gi|18390323	RAB14, member RAS oncogene family	2	14.4	3.1
gi|31543351	Neuron specific gene family member 1/ Calcyon	3	11.6	2.6
gi|22203763	Carboxypeptidase E	8	10.7	2.3
gi|23097346	Delta/notch-like EGF-related receptor	1	10.2	2.6
gi|26348058	KIAA1414	2	9.9	2.5
gi|31560090	Unnamed protein product: Laminin A domain	4	7.7	2.4
gi|33440473	Protein phosphatase 2 (formerly 2A), regulatory subunit A (PR 65), beta isoform	4	7.5	1.1
gi|34328185	Prosaposin	7	6.9	1.8
gi|38080221	similar to Elongation factor 1-alpha 1 (EF-1-alpha-1)	3	6.9	1.0
gi|28972311	Neurochondrin	2	5.7	0.6
gi|6679451	Palmitoyl-protein thioesterase 1	6	5.4	1.0
gi|6753102	Apolipoprotein E precursor (Apo-E)	5	5.4	1.0
gi|6753556	Cathepsin D	10	5.2	1.1
gi|6754186	Hexosaminidase B	10	4.7	1.2
gi|6754954	Sequestosome 1, oxidative stress induced	3	4.6	0.6
gi|7110627	Hexosaminidase A	2	4.5	0.7
gi|6755919	Ubiquitin B	5	4.3	1.2
gi|21735433	N-acylsphingosine amidohydrolase (acid ceramidase)-like; Asahl protein	4	4.3	1.1
gi|7242181	Phospholipase D3	7	4.3	1.2

Increased hemoglobins are not listed since it seems likely that intracardiac perfusion of the cachectic double mutant mice was inefficient. Exploratory experiments had shown that hemoglobins contaminate late-stage lysosomal fractions: A red band was visible in wildtype and cathepsin $B^{-/-}/L^{-/-}$ Percoll gradients which disappeared upon perfusion (data not shown).

References

1. **Aggelopoulos, N., J. G. Parnavelas, and S. Edmunds.** 1989. Synaptogenesis in the dorsal lateral geniculate nucleus of the rat. Anat Embryol (Berl) **180:**243-57.
2. **Authier, F., M. Kouach, and G. Briand.** 2005. Endosomal proteolysis of insulin-like growth factor-I at its C-terminal D-domain by cathepsin B. FEBS Lett **579:**4309-16.
3. **Authier, F., M. Metioui, A. W. Bell, and J. S. Mort.** 1999. Negative regulation of epidermal growth factor signaling by selective proteolytic mechanisms in the endosome mediated by cathepsin B. J Biol Chem **274:**33723-31.
4. **Bagshaw, R. D., D. J. Mahuran, and J. W. Callahan.** 2005. Lysosomal membrane proteomics and biogenesis of lysosomes. Mol Neurobiol **32:**27-41.
5. **Chandran, K., N. J. Sullivan, U. Felbor, S. P. Whelan, and J. M. Cunningham.** 2005. Endosomal proteolysis of the Ebola virus glycoprotein is necessary for infection. Science **308:**1643-5.
6. **Cool, D. R., E. Normant, F. Shen, H. C. Chen, L. Pannell, Y. Zhang, and Y. P. Loh.** 1997. Carboxypeptidase E is a regulated secretory pathway sorting receptor: genetic obliteration leads to endocrine disorders in Cpe(fat) mice. Cell **88:**73-83.
7. **Corrotte, M., S. Chasserot-Golaz, P. Huang, G. Du, N. T. Ktistakis, M. A. Frohman, N. Vitale, M. F. Bader, and N. J. Grant.** 2006. Dynamics and function of phospholipase D and phosphatidic acid during phagocytosis. Traffic **7:**365-77.
8. **DeKroon, R. M., and P. J. Armati.** 2001. The endosomal trafficking of apolipoprotein E3 and E4 in cultured human brain neurons and astrocytes. Neurobiol Dis **8:**78-89.
9. **Dekroon, R. M., and P. J. Armati.** 2001. Synthesis and processing of apolipoprotein E in human brain cultures. Glia **33:**298-305.

10. **Eiraku, M., Y. Hirata, H. Takeshima, T. Hirano, and M. Kengaku.** 2002. Delta/notch-like epidermal growth factor (EGF)-related receptor, a novel EGF-like repeat-containing protein targeted to dendrites of developing and adult central nervous system neurons. J Biol Chem **277:**25400-7.

11. **Eiraku, M., A. Tohgo, K. Ono, M. Kaneko, K. Fujishima, T. Hirano, and M. Kengaku.** 2005. DNER acts as a neuron-specific Notch ligand during Bergmann glial development. Nat Neurosci **8:**873-80.

12. **Ezaki, J., and E. Kominami.** 2004. The intracellular location and function of proteins of neuronal ceroid lipofuscinoses. Brain Pathol **14:**77-85.

13. **Felbor, U., L. Dreier, R. A. Bryant, H. L. Ploegh, B. R. Olsen, and W. Mothes.** 2000. Secreted cathepsin L generates endostatin from collagen XVIII. Embo J **19:**1187-94.

14. **Felbor, U., B. Kessler, W. Mothes, H. H. Goebel, H. L. Ploegh, R. T. Bronson, and B. R. Olsen.** 2002. Neuronal loss and brain atrophy in mice lacking cathepsins B and L. Proc Natl Acad Sci U S A **99:**7883-8.

15. **Foghsgaard, L., D. Wissing, D. Mauch, U. Lademann, L. Bastholm, M. Boes, F. Elling, M. Leist, and M. Jaattela.** 2001. Cathepsin B acts as a dominant execution protease in tumor cell apoptosis induced by tumor necrosis factor. J Cell Biol **153:**999-1010.

16. **Friedrichs, B., C. Tepel, T. Reinheckel, J. Deussing, K. von Figura, V. Herzog, C. Peters, P. Saftig, and K. Brix.** 2003. Thyroid functions of mouse cathepsins B, K, and L. J Clin Invest **111:**1733-45.

17. **Gocheva, V., W. Zeng, D. Ke, D. Klimstra, T. Reinheckel, C. Peters, D. Hanahan, and J. A. Joyce.** 2006. Distinct roles for cysteine cathepsin genes in multistage tumorigenesis. Genes Dev **20:**543-56.

18. **Goulet, B., A. Baruch, N. S. Moon, M. Poirier, L. L. Sansregret, A. Erickson, M. Bogyo, and A. Nepveu.** 2004. A cathepsin L isoform that is devoid of a signal peptide localizes to the nucleus in S phase and processes the CDP/Cux transcription factor. Mol Cell **14:**207-19.

19. **Hook, V., S. Yasothornsrikul, D. Greenbaum, K. F. Medzihradszky, K. Troutner, T. Toneff, R. Bundey, A. Logrinova, T. Reinheckel, C. Peters, and M. Bogyo.** 2004. Cathepsin L and Arg/Lys aminopeptidase: a distinct prohormone processing pathway for the biosynthesis of peptide neurotransmitters and hormones. Biol Chem **385:**473-80.

20. **Hook, V. Y.** 2006. Protease Pathways in Peptide Neurotransmission and Neurodegenerative Diseases. Cell Mol Neurobiol.

21. **Houseweart, M. K., L. A. Pennacchio, A. Vilaythong, C. Peters, J. L. Noebels, and R. M. Myers.** 2003. Cathepsin B but not cathepsins L or S contributes to the pathogenesis of Unverricht-Lundborg progressive myoclonus epilepsy (EPM1). J Neurobiol **56:**315-27.

22. **Houseweart, M. K., A. Vilaythong, X. M. Yin, B. Turk, J. L. Noebels, and R. M. Myers.** 2003. Apoptosis caused by cathepsins does not require Bid signaling in an in vivo model of progressive myoclonus epilepsy (EPM1). Cell Death Differ **10:**1329-35.

23. **Hu, J., J. Qian, O. Borisov, S. Pan, Y. Li, T. Liu, L. Deng, K. Wannemacher, M. Kurnellas, C. Patterson, S. Elkabes, and H. Li.** 2006. Optimized proteomic analysis of a mouse model of cerebellar dysfunction using amine-specific isobaric tags. Proteomics.

24. **Istvanffy, R., D. M. Vogt Weisenhorn, T. Floss, and W. Wurst.** 2004. Expression of neurochondrin in the developing and adult mouse brain. Dev Genes Evol **214:**206-9.

25. **Jenkins, G. M., and M. A. Frohman.** 2005. Phospholipase D: a lipid centric review. Cell Mol Life Sci **62:**2305-16.

26. **Junutula, J. R., A. M. De Maziere, A. A. Peden, K. E. Ervin, R. J. Advani, S. M. van Dijk, J. Klumperman, and R. H. Scheller.** 2004. Rab14 is involved in membrane trafficking between the Golgi complex and endosomes. Mol Biol Cell **15:**2218-29.

27. **Koike, M., H. Nakanishi, P. Saftig, J. Ezaki, K. Isahara, Y. Ohsawa, W. Schulz-Schaeffer, T. Watanabe, S. Waguri, S. Kametaka, M. Shibata, K. Yamamoto, E. Kominami, C. Peters, K. von Figura, and Y. Uchiyama.** 2000. Cathepsin D deficiency induces lysosomal storage with ceroid lipofuscin in mouse CNS neurons. J Neurosci **20:**6898-906.

28. **Koike, M., M. Shibata, S. Waguri, K. Yoshimura, I. Tanida, E. Kominami, T. Gotow, C. Peters, K. von Figura, N. Mizushima, P. Saftig, and Y. Uchiyama.** 2005. Participation of autophagy in storage of lysosomes in neurons from mouse models of neuronal ceroid-lipofuscinoses (Batten disease). Am J Pathol **167:**1713-28.

29. **Kroemer, G., and M. Jaattela.** 2005. Lysosomes and autophagy in cell death control. Nat Rev Cancer **5:**886-97.

30. **Ktistakis, N. T., C. Delon, M. Manifava, E. Wood, I. Ganley, and J. M. Sugars.** 2003. Phospholipase D1 and potential targets of its hydrolysis product, phosphatidic acid. Biochem Soc Trans **31:**94-7.

31. **Lezcano, N., L. Mrzljak, S. Eubanks, R. Levenson, P. Goldman-Rakic, and C. Bergson.** 2000. Dual signaling regulated by calcyon, a D1 dopamine receptor interacting protein. Science **287:**1660-4.

32. **Liu, N., S. M. Raja, F. Zazzeroni, S. S. Metkar, R. Shah, M. Zhang, Y. Wang, D. Bromme, W. A. Russin, J. C. Lee, M. E. Peter, C. J. Froelich, G. Franzoso, and P. G. Ashton-Rickardt.** 2003. NF-kappaB protects from the lysosomal pathway of cell death. Embo J **22:**5313-22.

33. **Mahley, R. W., K. H. Weisgraber, and Y. Huang.** 2006. Apolipoprotein E4: a causative factor and therapeutic target in neuropathology, including Alzheimer's disease. Proc Natl Acad Sci U S A **103:**5644-51.

34. **Mueller-Steiner, S., Y. Zhou, H. Arai, E. D. Roberson, B. Sun, J. Chen, X. Wang, G. Yu, L. Esposito, L. Mucke, and L. Gan.** 2006. Antiamyloidogenic and neuroprotective functions of cathepsin B: implications for Alzheimer's disease. Neuron **51:**703-14.

35. **Nakagawa, T., W. Roth, P. Wong, A. Nelson, A. Farr, J. Deussing, J. A. Villadangos, H. Ploegh, C. Peters, and A. Y. Rudensky.** 1998. Cathepsin L: critical role in Ii degradation and CD4 T cell selection in the thymus. Science **280:**450-3.

36. **Ohoka, Y., M. Hirotani, H. Sugimoto, S. Fujioka, T. Furuyama, and S. Inagaki.** 2001. Semaphorin 4C, a transmembrane semaphorin, [corrected] associates with a neurite-outgrowth-related protein, SFAP75. Biochem Biophys Res Commun **280:**237-43.

37. **Pedersen, K. M., B. Finsen, J. E. Celis, and N. A. Jensen.** 1998. Expression of a novel murine phospholipase D homolog coincides with late neuronal development in the forebrain. J Biol Chem **273:**31494-504.

38. **Reinheckel, T., S. Hagemann, S. Dollwet-Mack, E. Martinez, T. Lohmuller, G. Zlatkovic, D. J. Tobin, N. Maas-Szabowski, and C. Peters.** 2005. The lysosomal cysteine protease cathepsin L regulates keratinocyte proliferation by control of growth factor recycling. J Cell Sci **118:**3387-95.

39. **Shinozaki, K., H. Kume, H. Kuzume, K. Obata, and K. Maruyama.** 1999. Norbin, a neurite-outgrowth-related protein, is a cytosolic protein localized in the somatodendritic region of neurons and distributed prominently in dendritic outgrowth in Purkinje cells. Brain Res Mol Brain Res **71:**364-8.

40. **Siintola, E., S. Partanen, P. Stromme, A. Haapanen, M. Haltia, J. Maehlen, A. E. Lehesjoki, and J. Tyynela.** 2006. Cathepsin D deficiency underlies congenital human neuronal ceroid-lipofuscinosis. Brain **129:**1438-45.

41. **Simmons, G., D. N. Gosalia, A. J. Rennekamp, J. D. Reeves, S. L. Diamond, and P. Bates.** 2005. Inhibitors of cathepsin L prevent severe acute respiratory syndrome coronavirus entry. Proc Natl Acad Sci U S A **102:**11876-81.

42. **Steinfeld, R., K. Reinhardt, K. Schreiber, M. Hillebrand, R. Kraetzner, W. Bruck, P. Saftig, and J. Gartner.** 2006. Cathepsin d deficiency is associated with a human neurodegenerative disorder. Am J Hum Genet **78:**988-98.

43. **Stoka, V., B. Turk, S. L. Schendel, T. H. Kim, T. Cirman, S. J. Snipas, L. M. Ellerby, D. Bredesen, H. Freeze, M. Abrahamson, D. Bromme, S. Krajewski, J. C. Reed, X. M. Yin, V. Turk, and G. S. Salvesen.** 2001. Lysosomal protease pathways to apoptosis. Cleavage of bid, not pro-caspases, is the most likely route. J Biol Chem **276:**3149-57.

44. **Tohgo, A., M. Eiraku, T. Miyazaki, E. Miura, S. Y. Kawaguchi, M. Nishi, M. Watanabe, T. Hirano, M. Kengaku, and H. Takeshima.** 2006. Impaired cerebellar functions in mutant mice lacking DNER. Mol Cell Neurosci **31:**326-33.

45. **Tribl, F., M. Gerlach, K. Marcus, E. Asan, T. Tatschner, T. Arzberger, H. E. Meyer, G. Bringmann, and P. Riederer.** 2005. "Subcellular proteomics" of neuromelanin granules isolated from the human brain. Mol Cell Proteomics **4:**945-57.

46. **Tyynela, J., I. Sohar, D. E. Sleat, R. M. Gin, R. J. Donnelly, M. Baumann, M. Haltia, and P. Lobel.** 2000. A mutation in the ovine cathepsin D gene causes a congenital lysosomal storage disease with profound neurodegeneration. Embo J **19:**2786-92.

47. **Vitale, N., A. S. Caumont, S. Chasserot-Golaz, G. Du, S. Wu, V. A. Sciorra, A. J. Morris, M. A. Frohman, and M. F. Bader.** 2001. Phospholipase D1: a key factor for the exocytotic machinery in neuroendocrine cells. Embo J **20:**2424-34.

48. **Wille, A., A. Gerber, A. Heimburg, A. Reisenauer, C. Peters, P. Saftig, T. Reinheckel, T. Welte, and F. Buhling.** 2004. Cathepsin L is involved in cathepsin D processing and regulation of apoptosis in A549 human lung epithelial cells. Biol Chem **385:**665-70.

49. **Xiao, J., R. Dai, L. Negyessy, and C. Bergson.** 2006. Calcyon, a novel partner of clathrin light chain, stimulates clathrin-mediated endocytosis. J Biol Chem **281:**15182-93.

50. **Yasothornsrikul, S., D. Greenbaum, K. F. Medzihradszky, T. Toneff, R. Bundey, R. Miller, B. Schilling, I. Petermann, J. Dehnert, A. Logvinova, P. Goldsmith, J. M. Neveu, W. S. Lane, B. Gibson, T. Reinheckel, C. Peters, M. Bogyo, and V. Hook.** 2003. Cathepsin L in secretory vesicles functions as a prohormone-processing enzyme for production of the enkephalin peptide neurotransmitter. Proc Natl Acad Sci U S A **100:**9590-5.

51. **Zhan, S. S., K. Beyreuther, and H. P. Schmitt.** 1992. Neuronal ubiquitin and neurofilament expression in different lysosomal storage disorders. Clin Neuropathol **11:**251-5.

Figure 1

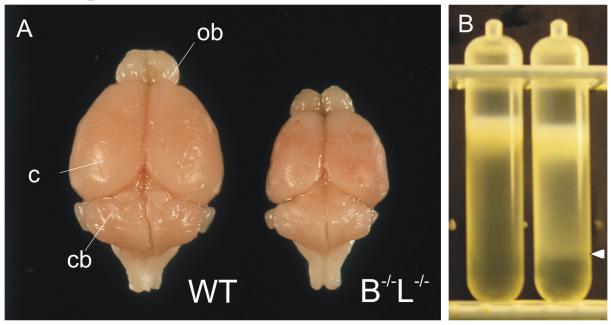
A
ob
c
cb
WT
B-/-L-/-
B

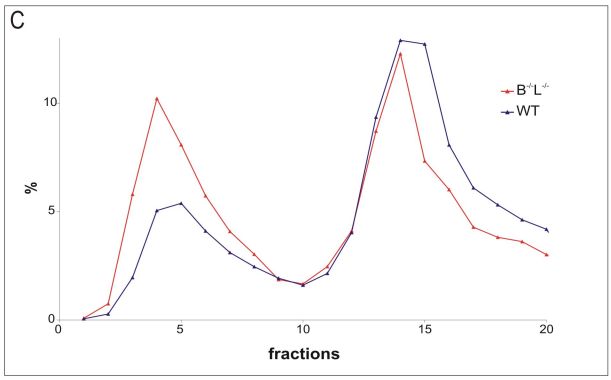
C
B-/-L-/-
WT
%
fractions

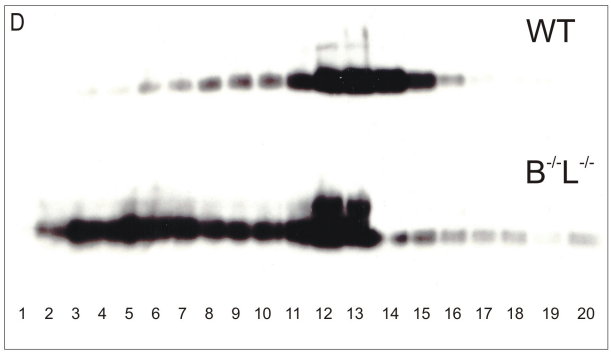
D
WT
B-/-L-/-
1 2 3 4 5 6 7 8 9 10 11 12 13 14 15 16 17 18 19 20

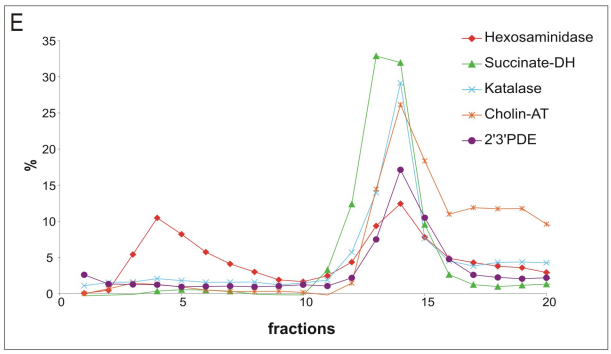
E
Hexosaminidase
Succinate-DH
Katalase
Cholin-AT
2'3'PDE
%
fractions

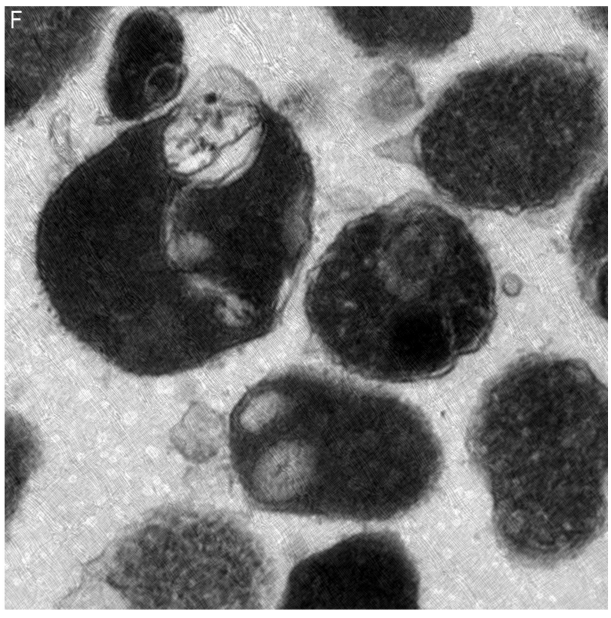
F

Figure 2

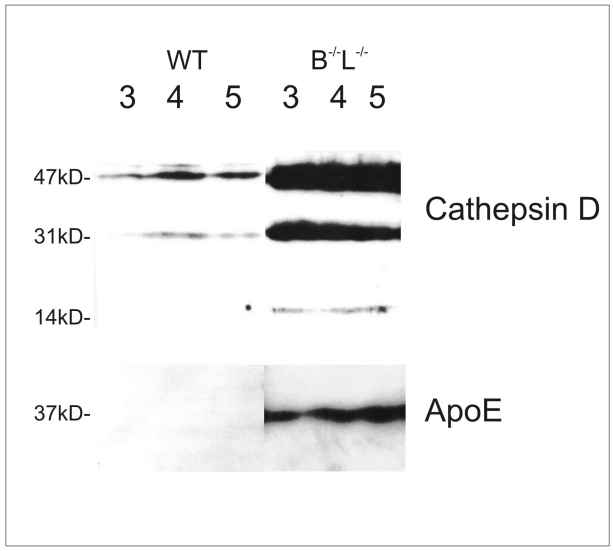

Anlage 3

Non–Heparan Sulfate-Binding Interactions of Endostatin/Collagen XVIII in Murine Development

Natalia Rychkova, Sonja Stahl, Sabine Gaetzner, and Ute Felbor*

Knobloch syndrome is characterized by a congenital generalized eye disease and cranial defect. Pathogenic mutations preferentially lead to a deletion or functional alteration of collagen XVIII's most C-terminal endostatin domain. Endostatin can be released from collagen XVIII and is a potent inhibitor of angiogenesis and tumor growth. We show differential expression of binding partners for endostatin, vascular endothelial growth factor (VEGF), and the collagen XV endostatin homologue in murine embryonal development using a set of alkaline phosphatase fusion proteins. Consistent with the human phenotype, vascular mesenchyme in the developing eye was identified as endostatin's primary target. While endostatin predominantly bound to blood vessels, the VEGF164 affinity probe labeled nonvascular tissues such as forebrain, hindbrain, the optic nerve, and the surface ectoderm of the future cornea. Strikingly increased staining specificity was observed with a non–heparin/heparan sulfate-binding endostatin probe. In contrast, elimination of the heparan sulfate binding site from VEGF led to complete loss of binding. The collagen XV endostatin homologue showed a highly restricted binding pattern. Oligomerization with endogenous endostatin was ruled out by use of collagen XVIII knockout mice. Our data provide strong evidence that collagen XVIII's C-terminal endostatin domain harbors a prominent tissue-binding site and that binding can occur in the absence of heparan sulfates in situ. ***Developmental Dynamics 232:399–407, 2005.*** **© 2004 Wiley-Liss, Inc.**

Key words: Knobloch syndrome; endostatin; collagen XVIII; vascular endothelial growth factor; heparan sulfate; brain and eye development

Received 28 June 2004; Revised 19 August 2004; Accepted 31 August 2004

INTRODUCTION

Knobloch syndrome (MIM# 267750) is an autosomal recessive disease mainly characterized by myopia magna (>20D), vitreoretinal degeneration, and congenital occipital encephalocele (Knobloch and Layer, 1971). High myopia has been diagnosed at birth and vitreoretinal degeneration as early as 3 days after birth (Sertié et al., 2000; Suzuki et al., 2002). Early recurrent retinal detachment, early cataract formation, and anterior segment disease including anterior iritis with posterior synechiae are further features of the eye defect in Knobloch syndrome. While the encephalocele can be corrected surgically within the first year of life, the ocular pathology is progressive in nature and shows poor response to surgical treatment. Patients experience a bilateral loss of vision during childhood.

Knobloch syndrome is caused by homozygous or compound heterozygous mutations in the *COL18A1* gene on 21q22.3 (Sertié et al., 2000; Suzuki et al., 2002; Kliemann et al., 2003; Menzel et al., 2004). Collagen XV and collagen XVIII are nonfibrillar collagens characterized by multiple interruptions in their central triple helical region and a unique highly homologous C-terminal domain (Oh et al., 1994). The 20-kDa C-terminal fragment of collagen XVIII can be proteolytically released (Wen et al., 1999; Felbor et al., 2000; Ferreras et al., 2000). It is a potent inhibitor of angiogenesis and

Department of Human Genetics, University of Würzburg, Biozentrum, Würzburg, Germany
Grant sponsor: Deutsche Forschungsgemeinschaft; Grant number: Fe 432/6-1, 6-2, 6-3.
***Correspondence to: Ute Felbor, M.D., Department of Human Genetics, University of Würzburg, Biozentrum, Am Hubland, D-97074 Würzburg, Germany. E-mail: felbor@biozentrum.uni-wuerzburg.de**

DOI 10.1002/dvdy.20222
Published online 20 December 2004 in Wiley InterScience (www.interscience.wiley.com).

tumor growth and was designated endostatin (O'Reilly et al., 1997). The crystal structure of endostatin predicted a prominent heparin/heparan sulfate binding site around arginines 158 and 270. Because heparan sulfate affinity is a feature of many growth factors such as vascular endothelial growth factor (VEGF), it was speculated that endostatin inhibits angiogenesis by binding to heparan sulfate containing proteoglycans on cell membrane surfaces (Hohenester et al., 1998). Subsequently, research has focussed on the characterization of endostatin's interaction with different heparin/heparan sulfate molecules (Sasaki et al., 1999; Dixelius et al., 2000; Karumanchi et al., 2001; Kreuger et al., 2002; Ricard-Blum et al., 2004). However, it remains unclear whether a high affinity endostatin receptor exists and whether heparan sulfate proteoglycans function as coreceptors that are required for local concentration of endostatin and mediate efficient binding of endostatin to a putative high affinity receptor. In addition, the physiological role of endostatin within collagen XVIII remains unknown.

Endostatin is encoded by exons 41 to 43 of the *COL18A1* gene (Rehn et al., 1996). Six of nine known independently arisen *COL18A1* mutations are located in exons 35, 36, 40, and 41 and lead to a premature stop just before or within the C-terminal endostatin coding region (Suzuki et al., 2002; Menzel et al., 2004). Furthermore, two missense mutations were recently located in the endostatin domain (Kliemann et al., 2003; Menzel et al., 2004). One of these mutations was shown to result in decreased affinity for laminin (Menzel et al., 2004). Thus, it is the most C-terminal endostatin domain that is either specifically deleted, interrupted or functionally altered in these Knobloch patients. It is conceivable that the endostatin domain is required for proper protein folding or protein stability of collagen XVIII. However, a stable truncated protein was isolated after deletion of the entire noncollagenous C-terminal domain of the *Caenorhabditis elegans* collagen XVIII homologue *cle-1* (Ackley et al., 2001). Alternatively, it is possible that binding of collagen XVIII to blood vessels and specific basement membranes is mediated by the endostatin domain. The latter alternative is supported by the observation that the binding pattern of hemagglutinin-tagged murine endostatin on adult human tissue sections closely resembled the distribution of its parent molecule collagen XVIII (Chang et al., 1999).

Histopathologic evaluation of a single enucleated eye from a Knobloch patient was not informative because it only showed unspecific late-stage gliotic changes of the detached retina (Cook and Knobloch, 1982). Thus, mouse models of Knobloch syndrome are important to elucidate early pathogenetic mechanisms. Collagen XVIII knockout mice show delayed regression of the hyaloid arteries and abnormal outgrowth of retinal vessels during the first 3 weeks of life (Fukai et al., 2002). They also develop age-dependent abnormalities in the iris, the ciliary body, and the retina (Marneros and Olsen, 2003; Ylikärppä et al., 2003a; Marneros et al., 2004) in agreement with altered endostatin immunoreactivity in retinae from patients affected with age-related macular degeneration (Bhutto et al., 2004).

The early onset of severe eye disease in Knobloch syndrome suggests that irreversible ocular damage occurs in utero. We localized and characterized endostatin binding partners in murine embryonal development. A systematic screen using alkaline phosphatase (AP) fusion proteins (Flanagan et al., 2000) identified vascular mesenchyme in the developing eye as endostatin's primary target, whereas the VEGF164 affinity probe prominently bound to nonvascular nerve tissues. Alanine in vitro mutagenesis of the heparin/heparan sulfate binding site within endostatin resulted in reduced binding affinity while elimination of the heparan sulfate binding site in VEGF led to complete loss of binding. Finally, inclusion of the non–heparan sulfate-binding collagen XV endostatin analogue into the screen demonstrated a striking spatial restriction and reduction in staining intensity when compared with endostatin.

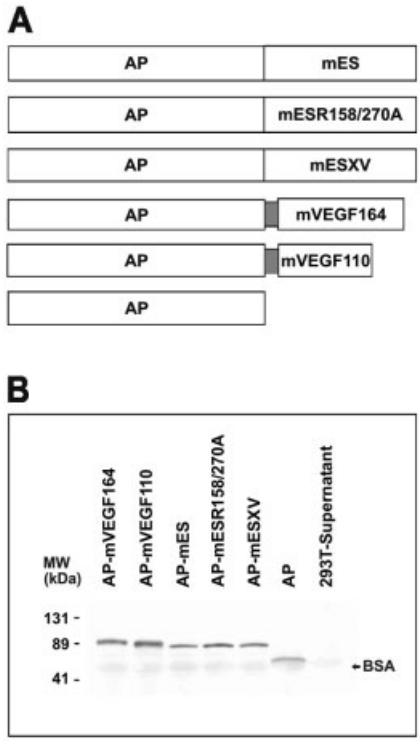

Fig. 1. Construction and expression of alkaline phosphatase (AP) fusion proteins. **A:** All fusion proteins consist of a heat-stable secreted form of human placental AP at the N-terminus which has a molecular weight of 67 kDa. Murine (m) endostatins (ES) and murine vascular endothelial growth factor (VEGF) isoforms were fused to the C-terminus. To increase the probability that the AP domain and the VEGF domains would function independently, they were separated by an additional 9-amino acid proline-rich linker (solid boxes). **B:** An anti-AP antibody was used to monitor the expression of AP fusion proteins by Western blotting. Endostatin monomers migrate at approximately 22 kDa under reducing conditions (O'Reilly et al., 1997; Felbor et al., 2000). Thus, AP–endostatin fusion proteins run at the expected size. AP–mVEGF fusion proteins are slightly larger than predicted, which suggests posttranslational modifications. The detection of unfused AP is reduced, because it migrates at a similar molecular weight as albumin (bovine serum albumin, BSA).

RESULTS

Generation of AP–Endostatin and AP–VEGF Fusion Proteins

To determine the expression profile of binding partners for endostatin in murine development, five dimeric AP fusion proteins (Fig. 1A) were designed that are expected to produce a pair of ligand moieties facing away from the tag in the same direction. Because endostatin is derived from the C-termi-

nal part of collagen XVIII, murine endostatin (mES) was fused to the C-terminus of heat-stable secreted human placental AP (AP–mES). To reduce nonspecific binding of endostatin to cell surfaces, two arginine residues responsible for heparan sulfate binding (Sasaki et al., 1999) were mutated to alanine by in vitro mutagenesis (AP–mESR158/270A). The highly homologous C-terminal fragment of collagen XV (endostatin-XV) lacks the evolutionarily conserved arginine at position 158 and does not bind to heparin. Whereas endostatin-XV showed anti-angiogenic activity in the chick chorioallantoic membrane angiogenesis assay (Sasaki et al., 2000), it did not inhibit outgrowth of endothelial cells from murine fetal bone explants (Gaetzner et al., in press). To further characterize the role of endostatin-XV, it was included in the present screen (AP–mESXV). Because endostatin can inhibit angiogenesis stimulated by VEGF (Yamaguchi et al., 1999; Kreuger et al., 2002), the murine 164- and 110-forms of VEGF were also fused to AP by means of a proline rich linker (AP–mVEGF164, AP–mVEGF110). Murine VEGF110 corresponds to a plasmin-generated fragment of human VEGF165 (Keyt et al., 1996). Like alternatively spliced VEGF121, it contains the N-terminal receptor binding determinants but lacks the C-terminal heparan sulfate binding domain and, therefore, is freely diffusable. Finally, pAPtag-4 was used to produce unfused AP as a negative control.

AP fusion proteins were produced in the extracellular supernatants of transiently transfected 293T cells. Expression of AP fusion proteins was monitored by quantitative measurement of AP activity in conditioned supernatants of transfected and nontransfected 293T cells. All supernatants of transfected cells demonstrated high and comparable AP activity, whereas the control supernatant of nontransfected cells showed only background activity (data not shown). Furthermore, expression of fusion proteins was assayed by immunoblotting with a polyclonal antibody against secreted human placental alkaline phosphatase. This antibody specifically detected AP fusion proteins of the expected sizes in supernatants of transfected but not of nontransfected cells (Fig. 1B). Ten-μl conditioned supernatants contained approximately 20 ng of fusion proteins (data not shown).

Differential In Situ Binding of Endostatins and VEGFs

The penetration of AP fusion proteins into unfixed whole-mount preparations of murine embryos was limited (data not shown). Therefore, fixed embryos were serial-sectioned in sagittal and transverse orientation. AP staining of midline sagittal sections with AP–mES (Fig. 2) demonstrated that endostatin bound to blood vessels in all organs examined. Nerve tissues in brain, spinal cord, and spinal ganglia did not stain specifically, whereas blood vessels of all sizes clearly did. Similarly, AP–mES detected blood vessels in adult murine brains (Fig. 3). As evidenced by strong staining of endothelial cells in small capillaries, endostatin not only bound to basement membranes and elastic fibers in vessel walls to epithelial basement membranes in a variety of organs (Fig. 2).

Incubation of sagittal sections with AP–mESR158/270A, which lacks the prominent heparan sulfate binding site resulted in a similar staining pattern. However, the staining required longer incubation times with the nitroblue tetrazolium/5-bromo-4-chloro-3-indolyl phosphate (NBT/BCIP) substrate (Fig. 2). Incubation with AP–mESXV and AP (Fig. 2) yielded no specific staining in midline sagittal sections. Unlike endostatin, AP–mVEGF164 staining was not predominantly vessel-associated in the embryonic day (E) 12.5–E14.5 murine tissues analyzed. Staining was prominent in liver tissue with active hematopoiesis but was also seen in forebrain, hindbrain, and basement membranes (Fig. 2). The elimination of the C-terminal heparan sulfate binding site in AP–mVEGF110 produced a perfect negative control (Fig. 2) akin to AP staining alone. That no general background staining was seen with AP, AP–mESXV, and AP–mVEGF110 and only very little with AP–mESR158/270A suggests that the background coloration observed with AP–mES and AP–mVEGF164 might be due to their high affinity for heparan sulfates.

Endostatin Binds to Blood Vessels in the Absence of Endostatin/Collagen XVIII

To rule out the possibility that endogenous endostatin interferes with endostatin binding in situ, collagen XVIII knockout embryos were incubated with AP fusion protein-containing supernatants. Prominent labeling of blood vessels and the pia mater in collagen XVIII null embryos demonstrated that endostatin binding in situ is not due to oligomerization with endogenous endostatin (Fig. 4A). In addition, the differential expression pattern of endostatin and VEGF binding partners was further confirmed because AP–mVEGF164 strongly stained forebrain and hindbrain in these sections (Fig. 4B). AP alone produced no background staining (Fig. 4C).

Non–heparin/Heparan Sulfate-Binding Endostatin Interacts Strongly With Mesenchymal Structures in the Murine Embryonal Eye

Staining of E12.5–E14.5 transverse sections with AP–mESR158/270A gave prominent signals in the hyaloid cavity between the lens and the neural layer of the retina, in the inner limiting membrane, the tunica vasculosa lentis, and the iridopupillary membrane. In addition, AP–mESR158/270A bound to vessels in the choroid (Fig. 5A,E) and in the developing E17.5 ciliary body (data not shown). Whereas incubation with AP–mESR158/270A led to little background coloration even upon overnight incubation with the NBT/BCIP substrate solution, AP–mES showed intense background staining if incubated overnight (Fig. 5B). Thus, elimination of the heparan sulfate–binding epitope resulted in significantly more specific endostatin staining patterns. The only structures that stained with AP–mESXV in our tissue collection were the tunica vasculosa lentis and the iridopupillary membrane (Fig. 5C,F). AP alone showed no specific staining (Fig. 5D).

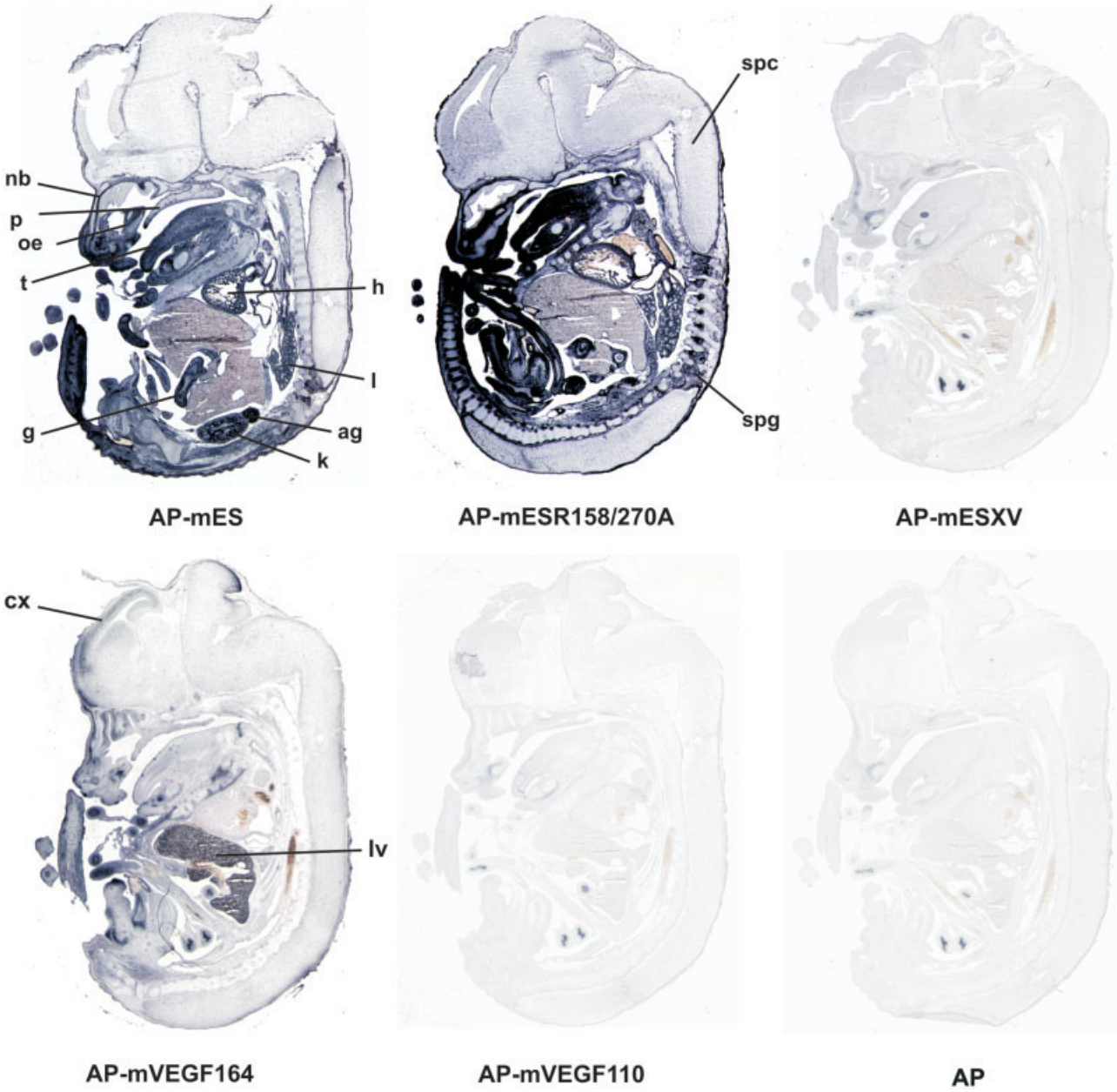

Fig. 2. Sagittal sections of embryonic day (E) 14.5 mice stained with alkaline phosphatase (AP) fusion proteins. AP–mES as well as the non–heparan sulfate-binding mutant AP–mESR158/270A both bound to blood vessels and epithelial basement membranes and, thus, showed very similar staining patterns (h, heart; l, lung; k, definitive kidney; ag, adrenal gland; nb, cartilage primordium of nasal bone; p, cartilage primordium of palatal shelf of maxilla; oe, olfactory epithelium; t, dorsal surface of tongue; g, gut; spc, spinal cord; spg, spinal ganglion). They only differed in length of incubation times: AP–mES stained after 1–2 hr of substrate incubation, whereas AP–mESR158/270A required overnight incubation. In contrast, non–heparan sulfate-binding AP–mVEGF110 did not stain basement membranes, liver tissue (lv), and the roof of the neopallial cortex, the future cerebral cortex (cx), which stained with AP–mVEGF164. AP–mES and AP–mVEGF164 sections were incubated with NBT/BCIP for 2 hr only, because overnight incubation resulted in strong background staining (see Fig. 5B). The remaining sections were all incubated overnight. AP–mESXV, AP–mVEGF110, and control AP showed no specific stain. mESXV, murine endostatin-XV; mES, murine endostatin.

While incubation with the NBT/BCIP substrate only takes 5 to 10 min to elicit a strong signal, weaker signals are known to take many hours to develop (Flanagan et al., 2000) most likely due to low receptor number resulting in a low amount of bound enzyme. Thus, experiments with varying substrate incubation times were performed (Fig. 6). A reduction of the incubation time with AP–mES fusion protein from 90 to 5 min did not lead to a relevant attenuation of the color reaction, indicating saturation of binding partners (data not shown). The use of higher AP fusion protein concentrations, therefore, was unnecessary.

AP–mESR158/270A labeled ocular structures rapidly. As early as 5 min after the addition of the substrate solution, the eyes showed a distinctive staining pattern (Fig. 6A), whereas blood vessels and basement mem-

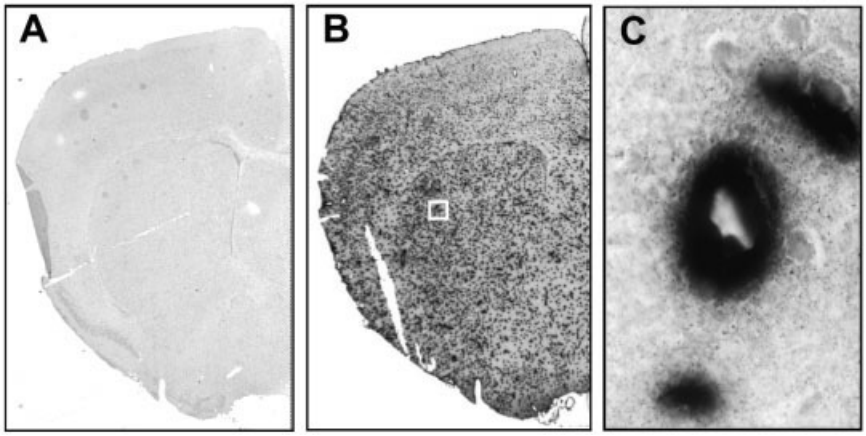

Fig. 3. **A,B:** Adult murine brain sections incubated with alkaline phosphatase (AP, A) and AP–mES (B) and counterstained with hematoxylin. **C:** Magnification of the area depicted by a square in B. The AP–mES probe clearly labeled blood vessels. mES, murine endostatin.

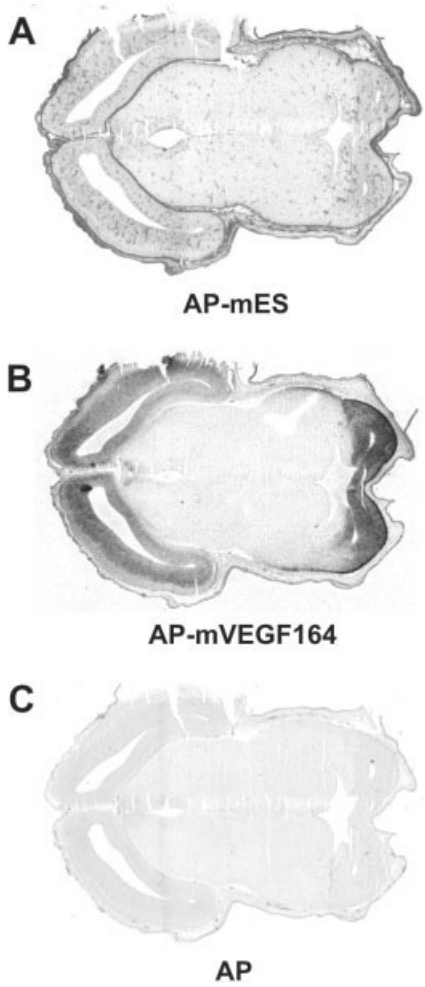

Fig. 4. **A–C:** Embryonic day (E) 14.5 transverse brain sections from collagen XVIII null mice stained with alkaline phosphatase (AP) -mES (A), AP–mVEGF164 (B), and AP alone (C). Because wild-type and collagen XVIII null vessels stain equally well with AP–mES, oligomerization with endogenous endostatin does not account for endostatin binding in situ. These stains further demonstrate differential expression of endostatin and VEGF receptors. VEGF, vascular endothelial growth factor; mES, murine endostatin.

branes in other organs required significantly longer incubation times. With AP–mESXV only a faint signal was detected after 1 hr. However, upon overnight staining, a highly specific labeling of the tunica vasculosa lentis was observed (Fig. 6B). Both heparin-binding AP–mES and AP–mVEGF164 led to background staining within less than 1 hr incubation with the substrate solution (Fig. 6C,D). AP–mVEGF110 and AP were negative even upon overnight incubation (Fig. 6E,F), indicating that there is no general background staining with our non–heparin-binding AP fusion proteins. Taken together, the heparan sulfate–binding sites within AP–mES and AP–mVEGF164 increase in situ binding at the expense of staining specificity.

DISCUSSION

In agreement with the observation that severe ocular alterations are present at birth in Knobloch syndrome, endostatin strongly bound to ocular mesenchyme during murine eye development. Prominent binding was observed within the hyaloid cavity, the future vitreous body, containing the vasa hyaloidea. These vessels supply the lens and the neural retina during embryonal life and regress after birth. In both wild-type and collagen XVIII knockout mice, the endostatin binding pattern (Figs. 5A,E, 6A) strikingly colocalized with the distribution of its parent molecule collagen XVIII (Sasaki et al., 1998) and defects in collagen XVIII knockout mice (Fukai et al., 2002; Marneros and Olsen, 2003; Ylikärppä et al., 2003a; Marneros et al., 2004). Similarly, the collagen XV endostatin homologue showed marked binding to the tunica vasculosa lentis (Figs. 5C,F, 6B), a structure immunopositive with an antibody against collagen XV and defective in collagen XV knockout mice (Ylikärppä et al., 2003b). Taken together with the observation that intact full-length collagen XVIII was localized within ocular basement membranes (Marneros et al., 2004), we conclude that an important tissue-binding site resides in collagen XVIII's C-terminal endostatin domain and that only a properly functioning endostatin domain guarantees correct binding to basement membranes. To further analyze the critical role of endostatin for tissue binding, it will be interesting to see whether mice lacking the endostatin domain will reveal improper localization of collagen XVIII within ocular basement membranes.

That the collagen XV endostatin homologue failed to bind to E12.5–E14.5 capillaries and epithelial basement membranes, the inner limiting membrane of the retina, the iris, and the ciliary body is consistent with a more restricted expression pattern of collagen XV during development and developmental shifts in the expression of collagen XV (Muona et al., 2002). Our data, therefore, emphasize the critical role of collagen XVIII in the eye, which cannot be compensated by collagen XV. They also provide an explanation for the lack of anti-angiogenic activity of endostatin-XV in a murine fetal bone explant angiogenesis model (Gaetzner et al., in press). However, the partially overlapping staining pattern in the eye suggests that the non–heparan sulfate receptor for endostatin-XV and -XVIII could be identical.

VEGF and endostatin both share an affinity for heparan sulfates, and the angiogenic activity of VEGF can be antagonized by endostatin in vitro (Yamaguchi et al., 1999; Kreuger et al., 2002). Therefore, we compared

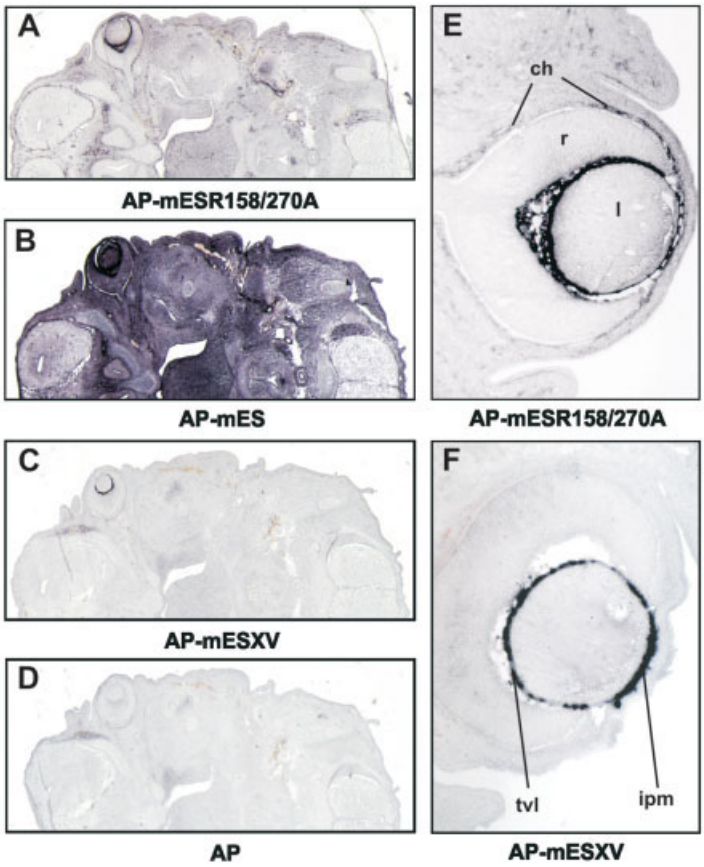

Fig. 5.

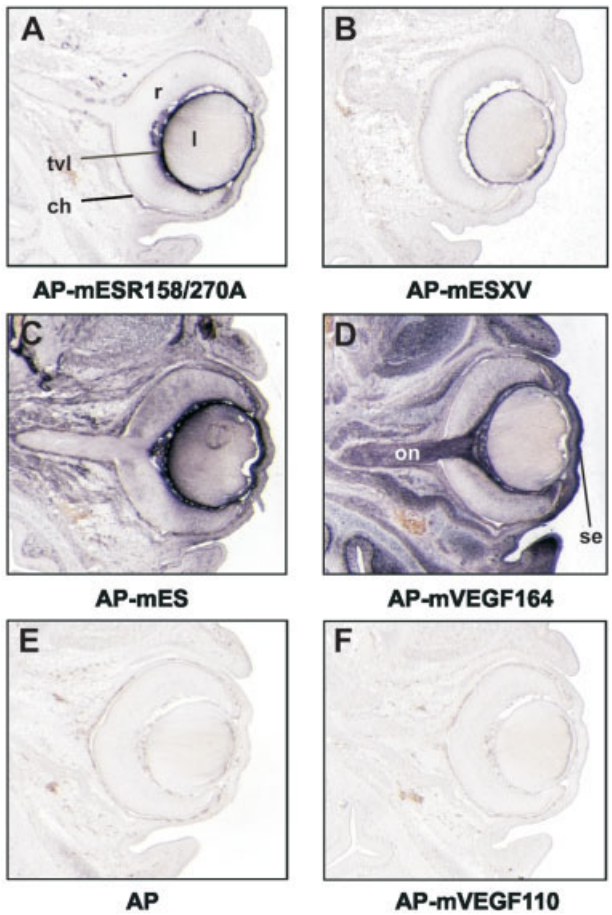

Fig. 6.

their binding patterns in situ. Endostatin binding was predominantly confined to the vasculature in the murine embryonic nervous system. Thus, the present results do not corroborate a role for endostatin in neuronal development as had been suggested by high expression of the *Caenorhabditis elegans* collagen XVIII homologue *cle-1* in neurons of the avascular nematode (Ackley et al., 2001). In contrast, the AP–mVEGF164 probe labeled forebrain in agreement with the expression of the VEGF receptor Flk-1 in E15 mouse forebrain neurons (Ogunshola et al., 2002). Distinct labeling of further nonvascular tissues such as the optic nerve and the surface ectoderm of the future cornea (Fig. 6D) extends the recent observation that VEGF receptors are found in developing neural retina (Robinson et al., 2001). Prominent staining of E14.5 liver (Fig. 2) coincides with the contribution of Flk-1 to definitive he-

Fig. 5. Transverse sections of embryonic day (E) 13.5 mice stained with alkaline phosphatase (AP) fusion proteins. All sections were incubated overnight with the substrate solution. **A–D:** Non–heparan sulfate-binding AP–mESR158/270A (A) and AP–mESXV (C) showed a highly specific staining pattern of structures in the eye, whereas AP–mES (B) resulted in unspecific background coloration of all tissues and unfused AP (D) was negative (the pigment layer of the retina is not pigmented because albino NMRI mice were analyzed). **E:** AP–mESR158/270A bound to vasa hyaloidea in the mesenchyme between the posterior pole of the lens (l) and the neural layer of the retina (r), which will form the future vitreous body as well as to the tunica vasculosa lentis, the iridopupillary membrane, and to vessels in the choroidal mesenchyme (ch). **F:** AP–mESXV labeled the tunica vasculosa lentis (tvl) and the iridopupillary membrane (ipm) only. mESXV, murine endostatin-XV.

Fig. 6. Time-course experiments on embryonic day (E) 14.5 murine eyes stained with alkaline phosphatase (AP) fusion proteins. **A:** AP–mESR158/270A gave strong and specific signals after 5 min of incubation with the NBT/BCIP substrate. This slide, however, was monitored for 1 hr before the reaction was stopped. **B:** AP–mESXV stained specifically but required overnight incubation. **C,D:** AP–mES (C) and AP–mVEGF164 (D) started to give background coloration within 1 hr. Note that AP–mVEGF164 also bound to structures in the optic nerve (on) and to the surface ectoderm (se) of the future cornea. **E,F:** AP (E) and AP–mVEGF110 (F) represented negative controls even after overnight incubation. mVEGF, murine vascular endothelial growth factor; mESXV, murine endostatin-XV.

matopoiesis during fetal development (Shalaby et al., 1997). The lack of VEGF staining in developing heart and lung can be explained with the observation that VEGF mRNA levels increase only in late embryonic stages in these organs (Ng et al., 2001). Both endostatin and VEGF binding colocalized in the hyaloid cavity of the eye. However, as opposed to endostatin, VEGF in situ binding depended on heparan sulfates, because the VEGF110 deletion mutant that contains the receptor binding sites but lacks affinity for heparan sulfates was negative (Fig. 6F). This observation is in agreement with a complete inhibition of VEGF165 binding to endothelial cells after pretreatment with heparinase (Rathjen et al., 1990) and a more than 100-fold decrease in endothelial cell mitogenic activity of VEGF110 and VEGF121 compared with VEGF165 (Keyt et al., 1996).

While RNA in situ hybridization and immunolocalization reveal highly specific molecular distributions in vertebrate embryos, the application of ligand fusion protein probes provides qualitatively different additional information, because novel binding partners can be mapped and characterized. This study addresses the controversial issue of endostatin's affinity for cell membrane heparan sulfates by use of a non–heparan sulfate-binding mutant AP–endostatin fusion protein probe in situ. Thus far, three studies implicated that endostatin binding (Chang et al., 1999; Wickström et al., 2003) and activity (Yamaguchi et al., 1999) are independent of heparan sulfates. In contrast, other studies showed that the recombinant non–heparan sulfate-binding mutant endostatin R158/270A protein is associated with reduced or lost biological activity in vitro (Sasaki et al., 1999; Dixelius et al., 2000; Javaherian et al., 2002; Schmidt et al., 2004) and that the inhibitory effect of wild-type endostatin on endothelial cell migration can be neutralized by heparin 12mers (Kreuger et al., 2002). Timed in situ-staining demonstrated that the AP–mESR158/270A probe specifically and rapidly bound to vascular mesenchyme in the murine embryonal eye (Figs. 5, 6). With lower affinity, it also labeled blood vessels in brain and other organs (Fig. 2). This finding indicates that endostatin interacts with a putative non–heparan sulfate high affinity receptor in situ, which is highly expressed in embryonal ocular mesenchyme. Based on our staining data, a cell line derived from embryonal hyaloid arteries would be ideal for expression cloning of this high affinity binding partner but is currently not available. Other vasculatures may contain the same receptor in lower density requiring heparan sulfates to, e.g., increase receptor binding. Alternatively, they may have different binding molecules. A variety of low affinity basement membrane binding partners such as fibulin-1, fibulin-2, laminin-1, and perlecan have been described (Sasaki et al., 1998). However, competition experiments with excess exogenous murine laminin-1 did not lead to altered endostatin binding in situ although AP–mES bound to laminin in solid phase assays (data not shown). This finding suggests that laminin is not an indispensable binding partner for endostatin in situ. In conclusion, it is conceivable that heparan sulfate binding is not essential for binding and proper anchoring of a structurally functioning collagen XVIII within ocular basement membranes, although it increases the biological activity of the proteolytic cleavage product endostatin in various angiogenesis assays.

EXPERIMENTAL PROCEDURES

Construction of Expression Vectors

Murine α1(XVIII) cDNA clone mc3b (Oh et al., 1994), murine α1(XV) cDNA clone mTS1-3 (Shinya and Olsen, unpublished), plasmid pSS9/TVA-VEGF164, and plasmid pSS10/TVA-VEGF110 (Snitkovsky et al., 2001) were used as templates to amplify the sequences of murine endostatin, murine endostatin XV, murine VEGF164, and murine VEGF110 with Pwo DNA polymerase according to the manufacturer's protocol (Roche). The following oligonucleotide primers were used: AP–murine endostatin: AP–mES5′, 5′-GGTTCCGGACATACTCATCAGGACTTTCAGCC-3′, AP–mES3′, 5′-GGAAGATCTCTATTTGGAGAAAGAGGTCATGAAG-3′; AP–murine endostatin XV: AP–mESXV5′, 5′-GGTCCGGATATGAGAGGCCTGTTCTGCACC-3′, AP–mESXV3′, 5′-GGAAGATCTTCACTTCCTAGTGTCTGTCATG-3′; AP–murine VEGFs: AP–Linkerfor, 5′-GGTTCCGGACCACCACCTGAACTCCTAGG-3′, AP–mVEGF164rev, 5′-ATGCTCGAGTCACCGCCTTGGCTTGTCAC-3′, AP–mVEGF110rev, 5′-ATGCTCGAGTCATGTTCTGTCTTTCTTTGGTC-3′.

In addition to the annealing sequence, forward primers contained a *Bsp*EI site at the 5′ end (AP–mES5′, AP–mESXV5′, AP–Linkerfor) and reverse primers contained a stop codon followed by a *Bgl*II (AP–mES3′, AP–mESXV3′) or a *Xho*I site (AP–mVEGF164rev, AP–mVEGF110rev) at the 3′ end. A DNA fragment encoding a proline-rich linker, PPPELLGGP, derived from the hinge region of a rabbit Fc chain had been placed at the N-terminal end of the coding sequences for murine VEGFs (Snitkovsky et al., 2001). After restriction and subcloning into the expression vector pAPtag-4 (obtained from D.A. Feldheim and J.G. Flanagan), the sequences of all inserts were confirmed by using Dye Terminator Cycle Sequencing (ABI). For in vitro mutagenesis with the QuikChange Site-Directed Mutagenesis kit (Stratagene), a PCR product encoding murine endostatin was first subcloned into the *Eco*RV and *Not*I restriction sites of pBluescript II SK(+) (Stratagene). After in vitro mutagenesis, it was PCR-cloned into pAPtag-4 as described above.

Expression of Recombinant Proteins

FuGENE 6 transfection reagent (Roche) was used to transiently transfect 12 μg of fusion plasmid DNA into 293T cells (human embryonic kidney cells, a gift from D.A. Feldheim and J.G. Flanagan) plated at 80% confluency on 150-mm tissue culture plates. The medium (DMEM with glutamax-I (GIBCO), 10% fetal bovine serum, 1% penicillin–streptomycin) was replaced 24 hr after transfection. Conditioned supernatants from transfected and nontransfected cells were collected after an additional 48–72 hr; centrifuged at 14,000 rpm (Eppendorf rotor

A-4-44); filtered through a 0.45-μm filter (Schleicher & Schuell); buffered with 10 mM HEPES, 0.05% NaN_3, pH 7.0; and stored at 4°C for immediate use or at −80°C for long-term usage.

Sodium Dodecyl Sulfate-Polyacrylamide Gel Electrophoresis/Western Blotting

A total of 15 μl of conditioned supernatants were loaded onto 5–15% sodium dodecyl sulfate-polyacrylamide gel electrophoresis gradient gels, run at 50 V for 18 hr, and wet-blotted onto nitrocellulose (Protran; Schleicher & Schuell) by using a TE42 Transphor transfer unit (Amersham Biosciences; 1.5 A for 1 hr at 4°C), because the semi-dry transfer was insufficient. Fusion proteins were detected with a rabbit polyclonal antibody against secreted human placental alkaline phosphatase (1:2,000, WAK-Chemie) followed by a horseradish peroxidase–conjugated anti-rabbit IgG (1:3,000, Santa Cruz) and enhanced chemiluminescence (Perkin Elmer/NEN). AP–mES and AP–mESR158/270A fusion proteins were quantified by Western blot analyses with known amounts of recombinant murine endostatin using a rabbit polyclonal anti-mouse endostatin antibody obtained from Cytimmune Sciences, Inc.

AP Activity Assay

A total of 100 μl unconcentrated supernatants were heat-inactivated for 10 min at 65°C to inhibit endogenous phosphatase activity. After centrifugation at 14,000 rpm (Eppendorf rotor F45-30-11), 20 μl were mixed with 380 μl HBAH buffer (see below) and 400 μl 2× AP substrate buffer (2 M diethanolamine, 1 mM $MgCl_2$, 18 mM *p*-nitrophenyl phosphate [AppliChem], pH 9.8), and incubated at room temperature. Absorbance at 405 nm was read at 30-sec intervals for 10 min in a spectrophotometer.

Staining of Tissue Sections

Timed-mated NMRI mice were ordered from Harlan Winkelmann. E12.5, E13.5, E14.5, and E17.5 embryos were dissected, fixed in 4% paraformaldehyde (in PBS) at 4°C overnight (E17.5 mice were decapitated and the head was fixed for 2 days; adult mice were perfusion-fixed with 10% neutral buffered formalin), transferred to 20% sucrose (in PBS) at 4°C on a shaker for 1 day, and frozen in OCT embedding medium (Tissue-Tek). Subsequently, E12.5–E14.5 mice were serial-sectioned in sagittal and transverse orientation, thaw-mounted on Polysine slides (Menzel Gläser), and stored at −80°C. For orientation, every 10th section was stained with methylene blue. AP staining of 10-μm cryosections was essentially performed as described in Flanagan et al. (2000). In brief, cryosections were thawed at 37°C for 5 min, washed in HBSS (150 mM NaCl, 20 mM HEPES, pH 7.0) for 10 min and in HBAH (HBSS, 0.5 mg/ml bovine serum albumin, 0.1% NaN_3) for 5 min twice. Then, tissues were covered with supernatants containing AP fusion proteins and incubated at room temperature for 90 min. Afterward, the sections were rinsed in ice-cold HBAH 6× for 2 min, fixed in acetone–formalin for 15 sec, washed in HBSS for 5 min twice, placed into preheated HBSS, and incubated in a 65°C water bath for 10 min to heat-inactivate endogenous phosphatase. Then, sections were washed in AP-staining buffer (100 mM NaCl, 5 mM $MgCl_2$, 100 mM Tris-HCl, pH 9.5) for 5 min and incubated with NBT/BCIP substrate (Roche) at room temperature under a shade of aluminium foil. Reactions were monitored under a dissecting microscope and stopped with 10 mM ethylenediaminetetraacetic acid (in PBS). Sections were fixed in 10% neutral buffered formalin (Sigma), and mounted with Kaiser's glycerin gelatin (Merck). Image acquisition was with a SZX9 stereomicroscope (Olympus) and the Spot Insight QE Color imaging software (Visitron). Higher magnifications were taken with a Zeiss Axiophot.

Collagen XVIII Null Mice

Mice with targeted disruption of *COL18A1* were a gift from Drs. N. Fukai and B.R. Olsen. Genotypes were determined by PCR amplification as described (Fukai et al., 2002).

ACKNOWLEDGMENTS

Drs. N. Fukai and B.R. Olsen are thanked for providing collagen XVIII knockout mice, Drs. D.A. Feldheim and J.G. Flanagan for the expression vector pAPtag-4, Drs. S. Snitkovsky and J.A.T. Young for plasmids pSS9/TVA-VEGF164 and pSS10/TVA-VEGF110, and I. Berger for subcloning AP–mVEGFs. U.F. receives an Emmy Noether-grant from the Deutsche Forschungsgemeinschaft.

REFERENCES

Ackley BD, Crew JR, Elamaa H, Pihlajaniemi T, Kuo CJ, Kramer JM. 2001. The NC1/endostatin domain of *Caenorhabditis elegans* type XVIII collagen affects cell migration and axon guidance. J Cell Biol 152:1219–1232.

Bhutto IA, Kim SY, McLeod DS, Merges C, Fukai N, Olsen BR, Lutty GA. 2004. Localization of collagen XVIII and the endostatin portion of collagen XVIII in aged human control eyes and eyes with age-related macular degeneration. Invest Ophthalmol Vis Sci 45:1544–1552.

Chang Z, Choon A, Friedl A. 1999. Endostatin binds to blood vessels in situ independent of heparan sulfate and does not compete for fibroblast growth factor-2 binding. Am J Pathol 155:71–76.

Cook GR, Knobloch WH. 1982. Autosomal recessive vitreoretinopathy and encephaloceles. Am J Ophthalmol 94:18–25.

Dixelius J, Larsson H, Sasaki T, Holmqvist K, Lu L, Engström Å, Timpl R, Welsh M, Claesson-Welsh L. 2000. Endostatin-induced tyrosine kinase signaling through the Shb adaptor protein regulates endothelial cell apoptosis. Blood 95:3403–3411.

Felbor U, Dreier L, Bryant RA, Ploegh HL, Olsen BR, Mothes W. 2000. Secreted cathepsin L generates endostatin from collagen XVIII. EMBO J 19:1187–1194.

Ferreras M, Felbor U, Lenhard T, Olsen BR, Delaissé J-M. 2000. Generation and degradation of human endostatin proteins by various proteinases. FEBS Lett 486:247–251.

Flanagan JG, Cheng H-J, Feldheim DA, Hattori M, Lu Q, Vanderhaeghen P. 2000. Alkaline phosphatase fusions of ligands or receptors as in situ probes for staining of cells, tissues, and embryos. Methods Enzymol 327:19–35.

Fukai N, Eklund L, Marneros AG, Oh SP, Keene DR, Tamarkin L, Niemelä M, Ilves M, Li E, Pihlajaniemi T, Olsen BR. 2002. Lack of collagen XVIII/endostatin

results in eye abnormalities. EMBO J 21:1535–1544.

Gaetzner S, Deckers MML, Stahl S, Löwik C, Olsen BR, Felbor U. 2005. Endostatin's heparin sulfate-binding site is essential for inhibition of angiogenesis and enhances in situ binding to capillary-like structures in bone explants. Matrix Biol (in press).

Hohenester E, Sasaki T, Olsen BR, Timpl R. 1998. Crystal structure of the angiogenesis inhibitor endostatin at 1.5 Å resolution. EMBO J 17:1656–1664.

Javaherian K, Park SY, Pickl WF, LaMontagne KR, Sjin RTT, Gillies S, Lo KM. 2002. Laminin modulates morphogenic properties of the collagen XVIII endostatin domain. J Biol Chem 277:45211–45218.

Karumanchi SA, Jha V, Ramchandran R, Karihaloo A, Tsiokas L, Chan B, Dhanabal M, Hanai JI, Venkataraman G, Shriver Z, Keiser N, Kalluri R, Zeng H, Mukhopadhyay D, Chen RL, Lander AD, Hagihara K, Yamaguchi Y, Sasisekharan R, Cantley L, Sukhatme VP. 2001. Cell surface glypicans are low-affinity endostatin receptors. Mol Cell 7: 811–822.

Keyt BA, Berleau LT, Nguyen HV, Chen H, Heinsohn H, Vandlen R, Ferrara N. 1996. The carboxyl-terminal domain (111-165) of vascular endothelial growth factor is critical for its mitogenic potency. J Biol Chem 271:7788–7795.

Kliemann SE, Waetge RTL, Suzuki OT, Passos-Bueno MR, Rosemberg S. 2003. Evidence of neuronal migration disorders in Knobloch syndrome: clinical and molecular analysis of two novel families. Am J Med Genet 119A:15–19.

Knobloch WH, Layer JM. 1971. Retinal detachment and encephalocele. J Pediatr Ophthalmol 8:181–184.

Kreuger J, Matsumoto T, Vanwildemeersch M, Sasaki T, Timpl R, Claesson-Welsh L, Spillmann D, Lindahl U. 2002. Role of heparan sulfate domain organization in endostatin inhibition of endothelial cell function. EMBO J 21:6303–6311.

Marneros AG, Olsen BR. 2003. Age-dependent iris abnormalities in collagen XVIII/endostatin deficient mice with similarities to human pigment dispersion syndrome. Invest Ophthalmol Vis Sci 44: 2367–2372.

Marneros AG, Keene DR, Hansen U, Fukai N, Moulton K, Goletz PL, Moiseyev G, Pawlyk BS, Halfter W, Dong S, Shibata M, Li T, Crouch RK, Bruckner P, Olsen BR. 2004. Collagen XVIII/endostatin is essential for vision and retinal pigment epithelial function. EMBO J 23:89–99.

Menzel O, Bekkeheien RCJ, Reymond A, Fukai N, Boye E, Kosztolanyi G, Aftimos S, Deutsch S, Scott HS, Olsen BR, Antonarakis SE, Guipponi M. 2004. Knobloch syndrome: novel mutations in *COL18A1*, evidence for genetic heterogeneity, and a functionally impaired polymorphism in endostatin. Hum Mutat 23: 77–84.

Muona A, Eklund L, Väisänen T, Pihlajaniemi T. 2002. Developmentally regulated expression of type XV collagen correlates with abnormalities in *Col15a1*−/− mice. Matrix Biol 21:89–102.

Ng Y-S, Rohan R, Sunday ME, Demello DE, D'Amore PA. 2001. Differential expression of VEGF isoforms in mouse during development and in the adult. Dev Dyn 220:112–121.

Ogunshola OO, Antic A, Donoghue MJ, Fan S-Y, Kim H, Stewart WB, Madri JA, Ment LR. 2002. Paracrine and autocrine functions of neuronal vascular endothelial growth factor (VEGF) in the central nervous system. J Biol Chem 277:11410–11415.

Oh SP, Kamagata Y, Muragaki Y, Timmons S, Ooshima A, Olsen BR. 1994. Isolation and sequencing of cDNAs for proteins with multiple domains of Gly-Xaa-Yaa repeats identify a distinct family of collagenous proteins. Proc Natl Acad Sci U S A 91:4229–4233.

O'Reilly MS, Boehm T, Shing Y, Fukai N, Vasios G, Lane WS, Flynn E, Birkhead JR, Olsen BR, Folkman J. 1997. Endostatin: an endogenous inhibitor of angiogenesis and tumor growth. Cell 88: 277–285.

Rathjen PD, Toth S, Willis A, Heath JK, Smith AG. 1990. Differentiation inhibiting activity is produced in matrix-associated and diffusible forms that are generated by alternate promoter usage. Cell 62:1105–1114.

Rehn M, Hintikka E, Pihlajaniemi T. 1996. Characterization of the mouse gene for the alpha 1 chain of type XVIII collagen (Col18a1) reveals that the three variant N-terminal polypeptide forms are transcribed from two widely separated promoters. Genomics 32:436–446.

Ricard-Blum S, Feraud O, Lortat-Jacob H, Rencurosi A, Fukai N, Dkhissi F, Vittet D, Imberty A, Olsen BR, van der Rest M. 2004. Characterization of endostatin binding to heparin and heparan sulfate by surface plasmon resonance and molecular modeling: role of divalent cations. J Biol Chem 279:2927–2936.

Robinson GS, Ju M, Shih S-C, Xu X, McMahon G, Caldwell RB, Smith LEH. 2001. Nonvascular role for VEGF: VEGFR-1, 2 activity is critical for neural retinal development. FASEB J 15:1215–1217.

Sasaki T, Fukai N, Mann K, Göhring W, Olsen BR, Timpl R. 1998. Structure, function and tissue forms of the C-terminal globular domain of collagen XVIII containing the angiogenesis inhibitor endostatin. EMBO J 17:4249–4256.

Sasaki T, Larsson H, Kreuger J, Salmivirta M, Claesson-Welsh L, Lindahl U, Hohenester E, Timpl R. 1999. Structural basis and potential role of heparin/heparan sulfate binding to the angiogenesis inhibitor endostatin. EMBO J 18:6240–6248.

Sasaki T, Larsson H, Tisi D, Claesson-Welsh L, Hohenester E, Timpl R. 2000. Endostatins derived from collagens XV and XVIII differ in structural and binding properties, tissue distribution and anti-angiogenic activity. J Mol Biol 301: 1179–1190.

Schmidt A, Wenzel D, Ferring I, Kazemi S, Sasaki T, Hescheler J, Timpl R, Addicks K, Fleischmann BK, Bloch W. 2004. Influence of endostatin on embryonic vasculo- and angiogenesis. Dev Dyn 230:468–480.

Sertié AL, Sossi V, Camargo AA, Zatz M, Brahe C, Passos-Bueno MR. 2000. Collagen XVIII, containing an endogenous inhibitor of angiogenesis and tumor growth, plays a critical role in the maintenance of retinal structure and in neural tube closure (Knobloch syndrome). Hum Mol Genet 9:2051–2058.

Shalaby F, Ho J, Stanford WL, Fischer K-D, Schuh AC, Schwartz L, Bernstein A, Rossant J. 1997. A requirement for Flk1 in primitive and definitive hematopoiesis and vasculogenesis. Cell 89:981–990.

Snitkovsky S, Niederman TMJ, Mulligan RC, Young JAT. 2001. Targeting avian leukosis virus subgroup A vectors by using a TVA-VEGF bridge protein. J Virol 75:1571–1575.

Suzuki OT, Sertié AL, Der Kaloustian VM, Kok F, Carpenter M, Murray J, Czeizel AE, Kliemann SE, Rosemberg S, Monteiro M, Olsen BR, Passos-Bueno MR. 2002. Molecular analysis of collagen XVIII reveals novel mutations, presence of a third isoform, and possible genetic heterogeneity in Knobloch syndrome. Am J Hum Genet 71:1320–1329.

Wen W, Moses MA, Wiederschain D, Arbiser JL, Folkman J. 1999. The generation of endostatin is mediated by elastase. Cancer Res 59:6052–6056.

Wickström SA, Alitalo K, Keski-Oja J. 2003. Endostatin associates with lipid rafts and induces reorganization of the actin cytoskeleton via down-regulation of RhoA activity. J Biol Chem 278:37895–37901.

Yamaguchi N, Anand-Apte B, Lee M, Sasaki T, Fukai N, Shapiro R, Que I, Löwik C, Timpl R, Olsen BR. 1999. Endostatin inhibits VEGF-induced endothelial cell migration and tumor growth independently of zinc binding. EMBO J 18:4414–4423.

Ylikärppä R, Eklund L, Sormunen R, Kontiola AI, Utriainen A, Määttä M, Fukai N, Olsen BR, Pihlajaniemi T. 2003a. Lack of type XVIII collagen results in anterior ocular defects. FASEB J 17:2257–2259.

Ylikärppä R, Eklund L, Sormunen R, Muona A, Fukai N, Olsen BR, Pihlajaniemi T. 2003b. Double knockout mice reveal a lack of major functional compensation between collagens XV and XVIII. Matrix Biol 22:443–448.

Anlage 4

Available online at www.sciencedirect.com

SCIENCE DIRECT

Matrix Biology 23 (2005) 557–561

MATRIX BIOLOGY

www.elsevier.com/locate/matbio

Short Report

Endostatin's heparan sulfate-binding site is essential for inhibition of angiogenesis and enhances in situ binding to capillary-like structures in bone explants

Sabine Gaetzner[a], Martine M.L. Deckers[b,1], Sonja Stahl[a], Clemens Löwik[b], Bjorn R. Olsen[c], Ute Felbor[a,*]

[a]*Department of Human Genetics, University of Würzburg, Biozentrum, Am Hubland, D-97074 Würzburg, Germany*
[b]*Department of Endocrinology and Metabolic Diseases, Leiden University Medical Center, Leiden, The Netherlands*
[c]*Department of Cell Biology, Harvard Medical School, Boston, MA, USA*

Received 19 August 2004; received in revised form 11 October 2004; accepted 12 October 2004

Abstract

The functional role of endostatin's affinity for heparan sulfates was addressed using an ex vivo bone angiogenesis model. Capillary-like sprouts showed prominent expression of collagen XVIII/endostatin. Outgrowth of endothelial cells was not altered in the absence of collagen XVIII but inhibited by the addition of recombinant endostatin. Mutant non-heparan sulfate binding endostatin and the collagen XV endostatin homologue were ineffective. The ability of mutant endostatin to bind to capillary structures was reduced when compared to endostatin. Endostatin-XV completely failed to bind to endothelial cells. Our data indicate that endostatin's angiostatic function is heparan sulfate-dependent, and that in situ-binding of endostatin to endothelial cells is increased by heparan sulfates.

Keywords: Endostatin; Collagen XVIII; Collagen XV; Heparan sulfate; Bone angiogenesis

1. Introduction

Endostatin, a 20-kDa proteolytic fragment from the C-terminal domain of collagen XVIII, is a naturally occurring inhibitor of angiogenesis and tumour growth whose affinity for heparin facilitated purification (O'Reilly et al., 1997). Replacing arginines 158 and 270 with alanines by in vitro mutagenesis resulted in loss of heparin and heparan sulfate binding associated with loss of anti-angiogenic activity in FGF-2-stimulated chick chorioallantoic membrane angiogenesis (Sasaki et al., 1999). The C-terminal domain of collagen XV (endostatin-XV) is highly homologous to endostatin but contains a four-residue deletion around arginine 158 and lacks heparin binding. While endostatin-XV did not affect endothelial cell proliferation (Ramchandran et al., 1999), it reduced angiogenesis in the chick chorioallantoic membrane (Sasaki et al., 2000). Further conflicting reports exist regarding the importance of heparin/heparan sulfate affinity for endostatin activity and binding. Four studies report loss of inhibitory activity of mutant endostatin R158/270A, whereas two studies demonstrate biological activity of non-heparin binding endostatin in various assay systems (Table 1). Binding of heparin mutant endostatin to the endothelial cells used in the respective assay was analyzed in only two studies with contradictory results. Javaherian et al. (2002) did not find binding of human Fc-endostatin R27/139A (which corresponds to R158/270A in the non-collagenous domain of

Abbreviations: VEGF, vascular endothelial growth factor; AP, alkaline phosphatase; ES, endostatin; AP-mES, alkaline phosphatase fused to the N-terminus of murine endostatin.

* Corresponding author. Tel.: +49 931 888 4097; fax: +49 931 888 4058.
E-mail address: felbor@biozentrum.uni-wuerzburg.de (U. Felbor).
[1] Current affiliation: Department of Cellular Biochemistry, The Netherlands Cancer Institute, Amsterdam, The Netherlands.

0945-053X/$ - see front matter © 2004 Elsevier B.V./International Society of Matrix Biology. All rights reserved.
doi:10.1016/j.matbio.2004.10.001

Table 1
Conflicting reports on the importance of heparan sulfates for endostatin activity and binding in various model systems

Activity of mutant* endostatin	Activity after heparin competition	Activity after heparitinase pretreatment	Cell/tissue binding	Model system	Reference
n.d.	n.d.	n.d.	Not reduced by heparin competition or heparitinase I+II	Human tissues	Chang et al., 1999
No	n.d.	n.d.	n.d.	CAM	Sasaki et al., 1999
Yes	n.d.	n.d.	n.d.	Migration/HUVECs	Yamaguchi et al., 1999
No	n.d.	n.d.	n.d.	CAM, apoptosis/IBE cells, kinase activity/ PAE cells	Dixelius et al., 2000
n.d.	n.d.	n.d.	Not reduced by heparin competition but by heparitinase I more pronounced than heparitinase III	CPAE cells	Karumanchi et al., 2001
No	n.d.	n.d.	No binding of mutant endostatin	Tube formation/ HUVECs	Javaherian et al., 2002
No	No	n.d.	n.d.	Migration/BCE cells	Kreuger et al., 2002
n.d.	n.d.	No	Not reduced by heparitinase III	RhoA activity, disassembly of actin cytoskeleton/HDMEC	Wickström et al., 2003
Reduced	n.d.	n.d.	Strong binding of mutant endostatin	Embryonic stem cell-derived vessels and endothelial cells	Schmidt et al., 2004
n.d.	n.d.	n.d.	Strong binding to vascular mesenchyme in the eye	Murine embryonal tissues	Rychkova et al., in press
No	Unclear	n.d.	Reduced binding of mutant endostatin	Tube formation/murine bone explants	Current study

*Mutant endostatin=non-heparin-binding endostatin, n.d.=not determined, CAM=chick chorioallantoic membrane angiogenesis assay, HUVECs=human umbilical vein endothelial cells, IBE cells=murine brain endothelial cells, PAE=porcine aortic endothelial cells, CPAE=cow pulmonary artery endothelial cells, BCE cells=bovine adrenal cortex endothelial cells, HDMEC=human dermal microvascular endothelial cells.

murine collagen XVIII) to the cell surface of human umbilical vein endothelial cells which were used in a Matrigel tube formation assay. However, Schmidt et al. (2004) showed prominent binding of biotinylated mutant mouse endostatin R158/184/270A to murine embryonic stem cell-derived endothelial cells which were assayed for proliferation, migration, and apoptosis. In order to further characterize mutant non-heparin binding endostatin, we analyzed both activity and binding of endostatin R158/270A in a murine multicellular collagen XVIII-producing bone angiogenesis model. We demonstrate that heparan sulfate binding is essential for anti-angiogenic activity of endostatin and enhances in situ binding to capillary-like networks in fetal mouse bone explants. Endostatin-XV lacks both the ability to inhibit outgrowth of capillary-like structures and to bind to endothelial cells.

2. Materials and methods

2.1. Generation of recombinant proteins

For activity assays, N-terminally flag-tagged human endostatins were constructed, expressed and purified as specified in Felbor et al. (2000). The R158/270A mutation was introduced by QuikChange™ Site-Directed Mutagenesis (Stratagene) in pBluescript II SK(+) (Stratagene). The human cDNA clone α1(XV) YMh4 (Muragaki et al., 1994) was used as template to PCR clone the sequences of human endostatin-XV with primers hESXV-N*flag*5′ (5′ -AGCGC-TAGCTGACTACAAGGACGACGATGACAAGTATGA-GAAGCCTGCTCTGCATTTG-3′) and hESXV-N*flag*3′ (5′ -GTCGGCGGCCGCTTACTTCCTAGCGTCTGTCAT GAAAC-3′). Direct binding of endostatins to sprouting endothelial cells was analyzed with the help of heat-stable alkaline phosphatase (AP) fused to the N-terminus of murine endostatins and murine vascular endothelial growth factor (VEGF) forms as described in Rychkova et al. (in press).

2.2. Bone explant angiogenesis assay

Cultures of 17-day-old murine fetal metatarsals were performed without coating of culture dishes according to Deckers et al. (2001). Stimulation of tube-like outgrowth with 100 ng/ml recombinant human VEGF (R&D) on days 3 and 10 was omitted in the activity assay (Fig. 2A) because the combination of wildtype endostatin and VEGF resulted in enlarged and fused vessels. Immunostaining was performed after 14 days in culture using the following antibodies: biotinylated monoclonal rat anti-mouse antibody ER-MP12/Biotin directed against murine PECAM-1 (1:200, BMA Biomedicals), polyclonal rabbit anti-mouse collagen

XVIII/NC11 antibody (1:500, Medical and Biological Laboratories, Japan), and polyclonal rabbit anti-mouse endostatin antibody (1:250, Cytimmune Sciences). Colour reactions were performed with the AEC chromogen kit (Sigma). Images were acquired with a Nikon Eclipse TE2000-U inverted microscope using the Spot Insight QE Color imaging software (Visitron). The total area of outgrowth from 24 C57BL/6 wildtype and 24 C57BL/6 collagen XVIII knockout metatarsals from four different litters were evaluated in four independent experiments with the MetaMorph Imaging Software (Visitron).

2.3. In situ staining of tube-like structures with AP affinity probes

Supernatants (250 μl) of transiently transfected 293 T cells were used for experiments after quantitation by AP activity assays and Western blot analyses. The generation of AP-endostatin and AP-VEGF fusion protein-containing conditioned media has been described in Rychkova et al. (in press). AP-staining of bone explant cultures was essentially performed as described (Flanagan et al., 2000), with small modifications. Bone cultures were fixed with acetone–formalin fixative for 15 s, and endogenous AP was heat-inactivated at 65°C for 120 min prior to the staining procedure. Addition of the AP inhibitor levamisole (2 mM, AppliChem) did not further reduce blue colouration of bones.

3. Results and discussion

To evaluate whether endostatin's parent molecule collagen XVIII plays an angiogenic role, fetal mouse bone explants were cultured. Capillary-like structures were identified using an antibody against the endothelial cell marker PECAM-1 (CD31). The structures also stained for collagen XVIII's N-terminal non-collagenous domain and its most C-terminal endostatin domain (Fig. 1A–C). Thus, the endothelial sprouts produced their own collagen XVIII containing vascular basement membranes. However, the formation of VEGF-stimulated PECAM-1-positive tube-like structures was only insignificantly attenuated in collagen XVIII-deficient metatarsals (Fig. 1D,F) when compared to wildtype metatarsals (Fig. 1A,F). Comparable results were obtained without VEGF-stimulation (data not shown). The absence of collagen XVIII did therefore not lead to any apparent functional consequences in this system. This is in agreement with the spatially restricted knock-out phenotype in vivo (Fukai et al., 2002).

Next, we analyzed whether the anti-angiogenic effect of endostatin is heparan-sulfate dependent in bone explants. Recombinant human and mouse (data not shown) endostatin inhibited the formation of capillary-like structures (Fig. 2A) while the non-heparan sulfate binding endostatin mutant R158/270A lacked anti-angiogenic activity in agreement with most previous experimental settings (Table 1). Endostatin-XV did not reduce endothelial cell sprouting from bone explants although endostatin-XV had been shown to reduce VEGF-stimulated angiogenesis in CAM assays (Sasaki et al., 2000).

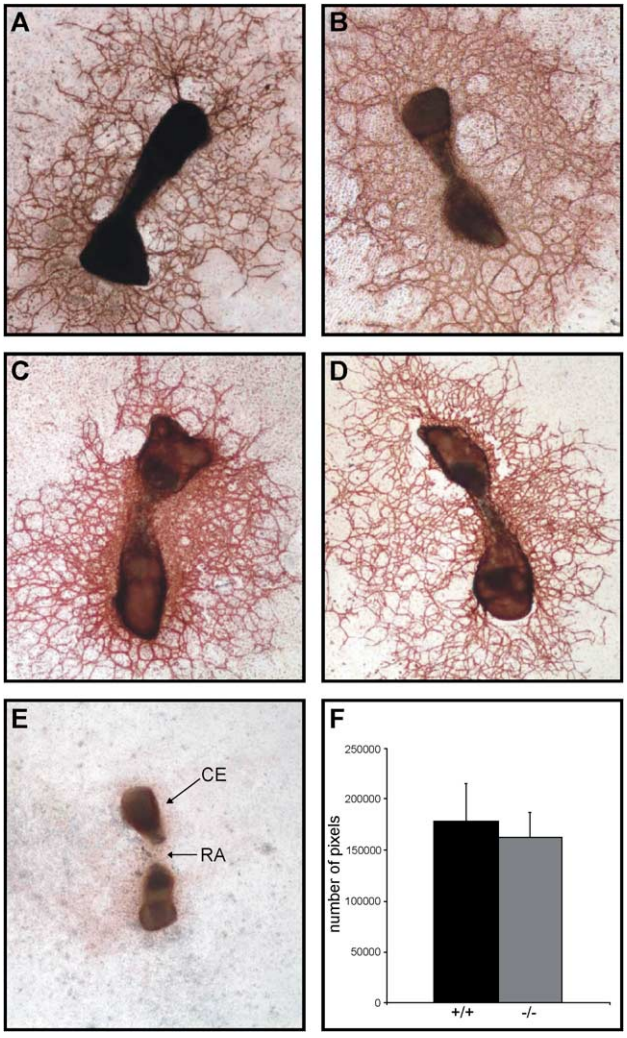

Fig. 1. Seventeen-day-old fetal mouse explants developed capillary-like structures in culture which reacted with antibodies against (A, D) PECAM-1, (B) collagen XVIII's N-terminal non-collagenous domain, and (C) collagen XVIII's C-terminal endostatin domain. The monolayer of fibroblast-like cells remained unstained. (E) No staining was observed without primary antibodies (CE=cartilage ends, RA=resorption area). The outgrowth of a PECAM-1-positive network from (D, F) collagen XVIII-deficient fetal bones (162,440±48,901 pixels) was not significantly reduced when compared to (A, F) the wildtype (178,643±72,814 pixels).

Since endostatin's heparan sulfate-binding site turned out to be required for inhibition of capillary-like outgrowth in bone explants, we examined its importance for endothelial cell binding in this model system. Murine endostatin fused to the C-terminus of heat-stable human AP (AP-mES) strongly bound to the capillary-like network (Fig. 2B,H). The non-heparan sulfate-binding mutant AP-mESR158/270A led to a weaker but specific staining of the endothelial network (Fig. 2C,I). Consistent with our activity data (Fig. 2A) and a striking spatial restriction of AP-mESXV-staining to the lense capsule in murine

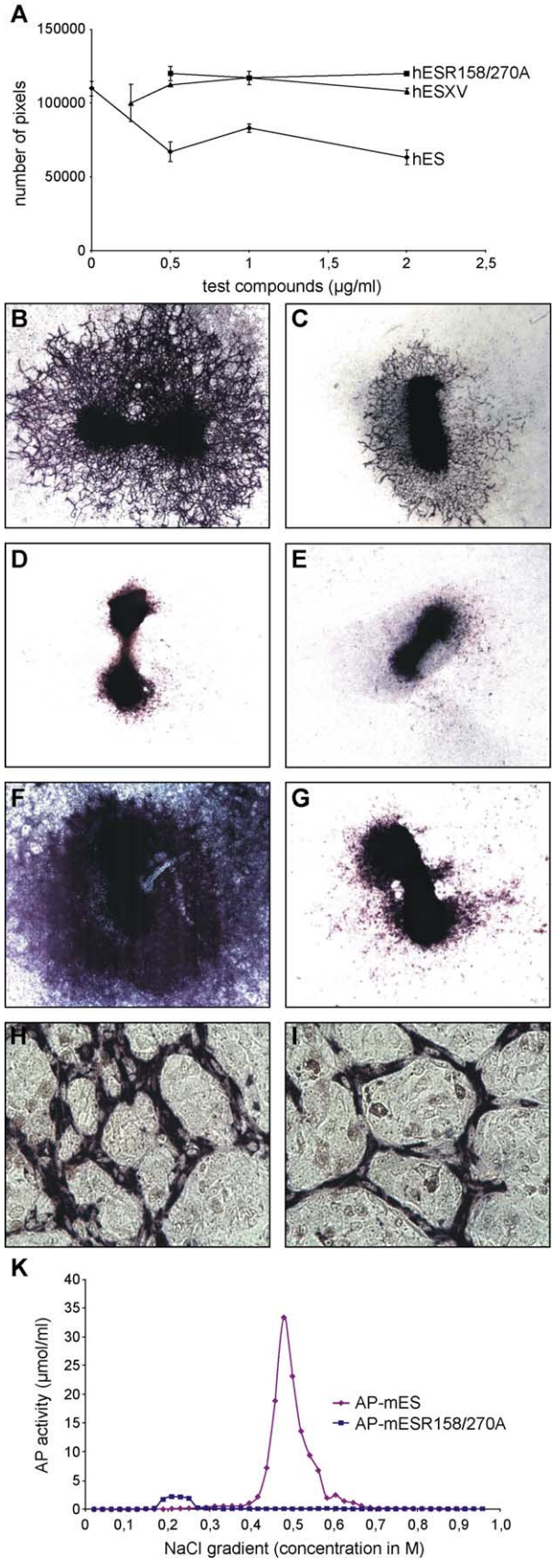

embryonal tissues (Rychkova et al., in press), AP-mESXV, like control AP, did not label endothelial cells (Fig. 2D,E). In contrast, AP-mVEGF164 reacted with both endothelial and fibroblast-like cells, while the non-heparan sulfate binding deletion variant AP-mVEGF110 was negative (Fig. 2F,G). Competition experiments with equimolar, 10- and 100-fold excess heparan sulfate from preparations known to contain 50% endostatin binding ≥12 mer molecules (Seikagaku) (Kreuger et al., 2002) did not reduce AP-mES binding to endothelial cells (data not shown). This might be explained by the fact that conditioned 293 T supernatants contain heparin/heparan sulfate binding molecules including endogenous C-terminal collagen XVIII fragments (heparin affinity chromatography data not shown). Alternatively, it is conceivable that exogenous heparin has enhancing effects on endostatin binding as has been described for VEGF (Gitay-Goren et al., 1992).

Lack of inhibitory effect on outgrowth of capillary-like structures (Fig. 2A) is associated with reduced binding of mutant endostatin (Fig. 2C). Thus, it seems plausible to assume that binding to heparan sulfates appears to be a major mechanism for activity and binding of AP-mES in bone explant angiogenesis. However, AP-mESR158/270A which was shown to have lost the ability to bind to heparin (Fig. 2K) still bound to endothelial cells with reduced affinity suggesting that this interaction occurs in the absence of heparan sulfates. This result contrasts with a previous binding assay in which non-heparan sulfate binding Fc-endostatin R27/139A failed to bind to human umbilical vein endothelial cells (Javaherian et al., 2002) but agrees with another recent study which demonstrated strong binding of biotinylated mutant endostatin R158/184/270A to murine embryonic stem cell-derived endothelial cells and

Fig. 2. (A) Effect of human endostatin (hES), non-heparin binding mutant human endostatin (hESR158/270A), and the recombinant C-terminal fragment of collagen XV (hESXV) on the formation of PECAM-1-positive tube-like structures. Only endostatin reduced outgrowth. Each compound was tested in sixtuple, and each experiment was repeated twice. (B–I) Incubation of bone explants with alkaline-phosphatase (AP) fusion proteins. (B, H) AP-mES as well as (C, I) non-heparin binding mutated AP-mESR158/270A labeled endothelial cells with their characteristic prominent nuclei in the capillary-like structures while (D) AP-mESXV and (E) AP alone did not. (F) AP-mVEGF164 labeled both the endothelial cells as well as the feeder layer of fibroblast-like cells whereas (G) the non-heparin binding form AP-mVEGF110 was negative. All explant cultures were incubated with AP fusion protein-containing supernatants for 90 min and with the NBT/BCIP substrate overnight. Staining was monitored periodically under a dissecting microscope. Blue colouration started to become visible after 1 h. The cartilage ends stained blue with the AP substrate BCIP/NBT despite 120 min heat inactivation of endogenous AP at 65°C prior to incubation with AP fusion proteins (original magnification: ×40 (B–G) and ×400 (H, I)). (K) AP-mES bound to heparin (60 ml supernatants were loaded onto HiTrap™ heparin affinity coloumns, Pharmacia) and started to elute at 0.4 M NaCl. AP-mESR158/270A was found in the unbound flow through (data not shown) and showed only residual affinity in the 180–240 mM NaCl eluate probably due to remaining arginine residues in the core protein. AP-activity measurements of the fractions were confirmed by Western blot analyses with anti-AP and anti-endostatin antibodies (data not shown).

tubes (Schmidt et al., 2004). In addition, AP-mESR158/270A strongly bound to vascular mesenchyme in the murine embryonal eye and labeled vessels of all sizes in other organs with lower affinity (Rychkova et al., in press). Furthermore, an alternative approach using pretreatment of human dermal microvascular endothelial cells with heparinase III did not decrease the association of endostatin with high and low density fractions of cell membranes but prevented recruitment of endostatin to lipid rafts and biological effects (Wickström et al., 2003). In conclusion, reduced but positive binding of AP-mESR158/270A to endothelial sprouts in the bone explant assay and to vasculatures in murine embryonal tissues implicates a complex spectrum of molecular interactions for the large multifunctional molecule endostatin including not only heparan sulfates, but also binding partners such as integrins (Rehn et al., 2001) and the matrix protein laminin (Javaherian et al., 2002).

Acknowledgements

We thank Dr. N. Fukai for providing collagen XVIII knockout mice, Drs. T. Sasaki and R. Timpl for the expression vector pCEP-Pu/AC7, Drs. D.A. Feldheim and J.G. Flanagan for the expression vector pAPtag-4, Cytimmune Sciences for the polyclonal rabbit anti-mouse endostatin antibody, and Medical and Biological Laboratories, Japan, for the polyclonal rabbit anti-mouse collagen XVIII/NC11 antibody. U.F. receives an Emmy Noether-grant from the Deutsche Forschungsgemeinschaft (Fe 432/6-1, 6-2, 6-3).

References

Chang, Z., Choon, A., Friedl, A., 1999. Endostatin binds to blood vessels in situ independent of heparan sulfate and does not compete for fibroblast growth factor-2 binding. Am. J. Pathol. 155, 71–76.

Deckers, M., van der Pluijm, G., Dooijewaard, S., Kroon, M., van Hinsbergh, V., Papapoulos, S., Löwik, C., 2001. Effect of angiogenic and antiangiogenic compounds on the outgrowth of capillary structures from fetal mouse bone explants. Lab. Invest. 81, 5–15.

Dixelius, J., Larsson, H., Sasaki, T., Holmqvist, K., Lu, L., Engström, Å., Timpl, R., Welsh, M., Claesson-Welsh, L., 2000. Endostatin-induced tyrosine kinase signaling through the Shb adaptor protein regulates endothelial cell apoptosis. Blood 95, 3403–3411.

Felbor, U., Dreier, L., Bryant, R.A., Ploegh, H.L., Olsen, B.R., Mothes, W., 2000. Secreted cathepsin L generates endostatin from collagen XVIII. EMBO J. 19, 1187–1194.

Flanagan, J.G., Cheng, H.-J., Feldheim, D.A., Hattori, M., Lu, Q., Vanderhaeghen, P., 2000. Alkaline phosphatase fusions of ligands or receptors as in situ probes for staining of cells, tissues, and embryos. Methods Enzymol. 327, 19–35.

Fukai, N., Eklund, L., Marneros, A.G., Oh, S.P., Keene, D.R., Tamarkin, L., Niemelä, M., Ilves, M., Li, E., Pihlajaniemi, T., Olsen, B.R., 2002. Lack of collagen XVIII/endostatin results in eye abnormalities. EMBO J. 21, 1535–1544.

Gitay-Goren, H., Soker, S., Vlodavsky, I., Neufeld, G., 1992. The binding of vascular endothelial growth factor to its receptors is dependent on cell surface-associated heparin-like molecules. J. Biol. Chem. 267, 6093–6098.

Javaherian, K., Park, S.Y., Pickl, W.F., LaMontagne, K.R., Sjin, R.T.T., Gillies, S., Lo, K.-M., 2002. Laminin modulates morphogenic properties of the collagen XVIII endostatin domain. J. Biol. Chem. 277, 45211–45218.

Karumanchi, S.A., Jha, V., Ramchandran, R., Karihaloo, A., Tsiokas, L., Chan, B., Dhanabal, M., Hanai, J.-I., Venkataraman, G., Shriver, Z., et al., 2001. Cell surface glypicans are low-affinity endostatin receptors. Mol. Cell 7, 811–822.

Kreuger, J., Matsumoto, T., Vanwildemeersch, M., Sasaki, T., Timpl, R., Claesson-Welsh, L., Spillmann, D., Lindahl, U., 2002. Role of heparan sulfate domain organization in endostatin inhibition of endothelial cell function. EMBO J. 21, 6303–6311.

Muragaki, Y., Abe, N., Ninomiya, Y., Olsen, B.R., Ooshima, A., 1994. The human alpha 1(XV) collagen chain contains a large amino-terminal non-triple helical domain with a tandem repeat structure and homology to alpha 1(XVIII) collagen. J. Biol. Chem. 269, 4042–4046.

Ramchandran, R., Dhanabal, M., Volk, R., Waterman, M.J.F., Segal, M., Lu, H., Knebelmann, B., Sukhatme, V.P., 1999. Antiangiogenic activity of restin, NC10 domain of human collagen XV: comparison to endostatin. BBRC 255, 735–739.

Rehn, M., Veikkola, T., Kukk-Valdre, E., Nakamura, H., Ilmonen, M., Lombardo, C.R., Pihlajaniemi, T., Alitalo, K., Vuori, K., 2001. Interaction of endostatin with integrins implicated in angiogenesis. Proc. Natl. Acad. Sci. U. S. A. 98, 1024–1029.

O'Reilly, M.S., Boehm, T., Shing, Y., Fukai, N., Vasios, G., Lane, W.S., Flynn, E., Birkhead, J.R., Olsen, B.R., Folkman, J., 1997. Endostatin: an endogenous inhibitor of angiogenesis and tumor growth. Cell 88, 277–285.

Rychkova, N., Stahl, S., Gaetzner, S. and Felbor, U. Non-heparan sulfate binding interactions of endostatin/collagen XVIII in murine development. Dev. Dyn., in press.

Sasaki, T., Larsson, H., Kreuger, J., Salmivirta, M., Claesson-Welsh, L., Lindahl, U., Hohenester, E., Timpl, R., 1999. Structural basis and potential role of heparin/heparan sulfate binding to the angiogenesis inhibitor endostatin. EMBO J. 18, 6240–6248.

Sasaki, T., Larsson, H., Tisi, D., Claesson-Welsh, L., Hohenester, E., Timpl, R., 2000. Endostatins derived from collagens XV and XVIII differ in structural and binding properties, tissue distribution and anti-angiogenic activity. J. Mol. Biol. 301, 1179–1190.

Schmidt, A., Wenzel, D., Ferring, I., Kazemi, S., Sasaki, T., Hescheler, J., Timpl, R., Addicks, K., Fleischmann, B.K., Bloch, W., 2004. Influence of endostatin on embryonic vasculo- and angiogenesis. Dev. Dyn. 230, 468–480.

Wickström, S.A., Alitalo, K., Keski-Oja, J., 2003. Endostatin associates with lipid rafts and induces reorganization of the actin cytoskeleton via down-regulation of RhoA activity. J. Biol. Chem. 278, 37895–37901.

Yamaguchi, N., Anand-Apte, B., Lee, M., Sasaki, T., Fukai, N., Shapiro, R., Que, I., Löwik, C., Timpl, R., Olsen, B.R., 1999. Endostatin inhibits VEGF-induced endothelial cell migration and tumor growth independently of zinc binding. EMBO J. 18, 4414–4423.

Anlage 5

Journal of Negative Results in BioMedicine

BioMed Central

Research

VEGF receptors on PC12 cells mediate transient activation of ERK1/2 and Akt: comparison of nerve growth factor and vascular endothelial growth factor

Ingrid Berger, Sonja Stahl, Natalia Rychkova and Ute Felbor*

Address: Department of Human Genetics, University of Würzburg, Germany

Email: Ingrid Berger - ingrid_berger@gmx.de; Sonja Stahl - sonja.stahl@biozentrum.uni-wuerzburg.de; Natalia Rychkova - nrych@mail.ru; Ute Felbor* - felbor@biozentrum.uni-wuerzburg.de

* Corresponding author

Published: 01 June 2006

Journal of Negative Results in BioMedicine 2006, **5**:8 doi:10.1186/1477-5751-5-8

Received: 04 February 2006
Accepted: 01 June 2006

This article is available from: http://www.jnrbm.com/content/5/1/8

Abstract

Vascular endothelial growth factor (VEGF) and endostatin are angiogenic and anti-angiogenic molecules, respectively, that have been implicated in neurogenesis and neuronal survival. Using alkaline phosphatase fusion proteins, we show that the PC12 neuronal cell line contains cell membrane receptors for VEGF but not for endostatin and the collagen XV endostatin homologue. Immunocytochemistry confirmed that proliferating and differentiated PC12 cells express VEGF receptors 1, 2 and neuropilin-1. While no functional effects of VEGF on PC12 cell proliferation and differentiation could be observed, a slight VEGF-induced reduction of caspase-3 activity in differentiated apoptotic PC12 cells was paralleled by transient activation of ERK1/2 and Akt. In direct comparison, nerve growth factor proved to be a strikingly more potent neuroprotective agent than VEGF.

Background

VEGF, VEGF receptor antagonists, and the C-terminal collagen XVIII fragment endostatin, an inhibitor of angiogenesis and tumor growth [1], have been tested for use in long-term therapies to enhance or reduce vascularisation [2]. Therefore, knowledge of VEGF and endostatin receptor expression patterns as well as of their non-endothelial cell functions is important. VEGF was originally identified as a vascular permeability factor [3] which turned out to be crucial for vasculo- and angiogenesis [4]. Later, non-endothelial VEGF target cells have been described in a variety of organs [5]. More recently, autocrine and paracrine functions have been observed in neurogenesis and neuronal survival in vitro and in vivo, both in the central nervous system and the peripheral nervous system [6]. Endostatin was implicated in neuronal cell migration and axon guidance in *Caenorhabditis elegans* [7]. Fc-endostatin dimers were also reported to have motogenic activity on rat pheochromocytoma PC12 cells cultured on Matrigel [8], an extracellular matrix preparation used for differentiation of endothelial cells into tube-like structures. NGF-treated PC12 cells are an established model for analysis of neuronal differentiation, neuronal survival and neurotrophin signal transduction [9]. Finally, increased neuronal and paracellular endostatin deposits were found in patients with Alzheimer's disease [10].

VEGF exerts its anti-apoptotic effect on hypoxic neurons via VEGF receptor 2 (VEGFR-2), neuropilin-1 (NRP1), the Ras/mitogen-activated protein kinase (MAPK) and the phosphatidylinositol 3-kinase (PI3K)/Akt kinase pathways [11-13] as in VEGFR-2-dependent endothelial sur-

vival [14]. Ras/MAPK and PI3K/Akt are also involved in PC12 cell survival signaling stimulated by nerve growth factor (NGF) [15,16]. Since VEGF has also been suggested to act as a neurotrophin in motoneuron degeneration [17], we intended to evaluate the effects of VEGF and endostatins on neuronal differentiation and survival in direct comparison with the prototypic neurotrophin NGF. PC12 cells were first probed with dimeric fusion proteins composed of the human placental isozyme of alkaline phosphatase (AP) at the N-terminus and murine (m) $VEGF_{164}$ or endostatins at the C-terminus. While the endostatin affinity probes did not react with PC12 cells, AP-m$VEGF_{164}$ strongly bound to proliferating and differentiated PC12 cells. Although PC12 cells were subsequently shown to express VEGF receptors 1, 2 and neuropilin-1, only a minor neuroprotective effect was observed for VEGF when compared to NGF.

Materials and methods

Cell culture

PC12 cells were a gift from Drs. M. Sendtner and S. Wiese (Department of Neurology, University of Wuerzburg, Germany). Cow pulmonary artery endothelial (CPAE) cells were purchased from ATCC (CCL-209). PC12 cells were cultured in DMEM with glutamax-I (Gibco) supplemented with 10% horse serum, 5% fetal bovine serum, 100 U/ml penicillin G, and 100 μg/ml streptomycin (Gibco) in 5% CO_2 at 37°C. For differentiation experiments, PC12 cells were plated on poly-L-ornithine coated tissue culture dishes and allowed to adhere over night (o/n). After one wash with serum-free DMEM, the cells were differentiated in serum-free DMEM containing 50 ng/ml human recombinant NGF (PAN Biotech) for 3 days [18]. Although Fc-endostatin dimer application induced the formation of multicellular PC12 aggregates on Matrigel [8], Matrigel was not chosen for the current study since it is an extracellular matrix preparation generally used for endothelial tube formation assays.

Alkaline phosphatase staining of PC12 cells

For construction and expression of AP fusion proteins see [19]. PC12 cells were either grown to 80% confluence or differentiated in 6-well plates, and AP staining was performed as described in [20]. Staining was monitored with a Nikon Eclipse TE2000-U inverted microscope and documented using the Spot Insight QE Color imaging software (Visitron). Quantitative measurement of AP fusion protein binding to proliferating PC12 cells was carried out as described previously [21].

Immunocytochemistry

PC12 cells plated on poly-L-ornithine coated glass coverslips were fixed in phosphate-buffered saline (PBS) containing 4% paraformaldehyde at room temperature for 20 min, washed three times in prewarmed tris-buffered saline (TBS) for 5 min, and incubated in blocking buffer (TBS with 10% goat serum) at room temperature for 1 h. After washing once with prewarmed TBS, the cells were incubated with anti-Flt-1 (sc-316), anti-Flk-1 (sc-504) or anti-Neuropilin (sc-5541) antibodies (2 μg/ml, Santa Cruz Biotechnology) in blocking buffer at 4°C o/n. Unbound primary antibodies were removed by washing, and the cells were incubated in 20 mM ammonium chloride solution for 30 min to reduce autofluorescence. Cells were stained for 1 h at 37°C with a secondary Cy3-conjugated goat anti-rabbit antibody (1:500, Dianova) in blocking buffer. After washing, the coverslips were mounted in Kaiser's glycerol gelatine (Merck). Fluorescent preparations of proliferating PC12 cells were documented at 600-fold magnification (Nikon Eclipse TE2000-U). Image acquisition of differentiated PC12 cells was performed with a Zeiss Axiophot at 1000-fold magnification.

Cell proliferation and cell death analyses

PC12 cell proliferation upon stimulation with 50 and 100 ng/ml $VEGF_{165}$ (R&D Systems) was assayed after 24 h, 48 h, and 72 h using the CellTiter 96® AQueous One Solution Cell Proliferation Assay (Promega). These assays were performed using two different cell densities (2×10^4 cells/cm^2 and 6.7×10^4 cells/cm^2) and full serum as well as serum-deprived conditions (0.1% and 0.4% horse serum). In addition, increasing $VEGF_{165}$ concentrations from 0.2 to 400 ng/ml were added to PC12 cells cultured in 5% fetal bovine serum, and [^{3}H]thymidine incorporation was measured 72 hours after onset of stimulation. The fluorometric CaspACE™ Assay System and western blot analyses with an anti-cleaved caspase-3 antibody (1:1000, Cell Signaling, #9664) were used to monitor apoptosis of differentiated PC12 cells (see below). All experiments were performed in triplicate.

SDS-PAGE/Western blot analyses of differentiated apoptotic PC12 cell lysates

PC12 cells were grown to 50% confluence in 10 cm tissue culture dishes and NGF-differentiated for 72 h in serum-free DMEM. For induction of apoptosis, cells were washed three times with serum-free DMEM and incubated for 7.5 h under serum-deprived conditions in NGF-free DMEM. After addition of exogenous recombinant human $VEGF_{165}$ (R&D Systems) for the indicated time frames, PC12 cells were washed once with ice-cold PBS containing 100 μM sodium orthovanadate, followed by centrifugation at 5000 rpm for 5 min at 4°C. The cells were lysed in 200 μl of ice-cold lysis-buffer (HEPES, pH 7.8, 150 mM KOAc, 50 mM ß-glycerolphosphate, 25 mM NaF, 10 mM $MgCl_2$, 5 mM EGTA, 1 mM EDTA, 10% glycerol, 1% Triton X-100, 0,05% (v/v) ß-mercaptoethanol, 1 μg/ml aprotinin, 6 μg/ml chymostatin, 1 μg/ml leupeptin, 1 μg/ml pepstatin A, 1 mM PMSF, 1 mM sodium orthovanadate). Supernatants were collected after centrifugation at 14 000 rpm for 10

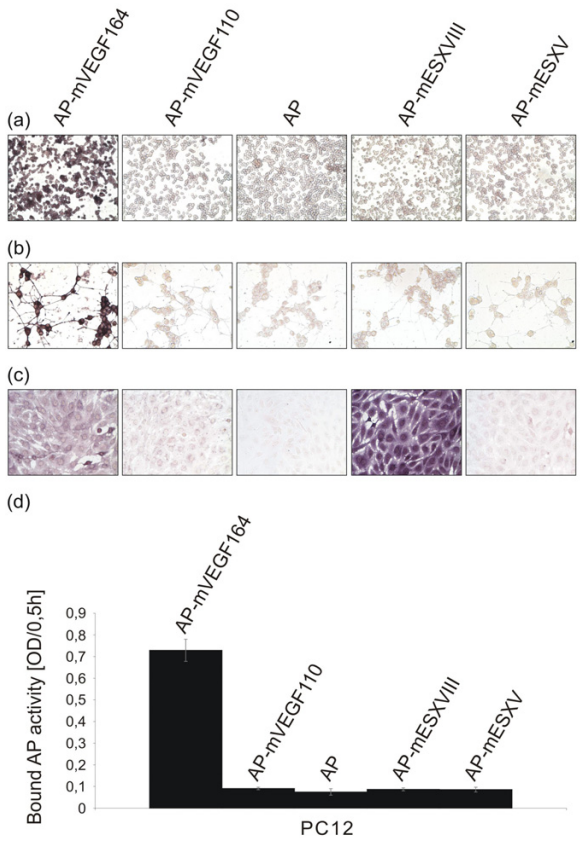

Figure 1
Alkaline phosphatase (AP) staining of (**a, d**) proliferating and (**b**) differentiated PC12 cells revealed binding of the AP-$mVEGF_{164}$ affinity probe while AP-murine endostatin (AP-mESXVIII) only stained (**c**) endothelial cells.

min at 4°C. Standardized samples containing 50 μg of whole protein (Bradford assay) were separated using 10–20% gradient gels. Proteins were wetblotted onto nitrocellulose and probed with anti-phospho-ERK1/2 (1:2000, Sigma, M8159) or anti-phospho-Akt-Ser473 (1:1000, Cell Signaling, #9271) antibodies. The blots were stripped and reprobed with antibodies detecting the respective non-phosphorylated proteins (anti-ERK1, 1:1000, Santa Cruz Biotechnology, sc-94; anti-Akt, 1:1000, Cell Signaling, #9272). Horseradish peroxidase-conjugated secondary antibodies (1:2000, Dianova) were visualized by enhanced chemiluminescence detection (Western Lightning™ Chemiluminescence Reagent System, PerkinElmer). Experiments were performed in triplicate.

Results

Differential cell binding of VEGF and endostatins

To determine the expression profile of binding partners for murine $VEGF_{164}$, endostatin and the collagen XV endostatin homologue on neuronal and endothelial cell lines, PC12 and CPAE cells were incubated with AP fusion proteins. The AP-$mVEGF_{164}$ affinity probe strongly stained proliferating and differentiated PC12 cells (Fig. 1a, b). In contrast, AP-$mVEGF_{110}$ which lacks the C-terminal heparan sulfate binding domain, the endostatin domain of collagen XVIII (AP-mESXVIII), and the collagen XV endostatin homologue (AP-mESXV) did not bind to PC12 cells. Both AP-$mVEGF_{164}$ and AP-mESXVIII labelled CPAE cells while AP-$mVEGF_{110}$, AP-mESXV and control AP did not (Fig. 1c). Quantitative measurement of AP fusion protein binding to proliferating PC12 cells confirmed the above results (Fig. 1d). In agreement with lack of AP-mESXVIII and AP-mESXV binding to PC12 cells, recombinant human endostatins [22] did neither promote nor inhibit PC12 cell differentiation (data not shown). Thus, PC12 cells are not a useful model for understanding endostatin effects on cells.

PC12 cells express high-affinity VEGF receptors

Consistent with AP staining, it was shown by immunofluorescence that PC12 cells express the high-affinity receptor tyrosine kinases VEGF receptor 1 and 2 (VEGFR-1, VEGFR-2) as well as the low-affinity receptor neuropilin-1 (Fig. 2). These receptors are expressed on the cell surface of proliferating (Fig. 2a–c) and differentiated (Fig. 2e) PC12 cells and seem to possess a clustered morphology reminiscent of activated tyrosine kinases. Comparable results were obtained with antibodies from Santa Cruz Biotechnology and Dianova (data not shown).

VEGF induces transient activation of ERK1/2 and Akt kinase in differentiated apoptotic PC12 cells

While the addition of $VEGF_{165}$ had no effect on PC12 cell proliferation and neurite formation, a consistent but non-significant reduction of caspase-3 activity became apparent when $VEGF_{165}$ was administered to differentiated apoptotic PC12 cells (data not shown). To analyze VEGF signaling in PC12 cell survival, the activation of extracellular signal-regulated kinases ERK1/2 and Akt was examined by Western blot analyses using phospho-specific antibodies and their respective non phosphorylated counterparts. Control cultures demonstrated that ERK1/2 (p44/p42 MAPK) and Akt activation are sustained for 79.5 h in the presence of NGF (Fig. 3, lane 1). Removal of NGF for 7.5 h after 72 hours of differentiation led to a significant reduction of ERK1/2 and Akt phosphorylation (Fig. 3, lane 2). Exogenous addition of 100 ng/ml $VEGF_{165}$ to NGF-deprived PC12 cells resulted in transient ERK1/2 activity within 7–10 min which decreased almost to control levels 20 min after stimulation (Fig. 3, lanes 3, 4, and data not shown). Higher concentrations of recombinant VEGF (200 ng/ml) did not increase or prolong ERK1/2 activity (data not shown). Similar activation kinetics were observed for phosphorylation of Akt at serine 473 (Fig. 3). For comparison of signaling mechanisms, apoptotic PC12

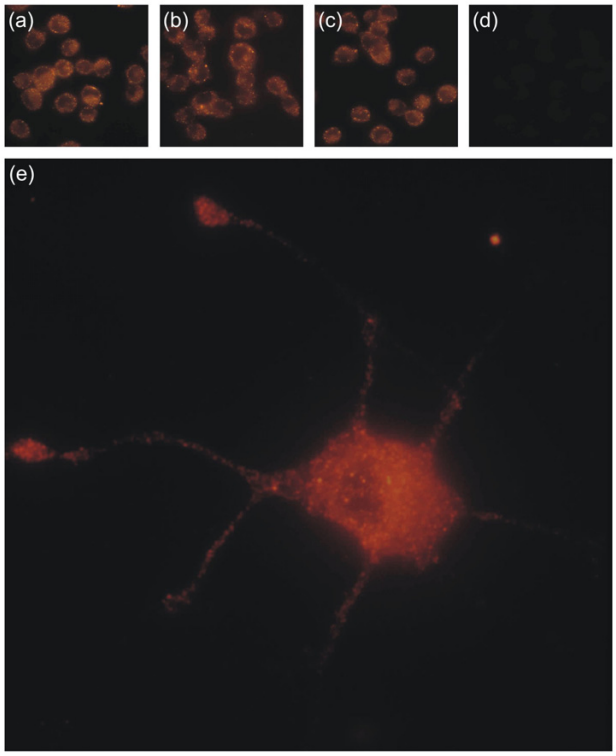

Figure 2
Immunodetection of VEGF receptors expressed on the cell surface of (**a-d**) proliferating and (**e**) differentiated PC12 cells. PC12 cells were stained with polyclonal antibodies against (**a**) VEGFR-1, (**b, e**) VEGFR-2, and (**c**) neuropilin-1. The primary antibody was omitted in (**d**) controls. Differentiated PC12 cells were also immunoreactive for VEGFR-1 and neuropilin-1 (data not shown).

cells were also NGF-stimulated. NGF-stimulation induced a much more pronounced and sustained activation of ERK1/2 and Akt which was even more prominent than in NGF treated non-apoptotic control cells (Fig. 3, lanes 5, 6).

Discussion

We here report that endostatin affinity probes derived from collagens XVIII and XV do not bind to PC12 cells indicating that these cells do not express endostatin cell membrane receptors. This observation is consistent with absent effects of recombinant endostatins on neurite outgrowth (data not shown) and lack of binding of AP-mESXVIII and AP-mESXV to murine embryonal nerve tissues [19]. AP-mESXVIII predominantly labelled blood vessels while AP-mESXV binding was restricted to the lense capsule [19] which correlates with the current results that only AP-mESXVIII, but not AP-mESXV, strongly stained CPAE cells. As opposed to the endostatin affinity probes, AP-mVEGF$_{164}$ showed strong binding to PC12 cells. Undifferentiated PC12 cells were known to express VEGF to stimulate angiogenesis [23]. We now demonstrate that proliferating and differentiated PC12 cells also express VEGFR-1 and -2 and NRP1. NRP1 acts as an isoform-specific VEGF co-receptor which only binds VEGF$_{165}$ [24]. Since C-terminally deleted AP-mVEGF$_{110}$ did not bind to PC12 cells, NRP1 appears to be required for the interaction of VEGF$_{165}$ with PC12 cells.

Despite prominent expression of VEGF receptors on PC12 cells, exogenous VEGF$_{165}$ had no effect on PC12 cell proliferation and neurite formation. One reason might be endogenous VEGF-expression of proliferating PC12 cells which is downregulated only 48 h after induction of differentiation with NGF [23]. This would also explain the slight anti-apoptotic effect of VEGF$_{165}$ on PC12 cells that had been differentiated for three days prior to VEGF$_{165}$ stimulation. However, only an insignificant decrease of cell proliferation could be observed upon treatment with an antibody against rat VEGF$_{164}$ (data not shown). Thus, our data are in line with the observation that VEGFR-1-expressing cells show a poor mitogenic response to VEGF stimulation [5]. Analysis of VEGF$_{165}$-induced signal transduction in differentiated apoptotic PC12 cells demonstrated activation of ERK1/2 and Akt. The transient nature of VEGF$_{165}$-triggered ERK1/2 phosphorylation in PC12 cells provides a further explanation for the observation that VEGF$_{165}$ was not able to induce PC12 cell differentiation which is known to require sustained activation of the MAPK cascade [25]. The inefficient rescue of PC12 cells from apoptosis through VEGF$_{165}$ is likely also due to its short-lived and relatively small effect on ERK1/2 and Akt.

VEGF-induced neuroprotective signaling via VEGFR-2, NRP1 and the two above-mentioned signaling cascades was shown in hypoxic and glucose-deprived hippocampal neuron × neuroblastoma (HN33) hybrid cells [11], in rat primary hippocampal neurons that had been exposed to glutamate [12], and in hypoxic murine primary cortical neurons [13]. In these in vitro model systems of cerebral ischemia, no comparison of VEGF and NGF activation kinetics was performed. Our results on growth factor stimulated PC12 cells show that both the anti-apoptotic effect and the activation of ERK1/2 and Akt were transient and minor when compared to NGF. It remains to be clarified whether this is a consequence of experimental conditions, cell line-specific or a general feature of VEGF-induced neuroprotection.

Conclusion

Based on experiments using growth factor deprivation, the present study suggests that NGF protects neuronal cells from cell death much more efficiently than VEGF$_{165}$. The significant NGF-induced reduction of caspase-3 activity in differentiated apoptotic PC12 cells correlates with a

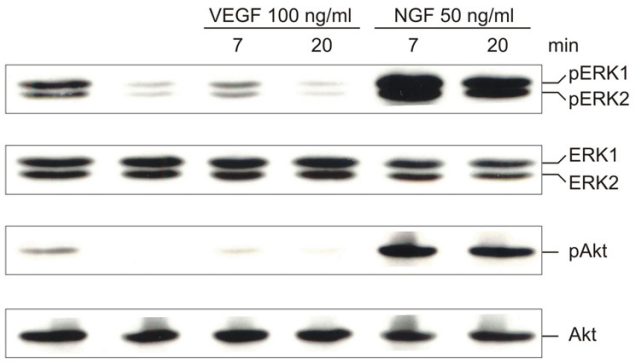

Figure 3
Western blot analyses of VEGF-induced signal transduction in differentiated PC12 cells after NGF withdrawal. Lysates of control cells maintained in the presence of NGF were loaded in lane 1. NGF-deprived PC12 cells (lane 2) treated with $VEGF_{165}$ (lanes 3, 4) or NGF (lanes 5, 6) demonstrated that $VEGF_{165}$ induced transient activation of ERK1/2 and Akt after 7 min. In contrast, NGF produced a stronger and persistent phosphorylation of ERK1/2 and Akt than $VEGF_{165}$.

much more pronounced and prolonged activation of downstream effectors when compared to $VEGF_{165}$. Thus, the angiogenic compound $VEGF_{165}$ may only be a minor player in neurogenesis and neuronal survival and may only have little therapeutic and side effects on neuronal cells.

Acknowledgements

This work was supported by an Emmy Noether-grant from the Deutsche Forschungsgemeinschaft (Fe 432/6-4). Sonja Stahl receives a stipend from the Graduiertenkolleg 1048.

References

1. O'Reilly MS, Boehm T, Shing Y, Fukai N, Vasios G, Lane WS, Flynn E, Birkhead JR, Olsen BR, Folkman J: **Endostatin: an endogenous inhibitor of angiogenesis and tumor growth.** *Cell* 1997, **88:**277-285.
2. Cross MJ, Dixelius J, Matsumoto T, Claesson-Welsh L: **VEGF-receptor signal transduction.** *Trends Biochem Sci* 2003, **28:**488-494.
3. Senger DR, Galli SJ, Dvorak AM, Perruzzi CA, Harvey VS, Dvorak HF: **Tumor cells secrete a vascular permeability factor that promotes accumulation of ascites fluid.** *Science* 1983, **219:**983-985.
4. Ferrara N, Gerber HP, LeCouter J: **The biology of VEGF and its receptors.** *Nat Med* 2003, **9:**669-676.
5. Matsumoto T, Claesson-Welsh L: **VEGF receptor signal transduction.** *Sci STKE* 2001, **2001(112):**RE21.
6. Storkebaum E, Lambrechts D, Carmeliet P: **VEGF: once regarded as a specific angiogenic factor, now implicated in neuroprotection.** *Bioessays* 2004, **26:**943-954.
7. Ackley BD, Crew JR, Elamaa H, Pihlajaniemi T, Kuo CJ, Kramer JM: **The NC1/endostatin domain of Caenorhabditis elegans type XVIII collagen affects cell migration and axon guidance.** *J Cell Biol* 2001, **152:**1219-1232.
8. Kuo CJ, LaMontagne KRJ, Garcia-Cardena G, Ackley BD, Kalman D, Park S, Christofferson R, Kamihara J, Ding YH, Lo KM, Gillies S, Folkman J, Mulligan RC, Javaherian K: **Oligomerization-dependent regulation of motility and morphogenesis by the collagen XVIII NC1/endostatin domain.** *J Cell Biol* 2001, **152:**1233-1246.
9. Kaplan DR, Miller FD: **Signal transduction by the neurotrophin receptors.** *Curr Opin Cell Biol* 1997, **9:**213-221.
10. Deininger MH, Fimmen BA, Thal DR, Schluesener HJ, Meyermann R: **Aberrant neuronal and paracellular deposition of endostatin in brains of patients with Alzheimer's disease.** *J Neurosci* 2002, **22:**10621-10626.
11. Jin KL, Mao XO, Greenberg DA: **Vascular endothelial growth factor: direct neuroprotective effect in in vitro ischemia.** *Proc Natl Acad Sci U S A* 2000, **97:**10242-10247.
12. Matsuzaki H, Tamatani M, Yamaguchi A, Namikawa K, Kiyama H, Vitek MP, Mitsuda N, Tohyama M: **Vascular endothelial growth factor rescues hippocampal neurons from glutamate-induced toxicity: signal transduction cascades.** *FASEB J* 2001, **15:**1218-1220.
13. Ogunshola OO, Antic A, Donoghue MJ, Fan SY, Kim H, Stewart WB, Madri JA, Ment LR: **Paracrine and autocrine functions of neuronal vascular endothelial growth factor (VEGF) in the central nervous system.** *J Biol Chem* 2002, **277:**11410-11415.
14. Gerber HP, McMurtrey A, Kowalski J, Yan M, Keyt BA, Dixit V, Ferrara N: **Vascular endothelial growth factor regulates endothelial cell survival through the phosphatidylinositol 3'-kinase/Akt signal transduction pathway. Requirement for Flk-1/KDR activation.** *J Biol Chem* 1998, **273:**30336-30343.
15. Xia Z, Dickens M, Raingeaud J, Davis RJ, Greenberg ME: **Opposing effects of ERK and JNK-p38 MAP kinases on apoptosis.** *Science* 1995, **270:**1326-1331.
16. Wert MM, Palfrey HC: **Divergence in the anti-apoptotic signalling pathways used by nerve growth factor and basic fibroblast growth factor (bFGF) in PC12 cells: rescue by bFGF involves protein kinase C delta.** *Biochem J* 2000, **352 Pt 1:**175-182.
17. Sopher BL, Thomas PSJ, LaFevre-Bernt MA, Holm IE, Wilke SA, Ware CB, Jin LW, Libby RT, Ellerby LM, La Spada AR: **Androgen receptor YAC transgenic mice recapitulate SBMA motor neuronopathy and implicate VEGF164 in the motor neuron degeneration.** *Neuron* 2004, **41:**687-699.
18. Gotz R, Karch C, Digby MR, Troppmair J, Rapp UR, Sendtner M: **The neuronal apoptosis inhibitory protein suppresses neuronal differentiation and apoptosis in PC12 cells.** *Hum Mol Genet* 2000, **9:**2479-2489.
19. Rychkova N, Stahl S, Gaetzner S, Felbor U: **Non-heparan sulfate-binding interactions of endostatin/collagen XVIII in murine development.** *Dev Dyn* 2005, **232:**399-407.
20. Flanagan JG, Cheng HJ, Feldheim DA, Hattori M, Lu Q, Vanderhaeghen P: **Alkaline phosphatase fusions of ligands or receptors as in situ probes for staining of cells, tissues, and embryos.** *Methods Enzymol* 2000, **327:**19-35.
21. Stahl S, Gaetzner S, Mueller TD, Felbor U: **Endostatin phenylalanines 31 and 34 define a receptor binding site.** *Genes to Cells* 2005, **10(9):**929-39.
22. Gaetzner S, Deckers MM, Stahl S, Lowik C, Olsen BR, Felbor U: **Endostatin's heparan sulfate-binding site is essential for inhibition of angiogenesis and enhances in situ binding to capillary-like structures in bone explants.** *Matrix Biol* 2005, **23:**557-561.
23. Claffey KP, Wilkison WO, Spiegelman BM: **Vascular endothelial growth factor. Regulation by cell differentiation and acti-**

vated second messenger pathways. *J Biol Chem* 1992, **267:**16317-16322.
24. Soker S, Fidder H, Neufeld G, Klagsbrun M: **Characterization of novel vascular endothelial growth factor (VEGF) receptors on tumor cells that bind VEGF165 via its exon 7-encoded domain.** *J Biol Chem* 1996, **271:**5761-5767.
25. Traverse S, Gomez N, Paterson H, Marshall C, Cohen P: **Sustained activation of the mitogen-activated protein (MAP) kinase cascade may be required for differentiation of PC12 cells. Comparison of the effects of nerve growth factor and epidermal growth factor.** *Biochem J* 1992, **288 (Pt 2):**351-355.

Anlage 6

Endostatin phenylalanines 31 and 34 define a receptor binding site

Sonja Stahl[1], Sabine Gaetzner[1], Thomas D. Mueller[2] and Ute Felbor[1,*]

[1]*Department of Human Genetics, and* [2]*Department of Physiological Chemistry II, University of Würzburg, Biozentrum, Am Hubland, D-97074 Würzburg, Germany*

Endostatin has achieved much attention as a naturally occurring inhibitor of angiogenesis and tumor growth. Endostatin is derived from collagen XVIII's C-terminal domain and deleted or truncated in most patients suffering from Knobloch syndrome blindness. To evaluate the functional significance of two surface-exposed hydrophobic phenylalanines at positions 31 and 34 of endostatin and two human sequence alterations within endostatin, A48T and D104N, we applied the alkaline phosphatase fusion protein method. Replacement of F31 and F34 with alanines led to complete loss of characteristic *in situ* binding while heparin binding remained intact. In contrast, a non-heparin binding alkaline phosphatase-tagged human endostatin lacking R27 and R139 bound to specific tissue structures. The two Knobloch syndrome-associated endostatin sequence variants did not result in altered *in situ* binding to murine embryonal tissues, human endothelial cells, heparin and immobilized laminin. However, expression of the endostatin mutant A48T was significantly reduced. This observation may be explained by a lower folding efficiency due to the structural constraints of A48 residing in the hydrophobic core. Our data suggest that residues F31 and F34 form a putative receptor binding site acting independently from heparan sulfate binding and that the A48T mutation destabilizes the endostatin molecule.

Introduction

Knobloch syndrome (MIM# 267750) is an autosomal recessive disorder characterized by an early onset progressive generalized eye disease and a congenital occipital encephalocele (Knobloch & Layer 1971; Czeizel *et al.* 1992; Seaver *et al.* 1993; Passos-Bueno *et al.* 1994; Wilson *et al.* 1998; Sniderman *et al.* 2000). High myopia and vitreoretinal degeneration are the main features of the ocular defect in Knobloch syndrome and lead to bilateral blindness during childhood in most cases. The cranial defect can be corrected surgically within the first year of life. It remains unclear whether other singular abnormalities such as lung hypoplasia, cardiac dextroversion, neuronal migration defects, dilatation of brain ventricles, unilateral duplicated renal collecting systems and generalized hyperextensibility of joints belong to the disease spectrum of Knobloch syndrome.

Communicated by: Yo-ichi Nabeshima
**Correspondence*: E-mail: felbor@biozentrum.uni-wuerzburg.de

Knobloch syndrome is caused by homozygous or compound heterozygous mutations in the *COL18A1* gene on 21q22.3 (Sertié *et al.* 2000; Suzuki *et al.* 2002; Kliemann *et al.* 2003; Menzel *et al.* 2004). Most mutations result in premature stop codons that affect all three alternatively spliced *COL18A1* isoforms. A homozygous splice site mutation that exclusively affects collagen XVIII's shortest isoform has been associated with a less severe ocular pathology and loss of vision beyond 20 years of age in a large consanguineous Brazilian kindred (Sertié *et al.* 2000). Consistent with the human phenotype, collagen XVIII knockout mice show complex ocular abnormalities including delayed regression of hyaloid arteries and abnormal outgrowth of retinal vessels during the first weeks of life (Fukai *et al.* 2002; Marneros & Olsen 2003; Ylikärppä *et al.* 2003; Marneros *et al.* 2004). On a specific C57BL background, collagen XVIII knockout mice also develop hydrocephalus, dilatation of brain ventricles, and markedly broadened basement membranes in atrioventricular valves of the heart and in the kidney tubules with elevated serum creatinine levels (Utriainen *et al.* 2004). This suggests that the absence of

DOI: 10.1111/j.1365-2443.2005.00890.x

a functional collagen XVIII molecule can cause other phenotypic alterations depending on genetic background.

Collagens XVIII and XV are non-fibrillar basement membrane molecules characterized by multiple interruptions in their central triple helical region and a unique highly homologous C-terminal domain (Oh *et al.* 1994a; Rehn & Pihlajaniemi 1994). This globular C-terminal 20 kDa endostatin domain of collagen XVIII is separated from a 50 residue association domain responsible for homotrimerization of collagen α1(XVIII) chains by a protease-sensitive hinge region (Sasaki *et al.* 1998). After proteolytic cleavage, endostatin is a potent inhibitor of angiogenesis and tumor growth (O'Reilly *et al.* 1997; Felbor *et al.* 2000). However, its receptors and mechanisms of action are still insufficiently characterized. As far as endostatin's physiological role within collagen XVIII is concerned, we recently suggested that endostatin harbors a prominent tissue-binding site for collagen XVIII, based on *in situ*-binding experiments to murine embryonal eye tissues (Rychkova *et al.* 2005). This notion agrees with the observation that deletion of the entire C-terminal non-collagenous domain of collagen XVIII still results in a stable truncated product in *C. elegans* (Ackley *et al.* 2001). Six of nine known independently arisen *COL18A1* mutations are located in exons 35, 36, 40 and 41, leading to a premature stop just before or within the C-terminal endostatin region encoded by exons 41–43 (Suzuki *et al.* 2002; Menzel *et al.* 2004). Assuming the importance of endostatin for tissue binding, these mutations would result in absent binding of collagen XVIII to vascular mesenchyme in ocular tissues and endothelial and epithelial basement membranes.

The only two known nucleotide substitutions associated with early-onset progressive Knobloch syndrome are also located within collagen XVIII's endostatin domain: two affected sibs have been reported with a homozygous replacement of a conserved alanine to threonine at position 48 within the endostatin domain (Kliemann *et al.* 2003). This A48T endostatin mutation corresponds to A179T in the non-collagenous domain of collagen XVIII, a terminology used by Kliemann *et al.* (2003). In addition, a compound heterozygous D104N endostatin polymorphism (dbSNP/rs12483377) was reported in two further Knobloch sibs (Menzel *et al.* 2004) but remains of unclear functional relevance (Antonarakis *et al.* 2005; Suzuki *et al.* 2005). While this particular variant has also been associated with increased risk for prostate cancer (Iughetti *et al.* 2001) recent *in vitro* angiogenesis studies suggest that the D104N endostatin variant is not functionally relevant on its own (Macpherson *et al.* 2004).

In the present study, we generated a systematic set of human alkaline phosphatase (AP) endostatin fusion proteins in order to analyze *in situ* binding of human endostatin mutants. We first show that the human endostatin domain of collagen XVIII binds to very specific structures such as the lense capsule in the eye which might suggest a lenticular contribution to the pathogenesis of Knobloch syndrome's myopia. Furthermore, we identify amino acid residues responsible for tissue binding and provide evidence that the recently reported human A48T amino acid substitution within endostatin is of functional significance.

Results

Complementary to expression pattern analyses based on RNA *in situ* hybridization and immunohistochemistry, dimeric APtags can be used to localize, characterize, and identify functionally active molecules that are capable of ligand-receptor binding (Flanagan *et al.* 2000). The AP-human endostatin (AP-hES) fusion proteins generated in this study are comprised of a heat-stable, secreted human placental isozyme of AP at the N-terminus and human endostatin at the C-terminus. Endostatin was fused to the C-terminus of AP because endostatin is the C-terminal domain of collagen XVIII. Two hydrophobic phenylalanines at positions 31 and 34 which are unusually exposed in the crystal structure of both murine and human endostatins were replaced by alanines: AP-hESF31/34A. In addition, the A48T replacement reported in two Knobloch sibs and the D104N endostatin polymorphism were introduced into AP-hES: AP-hESA48T and AP-hESD104N (for location of the above residues see Fig. 1A,B). Furthermore, two arginine residues known to be responsible for nonspecific binding of endostatin to heparan sulfate-containing proteoglycans on cell surfaces (Sasaki *et al.* 1999) were changed to alanines (AP-hESR27/139A). Since the murine equivalent of the arginine/alanine mutant is known to show reduced background staining on tissue sections after longer incubation times (Rychkova *et al.* 2005), the A48T replacement and the D104N endostatin polymorphism were combined with the arginine double substitutions to generate triple mutant proteins: AP-hESR27/139A/A48T and AP-hESR27/139A/D104N. Finally, unfused AP was used as a negative control.

Protein production by transiently transfected 293T cells was monitored using quantitative AP activity measurement and Western blot analyses. Apart from AP-hESA48T and AP-hESR27/139A/A48T, all fusion protein-containing supernatants and control AP had AP activities comparable to those obtained from conditioned

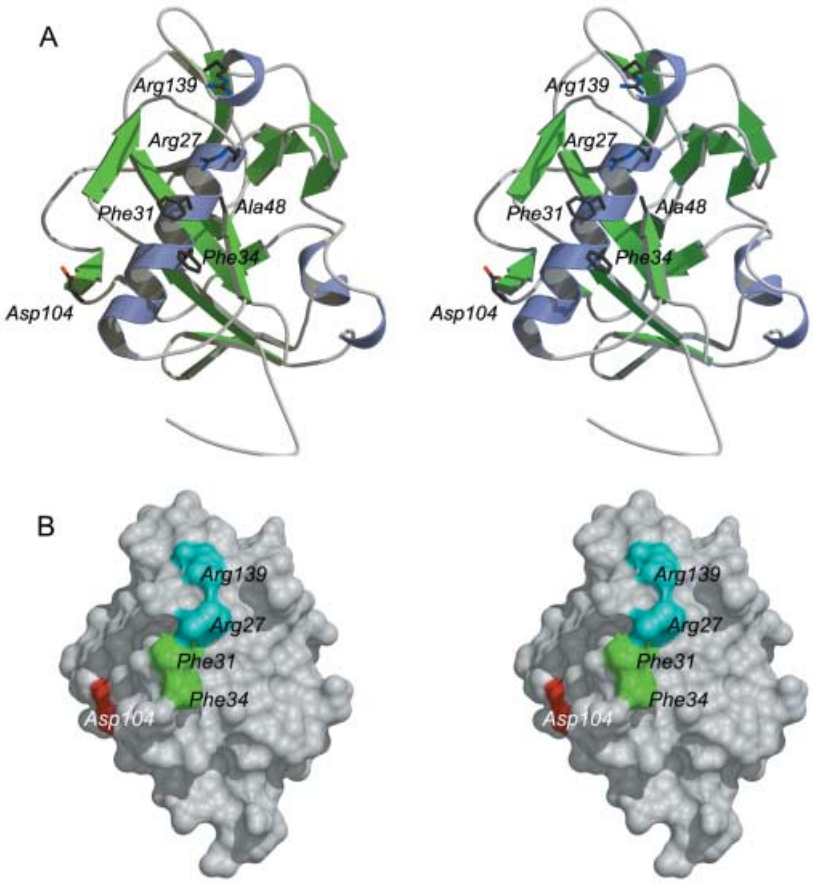

Figure 1 Stereo view of a ribbon (A) and the respective molecular surface representation (B) of human endostatin (PDB entry code 1BNL). (A) The side chains of residues R27, F31, F34, A48, D104, and R139 investigated in this study are shown as stick models and labeled accordingly. Ribbon and surface representation are oriented identically; the latter clearly shows that A48 is not accessible at the surface and hidden inside the hydrophobic core.

media containing murine endostatins fused to AP (AP-mES, AP-mESR158/270A, and AP-mESXV) which had been previously generated (Rychkova *et al*. 2005). Interestingly, cells expressing AP-hESA48T and AP-hESR27/139A/A48T repeatedly produced approximately 40% less (e.g. mean of 1.17 μmol/mL for AP-hESA48T instead of 2.023 μmol/mL for AP-hES, data not shown). The control supernatant of non-transfected 293T cells showed only background activity (data not shown). For all subsequent experiments, the supernatants were diluted to identical volume activities. Western blot analyses demonstrated that a polyclonal antibody against secreted human placental alkaline phosphatase reacted with AP fusion proteins of the expected size in supernatants of transfected cells whereas the supernatant of non-transfected cells did not react with this antibody (data not shown). Fusion proteins were also detected with a rabbit polyclonal anti-human endostatin antibody (Fig. 2A) and quantified by Western blot analyses with known amounts of recombinant human endostatin. Ten microliters conditioned supernatants contained approximately 20 ng of fusion proteins (Fig. 2B).

The equivalence of the highly conserved murine and human AP-endostatin fusion proteins was analyzed using *in situ* staining of 14-day-old (E14.5) murine embryonal eyes because murine endostatin as well as the murine non-heparin binding endostatin mutant bind particularly well to the tunica vasculosa lentis (Rychkova *et al*. 2005). Both endostatin affinity probes, AP-mES (data not shown) and AP-hES (Fig. 3A), stained the lense capsule equally well. In contrast, the AP-hESF31/34A fusion protein completely lacked characteristic staining of the lense capsule (Fig. 3B). The mutant AP-hESA48T, AP-hESD104N and AP-hESR27/139A probes resulted in comparable staining patterns (Fig. 3C–E). Control AP did not stain the eye section (Fig. 3F). These results were confirmed by *in situ* labeling of murine E14.5 sagittal sections (representative examples in Fig. 3G–I). Thus, stainings of all major tissues demonstrated that the observations obtained from ocular tissues can be generalized to endothelial and epithelial basement membranes.

For quantitation of AP fusion protein binding, cultured human dermal microvascular endothelial cells (HMEC-1) were incubated with AP affinity probes for

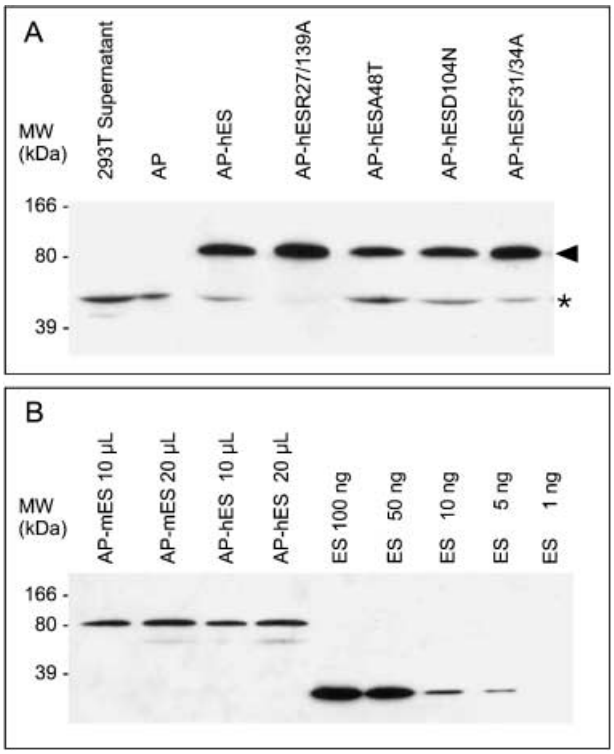

Figure 2 Representative Western blots probed with a polyclonal anti-human endostatin antibody. (A) All fusion proteins (arrow head) migrated at the expected molecular weight on 5–15% gradient SDS-PAGE gels (AP, alkaline phosphatase, 67 kDa; ES, endostatin, 20–22 kDa; h, human). Note that the antibody detects an endogenous endostatin-containing C-terminal fragment of collagen XVIII (*) indicating that 293T cells produce and process collagen XVIII. (B) Quantification of AP fusion proteins by Western blot analysis using known amounts of recombinant purified endostatin.

90 min, washed, lyzed, and assayed for bound AP activity. AP-mES showed stronger binding to HMEC-1 than AP-hES (Fig. 4A). The human A48T and D104N endostatin mutants did not show a statistically significant reduction in affinity to HMEC-1 when compared to AP-hES. In contrast, AP-hESF31/F34h did not bind to HMEC-1. The non-heparin/heparan sulfate binding mutants showed reduced cell binding (data not shown) indicating either that these cells do not contain a significant amount of high affinity receptors or that heparan sulfates are a prerequisite for endostatin binding to these cells.

Heparin/heparan sulfate affinity is a key feature of endostatin (Gitay-Goren *et al.* 1992; Sasaki *et al.* 1999) and many other growth factors such as vascular endothelial growth factor (Gitay-Goren *et al.* 1992; Sasaki *et al.* 1999). Therefore, we analyzed whether the human amino acid changes would lead to reduced/enhanced binding to heparin using affinity chromatography (Fig. 4B). AP-hES, AP-hESF31/34A, AP-hESA48T, and AP-hESD104N all bound to HiTrap™ heparin affinity columns (Pharmacia) and required 0.38 M NaCl for displacement. Thus, these amino acid changes do not influence endostatin's ability to bind to heparin. As expected, the non-heparin/heparan sulfate binding mutant AP-hESR27/139A had only residual affinity to the heparin affinity resin. The affinity of AP-hESF31/34A to heparin provides a possible explanation for the observed unspecific background staining in tissue sections (Fig. 3H).

Collagen XVIII has a polarized location in basement membranes with its C-terminal endostatin domain embedded in the basement membrane facing the endothelial/epithelial cell and the N-terminal non-collagenous domain located at the basement membrane–matrix interface (Fukai *et al.* 2002; Marneros & Olsen 2003; Ylikärppä *et al.* 2003; Marneros *et al.* 2004). Recently, a two receptor model for endostatin binding was proposed. In an *in vitro* Matrigel tube formation model system, oligomeric endostatin bound to heparan sulfates on cell surfaces and to laminin in the basement membrane (Javaherian *et al.* 2002). Binding of the immobilized trimeric-non-collagenous domain 1 of collagen XVIII to the extracellular matrix molecule laminin-1 had also been demonstrated in solid-phase assays (Sasaki *et al.* 1998). In these assays, monomeric endostatin was 100-fold less active. Since the APtag is dimeric and expected to produce a pair of ligand moieties facing away from the tag in the same direction (Flanagan & Cheng 2000), binding of our AP-endostatin fusion proteins to murine laminin-1 was analyzed in solid-phase assays. The AP-mES, AP-hES, AP-hESA48T, and AP-hESD104N probes showed similar affinity to laminin (Fig. 4C) which correlates with the results obtained from *in situ* labeling. Similarly, absent binding of AP-hESF31/34A to laminin reflected the results obtained from *in situ* analyses of murine tissues and human cells. As has been described earlier (Javaherian *et al.* 2002), the non-heparin/heparan sulfate binding mutant AP-hESR27/139A showed significantly reduced binding to laminin. Interactions of AP-mES and AP-hES with immobilized human $\alpha_5\beta_1$ integrin, another potential endostatin receptor (Rehn *et al.* 2001; Sudhakar *et al.* 2003; Wickström *et al.* 2003; Wickström *et al.* 2004), were negligible when compared to laminin and close to control AP (below 0.06 OD_{405nm}/10 min, data not shown).

Discussion

While endostatin's prominent affinity for heparan sulfates appears to be required for anti-angiogenic activity

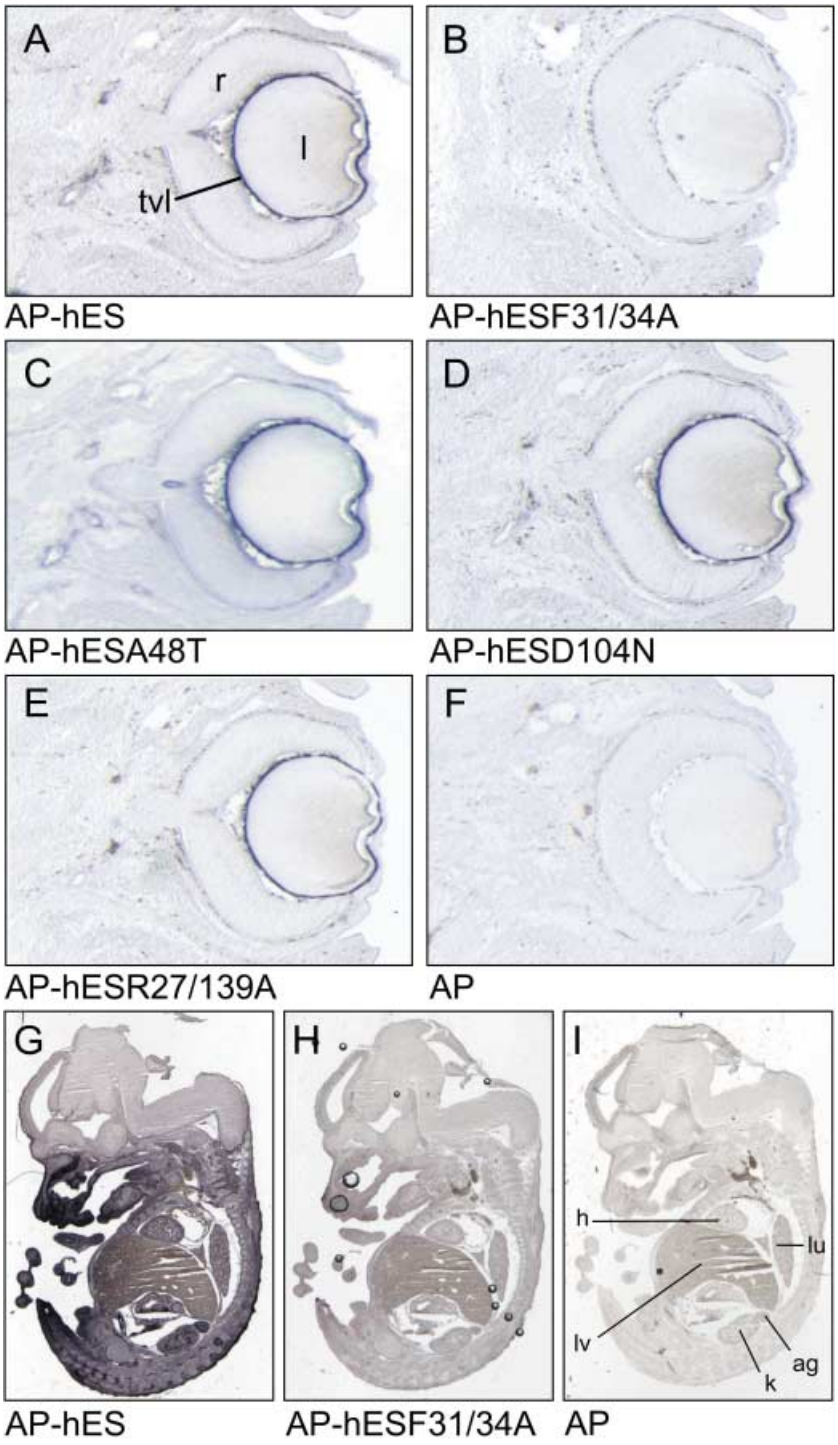

Figure 3 *In situ* staining of AP fusion proteins on E14.5 murine embryonal eyes and sagittal sections. (A) AP-hES, (C) AP-hESA48T, (D) AP-hESD104N and (E) AP-hESR27/139A stained the developing lense capsule equally well. (B) AP-hESF31/34A did not stain the lense capsule and (F) AP alone was also negative (m, murine; h, human; l, lense; r, retina; tvl, tunica vasculosa lentis). When compared to (G) AP-hES, (H) AP-hESF31/34A did not stain general basement membranes. AP-hESF31/34A gave only slight background staining when compared to (I) unfused AP. This unspecific staining increased upon longer incubation times while AP stayed negative (data not shown) (h, heart; k, definitive kidney; ag, adrenal gland; lu, lung; lv, liver). All sections were incubated with supernatants containing AP fusion proteins for 90 min which is sufficient to reach saturation of binding partners and with the NBT/BCIP substrate for 15 min (eye sections) or 1 h (sagittal sections) (Rychkova *et al*. 2005).

(reviewed in Olsson *et al*. 2004; Gaetzner *et al*. 2005), it is not essential for tissue binding (Rychkova *et al*. 2005). We here demonstrate that the two surface-exposed, highly conserved phenylalanines F31 and F34 are indispensable for *in situ* binding to murine tissues, human endothelial cells, and immobilized laminin. A dimeric AP-endostatin fusion protein in which F31 and F34 were replaced with alanines bound to heparin but lacked specific *in situ* binding in agreement with loss of anti-migratory activity of the murine F162/165 A endostatin

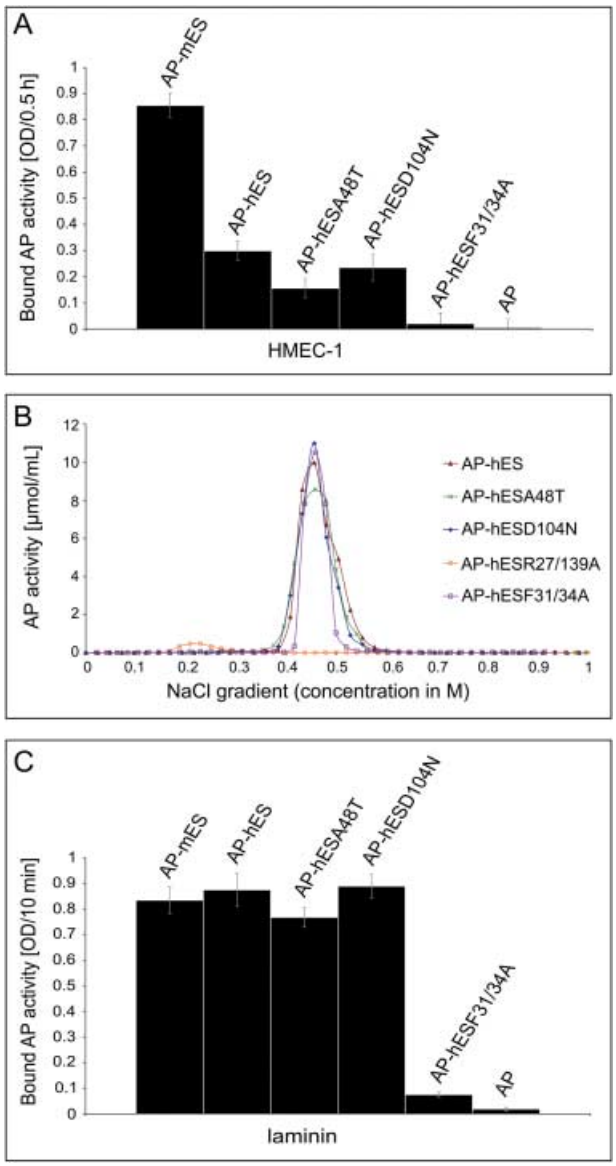

Figure 4 Quantitative analysis of AP fusion protein binding to the surface of cultured human microvascular endothelial cells (HMEC-1), heparin, and laminin. (A) Human fusion protein binding to HMEC-1 was weaker than murine. Binding affinities of the human A48T endostatin mutant and the D104N polymorphism were only slightly reduced while AP-hESF31/34A showed a statistically significant loss of binding ($P = 0.0077$). (B) Binding of AP-hESF31/34A, AP-hESA48T and AP-hESD104N to heparin affinity coloumns is not altered. AP-hES, AP-hESF31/34A, AP-hESA48T and AP-hESD104N showed identical profiles and started to elute at 0.38 M NaCl. AP-hESR27/139A was mainly found in the unbound wash through (data not shown) and retained only residual affinity at 0.18–0.26 M NaCl probably due to remaining arginine residues in the core protein. (C) Solid phase assays revealed strikingly reduced binding of AP-hESF31/34A to immobilized laminin when compared to AP-mES, AP-hES, AP-hESA48T and AP-hESD104N.

mutant on human umbilical vein endothelial cells (Karumanchi *et al.* 2001). F31 and F34 are highly conserved in vertebrates (Fig. 5). The crystal structures of endostatins derived from collagens XV and XVIII revealed that these two phenylalanine residues are in close proximity on the α1 helix at the center of an absolutely conserved patch (Ding *et al.* 1998; Hohenester *et al.* 1998; Sasaki *et al.* 2000). A comparison of different endostatin domains (PFAM database) from various species shows that the degree of conservation of solvent exposed residues is not randomly distributed with respect to their location on the endostatin molecule (Fig. 5A). The 'front' epitope (Fig. 5B, left panel) reveals ten highly conserved residues located within a 10Å radius with the two phenylalanines 31 and 34 in the center. The surface located on the 'back' harbors only very few residues which exhibit a similar degree of conservation (Fig. 5B, middle and right panel). In addition, several of those residues are either important for structural integrity (proline and glycine residues) or only partly accessible at the surface (A85, D107, L109, K117, L157) and their conservation might therefore be required for structure maintenance. Since conservation of solvent-exposed phenylalanines throughout evolution is rather unusual (Fig. 5A,B, left panel), this indicates that the epitope centered around the two phenylalanines 31 and 34 might represent an interface for protein-protein interaction and a putative endostatin high affinity receptor binding site (Hohenester *et al.* 1998). Since we could show that heparin binding is not affected by these phenylalanine to alanine substitutions, this epitope must represent a binding site to a new, so far unidentified receptor. However, the binding epitopes for heparan sulfate and the unidentified receptor might partially overlap due to their close proximity. Interestingly, in human endostatin crystals lattice contacts involve F31 and F34 from each monomer but it remained unclear whether these hydrophobic interactions occur *in vivo* (Ding *et al.* 1998). The crystal lattice contacts involving the two conserved phenylalanines are not only different between crystals of human and murine endostatin but also for crystals of murine endostatin with a different spacegroup (Hohenester *et al.* 2000). Therefore, these contacts rather display the 'stickiness' of the hydrophobic surface patch than dimerization through phenylalanines.

We also present the first functional evaluation of the homozygous A48T amino acid substitution found in two sisters affected with Knobloch syndrome but not in 100 control individuals (Kliemann *et al.* 2003). While *in situ* binding affinities were not altered, the production of AP-hESA48T was strikingly reduced when compared to wild-type endostatins. Since A48 is not accessible on the

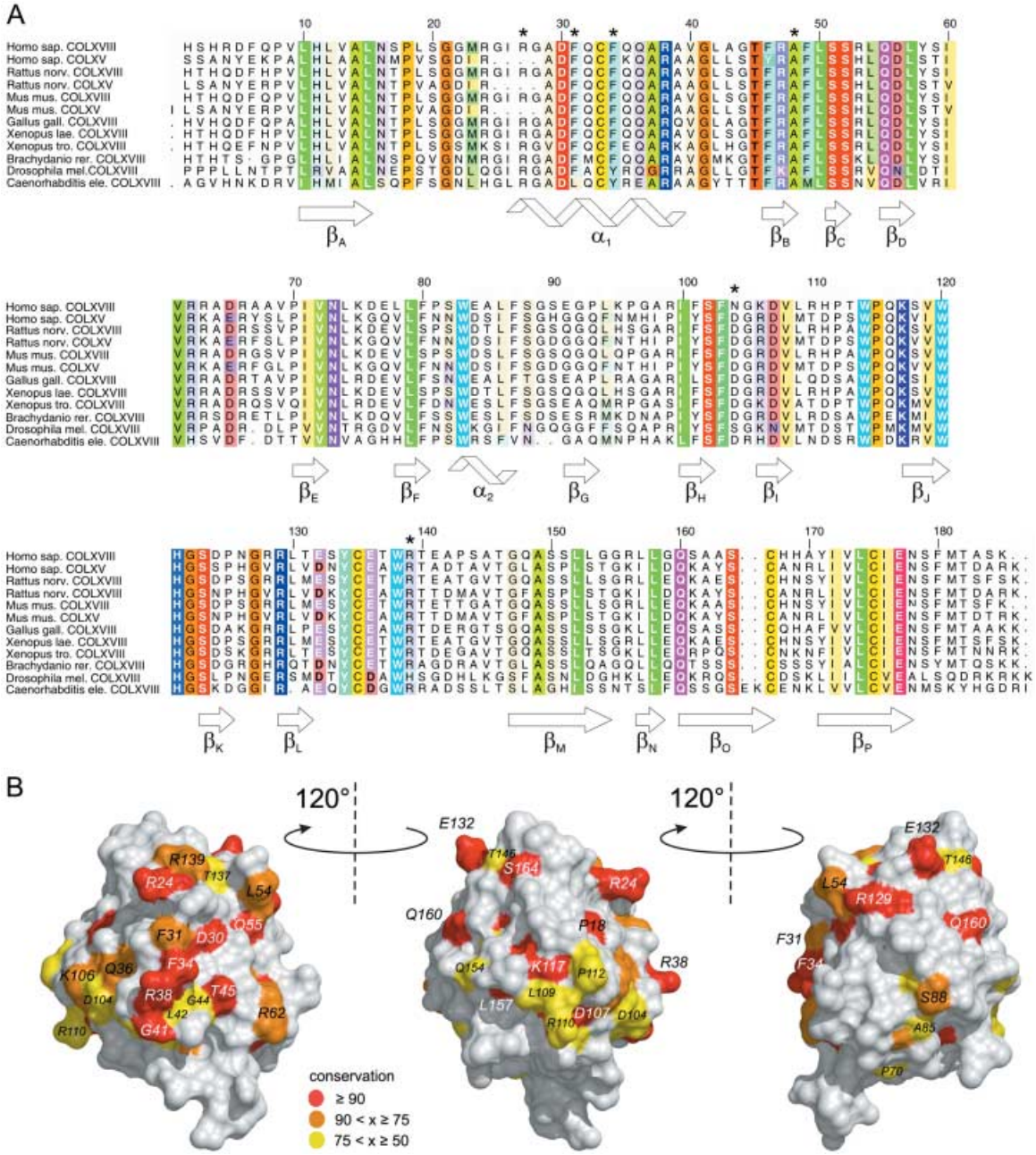

Figure 5 (A) Sequence alignment of a selection of endostatin domains from the 'full alignment' of the PFAM database (http://www.sanger.ac.uk/Software/Pfam/) and the NCBI protein database prepared with the software Jalview (Clamp *et al.* 2004). The Taylor color coding was used for the alignment, the color intensities are modulated by the degree of conservation, the color intensities shown were produced with a scale of 75 of the conservation tool in Jalview. Secondary structure elements are shown as arrows and helices according to Ding *et al.* (1998). Residues investigated in this study are marked by asterisks. (B) Surface representation of human endostatin (PDB entry code 1BNL) color coded according to the degree of conservation shown in (A). All residues which are still colored at a conservation level of 90 (Jalview tool conservation) are shown in red, residues marked at a level of 75 are shown in orange, whereas residues shown in yellow are colored only below a level of 75 but above 50. Therefore, residues in red mark the highest degree of conservation, residues in yellow the lowest. The orientation of the molecule shown in the left panel is identical with that in Fig. 1. The orientation of the molecule displayed in the middle and right panel is rotated by 120° around the *y*-axis, respectively. The figure clearly shows that the conservation of surface-accessible residues is not randomly distributed over the molecule's surface. Instead there is a clear clustering with the phenylalanines 31 and 34 in the center of a putative protein binding epitope.

endostatin surface (Fig. 1A,B), we conclude that the effect must be indirect. Analyzing the immediate environment of A48 reveals that its side chain is pointing into the interior of endostatin's hydrophobic core and is completely shielded from the solvent. Due to the tight packing of A48 by its direct neighboring residues I26, A29, D30 and L50 space for larger amino acid side chains is limited. Replacing the alanine with the more hydrophilic threonine side chain might therefore cause a lower folding efficiency. In the hydrophobic environment the polar hydroxyl group of threonine must be balanced by a hydrogen bond. Possible hydrogen bond donors/acceptors close in space are only the side chain carboxyl group or the main chain amide of D30. This stringent restraint might therefore lead to an increased amount of misfolded protein consistent with our findings that the expression rate of AP-hESA48T is reduced while the purified protein shows otherwise unaltered binding properties. A48's importance for the structural maintenance can also be deduced from the absolute conservation of the alanine residue at this position throughout all 40 endostatin domains in the PFAM database (http://www.sanger.ac.uk/Software/Pfam/). Although Kliemann *et al.* (2003) did only screen 25 of the 43 collagen XVIII exons by SSCP, it seems likely that A48T is a pathological mutation.

In contrast, our *in situ* stainings of tissues and cells, the heparin affinity chromatographies, and solid-phase assays did not provide evidence that the D104N amino acid substitution is of major pathological and clinical significance. Two recent studies have addressed functional aspects of D104N. Menzel *et al.* (2004) found impaired affinity of endostatin D104N for laminin by immunoprecipitation and Western blotting. However, this result might have been due to a different experimental approach in which Flag-tagged endostatin dimers were created via biotinylated anti-Flag IgG. Notably, Menzel *et al.* (2004) did not observe a reduced inhibitory activity of the D104N variant on migration of human dermal microvascular endothelial cells. In addition, it was shown that recombinant human D104 and D104N endostatins inhibit human umbilical vein endothelial cell tube formation equally well (Macpherson *et al.* 2004). The side chain of D104 is fully exposed to solvent and not involved in any non-covalent interactions that are required for structural integrity of the endostatin molecule (Fig. 1A,B). Replacement by the isosterical asparagine should therefore be without any consequences for the folding of the molecule. Taken together, the previous activity assays, our binding studies and the structural data do not confirm the hypothesis that the exchange of aspartic acid to asparagine at position 104 in endostatin (D104N) would directly lead to impaired anti-angiogenic activity and decreased affinity to other molecules (Iughetti *et al.* 2001).

As already pointed out by Menzel *et al.* (2004), it is possible that the two Hungarian Knobloch sibs carrying a heterozygous frameshift mutation and the endostatin D104N polymorphism may have an additional, yet undetected pathogenic mutation in e.g. regulatory elements or a large deletion. This possibility is supported by a recent report on a single unaffected mother of a Knobloch patient who carried a frameshift insertion in *trans* with the D104N polymorphism (Suzuki *et al.* 2005). Furthermore, the D104N variant is polymorphic in various populations with a frequency of 5.6–15% (Iughetti *et al.* 2001; Macpherson *et al.* 2004; Menzel *et al.* 2004), and homozygous individuals are healthy (Suzuki *et al.* 2005). Nevertheless it cannot be excluded that compound heterozygotes bearing one null allele in combination with the D104N allele show a reduced penetrance of the phenotype (Antonarakis *et al.* 2005).

Regarding predisposition to prostate cancer reported for the endostatin D104N polymorphism (Iughetti *et al.* 2001), no statistically significant association between the frequency of endostatin D104N and the incidence of androgen independent prostate cancer or survival was found in a larger case control group (Macpherson *et al.* 2004) and in tissues from prostate cancer patients (Li *et al.* 2005). However, the replication of association studies may not succeed due to different genetic backgrounds of the populations used and the heterogeneity of the disease studied. Therefore, it remains conceivable that the endostatin D104N polymorphism is in linkage disequilibrium with a collagen XVIII mutation of functional relevance.

Experimental procedures

Construction and expression of alkaline phosphatase fusion proteins

To generate human AP-endostatin fusion proteins, the human endostatin sequence was amplified from cDNA clone α1(XVIII) pNF18-2 (Oh *et al.* 1994b), mutated in pBluescript II SK(+) (Stratagene) using the QuickChange™ Site-Directed Mutagenesis kit (Stratagene), and subcloned into the expression vector pAPtag-4 (obtained from D.A. Feldheim and J.G. Flanagan, Harvard Medical School) using oligonucleotide primers AP-hES5′ (5′-GGT TCC GGA CAC AGC CAC CGC GAC TTC CAG-3′) and AP-hES3′ (5′-ATG CTC GAG CTA CTT GGA GGC AGT CAT GAA-3′) essentially as described (Rychkova *et al.* 2005). 293T cells (human embryonic kidney cells, a gift from D.A. Feldheim and J.G. Flanagan) plated at 80% confluence on 150 mm tissue culture plates were transiently transfected with 12 μg of fusion plasmid DNA using FuGENE 6 transfection reagent (Roche). Twenty-four hours

after transfection, the medium (DMEM with glutamax-I (Gibco), 10% fetal bovine serum, 1% penicilline-streptomycine) was replaced. Conditioned supernatants from transfected and non-transfected cells were collected after an additional 48–72 h, centrifuged at 1000 r.p.m. (Eppendorf rotor A-4-44), filtered through a 0.45 μm filter (Schleicher & Schuell), buffered with 10 mM HEPES, 0.05% NaN_3, pH 7.0, and stored at 4 °C for immediate use or at −80 °C for longterm usage.

Determination of AP activity

One hundred microliters supernatants were heat-inactivated for 10 min at 65 °C to inhibit endogenous phosphatases. After centrifugation at 14000 r.p.m. (Eppendorf rotor F45-30-11), 20 μL were mixed with 380 μL HBAH buffer (150 mM NaCl, 20 mM HEPES, pH 7.0, 0.5 mg/mL bovine serum albumin, 0.1% NaN_3) and 400 μL 2× AP substrate buffer (2 M diethanolamine, 1 mM $MgCl_2$, 18 mM p-nitrophenyl phosphate (AppliChem), pH 9.8), and incubated at room temperature. Absorbance at 405 nm was read at 30 s intervals for 10 min in a spectrophotometer. After AP activity measurement, the supernatants were diluted to obtain the same activity in each probe. In subsequent experiments, specific activities were compared to wild-type endostatin. AP fusion proteins were not affinity purified, quantitated, and titrated to perform exact enzyme kinetics.

SDS-PAGE / Western blotting

Fifteen microliters of conditioned supernatants were loaded on to 5–15% SDS-PAGE gradient gels, run at 50 V for 18 h and wet-blotted on to nitrocellulose (Protran; Schleicher & Schuell) using a TE42 Transphor transfer unit (Amersham Biosciences) 1.5 A for 1 h at 4 °C. The blots were incubated with a rabbit polyclonal antibody against secreted human placental alkaline phosphatase (1 : 2000, WAK-Chemie) or with a rabbit polyclonal anti-human endostatin antibody (1 : 2000, Cytimmune Sciences Inc.) followed by a horseradish peroxidase-conjugated anti-rabbit IgG (1 : 3000, Santa Cruz) according to standard procedures. The signals were visualized using enhanced chemiluminescence (Perkin Elmer/NEN).

Staining of tissue sections

Timed-mated NMRI mice were ordered from Harlan Winkelmann. E14.5 embryos were dissected, fixed in 4% paraformaldehyde (in PBS) at 4 °C overnight, transferred to 20% sucrose (in PBS) at 4 °C on a shaker for one day, and frozen in OCT embedding medium (Tissue-Tek). AP-staining of 10 μm cryosections thaw-mounted on to Polysine slides (Menzel Gläser) was essentially performed as described in Flanagan *et al.* (2000) and Rychkova *et al.* (2005).

Quantitative measurement of AP-endostatin binding to cell surfaces

Human dermal microvascular endothelial cells (HMEC-1 cell line kindly provided by the Centers for Disease Control and Prevention, Atlanta, GA, USA) were plated into six-well tissue culture plates and cultured for one day in Endothelial Basal Medium (Clonetics) supplemented with 10 ng/mL human epidermal growth factor (Clonetics), 1 μg/mL hydrocortisone (Clonetics), and 10% fetal bovine serum (Linaris). Confluent cells were washed once with cold HBAH buffer, incubated with 1 mL fusion protein-containing supernatants for 90 min at room temperature, washed with cold HBAH five times for 5 min and lyzed with 300 μL 1% Triton X-100, 10 mM Tris-HCl, pH 8.0. After collection of the lysates, the plates were rinsed again with an additional 200 μL of lysate buffer. The pooled lysates were vortexed, incubated at room temperature for 5 min, heat-inactivated at 65 °C for 10 min, placed on ice, and supplemented with an equal amount (400 μL) of 2× AP substrate buffer to measure the AP activity after 30 min as described above. The experiments were performed in triplicate. A detailed protocol for this procedure can be found in Flanagan & Cheng 2000).

Heparin affinity chromatography

Sixty milliliters of filtered supernatants adjusted to equal activities were applied to 5 mL HiTrap™ heparin affinity coloumns (Pharmacia) equilibrated in 0.05 M Tris-HCl, pH 7.4. The protein samples were eluted with a linear gradient of 0–1 M NaCl. The content of the individual fractions was determined by AP activity measurements and Western blotting with the anti-AP and anti-endostatin antibodies.

Solid-phase assays

Ninety-six-well flat bottom plates (Greiner) were coated with 1 μg purified murine laminin-1 (BD Biosciences) or 0.5 μg purified human $\alpha_5\beta_1$ integrin (Chemicon) per well at 4 °C overnight. After three washes with cold HBAH buffer, immobilized laminin was incubated with 100 μL AP affinity probes for 90 min at room temperature. The probes were supplemented with 2 mM $CaCl_2$, 1 mM $MgCl_2$, and 1 mM $MnCl_2$ in solid phase assays with $\alpha_5\beta_1$ integrin. Unbound protein was removed by three washes with HBAH buffer. One hundred microliters 2× AP substrate solution (2 M diethanolamine, 1 mM $MgCl_2$, 18 mM *p*-nitrophenyl phosphate (AppliChem), pH 9.8) was added to 100 μL HBAH buffer per well. Absorbance was measured at 405 nm after 10 min using a Dynatech MR5000 plate reader. Coated wells containing cell culture medium were used for zero adjustment. The experiments were performed in triplicate.

Acknowledgements

We thank Drs. B.R. Olsen and N. Fukai for cDNA clone α1(XVIII) pNF18-2, Drs. D.A. Feldheim and J.G. Flanagan for the expression vector pAPtag-4, Drs. E. Ades, F.J. Candal and T. Lawley for the HMEC-1 cell line, T. Neumann for her contribution to the biochemical experiments, and Dr. E. Conzelmann for helpful discussions. This work was supported by an Emmy Noether-grant from the Deutsche Forschungsgemeinschaft (Fe 432/6-4).

References

Ackley, B.D., Crew, J.R., Elamaa, H., Pihlajaniemi, T., Kuo, C.J. & Kramer, J.M. (2001) The NC1/endostatin domain of Caenorhabditis elegans type XVIII collagen affects cell migration and axon guidance. *J. Cell Biol.* **152**, 1219–1232.

Antonarakis, S.E., Reymond, A., Menzel, O., *et al.* (2005) A response to Suzuki *et al.* 'How pathogenic is the p.D104N/endostatin polymorphic allele of COL18A1 in Knobloch syndrome?'. *Hum. Mutat.* **25**, 316.

Clamp, M., Cuff, J., Searle, S.M. & Barton, G.J. (2004) The Jalview Java alignment editor. *Bioinformatics* **20**, 426–427.

Czeizel, A.E., Goblyos, P., Kustos, G., Mester, E. & Paraicz, E. (1992) The second report of Knobloch syndrome. *Am. J. Med. Genet.* **42**, 777–779.

Ding, Y.H., Javaherian, K., Lo, K.M., *et al.* (1998) Zinc-dependent dimers observed in crystals of human endostatin. *Proc. Natl. Acad. Sci. USA* **95**, 10443–10448.

Felbor, U., Dreier, L., Bryant, R.A., Ploegh, H.L., Olsen, B.R. & Mothes, W. (2000) Secreted cathepsin L generates endostatin from collagen XVIII. *EMBO J.* **19**, 1187–1194.

Flanagan, J.G. & Cheng, H.J. (2000) Alkaline phosphatase fusion proteins for molecular characterization and cloning of receptors and their ligands. *Methods Enzymol.* **327**, 198–210.

Flanagan, J.G., Cheng, H.J., Feldheim, D.A., Hattori, M., Lu, Q. & Vanderhaeghen, P. (2000) Alkaline phosphatase fusions of ligands or receptors as in situ probes for staining of cells, tissues, and embryos. *Methods Enzymol.* **327**, 19–35.

Fukai, N., Eklund, L., Marneros, A.G., *et al.* (2002) Lack of collagen XVIII/endostatin results in eye abnormalities. *EMBO J.* **21**, 1535–1544.

Gaetzner, S., Deckers, M.M.L., Stahl, S., Löwik, C., Olsen, B.R. & Felbor, U. (2005) Endostatin's heparan sulfate-binding site is essential for inhibition of angiogenesis and enhances in situ binding to capillary-like structures in bone explants. *Matrix Biol.* **23**, 557–561.

Gitay-Goren, H., Soker, S., Vlodavsky, I. & Neufeld, G. (1992) The binding of vascular endothelial growth factor to its receptors is dependent on cell surface-associated heparin-like molecules. *J. Biol. Chem.* **267**, 6093–6098.

Hohenester, E., Sasaki, T., Olsen, B.R. & Timpl, R. (1998) Crystal structure of the angiogenesis inhibitor endostatin at 1.5 Å resolution. *EMBO J.* **17**, 1656–1664.

Hohenester, E., Sasaki, T., Mann, K. & Timpl, R. (2000) Variable zinc coordination in endostatin. *J. Mol. Biol.* **297**, 1–6.

Iughetti, P., Suzuki, O., Godoi, P.H., *et al.* (2001) A polymorphism in endostatin, an angiogenesis inhibitor, predisposes for the development of prostatic adenocarcinoma. *Cancer Res.* **61**, 7375–7378.

Javaherian, K., Park, S.Y., Pickl, W.F., *et al.* (2002) Laminin modulates morphogenic properties of the collagen XVIII endostatin domain. *J. Biol. Chem.* **277**, 45211–45218.

Karumanchi, S.A., Jha, V., Ramchandran, R., *et al.* (2001) Cell surface glypicans are low-affinity endostatin receptors. *Mol. Cell* **7**, 811–822.

Kliemann, S.E., Waetge, R.T., Suzuki, O.T., Passos-Bueno, M.R. & Rosemberg, S. (2003) Evidence of neuronal migration disorders in Knobloch syndrome: clinical and molecular analysis of two novel families. *Am. J. Med. Genet.* **119A**, 15–19.

Knobloch, W. & Layer, J. (1971) Retinal detachment and encephalocele. *J. Pediatric Ophthalmol.* **8**, 181–184.

Li, H.C., Cai, Q.Y., Shinohara, E.T., *et al.* (2005) Endostatin polymorphism 4349G/A (D104N) is not associated with aggressiveness of disease in prostate cancer. *Dis. Markers* **21**, 37–41.

Macpherson, G.R., Singh, A.S., Bennett, C.L., *et al.* (2004) Genotyping and functional analysis of the D104N variant of human endostatin. *Cancer Biol. Ther.* **3**, 1298–1303.

Marneros, A.G. & Olsen, B.R. (2003) Age-dependent iris abnormalities in collagen XVIII/endostatin deficient mice with similarities to human pigment dispersion syndrome. *Invest. Ophthalmol. Vis. Sci.* **44**, 2367–2372.

Marneros, A.G., Keene, D.R., Hansen, U., *et al.* (2004) Collagen XVIII/endostatin is essential for vision and retinal pigment epithelial function. *EMBO J.* **23**, 89–99.

Menzel, O., Bekkeheien, R.C., Reymond, A., *et al.* (2004) Knobloch syndrome: novel mutations in *COL18A1*, evidence for genetic heterogeneity, and a functionally impaired polymorphism in endostatin. *Hum. Mutat.* **23**, 77–84.

Oh, S.P., Kamagata, Y., Muragaki, Y., Timmons, S., Ooshima, A. & Olsen, B.R. (1994a) Isolation and sequencing of cDNAs for proteins with multiple domains of Gly-Xaa-Yaa repeats identify a distinct family of collagenous proteins. *Proc. Natl. Acad. Sci. USA* **91**, 4229–4233.

Oh, S.P., Warman, M.L., Seldin, M.F., *et al.* (1994b) Cloning of cDNA and genomic DNA encoding human type XVIII collagen and localization of the alpha 1 (XVIII) collagen gene to mouse chromosome 10 and human chromosome 21. *Genomics* **19**, 494–499.

Olsson, A.K., Johansson, I., Akerud, H., *et al.* (2004) The minimal active domain of endostatin is a heparin-binding motif that mediates inhibition of tumor vascularization. *Cancer Res.* **64**, 9012–9017.

O'Reilly, M.S., Boehm, T., Shing, Y., *et al.* (1997) Endostatin: an endogenous inhibitor of angiogenesis and tumor growth. *Cell* **88**, 277–285.

Passos-Bueno, M.R., Marie, S.K., Monteiro, M., *et al.* (1994) Knobloch syndrome in a large Brazilian consanguineous family: confirmation of autosomal recessive inheritance. *Am. J. Med. Genet.* **52**, 170–173.

Rehn, M. & Pihlajaniemi, T. (1994) Alpha 1 (XVIII), a collagen chain with frequent interruptions in the collagenous sequence, a distinct tissue distribution, and homology with type XV collagen. *Proc. Natl. Acad. Sci. USA* **91**, 4234–4238.

Rehn, M., Veikkola, T., Kukk-Valdre, E., *et al.* (2001) Interaction of endostatin with integrins implicated in angiogenesis. *Proc. Natl. Acad. Sci. USA* **98**, 1024–1029.

Rychkova, N., Stahl, S., Gaetzner, S. & Felbor, U. (2005) Non-heparan sulfate–binding interactions of endostatin/collagen XVIII in murine development. *Dev. Dyn.* **232**, 399–407.

Sasaki, T., Fukai, N., Mann, K.G., Göhring, W., Olsen, B.R. & Timpl, R. (1998) Structure, function and tissue forms of the C-terminal globular domain of collagen XVIII containing the angiogenesis inhibitor endostatin. *EMBO J.* **17**, 4249–4256.

Sasaki, T., Larsson, H., Kreuger, J., *et al.* (1999) Structural basis and potential role of heparin/heparan sulfate binding to the angiogenesis inhibitor endostatin. *EMBO J.* **18**, 6240–6248.

Sasaki, T., Larsson, H., Tisi, D., Claesson-Welsh, L., Hohenester, E. & Timpl, R. (2000) Endostatins derived from collagens XV and XVIII differ in structural and binding properties, tissue distribution and anti-angiogenic activity. *J. Mol. Biol.* **301**, 1179–1190.

Seaver, L.H., Joffe, L., Spark, R.P., Smith, B.L. & Hoyme, H.E. (1993) Congenital scalp defects and vitreoretinal degeneration: redefining the Knobloch syndrome. *Am. J. Med. Genet.* **46**, 203–208.

Sertié, A.L., Sossi, V., Camargo, A.A., Zatz, M., Brahe, C. & Passos-Bueno, M.R. (2000) Collagen XVIII, containing an endogenous inhibitor of angiogenesis and tumor growth, plays a critical role in the maintenance of retinal structure and in neural tube closure (Knobloch syndrome). *Hum. Mol. Genet.* **9**, 2051–2058.

Sniderman, L.C., Koenekoop, R.K., O'Gorman, A.M., *et al.* (2000) Knobloch syndrome involving midline scalp defect of the frontal region. *Am. J. Med. Genet.* **90**, 146–149.

Sudhakar, A., Sugimoto, H., Yang, C., Lively, J., Zeisberg, M. & Kalluri, R. (2003) Human tumstatin and human endostatin exhibit distinct antiangiogenic activities mediated by alpha v beta 3 and alpha 5 beta 1 integrins. *Proc. Natl. Acad. Sci. USA* **100**, 4766–4771.

Suzuki, O.T., Sertié, A.L., Der Kaloustian, V.M., *et al.* (2002) Molecular analysis of collagen XVIII reveals novel mutations, presence of a third isoform, and possible genetic heterogeneity in Knobloch syndrome. *Am. J. Hum. Genet.* **71**, 1320–1329.

Suzuki, O.T., Bagatini, K., Sertié, A.L. & Passos-Bueno, M. (2005) How pathogenic is the p.D104N/endostatin polymorphic allele of COL18A1 in Knobloch syndrome? *Hum. Mutat.* **25**, 314–315.

Utriainen, A., Sormunen, R., Kettunen, M., *et al.* (2004) Structurally altered basement membranes and hydrocephalus in a type XVIII collagen deficient mouse line. *Hum. Mol. Genet.* **13**, 2089–2099.

Wickström, S.A., Alitalo, K. & Keski-Oja, J. (2003) Endostatin associates with lipid rafts and induces reorganization of the actin cytoskeleton via down-regulation of RhoA activity. *J. Biol. Chem.* **278**, 37895–37901.

Wickström, S.A., Alitalo, K. & Keski-Oja, J. (2004) An endostatin-derived peptide interacts with integrins and regulates actin cytoskeleton and migration of endothelial cells. *J. Biol. Chem.* **279**, 20178–20185.

Wilson, C., Aftimos, S., Pereira, A. & McKay, R. (1998) Report of two sibs with Knobloch syndrome (encephalocoele and viteroretinal degeneration) and other anomalies. *Am. J. Med. Genet.* **78**, 286–290.

Ylikärppä, R., Eklund, L., Sormunen, R., *et al.* (2003) Lack of type XVIII collagen results in anterior ocular defects. *FASEB J.* **17**, 2257–2259.

Received: 26 April 2005
Accepted: 23 June 2005

Anlage 7

Childs Nerv Syst
DOI 10.1007/s00381-006-0202-8

ORIGINAL PAPER

Clinical impact of *CCM* mutation detection in familial cavernous angioma

Oguzkan Sürücü · Ulrich Sure · Sabine Gaetzner · Sonja Stahl · Ludwig Benes · Helmut Bertalanffy · Ute Felbor

Received: 16 February 2006 / Revised: 21 April 2006

Abstract
Introduction and background A 3-year-old Bosnian girl with a large symptomatic brainstem and multiple supratentorial cavernous angiomas, who underwent neurosurgical treatment, is presented. As multiple cavernomas are more common in familial cases, genetic analyses and neuroradiological imaging were performed in the patient and her parents to see whether there was any evidence for inheritance. This information is important for genetic counseling and provision of medical care for at-risk relatives. Currently, no recommendation is available on how to manage these cases.
Results Genetic analyses demonstrated a novel *CCM1* frameshift mutation (c.1683_1684insA; p.V562SfsX6) in the child and the asymptomatic 27-year-old mother. Sensitive gradient-echo magnetic resonance imaging of the mother revealed multiple supratentorial lesions, whereas analogous imaging of the father showed no pathological findings.
Conclusion This case exemplifies that seemingly sporadic cases with multiple lesions might well be hereditary and that presymptomatic genetic testing of family members may identify relatives for whom clinical and neuroradiological monitoring is indicated.

O. Sürücü · U. Sure (✉) · L. Benes · H. Bertalanffy
Department of Neurosurgery,
Philipps-University Marburg,
Baldingerstrasse,
35033 Marburg, Germany
e-mail: sure@med.uni-marburg.de

S. Gaetzner · S. Stahl · U. Felbor
Department of Human Genetics,
University of Würzburg,
Würzburg, Germany

Keywords Cavernous angioma · Genetic testing · Cerebral cavernous malformation · CCM · Pontine hemorrhage · Gradient-echo MRI

Introduction

Cerebral cavernous malformations (CCM) occur sporadically or as an autosomal dominant trait with incomplete penetrance and variable inter- and intrafamilial expressivity. Causal mutations have been demonstrated in three genes, *CCM1*, *CCM2*, and *CCM3* [1, 8, 9]. Familial CCM is mostly associated with the occurrence of multiple lesions that increase in number and size with age [7]. Consistent with this observation, 4 out of 14 seemingly sporadic cases with multiple cavernomas were previously shown to be *CCM1* mutation carriers [15]. Because their parents were not analyzed, it remained unclear whether these had been inherited or were de novo mutations. In a further study, neuroimaging revealed that 17 out of 22 patients with multiple cavernous angiomas, but negative family history, had an asymptomatic relative with cavernomas [5, 7]. Thus far, six *CCM1*, four *CCM2*, and four *CCM3* mutations were detected in this cohort [1, 4, 5], indicating a mutation detection rate of at least 64% for seemingly sporadic cases with multiple cavernomas. It is interesting to note that two of the five patients without neuroradiologically affected relatives revealed *CCM3* mutations. One of these mutations was the de novo genomic deletion that led to the identification of the *CCM3* gene [1]. Further de novo *CCM* germline mutations have recently been reported [1, 10, 11]. In this study, we present combined genetic and neuroradiological data on a seemingly sporadic case of a patient who, in fact, inherited a previously undescribed maternal *CCM1* mutation.

Case report

History

A 3-year-old Bosnian girl was referred to our institution for operative treatment of a brainstem cavernoma 1 month after acute hemorrhage and neurological deterioration. She presented with somnolence, headache, right-sided hemiparesis with facial palsy, and speech disorder. The sudden aggravation was due to the enlargement and bleeding of a previously diagnosed pontine cavernoma associated with a mild hydrocephalus. Clinical stabilization and subsequent amelioration of neurological symptoms occurred under antiedematous therapy. Magnetic resonance imaging (MRI) revealed multiple cerebral cavernous malformations including an epileptogenic lesion in the left frontal lobe, which was treated medically (Fig. 1).

On admission, the patient suffered from truncal ataxia. She could hardly remain in sitting position and was unable to stand. She had mild facial palsy and high-grade hemiparesis with hyperreflexia and positive Babinski sign on the right side. Repeated MRI showed a left pontine cavernoma with a maximum size of 4×3.5×3 cm (Fig. 1).

Surgery

For brain relaxation, a right ventricular drainage of cerebrospinal fluid was placed before the microsurgical intervention. Our patient underwent a neuronavigated complete resection of the pontine cavernoma without any complications. The operation was performed in supine position with right-sided horizontal head turn. We chose a left subtemporal transtentorial approach targeting the anterolateral pons. Somatosensory and brainstem auditory evoked potentials were monitored throughout the operation.

Postoperative course

Postoperatively, her neurological symptoms improved constantly. Ten days after the operation, MRI was performed that confirmed the complete resection of the cavernoma and showed the decompression of the previously heavily

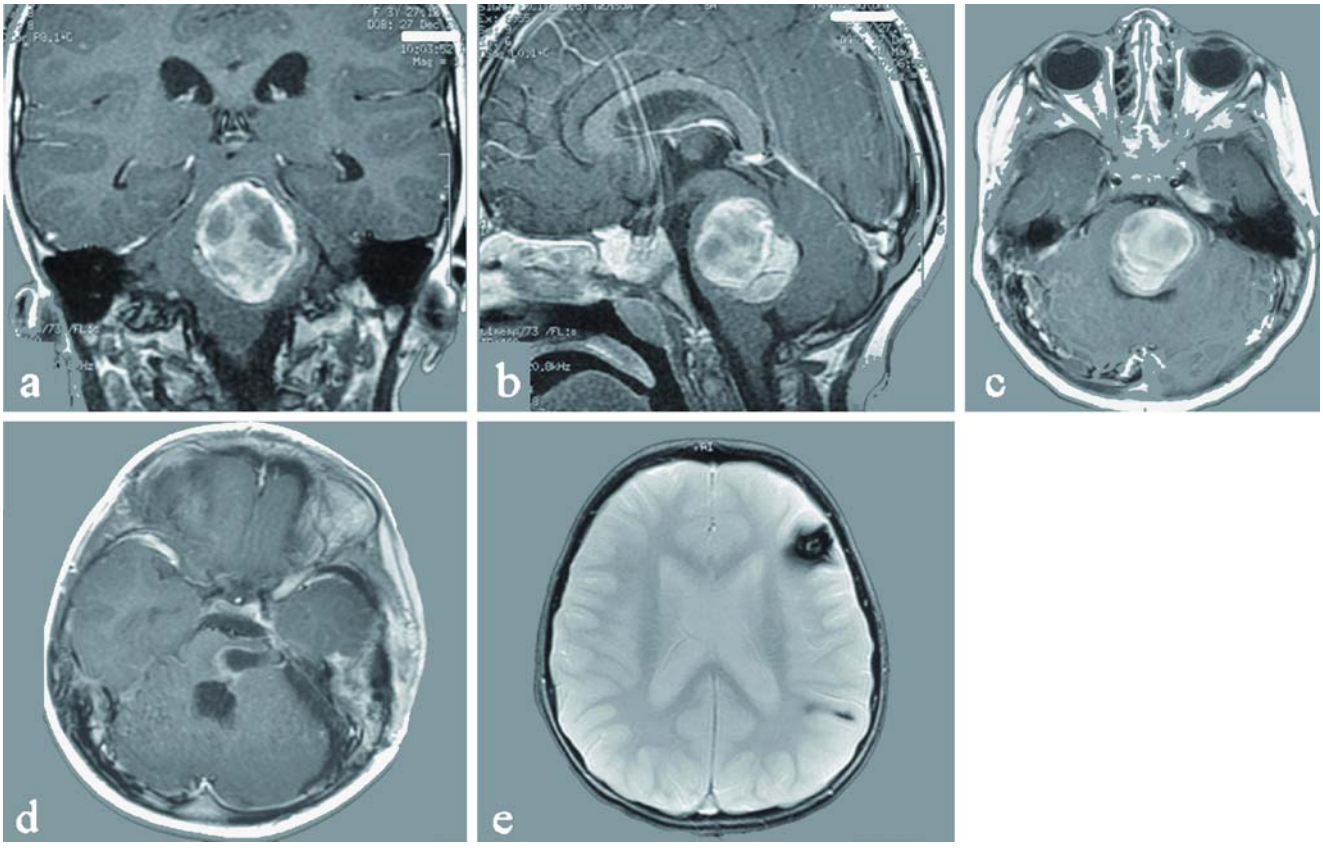

Fig. 1 **a–c** Contrast enhanced T1-weighted MR image showing the large pontine cavernoma of the child preoperatively. **d** Postoperative axial image showing complete resection of the cavernous malformation with recovered fourth ventricle size and brainstem decompression. **e** Gradient-echo MRI revealing additional supratentorial cavernous angiomas of the child (left frontal and parietal lobe)

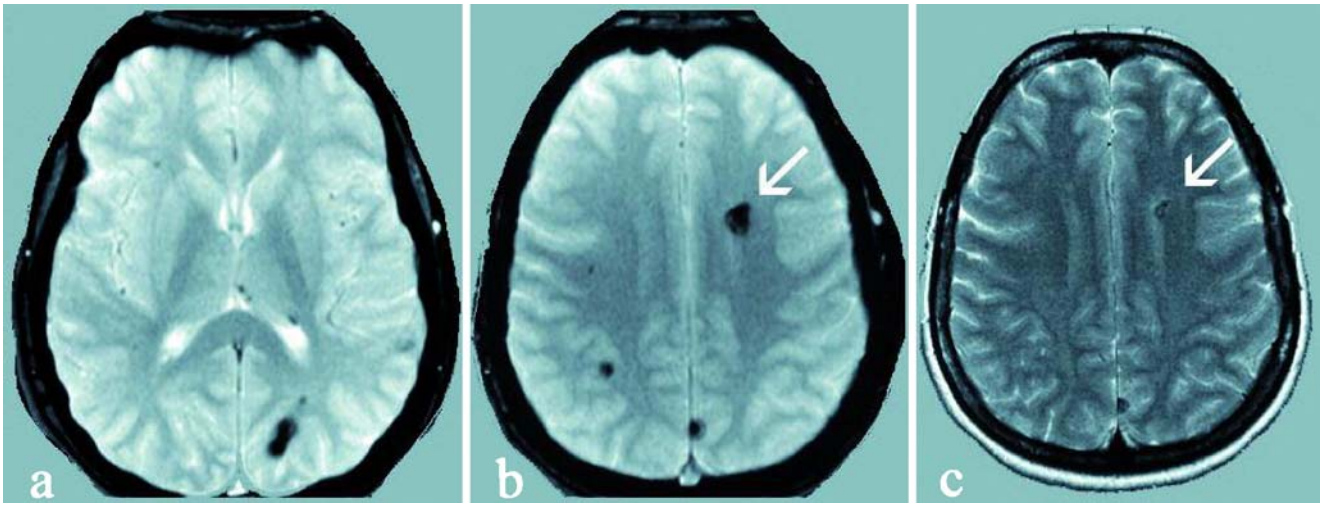

Fig. 2 **a**, **b** Multiple supratentorial cavernomas with typical hypointense signaling in the 27-year-old mother in gradient-echo MR scans. **c** The largest left frontal cavernoma can be seen in a routine T2-weighted MR scan of the asymptomatic mother (*white arrow*)

enlarged brainstem (Fig. 1). Strabismus and mild facial palsy were persisting within the 2 weeks of hospitalization. She was discharged for neurological rehabilitation in her home country. The excision of the symptomatic left frontal cavernoma (Fig. 1e) was offered to the parents (Fig. 2) but they did not yet favor a second surgery.

Genetic analyses

After having obtained informed consent, coding *CCM1*, *CCM2*, and *CCM3* exons with adjacent intronic sequences were PCR-amplified from lymphocyte DNA and directly sequenced on a Beckmann CEQ 8800 capillary electrophoresis system. A 1-bp insertion in exon 16 of the *CCM1* gene (c.1683_1684insA) was identified in the patient and her mother but not the father (Fig. 3).

Discussion

The novel p.V562SfsX6 frameshift mutation identified in our patient fits into the known scheme of truncating *CCM* mutations. Genetic testing and MRI of the asymptomatic parents revealed the same mutation and multiple cavernous angiomas in the 27-year-old mother (Fig. 2). Thus, our patient who was initially thought to be a sporadic case can now be classified as having familial CCM.

Multiple cavernomas and negative genetic analysis

CCM1, *CCM2*, and *CCM3* mutations are detected in 43–54, 13–22, and <10% of patients with familial CCM, respectively [1, 3, 4, 6, 9, 10, 13–16]. In about 30% of the patients, current genetic testing will not identify a mutation. This may for example be due to the existence of a fourth *CCM* gene, to mutations in the promoter regions of *CCM1–3*, or to limitations of the mutation detection method applied. For example, direct sequencing does not detect large deletions that have been described for *CCM2* and *CCM3* [1, 4]. To improve the mutation detection rate, we perform multiplex ligation-dependent probe amplification (MLPA) gene dosage assays for *CCM1–3* in addition to sequencing. If patients with multiple cavernomas have negative genetic screening results after sequencing and MLPA, we would propose gradient-echo MR scans of their relatives.

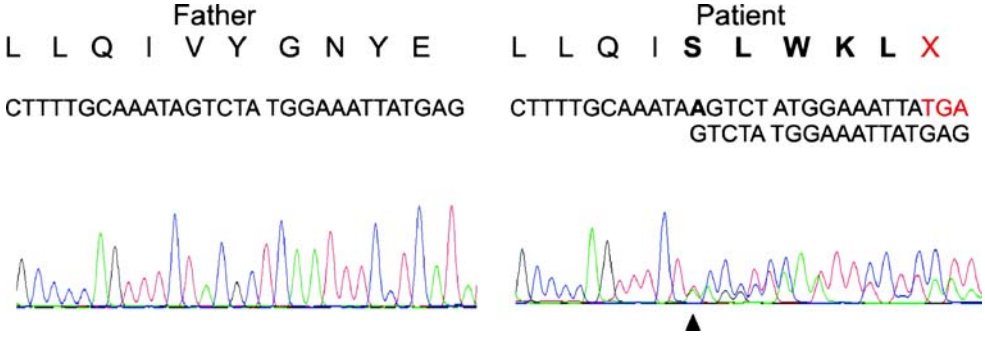

Fig. 3 Normal sequence of the patient's father and insertion of an adenine (A, *bold*) in the patient (*arrow head*) and her mother (data not shown) resulting in an altered reading frame and a premature stop codon (TGA, *red*). The first affected amino acid is valine (V) at position 562 which is changed to a serine (S, *bold*). The new reading frame ends after five amino acids in a stop (X, *red*) (p.V562SfsX6)

Multiple cavernomas and positive genetic analysis

After identification of a mutation in a seemingly sporadic case, genetic counseling and testing can be offered to the parents and further relatives. While screening *CCM1*, *CCM2*, and *CCM3* genes for mutations in the index patient may occasionally be laborious, genetic confirmation or exclusion of a previously detected mutation within the same family is quick and cost-effective when compared to MRI. Furthermore, genetic testing identifies mutation carriers even in the absence of clinical symptoms and neuroradiologically visible cavernomas. In the event that a parental mutation is confirmed, presymptomatic genetic testing of further family members selects those relatives who are at risk and truly require clinical and neuroradiological surveillance as described before [12]. Hence, we suggest to perform gradient-echo MR scans for asymptomatic family members with a confirmed *CCM* mutation to assess their current CNS involvement. Serial MR scans may be undertaken once per year. Depending on the findings and patient interests, even asymptomatic cavernomas can be removed surgically with a good outcome for prevention of consecutive bleeding and neurological deficits [2].

Sporadic cases with multiple cavernomas carrying a de novo mutation

If both parents carry the normal sequence and nonpaternity has been excluded, a new mutation must have occurred. In this case, relatives can be reassured with the exception of the proband's offspring and siblings. Patients with multiple cavernomas who carry a de novo *CCM* mutation have an almost 50% risk of transmitting their mutation to their children. In addition, the recurrence risk for siblings may not be completely negligible due to a possible germline mosaicism in an apparently noncarrier parent of the proband. However, this risk is unknown and difficult to assess because it depends on the proportion of mutated parental gametes. Genetic testing precisely determines whether children or siblings also carry the proband's mutation.

Conclusion

Because three *CCM* genes have now been identified, molecular genetic diagnosis is available for both familial CCM and sporadic cases with multiple lesions. If a *CCM* mutation is detected in a patient, genetic testing unambiguously identifies mutation carriers within his/her family and should be performed in conjunction with genetic counseling before neuroradiological screening of relatives. Individuals who test positive for a known mutation may require MRI examination and elective surgery. A negative test result would relieve relatives of clinical and neuroradiological monitoring and the fear to develop serious cavernoma-induced complications.

Acknowledgments Ute Felbor received an Emmy Noether grant from the Deutsche Forschungsgemeinschaft (Fe 432/6-4) and Sonja Stahl a stipend from the Graduiertenkolleg 1048. Genetic testing was approved by the local ethics committees of the Philipps-University Marburg, Study 149/05, and the University of Würzburg, Study 21/05.

References

1. Bergametti F, Denier C, Labauge P et al (2005) Mutations within the programmed cell death 10 gene cause cerebral cavernous malformations. Am J Hum Genet 76:42–51
2. Bertalanffy H, Benes L, Miyazawa T et al (2002) Cerebral cavernomas in the adult. Review of the literature and analysis of 72 surgically treated patients. Neurosurg Rev 25:1–53
3. Cavé-Riant F, Denier C, Labauge P et al (2002) Spectrum and expression analysis of *KRIT1* mutations in 121 consecutive and unrelated patients with Cerebral Cavernous Malformations. Eur J Hum Genet 10:733–740
4. Denier C, Goutagny S, Labauge P et al (2004) Mutations within the *MGC4607* gene cause cerebral cavernous malformations. Am J Hum Genet 74:326–337
5. Denier C, Labauge P, Brunereau L et al (2004) Clinical features of cerebral cavernous malformations patients with *KRIT1* mutations. Ann Neurol 55:213–220
6. Guclu B, Ozturk AK, Pricola KL et al (2005) Mutations in apoptosis-related gene, *PDCD10*, cause cerebral cavernous malformation 3. Neurosurgery 57:1008–1013
7. Labauge P, Laberge S, Brunereau L et al (1998) Hereditary cerebral cavernous angiomas: clinical and genetic features in 57 French families. Lancet 352:1892–1897
8. Laberge-Le Couteulx S, Jung HH, Labauge P et al (1999) Truncating mutations in *CCM1*, encoding *KRIT1*, cause hereditary cavernous angiomas. Nat Genet 23:189–193
9. Liquori CL, Berg MJ, Siegel AM et al (2003) Mutations in a gene encoding a novel protein containing a phosphotyrosine-binding domain cause type 2 cerebral cavernous malformations. Am J Hum Genet 73:1459–1464
10. Liquori CL, Berg MJ, Squitieri F et al (2006) Low frequency of *PDCD10* mutations in a panel of *CCM3* probands: potential for a fourth CCM locus. Hum Mutat 27:118
11. Lucas M, Costa AF, Montori M et al (2001) Germline mutations in the *CCM1* gene, encoding Krit1, cause cerebral cavernous malformations. Ann Neurol 49:529–532
12. Raychaudhuri R, Batjer HH, Awad IA (2005) Intracranial cavernous angioma: a practical review of clinical and biological aspects. Surg Neurol 63:319–328
13. Verlaan DJ, Davenport WJ, Stefan H et al (2002) Cerebral cavernous malformations: mutations in *Krit1*. Neurology 58:853–857
14. Verlaan DJ, Laurent SB, Rochefort DL et al (2004) *CCM2* mutations account for 13% of cases in a large collection of kindreds with hereditary cavernous malformations. Ann Neurol 55:757–758
15. Verlaan DJ, Laurent SB, Sure U et al (2004) *CCM1* mutation screen of sporadic cases with cerebral cavernous malformations. Neurology 62:1213–1215
16. Verlaan DJ, Roussel J, Laurent SB et al (2005) *CCM3* mutations are uncommon in cerebral cavernous malformations. Neurology 65:1982–1983

Anlage 8

For Peer Review

CCM1 gene deletion identified by MLPA in cerebral cavernous malformation

Journal:	*Neurosurgical Review*
Manuscript ID:	draft
Manuscript Type:	Case Report
Date Submitted by the Author:	n/a
Complete List of Authors:	Gaetzner, Sabine; University of Wuerzburg, Department of Human Genetics Stahl, Sonja; University of Wuerzburg, Department of Human Genetics Surucu, Oguzkan; University of Marburg, Department of Neurosurgery Schaafhausen, Anne; University of Wuerzburg, Department of Human Genetics Halliger-Keller, Birgit; University of Wuerzburg, Department of Human Genetics Bertalanffy, H.; University Hospital Marburg Sure, Ulrich; University of Marburg, Department of Neurosurgery Felbor, Ute; University of Wuerzburg, Department of Human Genetics
Keywords:	vascular malformations, cerebral cavernous malformations, genetics, MLPA, deletion

CCM1 gene deletion identified by MLPA in cerebral cavernous malformation

Sabine Gaetzner[1], Sonja Stahl[1], Oguzkan Sürüçü, MD[2], Anne Schaafhausen[1], Birgit Halliger-Keller[1], Helmut Bertalanffy, MD[2], Ulrich Sure, MD[2], Ute Felbor, MD[1]

[1]*Department of Human Genetics, University of Würzburg, Germany*

[2]*Department of Neurosurgery, University of Marburg, Germany*

To whom correspondence should be addressed to:

Dr. U. Felbor, MD

Department of Human Genetics

University of Würzburg

Biozentrum, Am Hubland

D-97074 Würzburg

Tel.: (+)49-931-888 4097

Fax: (+)49-931-888 4058

felbor@biozentrum.uni-wuerzburg.de

Running title: *CCM1* deletion detected by MLPA

Abstract

Familial cerebral cavernous malformations occur with a frequency of 1 in 2000 and may cause recurrent headaches, seizures, and hemorrhagic stroke. Exon-scanning based methods have identified intragenic mutations in three genes, *CCM1*, *CCM2*, and *CCM3*, in about 70% of familial CCM. To date, only two large *CCM2* and a single large *CCM3* deletion were published. In addition to direct sequencing of all three *CCM* genes, we have applied a newly developed multiplex ligation-dependent probe amplification gene dosage assay (MLPA) designed to detect genomic *CCM1-3* deletions/duplications. While direct sequencing did not reveal a mutation in the index case who presented with multiple cavernous angiomas that had caused a generalized tonic-clonic seizure with Todd's paralysis and headaches at the age of five, MLPA analyses detected a large deletion involving the entire *CCM1* coding region in the proband and further affected members of the German CCM family. The MLPA results were corroborated by analyses of single nucleotide polymorphisms within the *CCM1* gene and enabled predictive testing for at risk relatives. Our results confirm a loss-of-function mutation mechanism for *CCM1* and demonstrate that the use of MLPA enables a higher *CCM* mutation detection rate.

Key words: Vascular malformations; cerebral cavernous malformation; genetics; MLPA; deletion

Introduction

Familial cerebral cavernous malformations (CCM; MIM 116860, 603284, 603285) are autosomal dominantly inherited vascular abnormalities with genetic heterogeneity and likely interaction among gene products (10). Exon-by-exon screening approaches found *CCM1* mutations in 43-54% of familial CCMs (2, 9). Up to 22% were shown to carry a *CCM2* mutation (3, 6), and less than 10% a *CCM3* mutation (1, 4, 7, 9). Two large *CCM2* deletions (3) and one deletion involving the entire *CCM3* gene (1) have initially contributed to the identification of the *CCM2* and *CCM3* genes via loss-of-heterozygosity mapping. Since large genomic deletions escape detection by conventional mutation detection methods, we adopted the multiplex ligation-dependent probe amplification (MLPA) gene dosage assay to screen for large deletions/duplications in the *CCM1-3* genes. We here present the identification of a large deletion that encompasses the entire *CCM1* coding region.

Patients and methods

The index case is an 8-year-old boy (III-1, Fig. 1a) who experienced a generalized tonic-clonic seizure with Todd's paralysis and headaches at the age of five. Magnetic resonance imaging (MRI) of the brain showed multiple angiomas including a right temporomesial lesion (Fig. 1b, c). This symptomatic lesion with a diameter of 3,5 cm was completely excised microsurgically via a pterional approach. The postoperative course of the patient was uneventful. After six months, he did not require further antiepileptic medication.

Family history revealed a paternal grandfather with multiple intracranial lesions and fatal hemorrhage at age 47. The patient's father is clinically unaffected but MRI revealed multiple small cavernous angiomas that did not require surgical intervention so far (Fig. 1d). Neuroimaging of three further asymptomatic aunts (II-3, II-5, and II-7, Fig. 1a) revealed a small cavernoma in the basal ganglia of aunt II-5 (Fig. 1a, e).

Editorial Office, University Hospital Marburg, Baldinger Strasse, 35033 Marburg, Germany. Phone: +49-6421-28 65525

Genetic testing was approved by local ethics committees (University of Würzburg, Study 21/05; Philipps-University Marburg, Study 149/05). With informed consent, all coding *CCM1-3* exons were directly sequenced on a Beckmann CEQ 8800 capillary electrophoresis system according to published protocols with slight modifications (1-3).

Screening for large *CCM* alterations requires two MLPA kits (SALSA MLPA Kits P130 & P131 CCM, MRC Holland). *CCM1-3* MLPA analyses of four control individuals in each test and all 10 available family members were carried out according to the manufacturer's instructions using an ABI Prism 310 genetic analyzer. Haplotype analyses were performed for the index case and his parents using 19 intragenic single nucleotide polymorphisms (SNPs) (rs975707, 1064819, 1064820, 1064821, 11984192, 17164451, 2027950, 1034575, 10223994, 10282603, 10274699, 6953959, 12113704 11542682, 1052043, 1063658, 1063659, 11542681, 1063660) and five polymorphic markers flanking the *CCM1* locus (D7S2410, D7S1813, D7S2189, D7S646, and non-informative D7S689).

Results

Direct sequencing of all coding *CCM1*, *CCM2*, and *CCM3* exons and adjacent splice sites did not reveal any pathological intragenic alterations in the index patient. In contrast, only the index case but none of the controls displayed a large deletion encompassing all *CCM1* exons when tested by MLPA (Fig. 2b, e, f). *CCM2* and *CCM3* peaks and ratios did not differ between proband and controls (Fig. 2a, c, d). A second independent MLPA analysis included all 10 family members of the second and third generation (Figure 1a). The heterozygous *CCM1* deletion was confirmed in the three affected family members only (data not shown). Thus, the *CCM1* deletion was reproducible, segregates with the disease, and was not transmitted to children III-2 and III-3 and uncle II-6 (Figure 1A) rendering neuroimaging unnecessary for these individuals and their offspring.

Editorial Office, University Hospital Marburg, Baldinger Strasse, 35033 Marburg, Germany. Phone: +49-6421-28 65525

To further confirm the deletion detected by MLPA, haplotype analyses were performed with 19 intragenic *CCM1* SNPs, non of which was found to be heterozygous in the patient and his affected father. Only three SNPs turned out to be informative. While the patient's mother (II-2) is homozygous for G at rs975707, the father (II-1) is homo- or hemizygous for C (c.1-3078G>C). Since their son did not inherit a paternal C allele (Fig. 3), he is hemizygous for the maternal G allele. Similarly, the mother carries a homozygous C at rs2027950 and a homozygous T at rs6953959 (c.989+4389C>T) while the father's sequence revealed a G (c.989+63C>G) and a C, respectively. The proband only shows the maternal C and T alleles. On the basis of the order of microsatellite markers linked to the disease locus and intragenic SNPs as D7S2410-D7S1813-D7S2189-rs975707-rs2027950-rs6953959-D7S646, the proband and his mother share the haplotype 1-2-2-G-C-T-1. The son inherited the disease haplotype 2-3-3-del-del-del-2 from his father, and this haplotype clearly lacks a second allele for three intragenic *CCM1* SNPs (Fig. 3).

Discussion

The *CCM1* deletion was found in a total of five CCM families in which four novel intragenic *CCM* mutations had been identified by direct sequencing ((8) and unpublished data). Based on microsatellite genotyping and cDNA analyses, previous publications reported that two out of 10 *CCM2* mutations (3) and one out of eight *CCM3* mutations (1) were large deletions. An additional *CCM3* mutation was described as possibly due to a deletion of the genomic region that encompasses exon 5 (1). Furthermore, a genomic deletion involving the 3' end of *CCM1* exon 18 and part of intron 18 was detected (5). We anticipate that a significant proportion of CCM patients will display large deletions or duplications which remain undetected by direct sequencing. MLPA is a suitable method for identifying such *CCM* gene alterations and for

improving the mutation detection rate in CCM patients as well as predictive testing in at risk relatives.

Acknowledgements

The authors thank the patients and their family for their cooperation and MRC Holland for developing the MLPA kits. Ute Felbor receives an Emmy Noether-grant from the Deutsche Forschungsgemeinschaft (Fe 432/6-5) and Sonja Stahl a stipend from the Graduiertenkolleg 1048.

REFERENCES

1. Bergametti F, Denier C, Labauge P, Arnoult M, Boetto S, Clanet M, Coubes P, Echenne B, Ibrahim R, Irthum B, Jacquet G, Lonjon M, Moreau JJ, Neau JP, Parker F, Tremoulet M, Tournier-Lasserve E (2005) Mutations within the programmed cell death 10 gene cause cerebral cavernous malformations. Am J Hum Genet 76: 42-51

2. Cavé-Riant F, Denier C, Labauge P, Cecillon M, Maciazek J, Joutel A, Laberge-Le Couteulx S, Tournier-Lasserve E (2002) Spectrum and expression analysis of *KRIT1* mutations in 121 consecutive and unrelated patients with Cerebral Cavernous Malformations. Eur J Hum Genet 10: 733-740

3. Denier C, Goutagny S, Labauge P, Krivosic V, Arnoult M, Cousin A, Benabid AL, Comoy J, Frerebeau P, Gilbert B, Houtteville JP, Jan M, Lapierre F, Loiseau H, Menei P, Mercier P, Moreau JJ, Nivelon-Chevallier A, Parker F, Redondo AM, Scarabin JM, Tremoulet M, Zerah M, Maciazek J, Tournier-Lasserve E (2004) Mutations within the *MGC4607* gene cause cerebral cavernous malformations. Am J Hum Genet 74: 326-337

4. Guclu B, Ozturk AK, Pricola KL, Bilguvar K, Shin D, O'Roak BJ, Gunel M (2005) Mutations in apoptosis-related gene, *PDCD10*, cause cerebral cavernous malformation 3. Neurosurgery 57: 1008-1013

5. Laberge-le Couteulx S, Jung HH, Labauge P, Houtteville JP, Lescoat C, Cecillon M, Marechal E, Joutel A, Bach JF, Tournier-Lasserve E (1999) Truncating mutations in *CCM1*, encoding KRIT1, cause hereditary cavernous angiomas. Nat Genet 23: 189-193

6. Liquori CL, Berg MJ, Siegel AM, Huang E, Zawistowski JS, Stoffer T, Verlaan D, Balogun F, Hughes L, Leedom TP, Plummer NW, Cannella M, Maglione V, Squitieri F, Johnson EW, Rouleau GA, Ptacek L, Marchuk DA (2003) Mutations in a gene

encoding a novel protein containing a phosphotyrosine-binding domain cause type 2 cerebral cavernous malformations. Am J Hum Genet 73: 1459-1464

7. Liquori CL, Berg MJ, Squitieri F, Ottenbacher M, Sorlie M, Leedom TP, Cannella M, Maglione V, Ptacek L, Johnson EW, Marchuk DA (2006) Low frequency of *PDCD10* mutations in a panel of CCM3 probands: potential for a fourth CCM locus. Hum Mutat 27: 118

8. Surucu O, Sure U, Gaetzner S, Stahl S, Benes L, Bertalanffy H, Felbor U (2006) Clinical impact of *CCM* mutation detection in familial cavernous angioma. Childs Nerv Syst, in press.

9. Verlaan DJ, Roussel J, Laurent SB, Elger CE, Siegel AM, Rouleau GA (2005) *CCM3* mutations are uncommon in cerebral cavernous malformations. Neurology 65: 1982-1983

10. Zawistowski JS, Stalheim L, Uhlik MT, Abell AN, Ancrile BB, Johnson GL, Marchuk DA (2005) CCM1 and CCM2 protein interactions in cell signaling: implications for cerebral cavernous malformations pathogenesis. Hum Mol Genet 14: 2521-2531

Figure Legends

Fig. 1 (**a**) Pedigree of the German CCM family (black circle = affected female, black square = affected male). (**b**) Axial T2-weighted MR-image shows a large right temporomesial cavernoma (white arrows) in the index case (arrow in (**a**)) before microsurgical excision. (**c**) Additional asymptomatic cavernomas (black arrows) were diagnosed in both cerebral hemispheres by gradient echo MR-imaging. (**d**) Axial gradient echo MR-image of the boy's father shows two small asymptomatic cavernomas, left frontal and parietal (arrows). (**e**) One aunt (II-5 in (**a**)) also revealed an asymptomatic cavernoma in the left basal ganglia (arrow).

Fig. 2 MLPA data demonstrating a heterozygous deletion of the entire *CCM1* gene in the index case. Example of (**a**) normal and (**b**) pathological MLPA raw data (SALSA MLPA Kit P130). The electropherograms show reduced peaks for all *CCM1* exons in the proband (asterisks) while *CCM2* peaks (dots) are comparable between control and patient. Peaks from internal controls are not highlighted. (**e, f**) Quantitative analyses demonstrate that the relative peak areas are decreased to approximately 50% in the patient's two non-coding and 15 coding *CCM1* exons analyzed (black) when compared to internal (white) and (**c, d**) external controls and to (**e**) *CCM2* (grey) and (**f**) *CCM3* (grey) probes. Numbers below the coloumns in (**c, d**) indicate the *CCM1-3* exons analyzed according to the manufacturer's protocol.

Fig. 3 Haplotype analysis of the proband (III-1), his father (II-1), and mother (II-2). The haplotype associated with the CCM phenotype was determined as 2-3-3-del-del-del-2 (*boxed*) (del = deletion).

Fig. 3

	II-1		III-1		II-2	
D7S2410	4	2	2	1	1	3
D7S1813	1	3	3	2	2	4
D7S2189	1	3	3	2	2	4
rs975707	C	del	del	G	G	G
rs2027950	G	del	del	C	C	C
rs6953959	C	del	del	T	T	T
D7S646	4	2	2	1	1	3

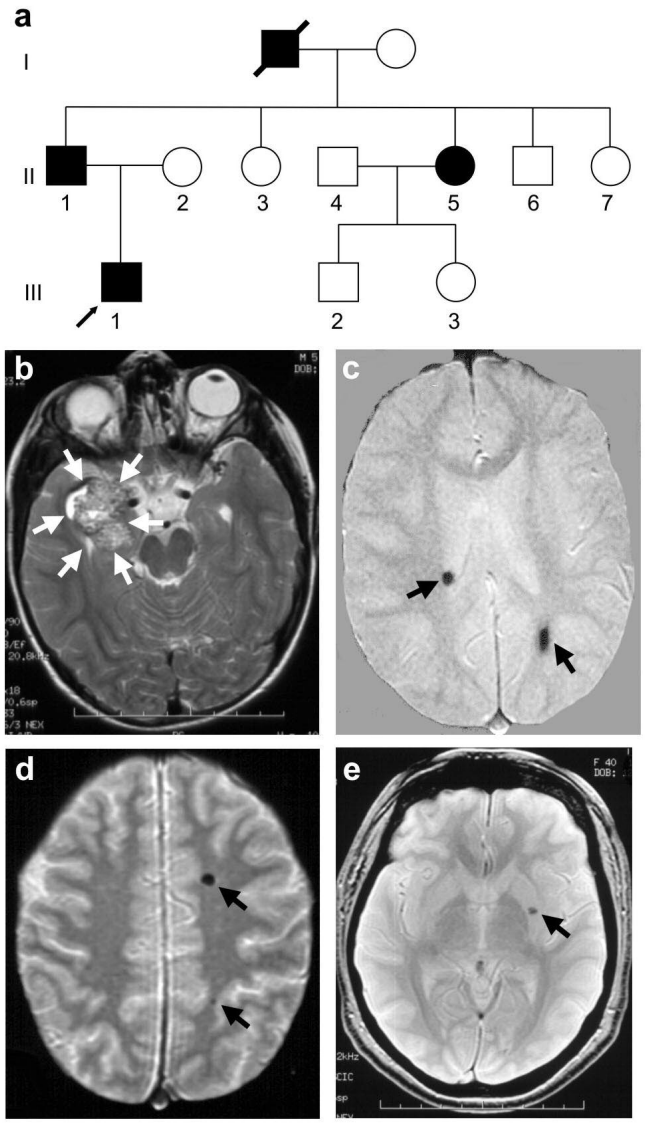
a
I
II
1
2
3
4
5
6
7
III
1
2
3
b
c
d
e

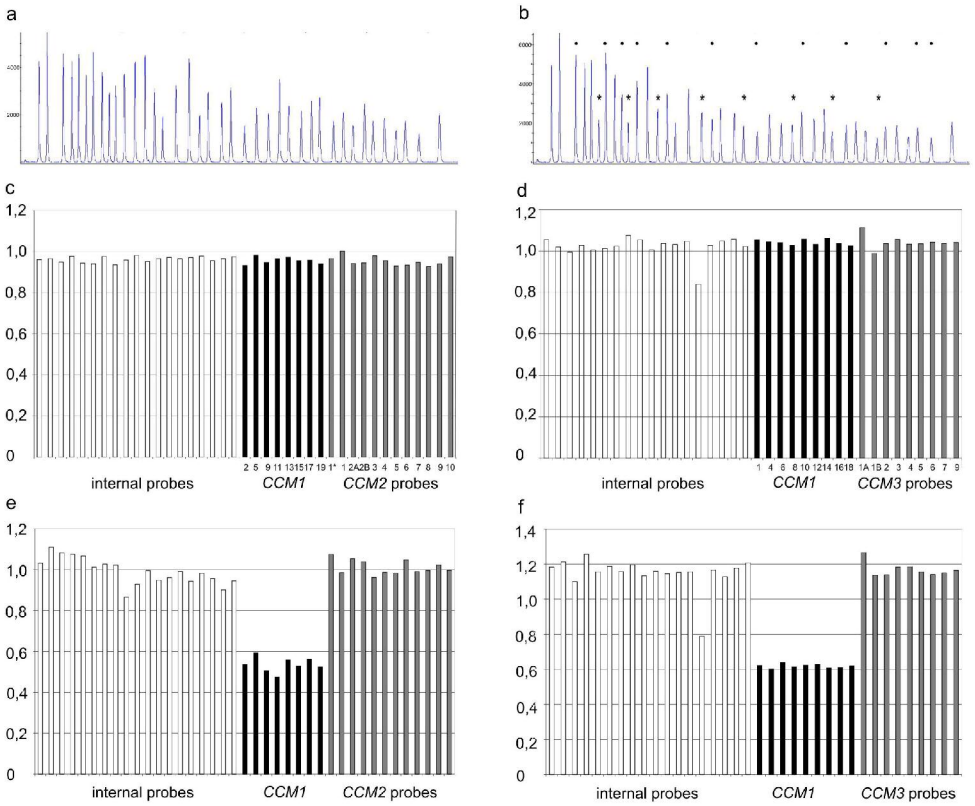
a
b
c
1,2
1,0
0,8
0,6
0,4
0,2
0
internal probes
CCM1
CCM2 probes
d
1,2
1,0
0,8
0,6
0,4
0,2
0
internal probes
CCM1
CCM3 probes
e
1,2
1,0
0,8
0,6
0,4
0,2
0
internal probes
CCM1
CCM2 probes
f
1,4
1,2
1,0
0,8
0,6
0,4
0,2
0
internal probes
CCM1
CCM3 probes

Anlage 9

Letters to the Editor

Stroke *welcomes Letters to the Editor and will publish them, if suitable, as space permits. They should not exceed 750 words (including references) and may be subject to editing or abridgment. Please submit letters in duplicate, typed double-spaced. Include a fax number for the corresponding author and a completed copyright transfer agreement form (published in every issue).*

Controversial Molecular Classification of Human Cerebrovascular Malformations

To the Editor:

The identification of underlying causal genes in familial forms of cerebrovascular malformations allows the dissection of an increasing number of these disorders at the molecular level. In recent years, mutations in *CCM1/KRIT1*, *CCM2/MGC4607*, and *CCM3/PDCD10* have been found to cause autosomal dominantly inherited cerebral cavernous malformations (CCM1, CCM2, and CCM3). Clinical penetrance appears to differ between the 3 CCM subtypes, but larger clinical studies are required to confirm this observation. A subset of patients with cerebral arteriovenous malformations also shows cutaneous capillary malformations attributable to mutations in the *RASA1* gene or is affected by hereditary hemorrhagic telangiectasias (HHT) resulting from mutations in the endoglin gene (*ENG*, HHT1), the activin receptor-like kinase1 gene (*ACVR1*, HHT2), and an as yet unidentified gene (*HHT3*). Disease severity seems to be milder in HHT2 when compared with HHT1, but the clinical course of individual cases remains unpredictable for CCMs and HHTs requiring the investigation of additional genetic and environmental factors that may contribute to the manifestation of these disease entities.[1–4]

Guclu et al[5] recently reported an interesting family in which the index case and her father were affected by CCMs, and the index case's sister had a cerebral venous malformation (CVM). The different vascular phenotypes within this single family were attributed to different genotypes. The sequence data shown demonstrated a stretch of 4 Ts at nucleotide positions 2055 to 2058 of the *CCM1* coding sequence in the index case and the father, but a stretch of only 3 Ts in the sister. The authors concluded that the 2 family members affected with CCM carry an insertion of a T in exon 19 of the *CCM1* gene causing the CCM phenotype, implying that CCMs and CVMs are genetically distinct.

We disagree with this interpretation of the sequence data. According to GenBank accession numbers U90268, AF296765, and AF388384, the *CCM1* sequences reported by Guclu et al[5] for the 2 individuals with CCM are in complete agreement with the wild-type sequence. Rather, the person affected with CVM carries a deletion of a thymine (c.2058delT) causing a genuine *CCM1* frameshift mutation (p.F686fsX706). In addition, the sequences shown were likely not derived from direct sequencing as described in the methods section and the figure legend. If these were direct sequences, the authors would have discovered the very first homozygous uniparental *CCM1* mutation. However, at least in mice, homozygous inactivation of the *CCM1* gene is embryonically lethal.[6]

The authors have sequenced all 3 known *CCM* genes in their patients. Nevertheless, a negative result obtained by sequencing does not exclude the existence of *CCM* mutations. Given a mutation detection rate of currently only about 70%,[7] affected individuals might still harbor a large *CCM1, CCM2* or *CCM3* deletion or insertion, a mutation in regulatory sequences of the *CCM* genes or a mutation in a fourth as yet unknown *CCM* gene. We conclude that the sequence data shown in the report by Guclu et al[5] do not support the existence of 2 distinct molecular entities. Under the assumption that the patients' samples had not been confounded, the data in the figure suggest that, like cavernous angiomas, CVMs might also in part be attributable to mutations in *CCM1*. Further genetic analyses of CVM patients will have to clarify whether CCM and CVM are molecularly distinct or whether both result from mutations in *CCM* genes.

Sources of Funding

U.F. received an Emmy Noether grant from the Deutsche Forschungsgemeinschaft (Fe 432/6-4) and S.S. a stipend from the Graduiertenkolleg 1048.

Disclosures

None.

Sonja Stahl
Ute Felbor, MD
Department of Human Genetics
University of Würzburg
Würzburg, Germany

1. Gault J, Sarin H, Awadallah NA, Shenkar R, Awad IA. Pathobiology of human cerebrovascular malformations: basic mechanisms and clinical relevance. *Neurosurgery*. 2004;55:1–16.
2. Marchuk DA, Srinivasan S, Squire TL, Zawistowski JS. Vascular morphogenesis: tales of two syndromes. *Hum Mol Genet*. 2003;12:R97–R112.
3. Plummer NW, Zawistowski JS, Marchuk DA. Genetics of cerebral cavernous malformations. *Curr Neurol Neurosci Rep*. 2005;5:391–396.
4. Boon LM, Mulliken JB, Vikkula M. RASA1: Variable phenotype with capillary and arteriovenous malformations. *Curr Opin Genet Dev*. 2005; 15:265–269.
5. Guclu B, Ozturk AK, Pricola KL, Seker A, Ozek M, Gunel M. Cerebral venous malformations have distinct genetic origin from cerebral cavernous malformations. *Stroke*. 2005;36:2479–2480.
6. Whitehead KJ, Plummer NW, Adams JA, Marchuk DA, Li DY. *Ccm1* is required for arterial morphogenesis: implications for the etiology of human cavernous malformations. *Development*. 2004;131:1437–1448.
7. Verlaan DJ, Roussel J, Laurent SB, Elger CE, Siegel AM, Rouleau GA. *CCM3* mutations are uncommon in cerebral cavernous malformations. *Neurology*. 2005;65:1982–1983.

(***Stroke*. 2006;37:2214.**)

***Stroke* is available at http://www.strokeaha.org** **DOI: 10.1161/01.STR.0000237168.16486.b7**

Anlage 10

Letters to the Editor

Stroke *welcomes Letters to the Editor and will publish them, if suitable, as space permits. They should not exceed 750 words (including references) and may be subject to editing or abridgment. Please submit letters in duplicate, typed double-spaced. Include a fax number for the corresponding author and a completed copyright transfer agreement form (published in every issue).*

Response to Letter by Stahl and Felbor

Response:

We would like to thank the authors Sonja Stahl and Ute Felbor for their very helpful comments on our article entitled "Cerebral Venous Malformations Have Distinct Genetic Origin from Cerebral Cavernous Malformations." In this article, we presented a rare family in which 2 family members, the father and daughter, had documented cerebral cavernous malformations (CCM), and another daughter had documented cerebral venous malformations (CVM). We had hypothesized that both types of lesions may be attributed to the same genetic defect, and proceeded to sequence all 3 genes known to cause CCM: *KRIT1, Malcavernin,* and *PDCD10*. As a result of our sequencing analysis, we determined that the father and daughter both possessed a frameshift mutation in exon 19 of the *KRIT1* gene, whereas the daughter with the CVM did not carry this mutation. We concluded that CCM and CVM were genetically distinct entities and used this data as further evidence to support the idea that CVMs are benign developmental anomalies that should not be treated clinically.

In their letter, Stahl and Felbor correctly point out that the string of 4 thymine residues (positions 2055 to 2058) is in fact the wild-type sequence and the published figure contains an error. In the original figure the family members affected with CCM were shown with the wild-type sequence and the individual with CVM was shown carrying the mutation. In fact the sequence traces were presented in reverse: the 2 family members with CCM should have been shown to carry the frame-shift mutation attributable to a T deletion, and the member with CVM should have been shown with the wild-type sequence. The corrected figure along with sequencing results of all family members, showing the frame shift mutation in the members affected with CCM, is now presented (Figure 1). As Stahl and Felbor also point out, the sequence traces presented in the original figure, and those presented here, have been TA cloned (Invitrogen), resulting in the presentation of the individual DNA strands clearly showing that the frame shift mutation is the result of a −T deletion. The original sequencing results that suggested the frame-shift mutation are now included (Figure 2). We have also replicated these results. We regret the confusion that our mislabeling of the original figure caused and trust that the new figure (Figure 1) resolves the central question raised by Stahl and Felbor.

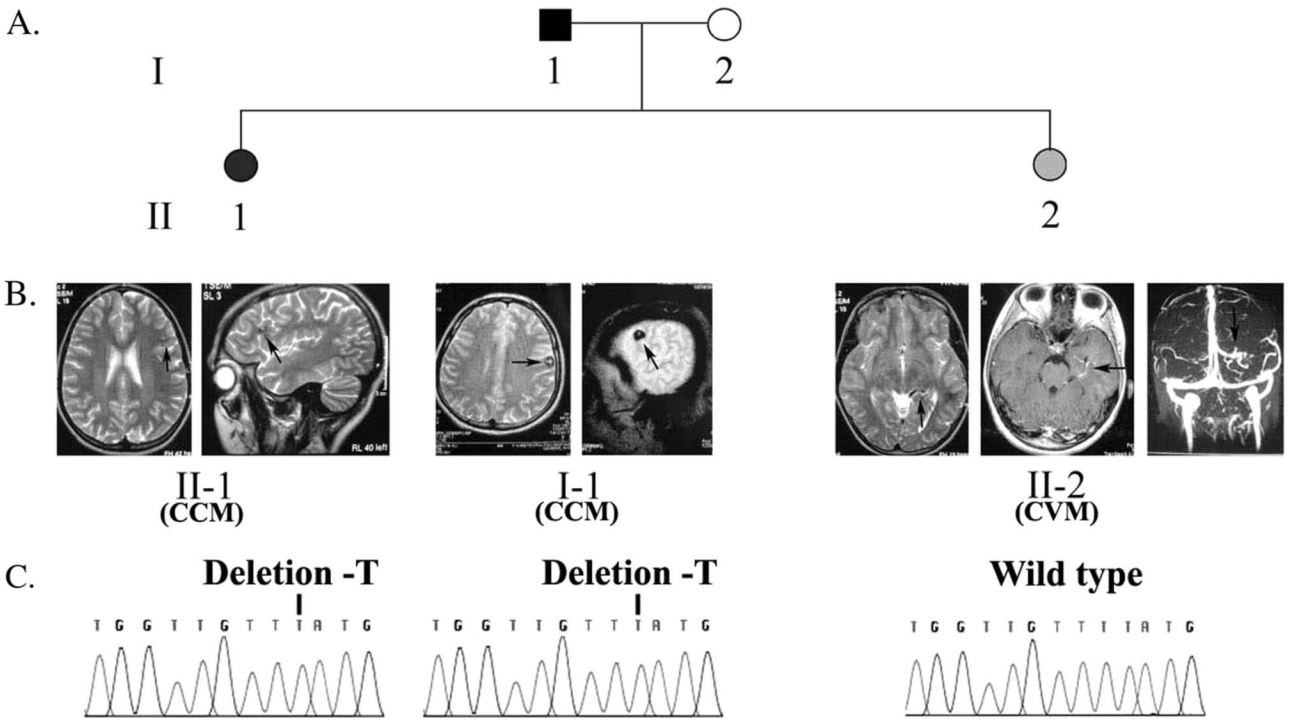

Figure 1. A, Pedigree of family CCM 2211. Filled symbols indicate CCM; gray symbol, CVM. B, Imaging studies of individuals I-1 and II-1 reveal typical CCM lesions (arrows). MRI of individual II-2 reveals the typical caput medusa appearance of a CVM in the posteromedial left temporal lobe (arrow) as confirmed by magnetic resonance venogram. C, Direct sequencing after TA cloning of exon 19 of the *KRIT1* gene reveals a -T deletion leading to a frameshift mutation for individuals I-1 and II-1. For individual II-2, who is known to harbor a large CVM, analysis reveals wild-type sequence for the *KRIT1* gene.

(*Stroke*. 2006;37:2215-2216.)

Stroke is available at http://www.strokeaha.org DOI: 10.1161/01.STR.0000237183.62327.c5

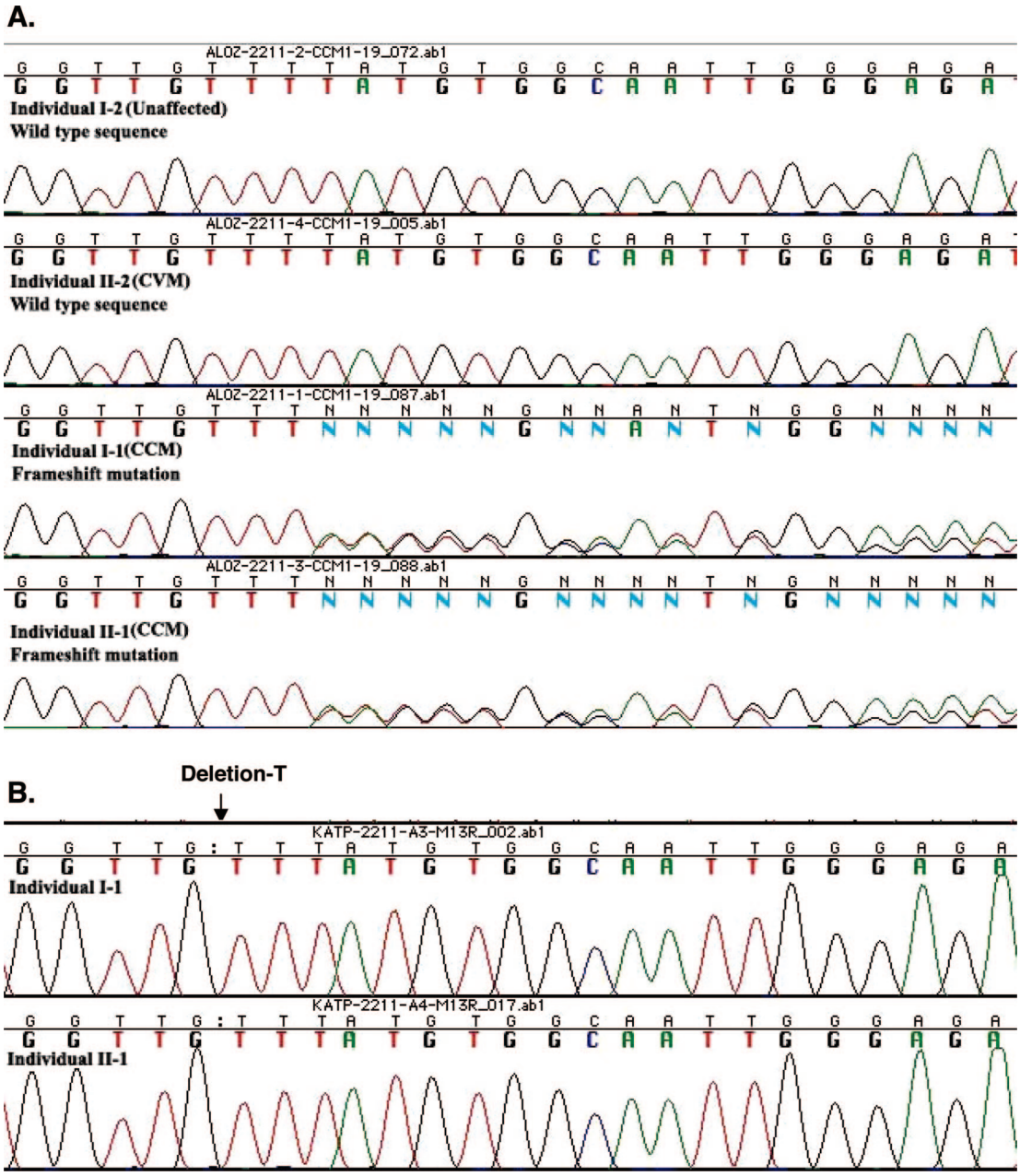

Figure 2. A, Direct sequencing of exon 19 of the *KRIT1* gene reveals the wild-type sequence in individuals I-2 (unaffected) and II-2 (who harbors CVM) and a frameshift mutation in individuals I-1 and II-1, both of whom have CCM. B, Direct sequencing after TA cloning of exon 19 PCR products in individuals I-1 and II-1 reveals a -T deletion causing a frameshift mutation.

In sum, the conclusions drawn in the published article, namely that CCM is attributable to a frameshift mutation in *KRIT1*, remain unchanged. These results strongly suggest that CCM is genetically distinct from CVM and that CVM, at least in this family, is not attributable to a mutation in the *CCM1* gene, *KRIT1*.

Disclosures

None.

Kaya Bilguvar, MD
Ali K. Ozturk, MD
Murat Gunel, MD
Yale University School of Medicine
New Haven, Conn

Bulent Guclu, MD
Yeditepe University
Istanbul, Turkey

Publikationsverzeichnis

Journalbeiträge:

Gaetzner S, Deckers ML, **Stahl S**, Löwig C, Olsen BR, Felbor U. Endostatin´s heparin-binding site is essential for activity and enhances *in situ*-binding to capillary-like structures from bone explants, Matrix Biol. 23(8), 557-61 (2005).

Rychkova N, **Stahl S**, Gaetzner S, Felbor U. Non-heparin binding interactions of endostatin/collagen XVIII in murine development, Dev Dyn. 232(2), 399-407 (2005).

Stahl S, Gaetzner S, Mueller TD, Felbor U. Endostatin phenylalanines 31 and 34 define a receptor binding site, Genes to Cells 10(9), 929-39 (2005).

Berger I, **Stahl S**, Rychkova N, Felbor U. VEGF receptors on PC12 cells mediate transient activation of ERK1/2 and Akt: Comparison of nerve growth factor and vascular endothelial growth factor, J. Neg. Res. BioMedicine 5:8 (2006).

Stahl S, Felbor U. Controversial molecular classification of human cerebrovascular malformations, Stroke 37(9), 2214 (2006).

Sürücü O, Sure U, Gaetzner S, **Stahl S**, Benes L, Bertalnaffy H, Felbor U. Clinical impact of *CCM* mutation detection in familial cavernous angioma, Childs Nerv. Syst. 16, (2006).

Gaetzner S, **Stahl S**, Sürücü O, Schaafhausen A, Halliger-Keller B, Bertalanffy H, Sure U, Felbor U. *CCM1* gene deletion identified by MLPA in cerebral cavernous malformation, Neurosurg. Rev. eingereicht

Stahl S, Reinders Y, Asan E, Conzelmann E, Sickmann A, Felbor U. Proteomic analysis of cathepsin B and L-deficient mouse brain lysosomes, vorbereitet für Mol. Cell. Prot.

Posterpräsentationen:

Hösl E, **Stahl S**, Asan E, Felbor U. Neural stem cell proliferation and differentiation in the absence of cathepsins B and L. ESHG Tagung in München 2004. Abstract in: Eur. J. Hum. Genet. 12 (Suppl. 1), 217 (2004).

Stahl S, Gaetzner S, Felbor U. Functional evaluation of nucleotide substitutions *in situ* using alkaline phosphatase fusion proteins. ESHG Tagung in München 2004. Abstract in: Eur. J. Hum. Genet. 12 (Suppl. 1), 319 (2004).

Stahl S, Reinders Y, Asan E, Conzelmann E, Sickmann A, Felbor U. Neurodegeneration in cathepsin B and L-deficient mice. 30th European Symposium on Hormones and Cell Regulation „Cell death and disease“ Meeting in Mt. St.-Odile, Frankreich 2005, S. 72.

Stahl S, Gaetzner S, Mueller TD, Felbor U. Endostatin phenylalanines 31 and 34 define a receptor binding site. DGFH Tagung in Heidelberg 2006. Abstract in: Med. Gen. 18, 48 (2006).

Gaetzner S, **Stahl S**, Kunze E, Bertalnaffy H, Sure U, Felbor U. Novel CCM1 mutations in familial and sporadic CCM with multiple cavernous angiomas. DGFH Tagung in Heidelberg 2006. Abstract in: Med. Gen. 18, 101 (2006).

Vortrag:
Retreat des Graduiertenkolleg 1048, „Molecular mechanisms of neurodegeneration in cathepsin B and L deficient mice“, Wildbad Rothenburg o.T. 2006.

Erklärung

Erklärung gemäß §4 Absatz 3 der Promotionsordnung der Fakultät für Biologie der Bayerischen Universität Würzburg vom 15. März 1999

1. Hiermit erkläre ich ehrenwörtlich, dass ich die vorliegende Dissertation selbstständig angefertigt und keine anderen als die angegebenen Quellen und Hilfsmittel benutzt habe.

2. Ich erkläre weiterhin, dass die vorliegende Dissertation weder in gleicher, noch in ähnlicher Form bereits in einem anderen Prüfungsverfahren vorgelegen hat.

3. Ich erkläre desweiteren, dass ich außer den mit den Zulassungsantrag urkundlich vorgelegten Graden keine weiteren akademischen Grade erworben oder zu erwerben versucht habe.

Steinfeld, den 25. September 2006 Sonja Stahl

Danksagung

Die vorliegende Arbeit wurde am Institut für Humangenetik der Bayerischen Julius-Maximilians-Universität Würzburg von Mai 2002 bis August 2006 unter der Anleitung von Frau Priv.-Doz. Dr. Ute Felbor angefertigt. Hiermit möchte ich mich bei allen bedanken, die zum Gelingen dieser Arbeit beigetragen habe:

Mein ganz besonderer Dank gilt Frau PD Dr. Ute Felbor für die interessanten Themen, für die überaus freundliche Betreuung und dafür, daß sie mir einen Auslandsaufenthalt an der Yale School of Medicine sowie verschiedene Kongressbesuche ermöglicht hat.

Herrn Prof. Dr. Höhn danke ich für sein Interesse an meiner Arbeit und die gute Ausstattung am Institut für Humangenetik.

Herrn Prof. Dr. Krohne möchte ich für seine Bereitschaft, das Zweitgutachten zu erstellen, danken. Herrn Prof. Dr. Sendtner möchte ich für die Mitbetreuung im Rahmen des Graduiertenkollegs 1048 danken.

Bei Herrn Prof. Conzelmann bedanke ich mich besonders für seine Betreuung von subzellulärer Fraktionierung und Leitenzymtests sowie für die kritische Durchsicht des Manuskripts. Seinen Mitarbeitern möchte ich für alle freundlichen Hilfestellungen danken. Frau Prof. Esther Asan möchte ich für ihre Unterstützung bei der Elektronenmikroskopie danken. Herrn Dr. Albert Sickmann und Frau Dr. Yvonne Reinders danke ich für die nette, erfolgreiche Kooperation. Herrn PD Dr. Thomas Müller und seiner Arbeitsgruppe bin ich für eine freundliche, konstruktive Zusammenarbeit dankbar. Bei Herrn Prof. Dr. Walter Mothes bedanke ich mich für seine nette Betreuung und die freundliche Aufnahme in seine Arbeitsgruppe in Yale für drei Monate.

Ein besonderer Dank gilt Frau Sabine Gätzner (BTA), die mir den Laboralltag nicht nur durch ihre technische Assistenz erleichterte. Meinen Laborkolleginnen Ingrid Berger, Evelyn Hösl, Tanja Neumann, Natasha Rychkova, Elisa Schleider, Sybille Ullrich und Katrin Voss möchte ich besonders, für ihre Hilfsbereitschaft und für das harmonische Arbeitsklima in Labor B324 danken. In diesem Zusammenhang auch vielen Dank an unsere F-Praktikantinnen Anne Wegehaupt und Juliane Klaes und unsere ehemalige technische Assistentin Nadine Rüttling.

Bei allen übrigen nicht namentlich erwähnten Mitarbeitern des Instituts für Humangenetik sowie den Mitarbeitern des Lehrstuhls für Physiologische Chemie II

und den Teilnehmern des Graduiertenkolleg 1048 möchte ich mich für die freundliche Arbeitsatmosphäre und die gute Zusammenarbeit bedanken.
Meinen Eltern möchte ich dafür danken, daß sie mir dieses Studium ermöglicht haben.
Meiner Schwester Petra, Lisa und Matthias danke ich für nette Gespräche und Dr. Matthias Wagner im Besonderen für die Durchsicht dieser Arbeit.

Ein ganz besonderes Dankeschön geht an Edgar für die schöne Zeit außerhalb des Labors.